Time - and Temperature - Dependant Properties of Structural Timber Adhesives used for Onsite Bonding

Muhammad Roseley, Adlin

Award date:
2013

Awarding institution:
University of Bath

ABSTRACT

Bonded-in technology for connections in timber structures relies on the effective bonding of steel or reinforced plastic rods to timber using room temperature cure epoxy adhesives. Thixotrophic adhesive are the best option for timber structural joints which require in-situ assembly. The only drawback with room temperature cured adhesive is their partially cure and possess relatively low glass transition temperature. There are concerns associated with the stability of these adhesive especially in service temperature which may reach up to 50°C.

This research investigated the creep properties of four commercially available epoxy-based adhesive. Prior to investigating the creep properties of the adhesives, their microstructure was analysed and the mechanical and thermal properties of the adhesives and bonded joints were evaluated. The adhesives investigated were partially cross-linked adhesive with a Tg value of 35.4°C to 53.4°C.

Creep testing of adhesive was conducted within a Dynamic Mechanical Thermal Analyser with a step-wise increase of temperature. The tests were conducted in tension loading in static mode at various stresses level. Under Tg and Tg + 15ºC all of the adhesives experienced creep to a limit conforming with the classic viscoelastic behaviour of polymers. Above Tg + 15ºC the adhesives behaved like rubbers. Therefore room temperature cured epoxy adhesives are still able to function above Tg under creep load. The adhesives tested in creep failed by rupture at high stresses and temperatures.

The performance of bonded-in connections under various combinations of temperature and relative humidity was also investigated. Creep experiment on specially designed model of bonded-in joint were conducted at temperatures of 20, 30, 40 and 50°C with corresponding levels of relative humidity (RH) of 65, 75, 85, and 95%. Under intermediate condition, secondary creep to a limit was observed. Tertiary creep to failure occurred on samples tested at maximum temperature and humidity.

ACKNOWLEDGEMENT

I would like to express my deepest gratitude to my supervisors, especially to Dr. Martin P. Ansell which has given me hope, inspiration and tireless mentoring for me to achieve my dreams. For the last four years he has been my mentor, a friend and a father figure to me. I would also like to thank Prof. Richard Harris for sharing his knowledge and guidance.

I wish to thank Dave Smedley of Rotafix Ltd on his valuable insight on the adhesive industry. The Rotafix family including Gareth Jones and Barbara has always been more than willing to offer technical help and their latest products for testing. Special thanks to all University of Bath's laboratory technicians which assisted me throughout my four year work. This includes the technical staffs from the Electron Microscopy unit, Ursula Potter and Hugh Perrott. I am also indebted to the support from Frank Hammet, Chris Arnold and Andrew from the Department of Mechanical Engineering. I've also received technical supports from the Civil Engineering and Architecture Department in which I'm fully grateful.

My deepest thanks goes to my colleagues in Bath including Ester Rojo, Parvez Alam, Simon, Franceso, Cesar, Umberto, Jon and others for encouragement and their part in knowledge sharing. My sincere thanks are offered to fellow Malaysian in Bath, including Umi, Shima, Tiea, Fatimah, Rahim, Hefni, Elina, Ridhwan, Azhar and others for being there when help is in need. I met Dr. Zakiah Ahmad just before coming to Bath. I am grateful for her continuous moral support and guidance throughout my study.

My four year studies in Bath have been supported by Malaysian's Ministry of Higher Education (MOHE) and Universiti Putra Malaysia (UPM). This financial support is greatly acknowledged.

Finally, I wish to thank my family who have been very understanding and continuously giving me encouragement and financial support. My warmest thank goes to both of my parents, Roseley and Noriah for their prayers. I'm indebted to my brother, Adli for taking care of my parents during my absence. This work is dedicated to all of you. Thank you again.

CONTENTS

LIST OF FIGURES

LIST OF TABLES

CHAPTER 1 : INTRODUCTION

1.1 BACKGROUND

Epoxy adhesives are available in a wide range of formulations, depending on the requirements of the application. The formulations for bonding wood are very effective due to their gap filling capability, ability to cure at room temperature and low clamping pressures required (Frihart, 2005). Epoxy adhesives have been used extensively for timber upgrading and in-situ restoration (Ansell and Smedley, 2007) due to their gap filling and shear thinning (thixotropic) capabilities and ability to cure at room temperature.

The use of adhesive bonding hardware such as pultruded rods and metal plates has increased substantially due to the results of research reported in the literature (e.g. Broughton and Hutchinson, 2001). The serviceability of adhesive bonding within wood structures has been widely discussed, particularly concerning the ability of adhesive to withstand load (Bainbridge *et al*., 2002, Madhoushi and Ansell, 2004 and Steiger *et al*., 2006).

However, the application of adhesive bonded joints in wood structures may be limited by temperature and high relative humidity. The ability of epoxy to withstand warm/moist service condition has long been a topic of concern and room temperature cure epoxies exhibit temperature-dependant properties such as creep since they are not fully cross-linked. Ashcroft *et al*. (2001) investigated the effect of environment on the strength of bonded joints and reported a transition from brittle to ductile behaviour as temperature increased due to the fact that room temperature curing epoxy adhesive possess low glass transition temperatures (T_g). Post curing of wood adhesives following bonding is likely to continue the cross-linking process and raise T_g.

The full potential of timber connection systems has not been reached due to lack of understanding of basic characteristics of the bonded interfaces. Attaining adequate

information on the effect of long term loading on time dependant properties such as creep is also very crucial. The European Community for standardisation has organised a specific research program (GIROD-Glued-In Rods) solely for the purpose of attaining data on the durability and creep property of bonded-in joints (Feligioni *et al*., 2003).

This research is also highly relevant to the current scenario in Malaysia. In order to change the misconception on the durability of tropical hardwood, the Malaysian government has taken active steps in promoting the use of indigenous hardwoods in construction. One of the prominent projects includes a large-scale glue-laminated timber (glulam) structure which was constructed using bonded-in joints. The bonded-in connection was made using a room temperature curing epoxy adhesive. Ambient-cured epoxy may take longer time to fully cure, although Malaysian hot tropical weather may help to accelerate the curing process. The performance of bonded connection under Malaysian weather of high temperature and humidity has been an interest of various studies (Smedley *et al*., 2012).

The most daunting task in researching the characteristics of adhesives under adverse environmental conditions is developing research method to obtain relevant and meaningful mechanical data. Such methods include Thick Adherend Shear Test, in creep and creep testing of bonded-in rods. The geometry and dimension of the joints and testing environment require much consideration. Ultimately, the aim is to predict service life through the testing of model bonded structures.

1.2 OBJECTIVES

The overall objective of the research is to characterise the creep behaviour of epoxy adhesives according to the following specific objectives:

1. To characterise the microstructure of room temperature curing epoxy adhesive which contain micro-size ceramic particles, nano-silica and rubber (CTBN) in relation to mechanical properties.

2. To evaluate the thermal stability of room temperature curing epoxy adhesives modified with nano-silica and by the introduction of liquid rubber and to evaluate changes in the glass transition temperature (Tg).
3. To evaluate the effect of various post-curing temperatures on the flexural, shear and fracture toughness of nano-silica modified epoxy bulk adhesives.
4. To analyse the shear properties of nano-silica modified epoxy adhesive using Thick Adherend Shear Test (TAST).
5. To evaluate creep and shear creep of bulk epoxy as a function of time and temperature using Dynamic Mechanical Analysis (DMA) technique.
6. To explore the static shear strength and failure mode of micro-ceramic and nano-silica modified epoxy adhesive bonded-in joints in Laminated Veneer Lumber (LVL).
7. To study the effect of micro- and nano-filler additions on creep performance of bonded-in joints due to exposure of various temperature and humidity level.
8. To utilise an existing model to describe creep behaviour of wood adhesives used for on-site bonding.
9. To demonstrate the suitability of room temperature cure epoxies for forming stable creep-resistant bonded-in connections in timber structures.

1.3 REPORT LAYOUT

This report is divided into sections which describe the following:

- Chapter 2 is a literature review based on the usage of wood as building material. The chapter discussed on wood as a sustainable building material which is derived from a renewable resource. Wood composite and engineered wood products were developed to sustain the increasing demand of wood material.
- Chapter 3 describes the types of joints and connectors types associated with structural timber bonding. Comparisons on the advantages and disadvantages of mechanical and adhesive bonded-joints were reviewed in this chapter.
- Chapter 4 reviews the bonded-in connection and factors which influences the durability of the joint. The chapter also features an example of bonded-in connected timber structure which uses room temperature curing epoxy adhesive.

- Chapter 5 discussed on epoxy adhesive as structural adhesive for bonding, restoration and upgrading of timber structure. The modification of epoxy adhesives by the addition of micro- and nano-particulate to increase the performance of the adhesive is also reviewed in this chapter.
- Chapter 6 reviews on the theoretical and empirical method in assessing the viscoelastic behaviour of polymer. This chapter contributes to the understanding creep and response of polymer under constant loading.
- Chapter 7 presents the investigation on the microstructure of epoxy adhesive. The results on the examination of micro- and nano-particle filled epoxy are presented based on the Scanning Electron Microscopy (SEM) and Transmission Electron Microscopy (TEM) findings.
- Chapter 8 describes the experimental procedures for static mechanical evaluation of adhesive which includes flexural, tensile, inter-laminar shear and fracture toughness testing. The static mechanical evaluations are presented with reference to flexural modulus, inter-laminar shear strength, critical stress intensity factor (K_{IC}), critical strain energy release rate (G_{IC}) and tensile modulus of elasticity.
- Chapter 9 reports on thermal properties of bulk epoxy adhesive using Dynamic Mechanical Thermal Analysis (DMTA). This chapter also examines the effect of micro- and nano-filler addition to the creep performance of adhesives via dynamic mechanical analysis.
- Chapter 10 presents the assessment of micro- and nano-filler additions on shear strength of lap joints. The thick adherent shear test (TAST) procedure was also described.
- Chapter 11 evaluates the shear strength of bonded-in joints based on steel and GFRP bonded into LVL. The fracture modes of test specimens are evaluated as a function of the thermal treatments.
- Chapter 12 reports on the investigation on the effect of temperature and humidity on the bonded-in joints models. The results is presented with reference to creep displacement.
- Chapter 13 reviews the results and discussions of the research presented in the thesis. The experimental evidence and analytical information is summarised. This chapter also proposes the direction of future work.

CHAPTER 2 : ENGINEERED WOOD

2.1 INTRODUCTION

Wood has been regarded as an essential building material since the early ages. Wood material has been of enormous economic significant based on its superior physical properties, aesthetic value, availability and workability.

Wood provides the advantage of high strength to weight ratio as compared to other building material such as steel and concrete. Figure 2.1 depicts the modulus of various materials which also includes wood, steel and concrete. This chart shows that all materials with modulus above 10GPa and density of more than 1.7 Mg/m^3 can be considered as high in modulus and density. In reference to Figure 2.1 the metal family (including steel) and non-technical ceramic (including concrete) are regarded as materials with high moduli and density (Ashby *et al.* 2010). By contrast, wood which is grouped in the natural material family has high moduli with a density of less than 1 Mg/m^3.

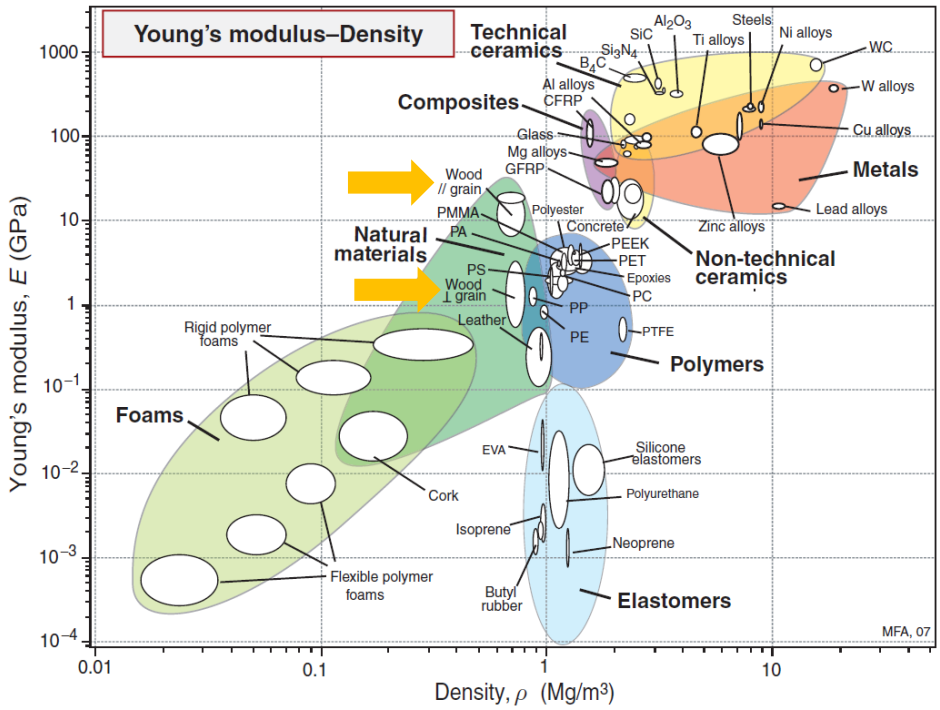

Fig. 2.1. Material chart on modulus and density properties of various materials. Wood material is indicated by arrows (Ashby et al., 2010).

Wood material is also cheaper than other conventional building materials. The cost of material is the most influential factor in construction. Engineered wood product offers the best option for strength, reliability and cost effective solution. Consider the chart in Figure 2.2 which depicts the modulus and relative prices per volume of materials. The chart concludes that wood and concrete as to compare to steel, is cheaper without too much compromising the strength of the material.

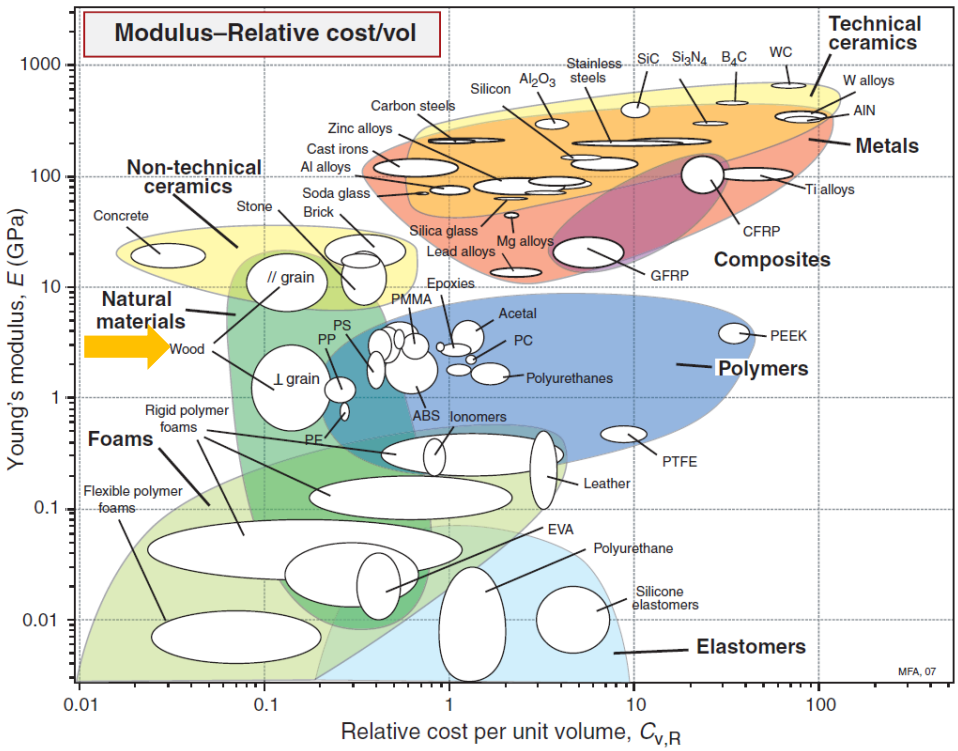

Fig. 2.2. Material chart on modulus and relative cost per unit volume of various materials. Wood material is indicated by arrows (Ashby et al., 2010).

Other justification on using wood as building material is because wood is a good insulating material. This is due to the inherent properties of the wood itself since it is primarily consists of hollow cellular structure. The cell cavity serves as air pockets for insulation. Wood products also require less energy to produce, hence lowering its carbon footprint. Steel and concrete both require more fossil fuel to produce. Wood is also a renewable and sustainable material which is mainly derived from sustainably managed forest and plantation. Forested areas offer benefit as carbon storage, oxygen generation and conservation of forest biodiversity.

Apart from its numerous advantages, wood has an issue in strength variability. Solid wood contains natural defects such as knots, spiral grain, reaction wood and density variation. Even wood of similar species has strength variation between trees and stand. The density of wood from the bottom of the log would differ from those obtained from the top log. Wood is an isotropic material in which the strength in tension and compression differs according to the direction of the grain.

Engineered wood based material was developed to produce wood of homogenous properties. This technology also allows the usage of logs from smaller diameter and wood material of lower quality range to meet raw material requirement. Exponential growth of demand for wood material to sustain the construction industry has caused for limited resource. Difficulties in obtaining suitable lumber sizes has persuaded for the development of engineered wood such as laminated veneer lumber (LVL), laminated strand lumber (LSL), parallel strand lumber (PSL) and glulam. Adhesive bonded structural connection has been used in many timber engineering techniques to produce large structural member from these composites.

2.2 ENGINEERED WOOD

Engineered wood is a specially designed material with the main purpose to out-perform the natural strength properties of solid wood. The process of reducing timber into smaller strips allows the defects to be removed or distributed throughout the composite. Knots, splits, reaction wood or sloping grain are considered as defects in wood. The removal of potential weak points produces composite of uniform quality, with strength and stiffness higher than original piece of timber. The process of breaking down and gluing the wood material back together allows boundless possibility on the shape of the final product. Structural composite lumber such as glulam can be produced according to specific curves and complex shapes. This technology also allows wider range of raw material capable to be processed. Source for composite lumber can either be from solid-sawn lumber, smaller diameter trees or even waste wood from other wood-based processes (Dinwoodie, 2000 and Berglund & Rowell, 2005).

2.2.1 GLUE LAMINATED LUMBER (GLULAM)

Glue laminated timber or glulam is the earliest established structural composite lumber, in which the first industrial patented use was in Germany in 1872). It was then introduced in 1893 for an auditorium in Switzerland (APA, 2002). The widespread use of glulam in timber structure was due to significant development in the glulam technology which includes:

- The improvement in processing technology (rapid heat and cure of adhesive using radio frequency energy)
- The introduction of water proof adhesives (phenol, resorcinol or melamine formaldehyde)
- Polymer composite reinforcement (fibreglass, carbon and polyester fibre) on the tensile face of glulam beam. This is to achieve stronger and stiffer beam with smaller cross-section (Dagher & Bragdon, 2001; Shmulsky & Jones, 2011).

The production of straight glulam beam is highly automated whilst curve beam requires manual production. Raw material for glulam will have to go through series of grade proof testing in which selections of high-grade wood are made based on strength and stiffness. Glulam is produced by face-laminating thick ply of wood (Figure 2.3). Each laminates has a thickness between 25 to 50mm. Individual pieces of wood are end-jointed using a scarf or finger joints to form a layer of continuous length (Figure 2.4). The locations of end joints are staggered across the layers to avoid formation of weak point. The individual layer finger joint is proof tested for bond strength before layering-up process. The lamination of layers is bonded in the direction of the grain along the parallel length of the lumber. Material of high strength and stiffness is located at the tension and compression zone of the laminated beam. Material of lesser quality is layered closer to the neutral axis of the beam (Shmulsky & Jones, 2011). The layers of laminae are face-coated using cold setting adhesives (eg. urea, resorcinol or phenol-resorcinol formaldehyde). The parallel layers are then fitted to a metal jig and clamped until the adhesive has set. Glulam can be produce in various shapes and strength classes depending on the

number and types of laminate used. Improvement in strength and stiffness of glulam is due to less material variability compared to solid wood. Under exposure to variation of moisture, glue laminated timber is also more dimensionally stable than solid wood (Dinwoodie, 2000).

Fig. 2.3 Glue laminated timber in existing timber structure

Fig. 2.4. Finger joints of glulam which can be in horizontal or vertical arrangement

The cost of producing glulam is two to three times than solid wood. As stated by Shmulsky & Jones (2011), high cost in production of glulam is attributed to several factors which include:

- Requirements for high-quality raw material
- Transportation cost between sawmill and glulam factory

- High capital investment and operating cost of glulam factory
- Glulam production requires relatively high spread rate of adhesive resin (340g of adhesive mix per square meter)

Glulam can be found in variety of applications including bridges, commercial building, residential, truck beds and marine construction. Glulam is suitable for application for wide-span stadium roof as can be seen in sports structures. PostFinance Arena which is built in Berne, Switzerland has glulam arches reaching up to 85 meters. The roof of Richmond Olympic Oval in Vancouver, British Columbia is made of 2400 cubic metres of Douglas-fir glulam beams (Naturally:Wood, 2012).

2.2.2 LAMINATED VENEER LUMBER (LVL)

LVL is a composite product made of multiple layers of veneers. The veneers are bonded with PF adhesive to build up member depths. The manufacturing process of LVL is much similar to plywood. Veneer for LVL is produced through rotary peeling of heated logs. The veneers are then clipped, dried and graded ultrasonically (Shmulsky & Jones, 2011). The thickness of veneer for LVL ranges from 1.5 to 6mm. Following grading, the veneers sheets are then glued and laid up for prepressing and hot pressing. The veneer orientation in LVL is similar to plywood except LVL veneer is oriented in a common grain direction. LVL is usually manufactured for end thickness of 21–75mm (Berglund & Rowell, 2005).

LVL is sold according to mechanical strength and stiffness. These are influenced by types of wood used and manufacturing properties. Two primary species used by Micro-lam LVL in United States is southern yellow pine and Douglas fir. Hardwood species such as gum and yellow poplar has also been cited as raw material for LVL. Other manufacturer such as Kerto-LVL in Norway uses Norway spruce. Market price on high grade LVL is higher than solid-sawn timber. This is due to many advantages of LVL over sawn timber such as uniform strength properties and good dimensional stability. Major application of LVL includes flanges for prefabricated wood I beams, scaffold planks, built-up girders and other application where high strength and stiffness is required (Shmulsky & Jones, 2011).

2.2.3 STRAND-BASED LUMBER

Parallel strand lumber (PSL) and laminated strand lumber (LSL) are the latest innovation in structural composite lumber. Both are sold for application which requires high bending strength. PSL and LSL can be found in many applications such as bridge stringers, cross- and switch-ties and wood trestle members. (Shmulsky & Jones, 2011).

The manufacturing process of PSL is similar to LSL except for the dimension of strands, types of wood material and adhesive used to bind the strands. PSL is produced from 2.5mm thick rotary peeled veneer strand of Douglas fir or Scots pine. The dimension of PSL strand is 2400mm in length by 3mm in width. LSL is made of aspen, yellow poplar or basswood strands. The strands are much thinner for LSL, with a length and width dimension of 300mm and 3mm respectively (Dinwoodie, 2000).

PSL is bonded using PF-based adhesive that contains high level of resin solids (up to 15%). This gives good dimensional stability and durability to PSL. LSL is produced using polymeric diphenylmethane diisocyanate (pMDI) resin adhesive which gives LSL lighter colour and waterproof quality. The strands are aligned parallel to each other before being pressed. High-frequency radio (radio or microwave) is used to cure phenolic resin in PSL. The resin-coated strands in LSL are cured using steam injection presses (Shmulsky & Jones, 2011).

2.3 CONCLUDING REMARKS

Wood provides the best option as building material, considering its renewability and sustainability, high strength to weight ratio, cost effectiveness, heat- insulation properties, less carbon footprint and other contributing factors which are equally important. There is the potential of engineered wood replacing solid wood in near future. The global trend of demand and supply indicates on significant increase of raw material consumption in line with growth of population. This justifies the urgent need

for technology development in engineered wood so as to discover new potential for wood and timber products.

CHAPTER 3: JOINTS AND CONNECTORS OF TIMBER

3.1 INTRODUCTION

The main purpose of timber jointing is to hold parts together. This can be achieved effectively by employing mechanical fastener, adhesive jointing or carpentry jointing. Mechanical fasteners such as nails, blots and screw are among the most commonly used joint. Adhesively bonded joints such as scarf joint, but joint and finger joint provide effective stress distribution within the joint and better load transfer between the connected elements. Carpentry joints such as mortice and tenon, tongue and groove, dowel and dovetail have been used for non-structural and structural application. Each technique is unique and provide different characteristic in terms durability, strength, flexibility and appearance. The application of joinery and connection techniques can be found in the manufacture of furniture (non-structural) to the construction of timbers structures such as buildings, towers and bridges (structural).

Within a timber structure, joint and connectors are the most crucial component.The strength and stability of a certain structure depends on the ability of the structural joint to transfer load between structural members effectively. Much consideration needs to be given on the performance of the structural joints since the load bearing capacity of a structure is governed by the strength properties of the timber members and the connecting joints. Timber connection is regarded as the weakest link within the structure and proper designing of the connection is crucial to ensure structural stability and rigidity. The performance of a joint in transferring load effectively depends on several factors which include the design of the joint on wood parallel and perpendicular to the grain, service condition and movement within the joint due to dimensional changes of the wood due to moisture. This chapter evaluates the types of mechanical fixings and adhesively bonded joints used in the construction of timber structure and the consideration taken during the construction of the joints.

3.1.1 CONSIDERATION IN SELECTION AND DESIGNING OF TIMBER CONNECTION

Following are factors which might affect the structural ability of the connection:

a) Moisture content

The most critical problem posed to timber connector is moisture content of the wood and changes of dimension due to moisture. Timber jointing using mechanical fastener can be assembled in green or dry state, although the later is preferable. Most adhesive for bonded joint require dry substrate, although some adhesives may have the ability to bond at 22% MC. Wood kept dry during service will last longer and maintain stronger joint. Exposure to moisture would lead to decay thus limiting its service life. During designing, it is crucial to consider the in-service moisture content such as whether the joint will be in continuously wet or dry condition. It is common practice to dry the timber within 3% of the moisture content in-service during the fabrication of the joint (Chu, 1987).

b) Shrinkage and swelling

Wood may shrink and swell due to drying and moisture uptake. Due to the cellular configuration, the behaviour and magnitude of dimensional changes would differ according to the orientation of the grain. It is important to take consideration on the direction of the load with regards to the direction of the grain during designing timber joints (Faherty, 1998).

c) Angle of load to grain

Apart from the effect on dimensional changes, orientation of the grain may also influence the mechanical strength of the joint. The type and placement of fastener may require proper consideration since ultimate strength in tension of connector placed perpendicular to grain is lower compared to parallel to the grain.

d) Grade and quality of wood

It is recommended that the grade oftimber used for constructionconform to the requirement with regard to the quality of the lumber as stated in grading

standards. Timber also needs to be sound and clear of visual defects such as check, knots, decay and splits.

e) Type of loading and duration of load

Long term loading would affect the duration of load of timber connectors. Duration of load can be defined as time to failure, which described the time between loading of a constant load and failure of the joint (Blass, 2003).Over a period of time, the load bearing capacity of connector will decrease thus increasing slip in loaded connection. Duration of load is strongly influenced by the movement in wood due to temperature and moisture changes.

A joint which is under a constant load over a long period of time will also experience creep. Creep in joint can be defined as the behaviour of joint deformation with respect to time. A study by Van de Kuilen (1999) has indicated on increase of creep in mechanical joints due to the mechano-sorptive behaviour of wood as a result to variation in relative humidity. The study also indicates that creep is greater in joints than in timber member. Moisture exchange at the end grain is greater than through side grain. Localised moisture changes caused deformation of fastener which is commonly located at the end of timber member. As for vibratory loads, a joint which is exposed to reversal stress is more suitable for bolts with shear plates or split ring than nails. In general, it is crucial to put the type of loading and duration of loading with regards to modification factor into consideration during designing (Blass, 2003).

f) Size, type and number of fasteners

These factors may affect the chance of error during installation and the cost of labour during construction. As cited by Faherty (1998), less number of fastener and connectors would reduce the cost of material. The chance of error and labour cost could also be reduced if the type and size of fastener is uniform throughout the structure. The magnitude of slippage at all joints could also be kept uniform if the structure is built using the same fastener.

g) Thickness and width of timber

The thickness and width of the timber would determine the type and size of the fastener. A basic rule applies when a timber is greater than 1 ½ inch (38.1mm) thick, nail fastener is recommended not suitable for the application. This also imply that any type of fastener is suitable for a timber which is thinner than 1 ½ inch (38.1mm). Higher load-bearing capacity would require fastener such as bolts, split rings, shearing plates, hanger are deemed more suitable for the application (Faherty, 1998).

The width of the timber may influence the load-bearing capacity of the joint with regards to direction of loading. Each increment of 25mm in width would result on 10% increase in load-bearing capacity when the connectors are bearing perpendicular to the grain (Rammer, 2010).

3.2 MECHANICAL JOINTS AND FIXINGS

3.2.1 TYPES OF MECHANICAL JOINTS AND FIXINGS

Mechanical fasteners can be classified into two main groups. The classification was made according to the method of the fasteners transfer load:

a) Dowel type fasteners:

These types of fasteners the method in transferring load is along the shank or length of the dowel. The strength of a joint is evaluated based on the resistance due to lateral and withdrawal loading. Lateral loading refers to the type of force perpendicular to the axis of the fastener whilst withdrawal loading results from force applied parallel to the axis of the fastener (Faherty, 1998). Dowel types fasteners include nails, screws, bolts and dowels.

b) Connectors:

Timber connectors or hardware transfer load at the surface of each member. Usually use in conjunction with dowel type fastener such as bolts. Shear plates, split rings will increasing the timber area to transmit load thus increasing the bearing area of the joint.

3.2.1.1 Nail

The most common and effective mechanical fastener is nails. It is regarded as effective since it can be placed closely together and can be driven without pre-drilling (Larsen, 2003). Nails are manufactured in various types and sizes and were specified according to length and diameter dimension. Within a joint, nails were used to resist withdrawal and lateral loading. Higher density timber tends to have higher resistance to withdrawal compared to lesser dense timber. The resistance to withdrawal loading is also determined by the diameter of the nail and depth of penetration of the nail into wood.Resistance to lateral loading in direction parallel to grain is almost two-thirds lesser than side-grain nailing.The strength of nailing is also affected significantly by the duration of loading. Among the contributing factorsto the increase of slip in loaded connection is the variation of temperature and humidity (Blass, 2003).The tendency of causing splits in nailing can be reduced by observing factors such as end distance, edge distance, spacing and size of the nails.

Modifications on the properties of the nails were made to improve the loading capacity of nails. Methods of surface modifications include coating using cement, galvanized, plastic and nylon (Rammer, 2010). Shapes modified nails such as barbed, helically and annually threaded nails have proven to be greater in withdrawal resistance compared to the common wire nails. Common wire nails were made by cold drawing a steel wire which will corrode due to the presence of moisture and when in contact with treated wood (preservative or fire retardant treated). Staining due to the reaction to wood extractive can be avoided by using nails made from copper, silicon bronze, stainless steel or hot-dipped galvanized nails (Rammer, 2010).

3.2.1.2 Screw

The design concept of wood screw is much similar to nail except it requires insertion by turning not driven by hammer (Faherty, 1998). It is also manufactured in varieties according to material, types, shape of head and diameter of the shank. Wood screws were classified according to types of its head which is either flat, oval or roundhead and were specifically designed for their appearance and usage.

The shank of the wood screws were threaded almost two-thirds of its length which provides extra resistance to withdrawal compared to other dowel type fasteners (Blass, 2003).Wood screw oriented perpendicular to the grain performed better in withdrawal resistance than screws oriented parallel to the grain. Withdrawalcapacity of wood screw is governed by the density of timber,length of engagement of the threaded portion and the diameter size of the screw (Chu, 1987 and Rammer, 2010). As for lateral resistance of wood screw in single shear, the capacity is determined by the thickness of the joined members, compressive strength of the wood and the dimension and yield strength of the screws (Faherty, 1998).

3.2.1.3 Bolt and dowel

Apart from nails, bolts are common fasteners used for timber jointing (Fig. 3.1). Bolts are generally used in the construction of large span trusses, arches, post and beam (Chu, 1987). Due to the thickness of timber member, bolts used for timber construction are much longer than ones used for steel construction. Bolts are commercially available in various sizesand should be quoted according to diameter (D) x length (L). Bolted joint has the capacity to connect single, double or multiple shear member. It is designed to resist lateral load perpendicular to the axis of the bolt. Pieces of assembled parts are joined by insertion of threaded bolt into the bolt hole and tightened using a nut. It is common practice to place washer under the bolt head and nut to reduce compression stress. The minimum required size and design stress for washer has been detailed in standards such as Eurocode 5 (Part1-1: 6.5.2) and MS 544(Part 5: 2001).

Dowels are mainly rod made of steel or glass fibre reinforced polyester (GFRP). Holes for dowel are usually tight fit or marginally undersized. During installation, dowels require light tapping with a wooden mallet to ensure it fits into the pre-drilled hole. Dowel has many end application which includes in construction of timber building. One prominent timber structure connected by dowel includes the building used during 1994 Winter Olympic in Norway (Larsen, 2003). Bolts and dowel has also been used together to take tensile and shear load.

Contrary to dowel holes, the holes for bolts were pre-drilled 1-2 mm oversized. Larger bolt hole diameter is required to accommodate shrinkage of the hole as the wood dries toequilibrium moisture content (Faherty, 1998). This will reduce the tendency of drying stress and splitting within the joint even though the gap might reduce the strength and stiffness of the joint (Larsen, 2003).

Among the factors which influence the strength of bolted joint is the L/D ratio. Studies indicate on the decline of proportional limit for bolt bearing stress as the L/D value increases (Rammer, 2010). The quality of the bolt hole should also be given consideration. Drilling using dull bits at ineffective feed rate and speed will produce rough holes. Smooth hole tend to produce higher bearing strength compared to bolted joints with rough holes. Other factors which affect the connection strength includes spacing of bolts, end distance, edge distance, number of bolts, quality of bolt and strength of timber (Rammer, 2010). Bolted joint are often used in conjunction with connectors in the joint surface for strength improvement (Larsen, 2003).

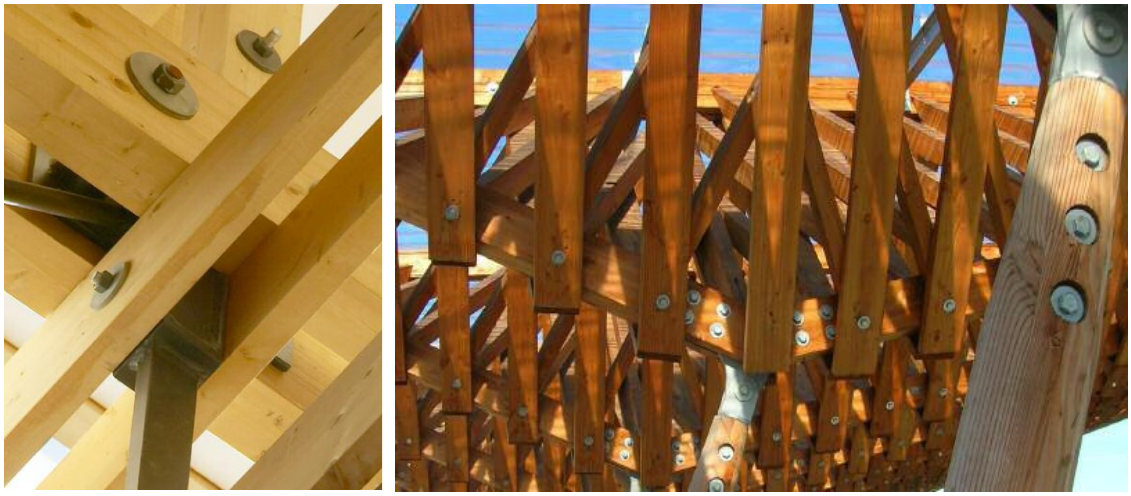

Fig. 3.1 Bolt connections as typically used in timber structures (TRADA Wood Information, 2007).

3.2.1.4 Connectors

Timber connectors such as split rings and shear plates as shown is Figure 3.2, are designed to increase the strength of the joint by providing larger timber area for

load transfer. Split ring and shear plates are used in timber to timber connection, embedded in the faces of timber to transfer load between the members.Shear plates are also used to transmit load from timber to a steel plates (eg. column to steel strap). Both connectors are used together with bolts to prevent separation of the members (Rammer, 2010).A split ring resembles a band of steel with a split in between. The purpose of the split is to allow timber movement due to shrinkage after installation. These connectors are commonly made of aluminium cast alloy, malleable iron or pressed steel and commercially available in various diameter size and gauges (regular and light) (Faherty, 1998).

Both split ring and shear plates require pre-cut groove and drilling using customised tools before installation, a step which may add up to the assembly cost of the connectors.The fabrication of the connectorismade at the factory. Only insertion of the bolt will be done at the site. This would required proper caution on the probability that the connectors disengaged during transportation. As detailed by Rammer (2010), among the factors which may affect the strength of connector joints are:

- size of the connector
- species of timber
- thickness and width of timber member
- end distance and spacing
- direction of load with regards to direction of the grain

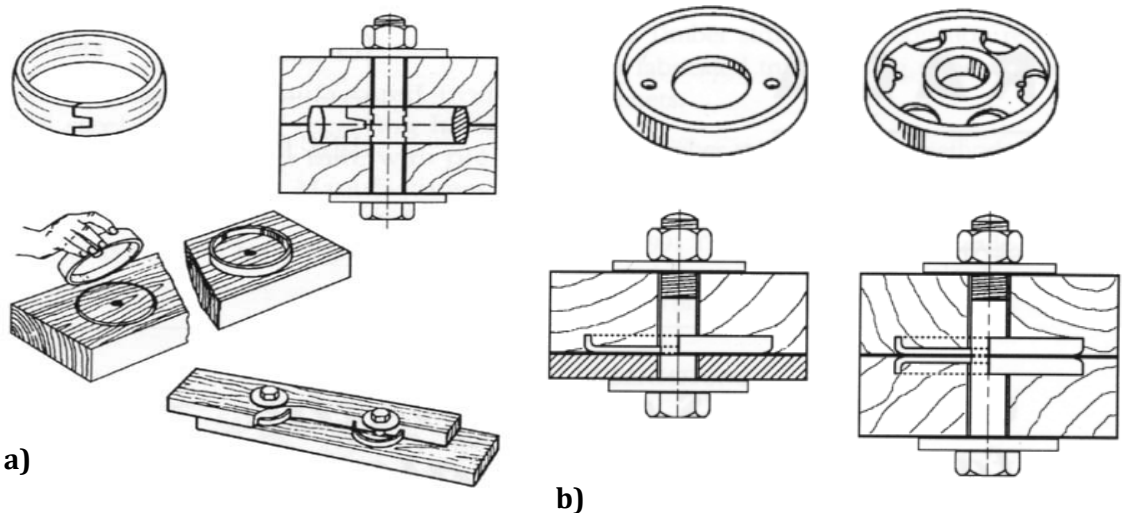

Fig. 3.2 Types of connectors: a) split ring and b) shear plates (TRADA Wood Information, 2003)

3.2.1.5 Other types of fastener

These fasteners can be grouped as two-dimensional plates and three-dimensional plates. Two-dimensional plates such as punched metal plates (Fig. 3.3a) are commonly used in jointing trusses, rafters and joists. It is common to find these fasteners connecting components of roof structure up to 30 – 40 m span.These connectors were designed to transmit load through teeth, plug or nails. Made of thin lightweight galvanized steel or zinc coated steel plates (1-2mm in thickness), punched metal plates are installed by using hydraulic pressing tools. Trusses are fabricated in the factory and assembled on site (Nielsen, 2003).

Three-dimensional plates include joist hangars, framing anchors, bracket and multi-angle connectors (Fig. 3.3b and 3.3c). These connectors were designed to provide strong shear connection and secure placement of timber members. Among application of these connectors are to fasten joist to headers and purlin to girder (Faherty, 1998).

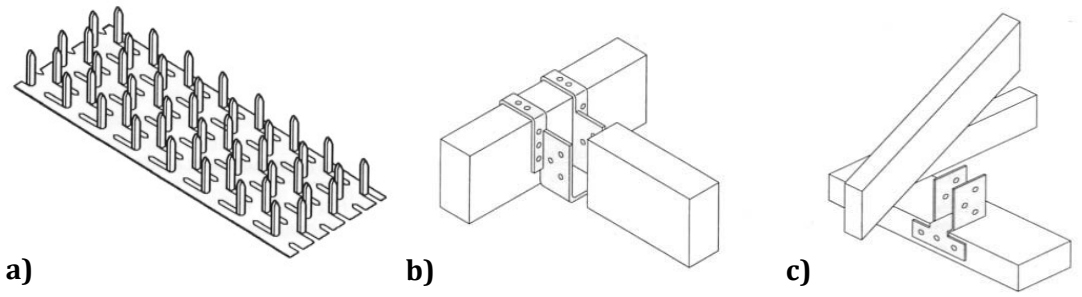

Fig.3.3 Types of connectors (a) punched metal plate (b) joist hanger (c) truss clip (TRADA Wood Information, 2003).

3.3 STRUCTURAL ADHESIVE JOINTS

3.3.1 INTRODUCTION

Adhesively bonded joints may provide numerous advantages compared to mechanically fastened timber joints. As cited by numerous studies, (Aicher, 2003 and Bainbridge & Mettem, 1998) structural adhesives performed better based on:

- Efficiency in distributing load evenly

- Superior rigidity
- Good strength to weight ratio than mechanical fastener such as bolts and split rings.
- May eliminate or minimise corrosion
- Aesthetic appearance due to concealed joints
- Excellent resistance to environmental degradation
- Protection of surrounding timber when exposed to fire but elevated temperature may degrade or deform the adhesive
- Higher load capacity over equal jointing area compared to mechanical fastener (shorter overlap length)

In general, adhesively bonded joints needs to be pre-fabricated at the factory, which may limit on-site manufacture. Other disadvantage of adhesively bonded joints as highlighted by several studies includes:

- Requirement of automated process during pre-fabrication (eg. fabrication of finger joints)
- May require highly skilled worker
- Special requirement to adhere according to the adhesive manufacturer's recommendations regarding glue mixing, spreading, storage time ("open" or "close"), temperature, curing period, surface properties of timber and bonding pressure.
- Strict quality control during manufacturing to maintain bonding quality

This section will discuss on the type of structural adhesive jointing which includes two main groups: pure wood to wood and hybrid joints. Figure 3.4 depicts typical wood to wood adhesively bonded joints used for structural and non-structural connection as cited by Frihart and Hunt (2010).

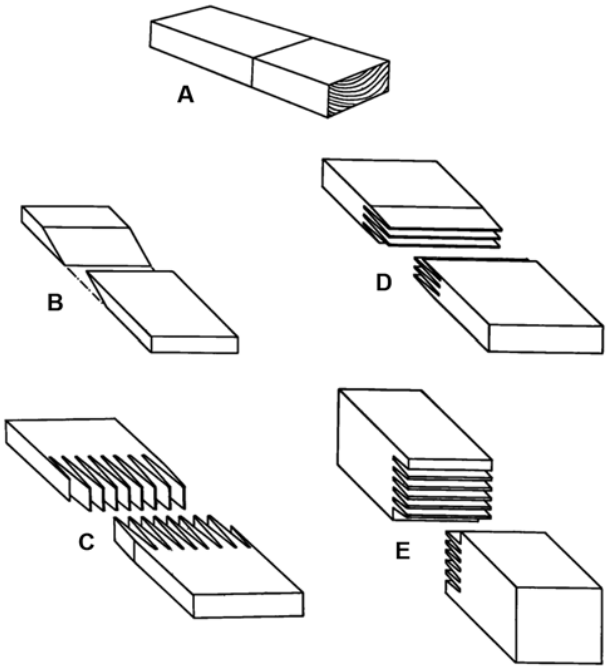

Fig. 3.4 End grain joints for structural and non-structural connections: A, butt joint; B, scraf joint; C, vertical structural fingerjoint; D, horizontal structural fingerjoint; E, non-structural fingerjoint (Frihart & Hunt, 2010).

3.3.2 TYPES OF STRUCTURAL ADHESIVE JOINTING

3.3.2.1 Pure wood to wood jointing

A) END JOINTS, KNEES AND REINFORCEMENTS

- SCARF JOINTS

Scarf joint is one of the most effective joint in delivering high strength. Similar to the butt joint, scarf joint was developed for end to end jointing in creating timber of continuous length. The high strength is mainly attributed to the increase of bonded surface area, reduction in stress concentrations and penetration of adhesive into the substrate. This is achieved by machining the wood at an angle, hence producing member with tapered ends. The tapered ends will then glued together to attain fibre to fibre surface area. The scarf joint angle α, can be expressed as l/t, where l is the overlap length and t as thickness of the member. The l/t ratio has an effect on the mean shear and normal stresses (also denoted as peel stresses), τ and σ. As cited by Aicher (2003), reduction of slope will also reduce the peel stress (normal) and shear stress, σ_n and τ, along the glueline of axially loaded scarf joint.

- FINGER JOINTS

Finger joint is the improved version of scarf joint. A scarf joint may have disadvantages due to requirement of longer overlap length. Finger joint on the other hand has the capacity in delivering high strength joint with less overlap lap length. This is achieved through multiple scarf joints which run in horizontal or vertical arrangement to the longitudinalorientation of the member. A good quality finger joint might attain 90% of the ultimate tensile strength of an un-jointed wood (Frihart and Hunt, 2010). In structural application, finger joints can be classified into two types. The first type of finger jointing is used for end jointing in glulam lamination. Larger finger joint is employed purposely to joint full cross-sectional area of glulam. It is commonly used to bond corner pieces of glulam. The geometry of finger joint is the main factor that contributes to tension or bending strength. Other contributing factors include the property of the adhesive, manufacture quality and curing condition (Aicher, 2003)

- GLUED CROSS-LAPPED JOINTS

Lap joint is classified as flat grain jointing, where two parts of grain surface is bonded to each other. The joint capacity is determined by the length of the bonded area, type of adhesive, angle between jointed components and material properties such as density of the wood (Glos & Horstmann, 1989). As depicted in Figure 3.5, glued cross-lapped joint is designed as a full-moment resisting joint and manufactured by gluing and cross-lapping multiple timber members. It is extensively used in the manufacturing of timber trusses and portal frame knee joints. Among advantages of this joint is the ability to provide high strength and rigid joint, neater appearance and fire resistance although it may require high level of quality control during manufacture (Batchelar & McIntosh, 1998).

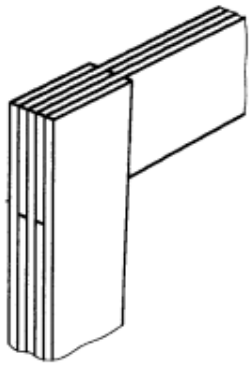

Fig. 3.5 Glued cross-lapped joints (Batchelar & McIntosh, 1998)

- KNEE AND TRUSS JOINTS WITH GUSSET JOINTS USING PLYWOOD OR LVL

As cited by Aicher (2003), plywood/LVL gusset joint was introduced in the 1950's and is now gaining acceptance due to several factors such as:

a. advancement in the concept in architectural design
b. efficiency in providing stiff joint for wide-span truss structure
c. good economic value
d. improvement in technology of gluing and cramping

Generally, the thickness of plywood/LVL gusset is one-fifth of the thickness of glulam/timber member. The thickness can be reduced by replacing it with high tensile steel reinforcement or glass/carbon fibre plates (Buchanan, 2007). Plywood/LVL gusset joints can be manufactured in four variations namely internal haunch, external haunch, mitred knee and apex joint as depicted in Figure 3.6. An extensive investigation on 1000 sample of gusset joint by Kalina (1965) has indicated that the global shear strength of the joint was significantly affected by size of the bonded area. Fibre angle of the joint has less influence on the shear strength of gusset joint.

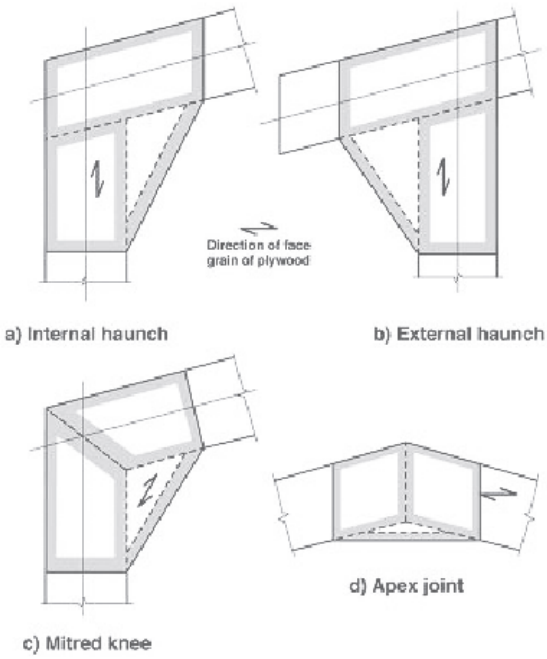

Fig. 3.6 Variation of gusset joints (Buchanan, 2007)

B) SPECIAL (FORMWORK) I-BEAM JOISTS

- LATTICE AND PANEL WEB JOINTS

I-beam joist has been used extensively in construction as truss support beams, floor joist and framing components. Wood composite I-beams primarily consist of flanges and web. The flanges are designed to carry high tension and compression stresses and are generally made of machine stress-rated (MSR) lumber and laminated veneer lumber (LVL). The middle section of I-beam, which is the web, is designed from high shear modulus and shear strength materials such as plywood, particleboard, waferboard, oriented strand board (OSB) and hard board (Leitchti et al, 1990).

Structural joints of flange to web connections are mainly of finger joints and scarf joints (Fig. 3.7). The joints act as bonding mechanism which transmits stresses from flanges to the web. In general, factory-prefabricated composite I-beam is assembled using rigid adhesive which contributed to the rigidity of the joint (River and Gillespie, 1981). Ensure a good bond in flange to web jointing eliminates shear slip at this joint.

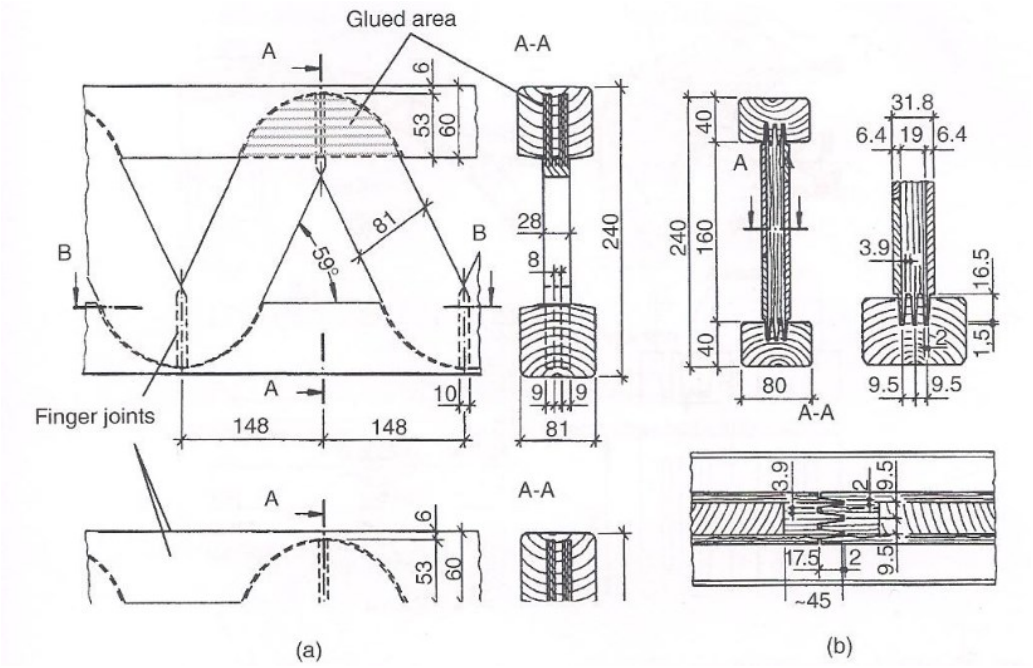

Fig. 3.7. Formwork of I-beam (a) glued lattice web beam (b) glued panel web beam (Aicher, 2003).

3.3.2.2 Hybrid joints

- JOINTS WITH GLUED-IN RODS

The term hybrid joints may be referred to joints which were made of combination of materials. This may include connectors made from combination of wood materials such as solid wood of structural composite lumbers (eg. LVL, SCL, PSL) and non-wood material. The non-wood materials are mainly of high strength and stiffness materials which includes steel or Fibre Reinforce Plastic (FRP). In general, the non-wood materials were served as connectors by gluing in to timber as depicted in Figure 3.8. The topic of glued-in connectors will be discussed extensively in Chapter 4.

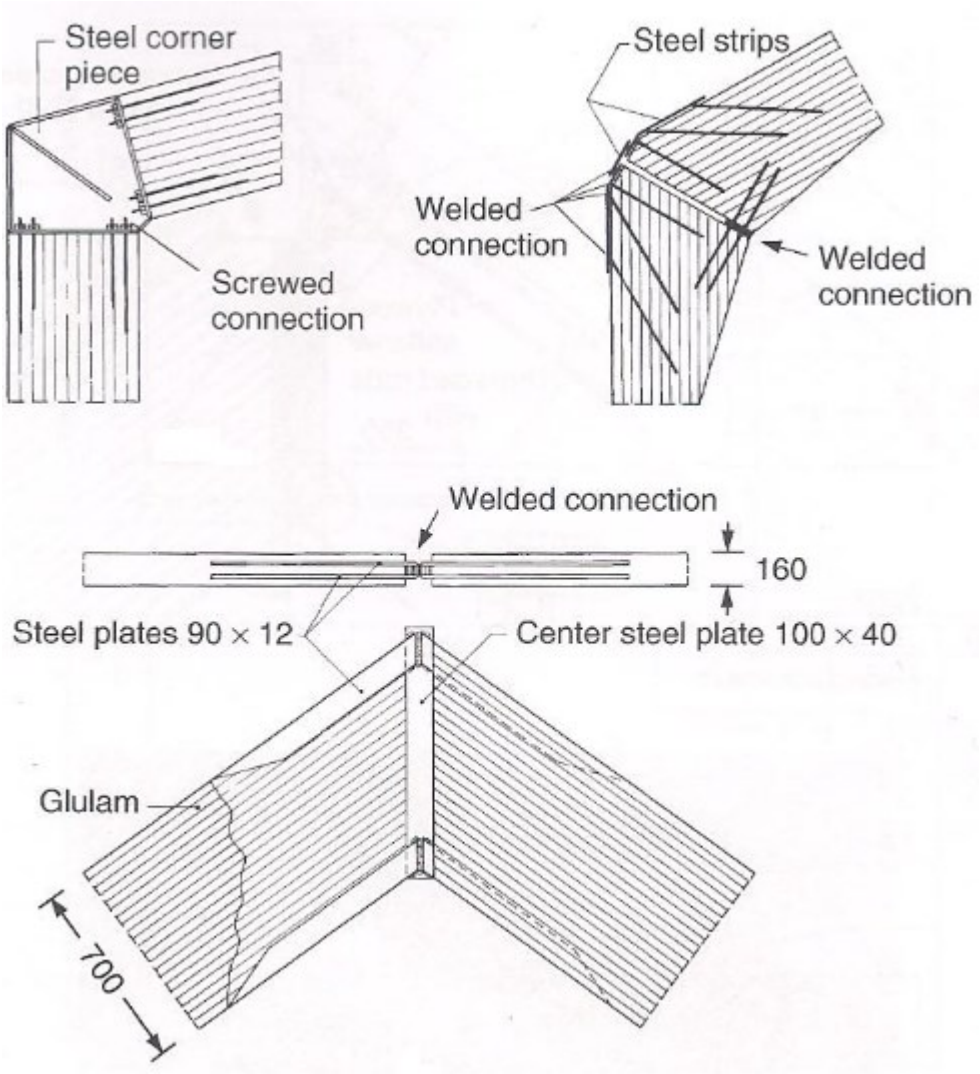

Fig. 3.8 Frame corners using bonded-in rod or steel plates (Aicher, 2003)

3.4 CONCLUDING REMARKS

Adhesively bonded joints are gaining acceptance since the have been used extensively in structural application. As compared to mechanical joints, adhesive bonded joints offer numerous advantages which may overcome many issues regarding stress transfer distribution and joint appearance. However, design consideration needs to be further emphasized, in particular issues concerning type of load, duration of load and service condition.

CHAPTER 4 : BONDED-IN CONNECTIONS

4.1 GLUED-IN JOINTS

4.1.1 INTRODUCTION

Adhesive bonded timber connectors such as rods, dowels and plates have been widely used for the purpose of upgrading and repairing of timber structures. Metal plates are used to increase stiffness and strength of structural member due to its effectiveness to transmit shear forces, axial loading and bending moments between timber members (Broughton & Hutchinson, 2001b). It is however, less popular due to its visible joints. Concealed bonded-in connection with threaded or deformed rod is considered more popular and efficient due to its interlock mechanism (Figure 4.1 and 4.2).

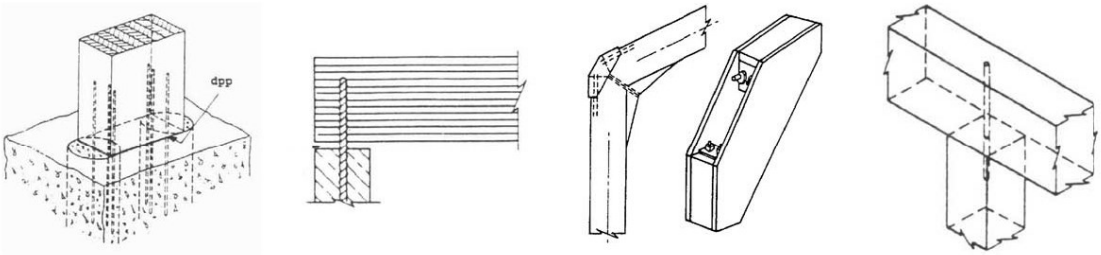

Fig. 4.1. Connection methods employing bonded-in rods (Bainbridge et al. 2002)

Strong and stiff joints of bond-in rods with excellent performance in load transfer has been used for glued-laminated timber (Serrano 2001). Steel rods, glass fibre-reinforced plastic (GFRP) and the potential use of carbon fibre-reinforced plastic (CFRP) reinforcing bars has been used to confer superior properties as reinforcement materials (Harvey & Ansell, 2000). Moreover, bonded in-rod is also less in weight, less grain-end splitting tendency and also has greater fire resistance ability (Broughton & Hutchinson, 2001a). The most important component within a connection system would be types of adhesive used. The adhesive provide bond between the wood material and rod. It is crucial for the adhesive to be able to fill voids and cavities in order to effectively transfer and sustain loads.

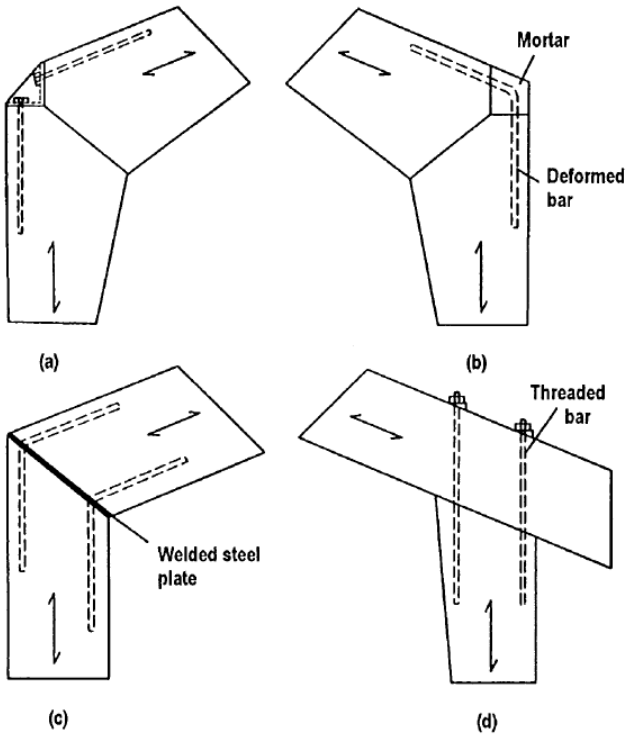

Fig. 4.2. Various bonded-in connection details (Broughton & Hutchinson, 2001a)

4.1.2 TYPES OF RODS

The function of rod within a bonded joint is to transfer forces between structural elements. It is one of the most important components of the joint other than substrate and adhesive.

Common types of bonded-in rods includes wood (eg. dowel), steel and Fibre reinforce polyester (FRPs) with carbon, Kevlar or glass fibres. Each types of rod made from any particular material may has its advantages over the other materials. The use of Glass Fibre Reinforced Polyester (GFRP) rod as jointing material is gaining acceptance due to its high strength to weight ratio. This produces lightweight connection and easier handling (Harvey & Ansell, 2000). GFRP rod is also suitable for high humidity application due to its resistance to corrosion. GFRP rod material is similar to timber and adhesives in terms of mechanical properties and thermal expansion coefficient. Under exposure to high temperature, the differences in thermal expansion coefficient between the rod and substrate may lead to internal stress within the glueline as reported by Aicher *et al.* (1998). Special

application such as in Magnetic Resonance Imaging rooms may require bonded material which is non-magnetic such as GFRP (Harvey & Ansell, 2000).

4.1.3 TYPES OF ADHESIVES

Alternative structural timber adhesives are the types of adhesive that are not included in test methods, codes and standard for structural timber adhesives in the UK (Davis 1997). Epoxy resins, polyurethanes, acrylic resin and emulsion polymer isocynates were included under this category.

Basically, adhesives for wood strengthening are required to exhibit several properties as indicated by Broughton and Hutchinson (2003). Adequate adhesion to wood with good resistance to shear is one of the most important. The adhesive should also be resistant towards variation of moisture content of the wood (less than 18%) and sustain loading. Tensile test on the adhesive should exhibit modulus of elasticity more than 1GPa and shear and tensile strength of more than 12MPa at 20^{o}C. In terms of glass transition temperature, the Tg value of the adhesive should be higher than 50^{o}C. The adhesive is also required to be gap-filling, able to suit application temperature and thixotropic. Of all alternative adhesive mentioned above, only epoxy resin meets the standards (Table 4.1).

Table 4.1. Types of structural adhesive used with timber

Generic resin types	Nature and behaviour	Practicality for repairs
Phenolics and aminoplastics	• Limited to bondline thickness approx. 1.5mm • Some types require heat during cure • Higher shrinkage than specially adapted gap-filling epoxies	Not practical for in-situ repairs. Best suited to workshop and factory fabrication because of bond line
Polyesters	• General require application of pressure during cure • Some have less resistance to creep deformation than specialised epoxies • Lower tolerance of damp conditions than specialised epoxies	

Polyurethanes	• High strength and stiffness • Primarily contact adhesives rather than large gap fillers • Unestablished resistance to deformation over time • Lower tolerance of damp conditions during cure than specialised epoxies	preparation and curing conditions required
Epoxy resins	• High strength, stiffness compatible with timber • Tolerance of surface conditions and environment • Low shrinkage, non-cracking system evolved for structures	Most frequent choice for in-situ repairs

Source: LICONS: Low intrusion conservation system for timber structure (Broughton and Hutchinson, 2003)

Epoxy modified with nanosilica has been used extensively in timber upgrading and in-situ restoration due to its thixotrophic properties, gap filling abilities and room temperature cure (Davis, 1997 and Ansell & Smedley, 2007). For the purpose of structural repair, epoxies may be categorise base on the physical form that it is used. The first form is grouts, a type of easy flow resin system and the application of it may require it to be poured, injected or pumped with the placement of shuttering to contain the material in the repair (Figure 4.3).

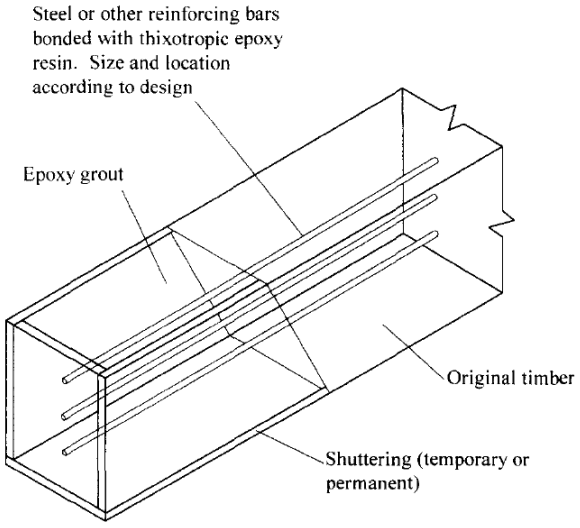

Fig. 4.3. Sample of epoxy grout in a bonded-in rod jointing system (Davis, 1997)

The second form is adhesives which is applicable for bonding of reinforcement. Mortars are small patch repairs to fissures, notches and cavities (Broughton & Hutchinson, 2001a). Reinforcing materials such as steel rods, metal plates and reinforced-fibres plastics are widely used in structural repair. The role of adhesive together with reinforcement materials is to bond between two materials that is different in terms of strengths and characteristics. The adhesive is responsible to transfer load between timber members, particularly in tension and shear. Bond strength of epoxy resin is however, affected severely by creep strain. The tendency of epoxy-bonded wood to creep is mainly due to its limited ability to deal with moisture changes (Frihart, 2005).

4.2 FACTORS AFFECTING DURABILITY OF BONDED-IN CONNECTIONS

The durability of epoxy in withstanding warm/moist service condition has long been a topic of concern. This is particularly important in predicting long-term performance of bonded connections. The effect of ageing and environment on epoxies adhesive joints investigated by Ning Su *et al*. (1991) indicates on damage on load bearing capability of adhesive joints due to exposure to high humidity. Broughton and Hutchinson (2001b) investigated the effect of timber moisture content on bonded-in rods which indicated on the reduction of pull-out strength with increasing of moisture content. Moisture ingress into a polymer matrix can lead to irreversible damage as indicated by Apicella *et al.* (1979) but short term absorption of moisture is reversible. It is assumed that moisture has the tendency to form microcavities in epoxy resin in which part of the water molecules will subsequently disperse into polymer and resides into the microcavities. As have been observed by Comyn (1989), microcracks and microcrazes as a result of growth from microcavities occurred due to degradation of the resin matrix or existence of residual by-products from the synthesis of resin. Ivanova *et al.* (2000) has suggested on the influence of moisture to polymer plasticisation causing weakening of intermolecular interaction of functional group within the chain. An examination on bondline failure by Frihart (2005) has suggested a slight different approach on the cause and effect of moisture on epoxy resin. The research has shown that the main cause for bond failure was due to differences in the expansion coefficient between the cured epoxy and the wood during wetting of the sample. His observation has indicated that epoxy absorbs less water and does not swell as the same degree as wood. Stresses due to

the swelling have resulted on strain on the rigid bondline thus causing fracture at the epoxy-wood interface layer.

Apart from moisture, epoxy's mechanical strength is also extremely sensitive to temperature. Room temperature cure epoxies exhibit temperature-dependant properties since it is not fully cross-linked. Ashcroft *et al*. (2001) has investigated on the effect of environment on bonded joints which indicates on the tendency of epoxy resin to change from brittle to ductile as temperature increase. The sample tested under various temperature conditions also exhibits reduction in Young's modulus, yield stress and ultimate tensile stress (UTS) with an increase in strain to failure. Cruz *et al.* (2004, 2005) and Cruz and Custódio (2006) assessed the influence of temperature variation ranging from 23°C at 50% RH to 80°C at 25%RH on bonded-in joints. The study discovered that timber covering had small influence in damping and delaying temperature peaks on the glueline. This finding is supported by an earlier study by Aicher *et al*. (1998, 2002) which discovered on reduction in duration of load due to low temperature damping within bonded-in glulam joints.

Under sustained loadings and harsh environmental condition, viscoelastic deformation may occur on epoxy bonded joints. Lack of information in the mechanism of viscoelastic behaviour has brought great importance in assessing the long term performance of epoxy-based structural adhesives. The service life of adhesive bonded structure may up to tens of years, which made it essential to establish fundamental knowledge on its time-dependant behaviour. It might be impractical and expensive to perform conventional creep testing over the total service life. Therefore, this type of study requires accelerated testing scheme that will able to predict long-term properties of stiffness and strength based on typical short-term tests. McMurray and Amagi (1999), Miyano *et al.* (2000), Huiwen and Sun (2000) and Feng *et al.* (2005) investigated the time dependence of flexural strength through creep and fatigue testing. All tests were exposed to various temperatures and environmental condition to imitate thermal and/or moisture aging during service.

The occurrences of mechanical weakness due to the influence of environment condition have led to numerous efforts in improving the resin properties. Fillers are often incorporated into uncured epoxy resin which has the capacity to improve mechanical

properties, reduce production cost and moisture sensitivity (Ivanova *et al.* 2000). Initial investigation by Brown (1982) has suggested on increase in modulus and toughness depending on the type and amount of filler. Kim *et al.* (1996) has indicated on the enhancement of fracture toughness for less crosslinked epoxy resin as particle size of filler decreases. The effect of time and temperature on flexural creep and fatigue strength of silica particle filled epoxy resin was investigated by Nishimura *et al.* (1989) with similar study by McMurray and Amagi (1999). Both of these studies have indicated on an increase in creep damage dependency with temperature elevation. At low temperatures, the initiation of fracture began in the silica particles while at high temperatures and the major cause of failure originated from the particle-resin interface. The effect of humidity and temperature on liquid rubber (carboxyl terminated butadiene acrylonitrile-CTBN) nano-filled epoxy resin was investigated by Ahmad *et al.* (2006) which concluded on significant increase in tensile and shear strength of bonded-in timber connection. Silicates and silica were also included in resin formulation as either hydrophobic or hydrophilic reinforcing filler particles.

Until the basic characteristics such as durability of epoxy bonded joints are fully understand, it is generally accepted that the utilisation of epoxy resin should be limited to certain working condition. The Eurocodes 5 (ENV 1995:1997) has been regarded as guideline to engineers in designing structures according to the structure's service life with respect to timber's interaction with its immediate environment. Referring to Bainbridge *et al.* (2002), the usage of epoxy bonded-in rods is limited to service classes 1 and 2 (Table 4.2). On realizing the limitation of knowledge on the durability and creep property of bonded-in joints, a specific research program called GIROD (Glued-In Rods) financed by the European Community for standardisation, was established. The main objective of the project was to provide information for the establishment of standards thus putting bond-in rod joints to a much advance and greater use.

Table 4.2. Eurocode 5 Service Classes (Bainbridge et al. 2002)

	Service Class 1	Service Class 2	Service Class 3
Definition	Moisture content corresponds to a temperature of 20°C. Relative humidity exceeding 65%.	Moisture content correspond to a temperature of 20°C Relative humidity exceeding 85%	Climatic conditions leading to higher moisture contents than in Service Class 2
Effect on timber	Average moisture content in most softwood will not exceed 12%	Average moisture content in most softwood will not exceed 12%	Average moisture content in most softwood will exceed 12%
Example of used	Timber in building with heating and protected from damp conditions. Examples are internal walls, internal floors (other than ground floors) and warm roofs	Timber in covered buildings. Examples are ground floor structures where no free moisture is present, cold roofs, the inner leaf of cavity walls and external single leaf walls with external cladding	Timber fully exposed to the weather. Examples are the exposed parts of open buildings and timber used in marine structures

4.3 BONDED-IN JOINT IN EXISTING STRUCTURE: THE MALAYSIAN GLULAM PROJECT

The Malaysian Timber Industrial Board (MTIB) exhibition hall is Malaysian first glue laminated timber structure which was constructed using bonded-in connections (Figure . The exhibition hall and administration centre which covers 4686m^2 of floor area is situated on a 1.96 hectare site in the capital state of Johor.

The building was designed of 3 arch-shaped halls which are mainly of Malaysian hardwood glulam. The architectural design of the building preserved the dominance of wood as building material. Two Malaysian indigenous wood species, Keruing (*Dipterocarpus spp*.) and Resak (*Vatica spp*.) was selected as glulam material for this project. The selection was made based on the natural durability and superior mechanical properties of the wood. The glulam material was manufactured in Johor and supplied by Woodsfield glulam.

Fig. 4.4. Malaysian Timber Industrial Board (MTIB) exhibition hall in Johor

Each glue laminated section 130mm x 600 mm has a total span of 3 to 7 meters. The section elements were bonded-in using steel rod to form arches. An epoxy based room temperature curing structural adhesive supplied by Rotafix Ltd. was used to bond the metal rod to timber. Bonding of galvanised steel rods to pre-drilled glulam was made at Woodsfield (Figure 4.5). A total of 39 glue laminated arches were required to erect the exhibition hall. Overall, the structure required 351 moment resisting adhesive bonded joints to link the arches. Some of the adhesive bonded connections in details are shown in Figure 4.6. Figure 4.7 features a close-up of the connections during arch construction. The arches were crane lifted and bolted to the elevated concrete runners (Figure 4.8). The glue laminated arches were then covered by water boil proof (WBP) plywood and thick rolled zinc sheet as protective function. Belian wood (*Eusideroxylon zwageri*) shingles of 0.35mm x 100mm x 450mm dimension were installed as arch covering to maintain the aesthetic look of the exhibition hall (Figure 4.9). Balau (*Shorea spp*.) and Keranji (*Dialium spp*.) tongue and groove panels were installed between the internal section of the rib walls and roof of the hall (Figure 4.10).

Fig. 4.5 Bonding of galvanised steel to glulam using Rotafix epoxy adhesive

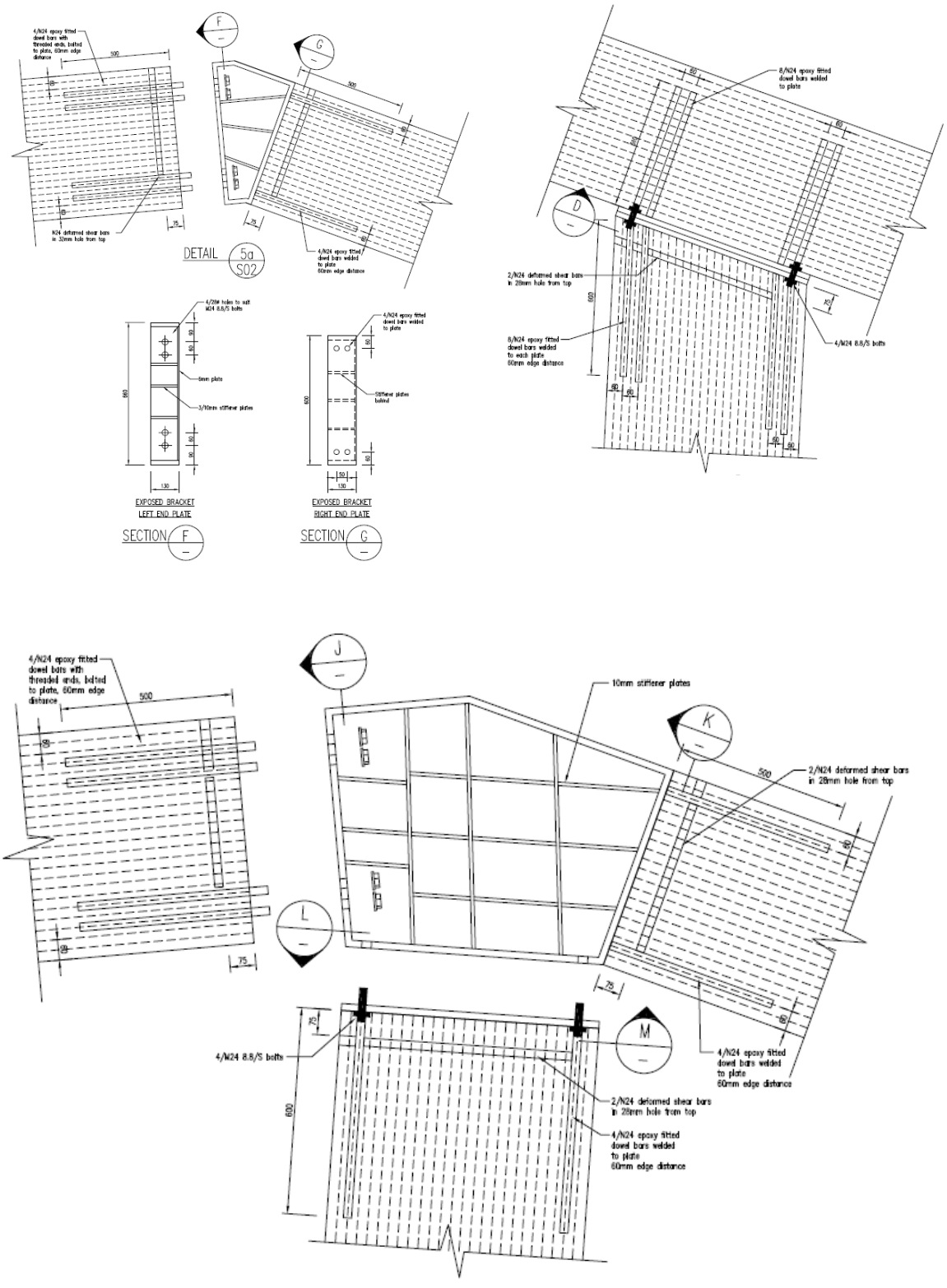

Fig. 4.6. Connection details

Fig. 4.7. Close up of bonded-in connection

Fig. 4.8. A crane lifting a section of the arch

Fig. 4.9 Berlian shingles

Fig. 4.10. Balau and Keranji panels

The justification in featuring this particular section is to highlight several interesting questions, which are related to the main purpose of this thesis. The issues to be address can be listed as:

a) Types of adhesive used in bonded-in joint.

The galvanised steel rods were bonded into pre-drilled glulam using a room temperature curing epoxy adhesive. According to LICONS guidelines the modulus of the epoxy should be more than 1GPa and shear and tensile strength of more than

12MPa at 20^{o}C. The T_g value of the epoxy should also be higher than 50^{o}C (Broughton & Hutchinson, 2003). As known, an epoxy which cures at ambient temperature is not a fully cured adhesive. This posed questions on the mechanical properties of an un-fully cross-linked adhesive and possibility of post-curing due to hot Malaysian weather. These questions provides the justification on the investigation of adhesive mechanical properties as presented in Chapter 8 and the thermal properties of epoxy resin in Chapter 9.

b) Types of wood material.

This project employs tropical hardwood species as glulam material. It is known that hardwood may have higher extractive content than softwood. Wood extractives may include complex mixture of chemicals such as tannins, anthocyanins, flavonesand and lignin. Keruing timber contains oleo-resin, which in some species is exuded on the end grain. The presence of extractive may interrupt bonding mechanism of adhesive, which makes hardwood more difficult to glue. This gives a solid background to assess the bond strength of Malaysian hardwood species. The study on the pull-out strength of Resak, Yellow resak and Keruing was thoroughly discussed and presented in Chapter 11.

c) Temperature and humidity.

Malaysia observes tropical weather with a temperature range of 22°C to 33°C (average 27°C). Annual precipitation Malaysia is 2500mm and relative humidity (RH) may range from 58% to 97%. As stated by the Eurocodes 5 (ENV 1995:1997) the usage of epoxy bond-in rod is only limited to service classes 1 and 2 (Table 2). All bonded-in connections are within enclosure of the building, which places this application under service class 2. It is important to consider the effect of service temperature on the durability of the adhesive. A close monitoring of temperature and displacement on the MTIB glulam structure was conducted by Smedley *et al.* (2012) and still on-going. On realizing the limitation on the information on the performance of joints under constant loading at high temperature and humidity, several studies were proposed. Chapter 9 presents the response of creep in bulk epoxy in relation to temperature increase. The effect of temperature and humidity on model of bonded joints is presented in Chapter 12.

4.4 CONCLUDING REMARKS

Bonded-in technology for connections in timber structures relies on the effective bonding of steel or reinforced plastic rods to timber using room temperature cure epoxy adhesives. Extensive research is the solution to the present lack of information on the effective and safe application of bonded-in technology. Key issues include deformation and durability under creep loads at elevated temperatures and high relative humidity. This thesis examines creep behaviour of modified epoxies and bonded-in connections under these conditions.

CHAPTER 5 : EPOXY RESIN ADHESIVES

5.1 INTRODUCTION

Epoxy resin adhesive is one of the most popular adhesives due to its versatility. The history of epoxy commercialisation started in 1927 when it was first introduced by Dr. Pierre Castan of Switzerland and Dr. S.O. Greenlee of United States. Today, epoxy resin has found its way in a wide range of applications from consumer-based markets in furniture to structural applications in construction as well as high performance end-uses such as the aerospace and automotive industry. The application of epoxy resin is not limited by the type of substrate due to its ability to bond to any type of material. Although epoxy is considered new for timber application, it has actually long been used for bonding of metal and plastic parts in motor vehicles and aircraft (e.g De Havilland Mosquito). Epoxy adhesives have a good reputation for bonding various types of substrates such as glass, concrete, wood, aluminium, alloy and fibre-reinforced plastics. Epoxy as a bonding material in structural joints performs better than metal connections (bolts and rivets) due to the weight to strength ratio of the joint and elimination of galvanic corrosion. During cure, epoxy releases very minimal volatile compounds and forms a hard structure with almost negligible shrinkage thus minimizing internal stress. Application of epoxy as a wood adhesive has been effective due to its gap filling and room temperature curing capabilities and low clamping pressure (Frihart 2005). As compared to other timber adhesive, epoxy resin has an advantage due to its wide range of service temperature (-30^{o}C to 60^{o}C). Epoxies are also available in many formulations, depending on the requirements of the application. Epoxies can be formulated to cure rapidly at room temperature (minimum time ~45s) or at high temperatures. Strength properties, the duration of pot life and resistance to working environmentsmay be customised according to the specific end-use. Customisation of epoxy resin depends largely on the chemistry used for the formulation of the epoxy resin base and the type of hardener used in curing.

The fundamental chemical compound within the epoxy is the oxirane ring (as depicted in Figure 5.1) which can be characterized by two carbon atoms singly bonded to an oxygen atom. The three-membered ring is the signature of the epoxy group.

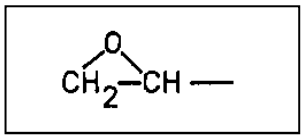

Fig. 5.1 Chemical structure of epoxy (oxirane ring) (Goulding, 1994)

Epoxy resins can be formulated in many different ways, but the most common is the diglycidylether of bisphenol A or known as DGEBA which is formulated from the reaction of epichlorohydrin and BisphenolA (Figure 5.2). The reaction of epichlorohydrin with hydroxyl group causes dehydrochlorination.

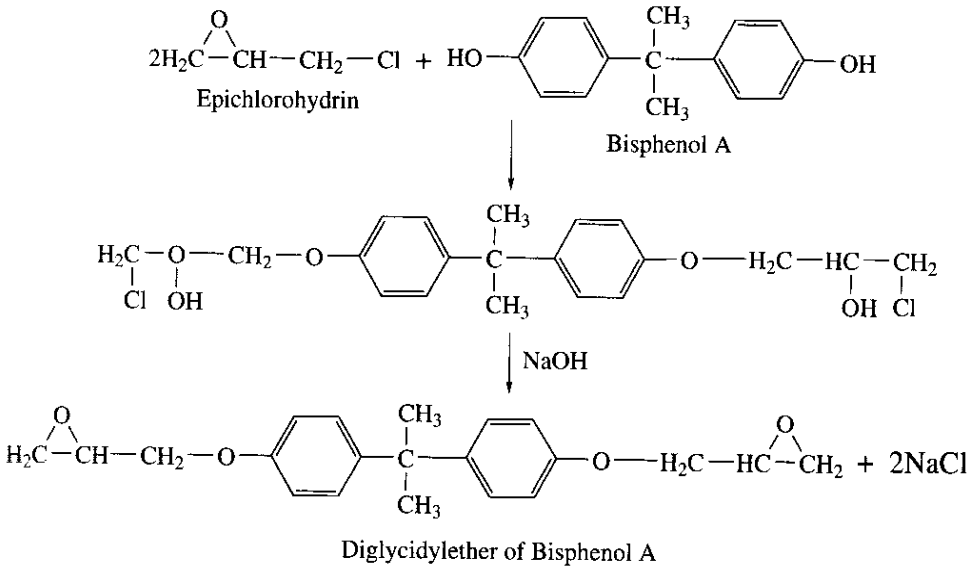

Fig. 5.2 Chemical structure of epichlorohydrin, bisphenol A and Diglycidylether of bisphenol A (Bishop, 2005a)

The result of the reaction is an epoxy resin with the molecular structure presented in Figure 5.3. Epoxy resin is mainly of rigid to ductile condition which determined by the degree of chain extension. As referred to Figure 5.3, the degree of polymerised subunits is denoted as *n*. Most commercially available epoxy resins for adhesive applications are

in liquid form with *n* between 0 and 1 (Goulding, 1994) or 0.15 to 0.25 (Bishop, 2005). Epoxy with higher values of *n* appears asbrittle solid. Other epoxyformulations which are commercially available are cycloaliphatic, glycidylamine, hybrid glycidylester/glycidylamine and glycidylester.

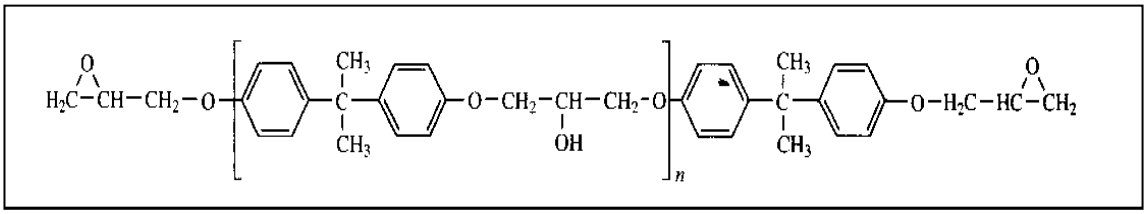

Fig. 5.3 General structure of Diglycidylether of Bisphenol A (Bishop, 2005a)

By reacting phenolic compoundswith the epichlorohydrin, epoxidizednovolacphenolic resins can be produced. Reaction of epichlorohydrin with aromatic amines and aromatic amino alcohols has also been investigated, resulting in resin materials such as tetraglycidyl methylene dianiline (TGMDA) and triglycidyl p-amino phenol (TGAP). These formulations are not as commonly used as DGEBA formulation since it requires additional care for storage. At room temperature, both TGMDA and TGAP have the tendency to react slowly hence they must be stored in a refrigerator.

Epoxy base resin can also be formulated to suit special application requirements. Cycloaliphatic epoxy is used specifically for electronic applications. Common DGEBA resin is not suitable for these applications since it is based on epichlorohydrin which contains chloride ions and hydrolyzable chloride. Under high humidity, these two components can cause corrosion of electronic components. Cycloaliphatic epoxy is formulated by oxidation of vinyl groups and double bonds in unsaturated rings (Figure 5.4). Since it is formed by peroxidation, this resin has very low chloride content which makes it suitable for electronic application (Pocius, 2002).

The cross-linking of epoxy resin results in an infusible polymer of considerable bonding strength. The cross-linking can only take place in the presence of a curing agent. The resulting adhesive may be limited by its brittleness and low-impact properties which can be modified by the inclusion of other compounds such as reactive diluents, fillers and toughening materials.

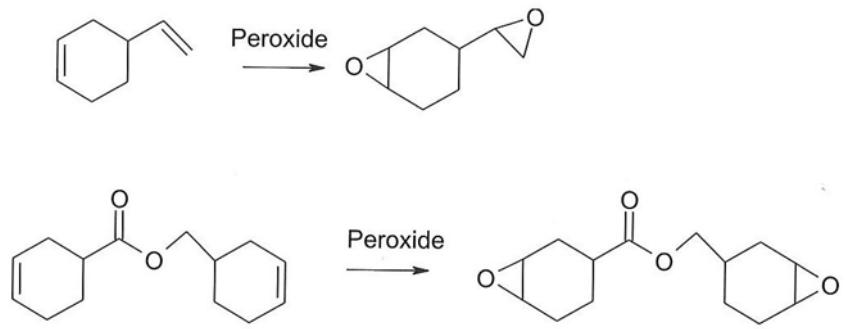

Fig. 5.4 Synthesis of two cycloaliphatic epoxy resin (Pocius, 2002)

5.2.1 CURING AGENTS, REACTIVE DILUENTS, FILLERS, ADDITIVES AND THEIR EFFECT ON THE PROPERTIES OF EPOXIES

5.2.1.1 Hardeners

The type of hardener used in the system strongly determines the properties of the epoxy resin. Hardeners of epoxy include amines, thiols (eg. Polythiols),mercaptants, alcohols, anhydrides, Lewis acids, organic acids or Lewis bases. Lewis acids act as curing agents for epoxy by acting as a catalyst for the cationic polymerisation of oxirane-based resins. Epoxy can also be reacted with alcohol from phenol or the reaction of oxiranes with alcohol. This reaction which commonly takes place at temperatures higher than 120°C generates ether alcohols. Accelerated curing of epoxy at room temperature can be achieved by reaction with mercaptans in the presence of tertiary amine catalyst (trisdimethyl amino phenol). Hardeners such as polythiols have also been formulated to cure epoxies rapidly and can be applied as fast-curing adhesives for steel. (Pocius, 2002).

As mentioned in the previous section, cycloaliphatic epoxy is an epoxy base resin formulated specially for the electronic industry due to its anti-corrosion requirements. This base formulation requires special hardeners such as anhydride. The reaction occurs at elevated temperature. During reaction, anhydride will react with alcohol to form ester and carboxylic acid. Crosslinking occurs when the carboxylic acid reacts with the oxirane group. Figure 5.5 summarise the chemistry of curing reactions for epoxy resins as described by Pocius (2002).

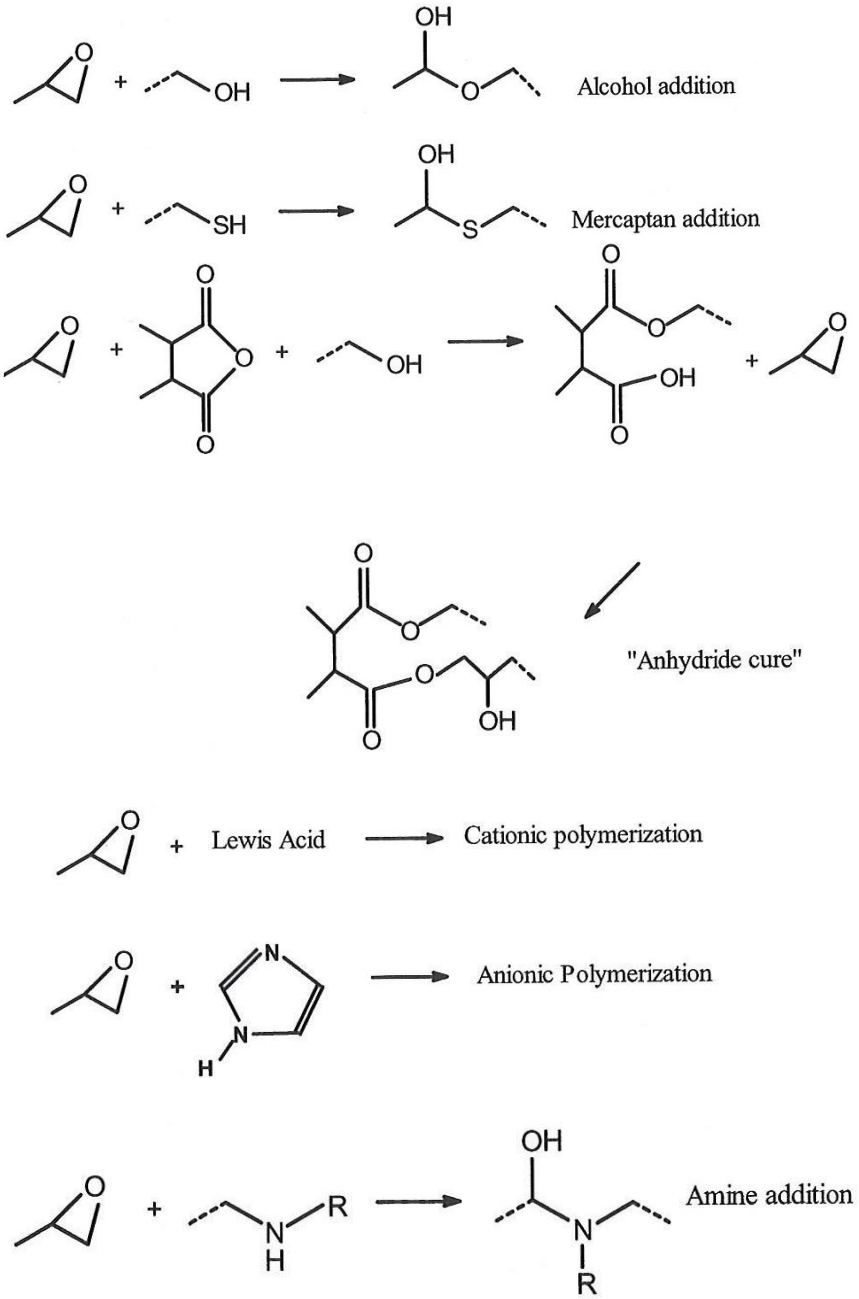

Fig. 5.5 Various curing reactions for epoxy resins (Pocius, 2002)

Latent hardeners such as dicyandiamide (*amides*) (Figure 5.6) arethe most widely used type of hardener which have low reactivity under 150°C and a long pot lives (a year to 18 months). At elevated temperatures (150°C to 180°C), however, dicyandiamide reacts quickly (Bishop, 2005). Mixing of the resin and dicyandiamide is easy due to its low volatility and irritancy and non-critical mix ratio. It has a fairly high heat distortion

temperature (tendency to soften at elevated temperatures) but this will be reduced as the content of the hardener increased.

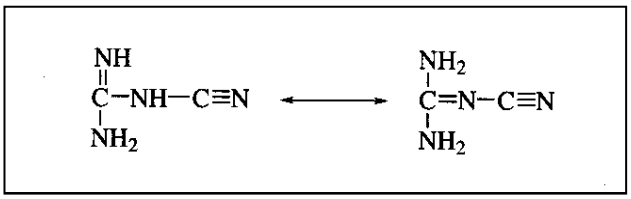

Figure 5.6 Dicyandiamide (Bishop, 2005b)

Other types of hardener may include aliphatic and aromatic amine based hardeners. Aromatic primary amines as indicated in Figure 5.7 (eg. Diethylenetriamine, tetraethylenepentamine, isophoronediaminea), , have better room-temperature curing properties thandicyandiamide but are unfavourable due to the complexity of mix ratios and strongly irritant properties (Goulding, 1994). Aromatic amines on the contrary cure at an elevated temperatures. The type of hardener may strongly influence cure rate and cure temperature.

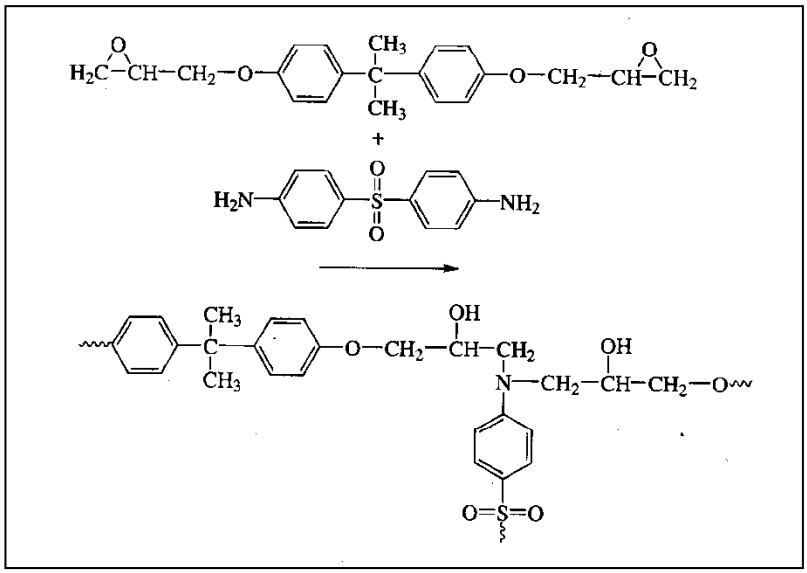

Fig. 5.7 Curing of aromatic primary amine (hardener) and epoxy resin (Bishop, 2005b)

5.2.1.2 Reactive diluents, fillers and additives

Apart from hardeners, other compounds which catalyze the curing process include reactive diluents (eg. Triphenyl phosphate, lactams and furfuryl alcohol), although they are known to degrade the performance of the adhesive.

Fillers and additives are typically added to epoxy resins to modify specific properties and they range from relatively low cost silica to the much higher priced micro-balloons. Fillers and additives control thixotropy, abrasion resistance, production price, gap-filling properties and shrinkage reduction (Harani*et al*., 1998 and Wetzel *et al*., 2003). Fibrous fillers such as glass improve tensile strength and impact resistance. Chemical agents such as fumed silica are used in minimal amounts (usually 0.1 to 3%) to modify viscosity and thixotropy and improve gap filling properties (Kinloch et al., 2005). Thixotropic properties are vital for structural adhesive or adhesive used in structural restoration where they are applied on vertical surfaces or overhead (Roseley et al., 2010). In depth discussion on the modification of epoxy resin will be discussed in section 6.5.

5.3 TIME-TEMPERATURE-TRANSFORMATION CURE DIAGRAM OF EPOXY RESIN

To further understands the mechanism of epoxy curing and the physical properties of the epoxies, a diagram which describes isothermal cure temperatures corresponding to time was proposed. This concept was introduced by J.K Gillham (1982) to describe cure and properties of thermosetting polymers and later was adopted by A.V Pocius (2002) and a typical diagram is shown in Figure 5.8.

The time-temperature-transformation (T-T-T) diagram simplifies the transitions between curing phases of epoxy in relation to changes in temperature. These phases include phase separation (as for rubber modified system), gelation, vitrification and full cure. An earlier version of the T-T-T diagram by Gillham (1982) also mentioned additional phases such as devitrification and char of the thermosetting polymer. The gelation phase corresponds to the retardation of microscopic flow of the liquid due to formation of molecular network. Vitrification signifies the retardation of chemical reactions which brings the transformation to the glassy state (formation of solid gel).

The horizontal divisions of the diagram indicate physical properties of the thermoset corresponding to curing temperature. The lowest division (ungelled glass region) corresponds to the initiation of the curing process. As the curing temperature increases,

transition of divisions from liquid region to gelled glass region and subsequently the fully cured region is indicated. The diagram also indicates three Tg's to characterise the state of curing of the thermoset. The $T_{g,resin}$ corresponds to the glass transition temperature of the uncured resin whilst $T_{g,gel}$ represents the glass transition temperature of the gel of the resin. The ultimate glass transition temperature which is obtained when the polymer has fully cured is represented by $T_{g\infty}$.

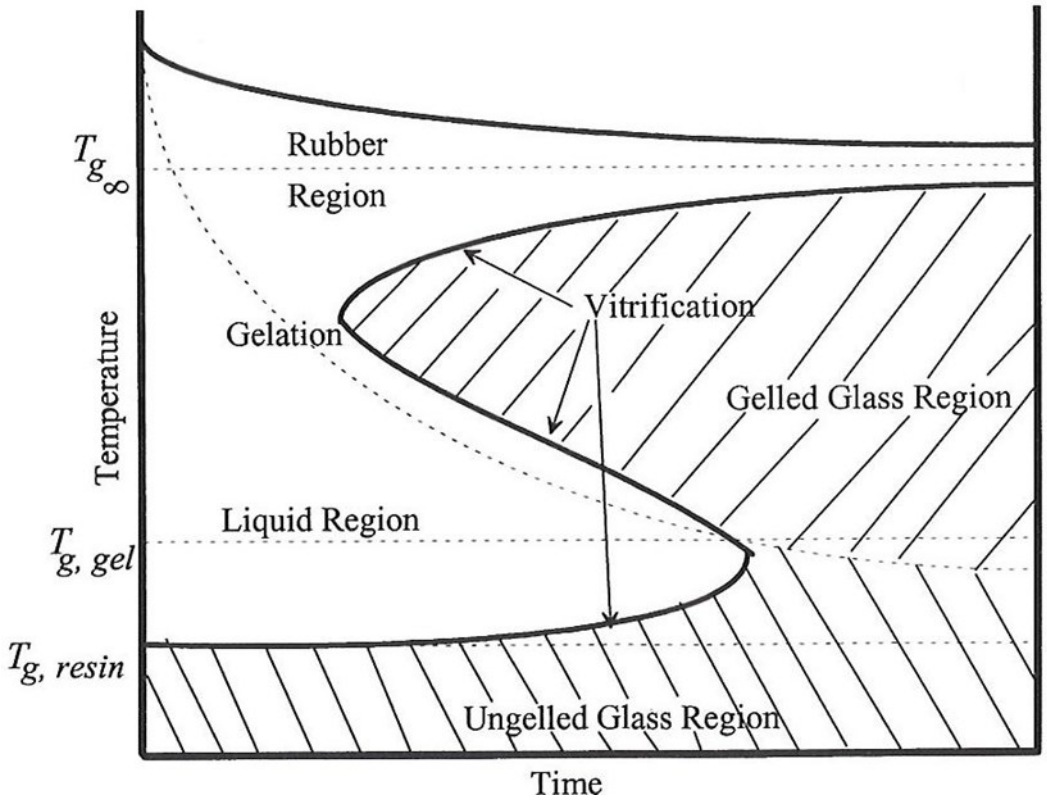

Fig. 5.8 Time-Temperature-Transformation (T-T-T) diagram for thermosetting resins (Pocius, 2002)

These diagrams explains the curing of room temperature epoxy system.The first phase between $T_{g,resin}$ and $T_{g,gel}$ indicates that the thermoset vitrifies before gelation. At the point just below $T_{g,gel}$the gelation line intersect with vitrification which indicates both vitrification and gelation occurs at the same time. The subsequent region between $T_{g,gel}$ and $T_{g\infty}$indicates that corresponding to the curing temperature, the thermoset is likely to gel and then vitrify. For an ambient temperature curing system, provided that the curing temperature is below than $T_{g\infty}$,it is likely that the chemical reaction of the epoxy has not been completed.As indicated in numerous publications, a room temperature curing

epoxy system (eg. two-part epoxy) is not a fully cured system become chemical reactions are incomplete. Pocius (2002) also indicates that there is a discrepancy in the methods of measuring T_g of ambient temperature curing epoxy since current methods (DMTA and DSC) require the polymer to temperature temperature above Tg. At that stage, post-curing might have taken place and it is likely that the measured $T_g$reflects the T_g of post-cured resin.

5.4 MODIFICATION OF EPOXY ADHESIVE AND POLYMER MECHANICAL TESTING

Epoxy resins are well established commercial adhesive systems due to their good adhesion properties which correspond to high wetting ability and low cure shrinkage. They exhibit high resistance to creep, heat and chemicals due to their cross-linked nature (Arias *et al*., 2003). Epoxy adhesive have been extensively used as structural adhesive and for composite matrices due to its superior mechanical strength. The applications of epoxy resin is only limited by their brittleness which is exhibited by low resistance to impact and crack initiation. The toughness characteristic of epoxy resin can be significantly improved by modification or addition of a rigid phase or resinous modifiers. To characterise the improvement due to the modification of the epoxy, various mechanical tests were introduced.

Standards for adhesives play a vital role in current technology since the global market for adhesives demands high levels of quality assurance. Various organizations are involved in governing standards and some of the most quoted are British Standards Institution (BSI), the Comité Européen de Normalisation (CEN), the American Society for Testing and Materials (ASTM) and the International Organization for Standardization (ISO). Tests for adhesives can be categorised into three main types namely viscosity, solid content and density as indicated by Millington (2005).. Millington (2005) has also identified tests to determine the curing or setting behaviour and the bonding strength of the adhesive.

The need to evaluate the strength properties of adhesives has led to various methods for mechanical testing in tension, compression and shear. Normal or direct stresses act at

right angles to the plane of the tested material as opposed to the shear stresses which act parallel to the plane of the material. The three-point flexural test (BS EN ISO 178) and inter-laminar shear (ILS) test (EN 658-5:2002 (E)) have been widely used to assess the mechanical properties of adhesives. Both of these tests employed the simple application of a 3-point bending load. The shear test also uses the same test geometry but differs in terms of the sample size which is smaller (with a length to thickness aspect ratio of 5:1) than for the flexural test. For three-point bending a minimum span to thickness ratio of 16 is normal but for the ILS test, this ratio is equal to 5 in order to maximise the shear stress at the central region of the tested sample. Fracture toughness testing is a method used for measuring the resistance of a material to fracture. This method is suitable for a brittle material such as an epoxy in order to quantify the ability of a material which contains cracks to resists the propagation of fracture. One of the methods for determining the fracture toughness of a material is to apply a three-point bending test on a sample with a central crack samples. In a single-edge notch bend test (SENB), a central hairline crack is induced and the fracture toughness is quantified by the critical stress intensity factor (K_{IC}) and strain energy release rate (G_{IC}). During the propagation of a crack, new surfaces are created. Energy dissipated during the formation of new surfaces is quantified by the strain energy release rate (G_{IC}). Properties such as flexural and shear strength and modulus fracture toughness vary according to the modification of the epoxy.

Rigid materials such as silica, kaolin, glass beads and $CaCO_3$ (chalk) are fillers used by the plastics industry to reduce cost (Harani*et al*., 1998). Modification with rigid particles increases mechanical properties such as tensile, flexural and impact strength and fracture toughness. A study by Wetzel *et al*. (2003) on the mechanical performance of epoxy modified with macro and nano-scale calcium silicate ($CaSiO_3$) particles has indicated an improvement in elastic modulus achieved with an optimum ratio of both particle sizes. Structure, shape and size of particles had a strong influence on the mechanical properties (tensile, fracture toughness and strength) as indicated in various studies (Yamamoto *et al*., 2003 and Nakamura *et al*., 1992). A similar study on particles of different sizes was reported by Kwon *et al*. (2008a) on spherical silica particles. The study concluded that the composition ratio has a significant effect on the yield strength, σ_y, and fracture toughness, K_{IC}, and less significant effect on Young's modulus, E. A subsequent study by Kwon *et al*. (2008b) concluded that fracture toughness of nano and

micro particles epoxy composites was dependant on temperature. A detailed study of toughening mechanism using the single-edge notch bend (SENB) test was proposed by Johnsen *et al*. (2007) on nanoparticle-modified epoxy polymers. The nano particles were introduced via a sol-gel technique to give a well dispersed phase. An increase of fracture energy from 100 J/m^2 for neat epoxy to 460 J/m^2 for epoxy modified with 13% vol nano silica was measured. This contradicts the findings of Imanaka *et al*. (2001) using double cantilever beam (DCB) beam specimens. The study concludes that fracture toughness of DCB specimens increases with the size of the micro-silica particles.

A more recent approach to improving toughness of resin is the addition of resinous modifiers such as rubber particles as a second phase. Studies have been made by Pearson and Yee (1991) and later on by Arias *et al*. (2003) and Russel and Chartoff (2005) using liquid carboxyl-terminated acrylonitrile-butadiene rubber (CTBN) to toughen epoxy resin. Nigam *et al*. (2003) used carboxy terminated polybutadiene (CTPB), Chiki*et al*. (2002) used amine-terminated butadiene acrylonitrile (ATBN) and Ratna and Banthia (1999) used modified epoxy resin with carboxyl terminated poly(2-ethylhexyl acrylate) (CTPEHA). The mixture of epoxy oligomer (diglycidyl ether of bisphenol A) and liquid rubber together with a curing agent started as a single phase system. As the curing progresses, rubber precipitation occurs and spherical rubber domains or rubber particles develop. The rate of precipitation occurs at different stages depending on the molecular weight of the liquid rubber. Chen and Jan (1992) studied a bimodal rubber-particle size distribution by simultaneously adding two types of liquid rubber. The study concluded that liquid rubber which precipitates at latter stage of curing produces a larger particle size, hence creating a two-size rubber particle system. Bimodal/unimodal rubber particles precipitation is also determined by the type of curing agent as reported by Arias *et al*. (2003). The degree of phase separation between rubber particles and the resin matrix can be calculated from the volume fractions. Phase separation between rubber and matrix resin is regarded as incomplete if the calculated volume fraction is less the amount of added rubber. The residual rubber is thought to still remain in the resin phase and this will subsequently diminish the properties of elastic modulus and glass transition temperature (Kinloch and Young, 1983, Chen and Jan, 1992, Arias *et al*., 2002 and Russell and Chartoff, 2005). Significant improvement in fracture toughness is attainable without compromising other mechanical properties (flexural and tensile) at an optimum rubber concentration. Nigam *et al*. (2003) reported

on the tensile, flexural and impact strength of neat resin and rubber-epoxy blends (5 wt %, 10 wt %, 15 wt % and 25 wt %) and concluded that the highest strength is achieved at 10 wt % before diminishing at higher percentages. This result is consistent with other studies by Yee and Pearson (1986), Pearson and Yee, (1989) and Nigam et al. (1998). Ratna and Banthia (2000) have reported on the decrease of tensile strength due to an increase in flexibility caused by the presence of low modulus rubber particles.

The possibility of having hybrid systems which improve the toughness by using rigid phase fillers and resinous modifiers has been described in recent studies. A study by Kinloch *et al*. (2005) on the effect of silica nano particles and rubber particles (CTBN) on thermosetting epoxy has indicated an increase in fracture toughness. A very significant increase in the values of stress intensity factor, K_{IC}, and the value of fracture energy, G_{IC}, was observed through the introduction of a three-phase rubber-silica epoxy system. These results are in agreement with an earlier study by Kinloch *et al*. (1985a and 1985b). Matějka *et al*. (2000) investigated the temperature dependence of storage modulus and loss factor to evaluate the phase structure and interaction between epoxy and silica particles. The study observed a significant increase in modulus due to an increase in crosslinking between the silica phase and the polymer. An increase in Young's modulus, E, and yield stress, σ_y, was reported by Young *et al*. (1986) for multiphase thermosetting polymers of carboxyl-terminated random copolymer of butadiene and acrylonitrile (CTBN) by adding 18 wt% content of glass beads. A latter study by Zhang and Berglund (2004) showed that the inclusion of glass beads to the CTBN had only a little effect on the yield stress but made a significant contribution to fracture toughness. A related study by Maazouz *et al*. (1993) found a significant improvement in fracture energy and a synergistic effect due to the presence of both kinds of particles (rubber and glass beads).

The inclusion of modifying elements within the polymer and the interaction between the modifiers are best described using microscopy techniques.

The study of phase morphology and failure mechanisms has been extensively characterised using both optical and electron microscopes.

A study on the phase separation mechanism of rubber-modified epoxy was conducted by Yamanaka and Inoue (1990). Observation under light microscope indicates an onset of phase separation when the temperature was elevated, exhibiting development of a structure with curing (Figure 5.9).

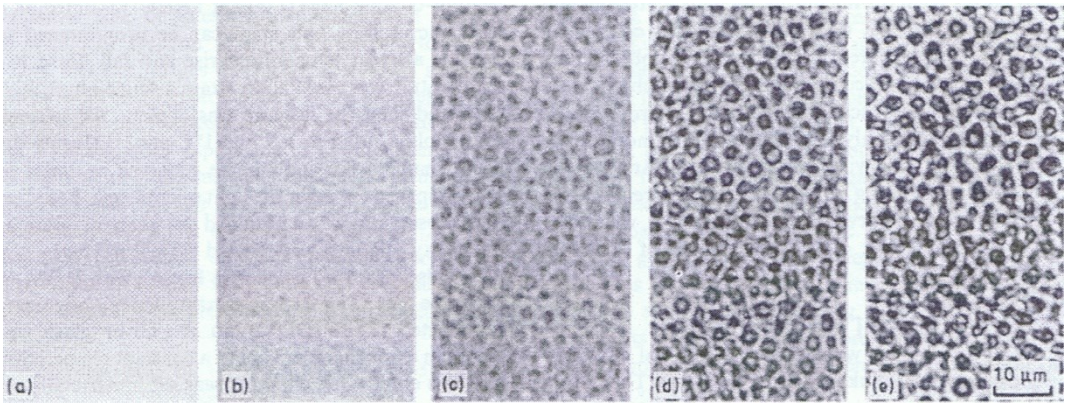

Fig. 5.9 Various stage of curing of a rubber-modified epoxy at 100°C observed under light microscope. (a) 1 min, (b) 8 min, (c) 17 min, (d) 32 min, (e) 360 min (Yamanaka and Inoue, 1990).

A phase morphology study using scanning electron microscope (SEM), transmission electron microscope (TEM) and atomic force microscope (AFM) imaged the formation of spherical domain structures or rubber particles (Chen and Jan, 1992, Nigam *et al*., 2003, Russel and Chartoff, 2005) (Figure 5.10). As reported by Manzione *et al*. (1980), the particles are precipitated rubber which begins to form at the cloud point and ends at the gel point.

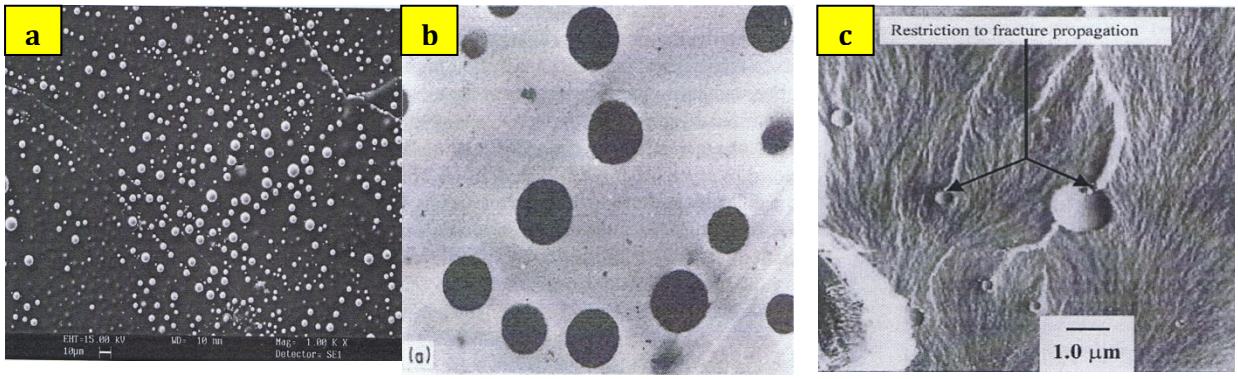

Fig. 5.10 (a) SEM (Russell and Chartoff, 2005), (b) TEM (Chen and Jan, 1992), and (c) AFM (Nigam et al., 2003) micrographs of rubber-modified epoxy exhibiting spherical domain.,

Using SEM, Imanaka*et al*. (2001) and Kwon *et al*. (2008b) (Figure 5.11a) concluded that silica nano and micro particles were spherical in shape. Various studies using TEM (Figure 5.11b) and AFM were conducted on epoxy modified polymer of either micro or nano or composition of both particles (Wetzel *et al*., 2003, Zhang *et al*., 2008, and Kwon *et al*., 2008). The recent interest in using smaller particles at nano scale is due to the particles' higher interface area then micro particles. Haupert and Wetzel (2005) discussed the importance of homogeneity in particle distribution due to its significant effect on the wear performance of epoxy composite. The distribution of particles depends highly on the technique and condition of introduction (eg. chemical or mechanical technique), particle size and type, surface area and volume content.

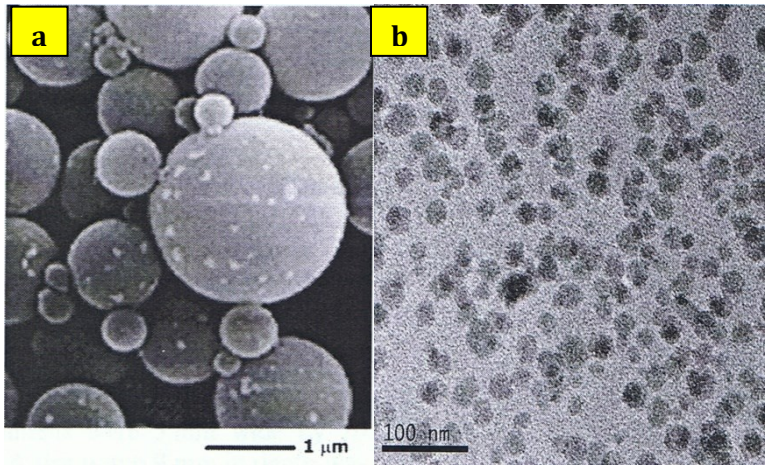

Fig. 5.11 (a) SEM (Kwon et al., 2008b) and (b) TEM (Zhang et al., 2008) micrograph taken from epoxy-based silica filled micro and nanocomposite.

Pearson and Yee (1989) studied the deformation mechanisms of single-edge notch rubber modified epoxy specimens. They used the single-edge notch bending (SENB) test to investigate the fracture toughness, K_{IC}, of the epoxy material. The study which employed SEM and TEM showed cavitation of rubber particles and formation of shear bands due to the fracture. Stress-whitened zones also formed on an unstable fractured surface. Similar findings have been reported in almost all studies on the fracture analysis of mechanically tested rubber modified epoxy polymer (Arias *et al*., 2003, Yamaka and Inoue, 1990, Ratna and Banthia, 2000). Sue (1992) has reported on the formation of particle-cavitation line arrays termed as croids, as derived from the word 'crack' and void'.

In rigid particle-modified epoxy polymers, fractography analysis is conducted on fracture toughness and flexural tested samples to analyse crack morphology and matrix-particle interaction. Johnsen *et al*. (2007) reported on the evidence of particles debonding and plastic void growth due to the toughening mechanism of SENB tested sample of modified polymer (Figure 5.12). The study also concluded on crack deflection as it encounters nanosilica particles. Crack pinning, identified as bowing lines, was also observed on the fractured surface although it is unlikely to contribute to the increased toughness.

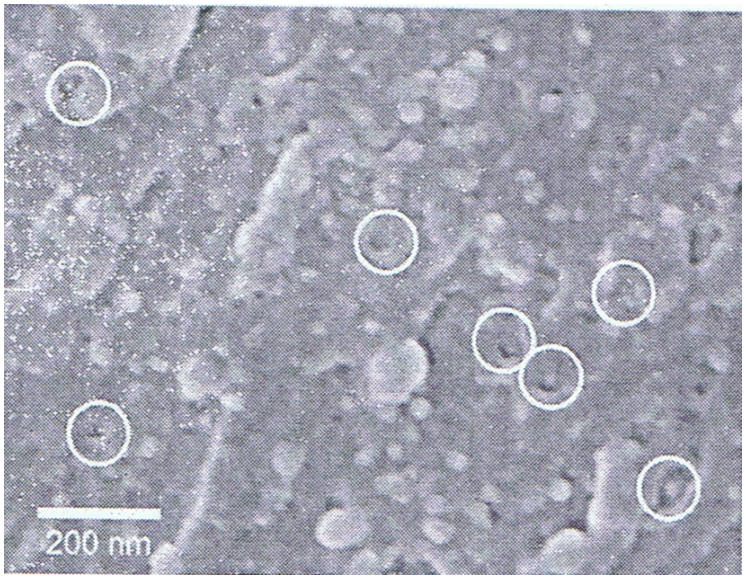

Fig. 5.12 SEM of nanosilicaparticles debonding (encircled) and plastic voids (Johnsen et al., 2007).

Similar finding on particle debonding was reported by Kwon *et al*. (2008) with critical crack propagation through the epoxy matrix. Kanchanomai*et al*. (2005) studied on the effect of loading rate on fracture behaviour of SENB tested sample. Based on SEM micrographs analysis, the study reported on the formation of shear lip, stretch zone and localized plastic deformation corresponding to the loading rates (Figure 5.13).

Fig. 5.13 SEM of stretch zones on modified DGEBA resin with low viscosity (Kanchanomaiet al., 2005).

Fractography of flexural tested sample was reported by Wetzel *et al*. (2003) on a calcium silicate ($CaSiO_3$) and alumina (Al_2O_3) particle-modified epoxy. Examination by SEM revealed shear deformation and surface roughness (Figure 5.14). Deviation and branching occurred when the crack passed around the particles. In areas where the crack passed through the particle, debonding and failure of the particle was observed. A related study by Kwon *et al*. (2008) has also reported on the occurrence of particle debonding.

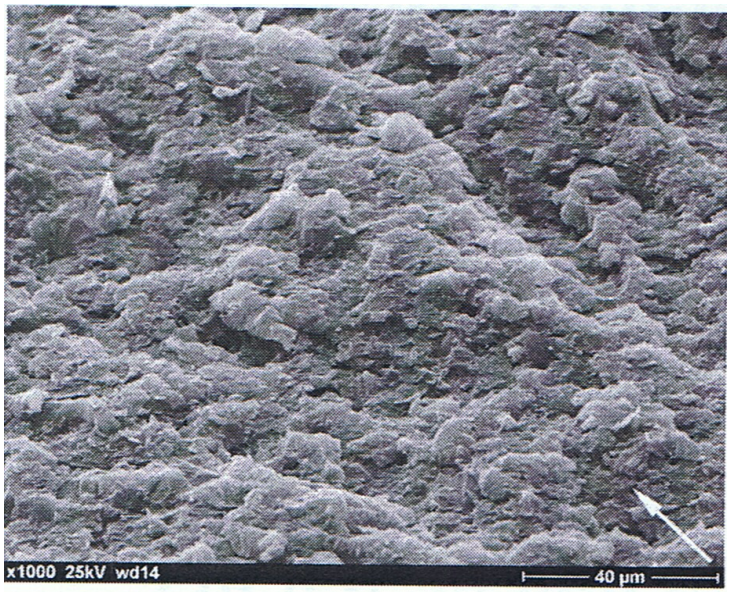

Fig. 5.14 Surface roughness of flexure sample of calcium silicate ($CaSiO_3$) and alumina (Al_2O_3) particle-modified epoxy. Arrow mark direction of crack propagation (Wetzel et al., 2003).

5.6 CONCLUDING REMARKS

Epoxy is a versatile adhesive which can be modified to suit specific need. This includes special properties such as gap-filling ability (thixotropicity) and curing temperature. Modification of epoxy by addition of micro-particulate, nano- fillers and liquid rubber is made to enhance the mechanical performance of epoxy adhesive. The growing advancement in research and usage of epoxy as structural adhesive has given many advantages to the usage of timber as construction material although it is an expensive adhesive. Room temperature curing epoxies are potentially disadvantaged by their low Tg which may allow creep to occur in bonded-in connections. The thesis will evaluate the performance of modified epoxy adhesives under creep loads.

CHAPTER 6 : VISCOELASTICITY

6.1 INTRODUCTION

One of the most studied areas on the mechanical response of materials is viscoelastic behaviour. The term defines property of material which exhibit both elastic and viscous behaviour. The viscoelastic response is further detailed in the next section which includes theories in relation to stress and strain and models that were developed to describe viscoelastic behaviour.

6.2 TYPES OF VISCOELASTICITY

Maxwell, Boltzman and Kelvin have made important discoveries on the relation of stress and strain by experimenting with creep and recovery of metals, glasses and rubbery materials. Viscoelasticity describes the flow of materials under applied force and temperature. In this sense, the behaviour of liquid-like flow can best be described by the Newtonian model.

6.2.1 NEWTON'S LAW OF VISCOSITY

As described by Ward and Sweeney (2004), Newton's law on viscosity η, defines the relation of stress σ being proportional to the liquid's velocity gradient. In this equation the velocity and velocity gradients are represented by the variable V and y respectively:

$$\sigma = \eta \frac{\partial V}{\partial y} \qquad \text{(Eq. 6.1)}$$

As for velocity gradient which acted on *xy* plane, the equation can be described by the following:

$$\sigma_{xy} = \eta \left(\frac{\partial Vx}{\partial y} + \frac{\partial Vy}{\partial x} \right) \qquad \text{(Eq. 6.2)}$$

The velocity gradient in x and y direction are indicated as ∂Vx/∂y and ∂Vy/∂x in Eq. 6.2. The diagram below (Figure 6.1) describes the velocity gradients in y direction.

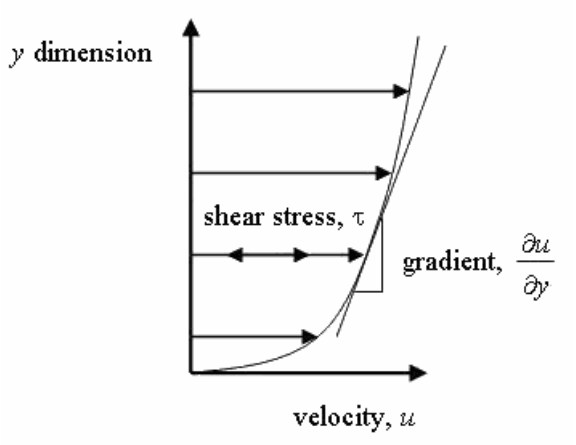

Fig. 6.1 The velocity gradient (Ward & Sweeney, 2004).

By placing *u* and *v* as the displacement in x and y direction, Eq. 6.3 can be written as:

$$\sigma_{xy} = \eta \left[\frac{\partial}{\partial y}\left(\frac{\partial u}{\partial t}\right) + \frac{\partial}{\partial x}\left(\frac{\partial v}{\partial t}\right)\right]$$

$$= \eta \frac{\partial}{\partial t}\left(\frac{\partial u}{\partial y}\right) + \left(\frac{\partial v}{\partial x}\right)$$

$$= \eta \frac{\partial e_{xy}}{\partial t}$$

(Eq. 6.3)

This equation shows that the change of shear strain or strain rate has a proportional influence on shear stress σ_{xy}. As mentioned by Menard (2008), the rate of flow of material increases with the increase in shear rate. Materials which conforms to this law is categorised as Newtonian material. For a Newtonian fluid, the stress is linearly proportional to the rate of change in strain. Some other materials which deviate from the linear relationship are called the Non-Newtonian materials. These material exhibits several types of deviations which are depicted in the following figure.

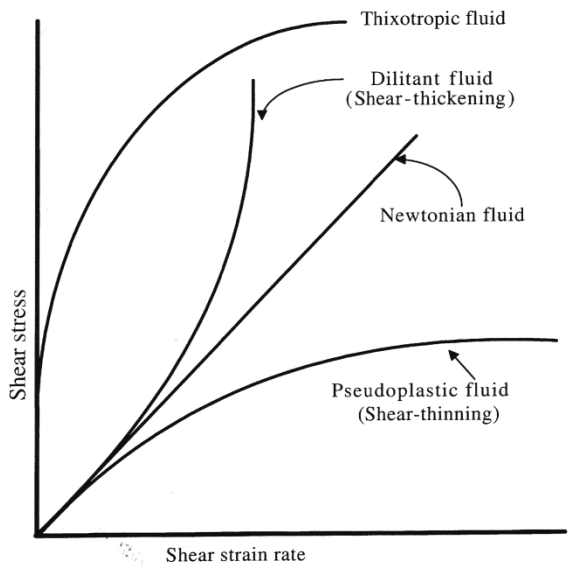

Fig. 6.2 Shear stress-strain rate of Newtonian and Non-newtonian liquid (Pocius, 2002)

Figure 6.2 shows the shear stress and shear strain rate curve of both Newtonian and Non-Newtonian fluids. As depicted by the Newton law of viscosity equation, the stress-strain rate curve of a Newtonian fluid conforms to the linear response. A non-linear response of shear stress to strain rate curve which bends towards the y-axis is known as dilatant fluid. This material exhibit the behaviour of 'shear thickening' which increases their viscosity as the shear rate increases. A material which decreases in viscosity as strain rate increases is known as pseudoplastic fluid. The pseudoplastic fluid exhibit 'shear thinning' effect as shear rate increases. The Newton, dilatant and pseudoplastic curves have a common initial position. All mentioned curves have zero intercept on the shear stress and shear rate axis. Other materials which exhibits non-zero intercept behaviour are known to be displaying 'yield stress'. Solid such as Bingham plastic displays Newtonian behaviour upon yielding. Yield stress behaviour is also observed in thixotropic materials. Thixotropic materials decrease in viscosity at constant shear/strain rate. This behaviour is a very important feature in the development of adhesive when practicality is the most important consideration (Pocius, 2002), for example the adhesive must be thixotropic when injecting them into overhead cavities.

Another important variable which shaped the viscoelastic behaviour of material apart from stress and strain is time. Transient experiment which is conducted by placing load to deform the material in relation to time often results two types of viscoelastic

response. In creep experiment, the stress is held constant resulting increase in strain with time. Figure 6.3 exhibit the strain response to constant stress over a range of time. Creep compliance as represented by *J(t)* denotes the rate of strain-stress. Stress relaxation behaviour described the decline of stress when strain in held constant. As shown in Figure 6.4, the relaxation modulus decreases away with time. Both theory on creep and stress relaxation behaviour will be discussed further in section 6.3.

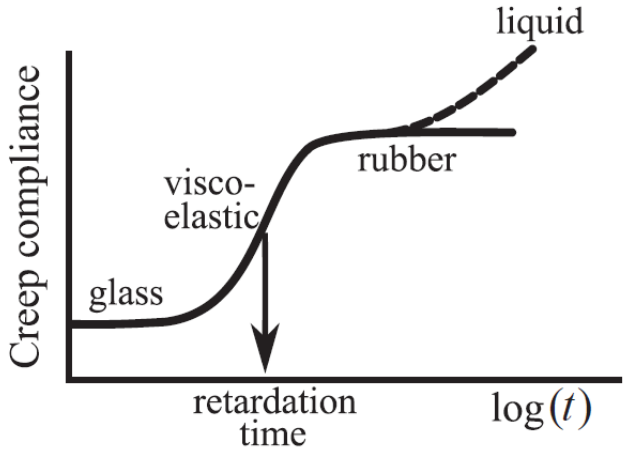

Fig. 6.3 Creep compliance as a function of time (Vincent, 2012)

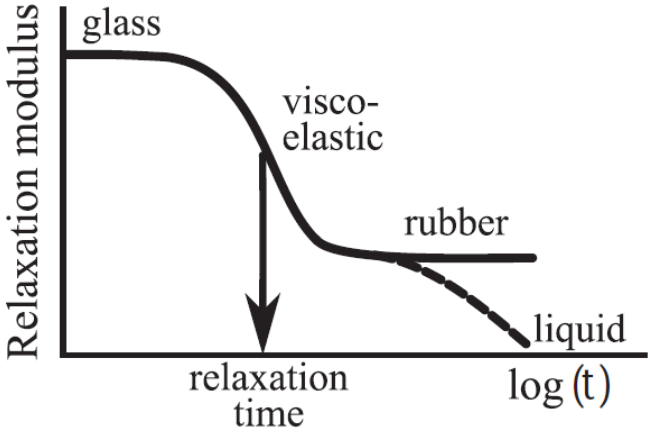

Fig. 6.4 Relaxation modulus as a function of time (Vincent, 2012)

Viscoelasticity could also be described as linear and non-liner viscoelastic. The linear viscoelasticity theory is most applicable for small deformations whilst nonlinear is best for materials with large deformation with changes in properties due to deformation. The models of linear viscoelasticity will be discussed at greater length in the next section.

The linear viscoelasticity can be defined by means of three approaches. The first approach is known as the Boltzman superposition or the integral representation of linear viscoelasticity. Viscoelasticity could also be modelled based on the assembly of Hookean springs and Newtonian dashpots models. The second approach is known as the differential representation which is based on linear differential equation. The final approach on modelling linear viscoelasticity would be based on the theory of the molecular model via dynamic test. All models presented were described in response to creep and stress relaxation.

6.3.1 BOLTZMAN SUPERPOSITION (INTEGRAL MODEL)

The Boltzman (1876) superposition theory was established based on two principles:

a) *The creep is a function of the entire past loading history of the specimen.*
b) *Each loading step makes an independent contribution to the final deformation, so that the total deformation can be obtained by the addition of all the contribution.*

It is noted that the first condition refers to the influence of memory function on the deformation of the material. The theory implies on the importance to consider the history of past loading since this will influence the behaviour of the material at present. The second condition states that a specimen under creep load will experience a similar amount of creep amount for each extra load. This can be explained through Boltzman's transient experiment on creep response to multistep loading programme (Figure 6.5)

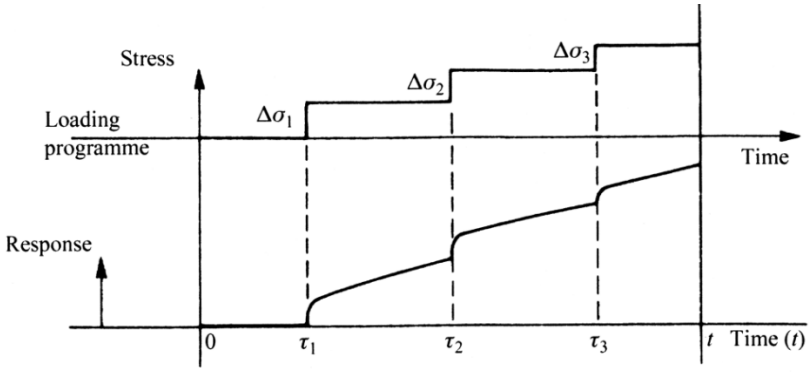

Fig. 6.5 Multistep loading creep behaviour (Ward & Sweeney, 2004)

Each step of loading carries incremental stresses (Δσ) which adds at subsequent time (τ) respectively. The total sum of strain at time *t* is given by:

$$e(t) = \Delta\sigma_1 J\,(t-\tau_1) + \Delta\sigma_2 J\,(t-\tau_2) + \Delta\sigma_3 J\,(t-\tau_3) + \ldots\ldots \quad \text{(Eq. 6.4)}$$

Both J and J(t – τ) represents the compliance of the material and creep compliance function respectively. The equation can be further generalised as:

$$\varepsilon\,(t) = \int_{-\infty}^{t} J\,(t-\tau_n) + d\sigma(t_n) \quad \text{(Eq. 6.5)}$$

The equation can be rearranged by separating the immediate elastic response, ε (Eq.6). The variable G_u in the equation denotes the unrelaxed modulus. This brings to the final equation which separates the time-independent and time-dependant function in terms of stress-relaxation modulus, G_r (Eq.7).

$$\varepsilon\,(t) = \left[\frac{\sigma}{G_u}\right] + \int_{-\infty}^{t} J\,(t-\tau_n)\,\frac{d\sigma(\tau_n)}{d\tau_n}\,d\tau_n \quad \text{(Eq. 6.6)}$$

$$\sigma(t) = [G_r\varepsilon] + \int_{-\infty}^{t} J\,(t-\tau_r)\,\frac{d\varepsilon(\tau_r)}{d\tau_r}\,d\tau_r \quad \text{(Eq. 6.7)}$$

6.3.2 MAXWELL, KELVIN-VOIGT AND THE STANDARD LINEAR SOLID MODEL (DIFFERENTIAL MODEL).

This section describes a common method in modelling viscoelastic behaviour through mechanical models of spring and dashpot. The spring and dashpot represent the elastic and viscous element within a viscoelastic material.

6.3.2.1 The Maxwell model

As similar to the other models, the Maxwell model is consists of two important elements of Hookean spring and Newtonian dashpot (Figure 6.6).

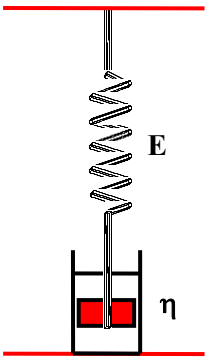

Fig. 6.6 The Maxwell unit

These gives two sets of equation relating to stress and strain. Equation 6.8 and 6.9 relates to the stress-strain relationship in the spring and dashpot respectively.

$$\sigma_1 = E_m \varepsilon_1 \qquad \text{(Eq. 6.8)}$$

$$\sigma_2 = \eta_m \frac{d\varepsilon_1}{dt} \qquad \text{(Eq. 6.9)}$$

In Maxwell model, the spring and dashpot is arranged in series which gives each element an equal stress; $\sigma = \sigma_1 = \sigma_2$ whilst total strain is given as $\varepsilon = \varepsilon_1 + \varepsilon_2$. The total stress-strain relation can be expressed by adding Eqs. 6.8 and 6.9 to give:

$$\frac{d\varepsilon}{dt} = \frac{1}{E_m}\frac{d\sigma}{dt} + \frac{\sigma}{\eta_m} \qquad \text{(Eq. 6.10)}$$

In modelling stress relaxation experiment via Maxwell approach, the strain (length) is held at constant. Therefor,

$$\frac{d\varepsilon}{dt} = 0\,, \quad \frac{1}{E}\frac{d\sigma}{dt} + \frac{\sigma}{\eta_m} \qquad \text{(Eq. 6.11)}$$

which can also be written as

$$\frac{d\sigma}{\sigma} = -\frac{E_m}{\eta_m}\,dt \qquad \text{(Eq. 6.12)}$$

It is given that during the initial stages of stress-relaxation, $t = 0$ and $\sigma = \sigma_0$ and integrating to Eq. 6.12, giving

$$\sigma = \sigma_0 \exp\left(-\frac{E_m}{\eta_m}\right) t \qquad \text{(Eq. 6.13)}$$

The following equation expressed exponential decline of stress as according to characteristic time constant $\tau = \eta_m / E_m$. The variable τ in this equation represents the relaxation time.

$$\sigma = \sigma_0 exp\left(\frac{-t}{\tau}\right) \qquad \text{(Eq. 6.13)}$$

The Maxwell model is unsuitable for creep behaviour since the dashpot have the tendency to permit viscous flow under the condition of constant stress. This will cause the spring to be in constant tension. Creep behaviour requires a more complex modelling as indicated by experiment based on Kelvin-Voigt model (Ward & Sweeney, 2004).

6.3.2.2 The Kelvin-Voigt model

The obvious difference between Kelvin-Voigt and Maxwell model is in the arrangement of the elements. The spring and dashpot element for Kelvin-Voigt model is arranged in parallel configuration as indicated in Figure 6.7.

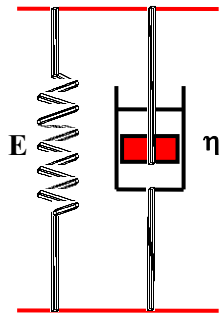

Fig. 6.7 The Kelvin-Voight unit

In this model, retardation by the dashpot element prohibits instantaneous response in the spring element. The stress-strain relation for the spring and dashpot gives rise to the expression:

$$\sigma_1 = E_K \varepsilon_1 \qquad \text{(Eq. 6.14)}$$

$$\sigma_2 = \eta_K \frac{d\varepsilon_2}{dt} \quad \text{(Eq. 6.15)}$$

Since the spring and dashpot are parallel in arrangement, the total stress σ is shared between the elements: $\sigma = \sigma_1 + \sigma_2$. The total strain equals to the strain of each component as $\varepsilon = \varepsilon_1 = \varepsilon_2$. Thus equation 6.14 and 6.15 can be added to give

$$\sigma = E_K \varepsilon + \eta_K \frac{d\varepsilon}{dt} \quad \text{(Eq. 6.16)}$$

At $0 < t < t_1$ and stress is σ,

$$\frac{E_K}{\eta_K} \int_0^t dt = \int_0^\varepsilon \frac{d\varepsilon}{(\sigma/E_K) - \varepsilon}$$

where η_K / E_K is a function of time. Integrating the last equation we obtain

$$\frac{t}{\tau} = \ln\left(\frac{\sigma/E_K}{(\sigma/E_K) - \varepsilon}\right)$$

where τ represents the retardation time and can be written as

$$\frac{\sigma}{E_K} = \left(\frac{\sigma}{E_K} - \varepsilon\right) exp(t/\tau)$$

Simple rearrangement of the above equation gives

$$\varepsilon = \frac{\sigma}{E_K} [1 - exp(-t/\tau)] \quad \text{(Eq. 6.17)}$$

6.3.2.3 The Standard Linear Solid

In Standard Linear Solid model, both Maxwell and Kelvin-Voigt model were combined to represent the stress relaxation and creep behaviour of viscoelastic material (Fig.6). This is made possible by the addition of second spring of modulus, E_a to the Maxwell spring-dashpot unit (Ward & Sweeney, 2004). The stress-strain relationship of Standard Linear Solid model is given as

$$\sigma + \tau \frac{d\sigma}{dt} = E_a \varepsilon + (E_a + E_m)\tau \frac{d\varepsilon}{dt} \quad \text{(Eq. 6.18)}$$

6.3.3 THE MOLECULAR MODEL

The final approach on modelling the behaviour of viscoelasticity is to study the molecular changes in response to stress and strain. The first and second methods (integral and differential models) were established based on transient experiment. Transient experiment implicates the study on deformation of material in response to loading. The molecular model applies dynamic test in which sinodssoidal stress and strain is imposed on a material. Dynamic testing is more flexible due to its suitability by a wide range of testing condition (eg. frequencies, temperature, test rig geometries, time). An important apparatus in dynamic study is the dynamic mechanical analysis which will be discuss in great length in the next section.

6.4 DYNAMIC MODULUS

This section addresses dynamic mechanical analysis as an analytical tool in the study of deformation and flow of material.

6.4.1 THEORY OF DYNAMIC MODULUS

Menard (2008) defined Dynamic Mechanical Analysis (DMA) as applying an oscillating force to a sample and analysing the material's response to that force. In dynamic test, the specimen is subjected to oscillating stress while the resulting deformation is being measured. The study of viscoelastic materials can best be explained through describing the two extreme behaviour of material, elastic and viscous. The section below describes the response of each material to the oscillating stress.

A material which is elastic in behaviour (spring-like nature) responds with in-phase stress and strain. A viscous material (dashpot) has the tendency to exhibit an out-of-phase response. The phase difference between stress and strain of viscous material occurs due to the strain lags stresses by 90° or $\pi/2$ radian. The nature of viscoelastic material lies in between being elastic and viscous. Apart from displaying instantaneous response, a viscoelastic material also exhibit a certain degree to phase lag in strain. Figure 6.8 summarise the stress-strain wave of elastic, viscous and viscoelastic materials with response to oscillating stress.

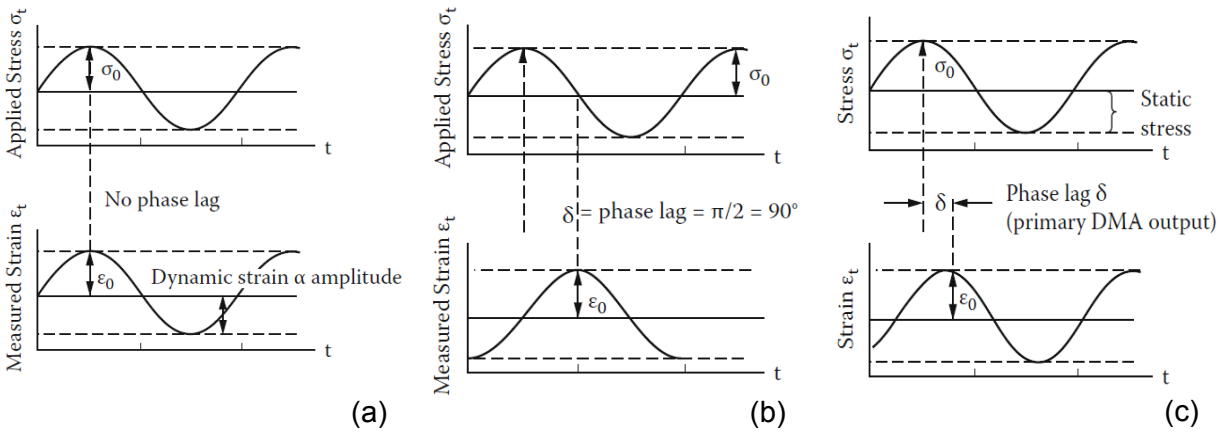

Fig. 6.8 The applied stress and strain response of (a) elastic material (b) viscous material and (c) viscoelastic materials (Menard, 2008)

The stress and strain relationship of viscoelastic material can be given as:

$$\varepsilon = \varepsilon_0 \sin(t\omega) \qquad \text{(Eq. 6.19)}$$

$$\sigma = \sigma_0 \sin(t\omega + \delta) \qquad \text{(Eq. 6.20)}$$

where δ is the phase angle, t is time and ω denotes the frequency of strain oscillation.

Data for DMA were then calculated based on the response of stress and strain sine wave under sinusoidal stress. Two types of moduli can be measured to define the characteristic of viscoelastic materials. The storage modulus (E') defines the elastic portion and the stored energy of the material. The loss modulus (E") represents the viscous characteristic of the material. This modulus expresses the loss of energy which dissipated as heat due to friction and internal motion. Both moduli can be defined as below:

$$E' = (\sigma^0/\varepsilon^0)\cos\delta = (f_0/bk)\cos\delta \qquad \text{(Eq. 6.21)}$$

$$E'' = (\sigma^0/\varepsilon^0)\sin\delta = (f_0/bk)\,sin\delta \qquad \text{(Eq. 6.22)}$$

in which δ represent the phase angle, b is the term of sample geometry, f_0 is the applied peak force and k denotes the displacement of sample. The vector sum of storage and loss modulus later gives the value of complex modulus, E*.

$$E^* = E' + iE'' \quad \text{(Eq. 6.23)}$$

where $i^2 = -1$.

The storage and loss modulus is closely related to the complex modulus and tangent of the phase angle (tan δ) which can be described graphically as:

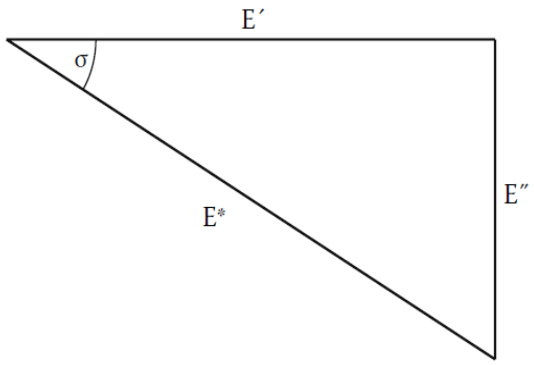

$$\text{TAN}\,\delta = \frac{E''}{E'} \quad \text{(Eq. 6.24)}$$

Fig. 6.9 Relationship between phase angle, E, E' and E'' (Menard, 2008)*

The tangent of the phase angle (tan δ) represents the damping characteristic of the material. Damping is an effect of energy loss due to molecular rearrangements and internal friction (Menard, 2008). It also can be used to indicate the possibility of error in measurement since tan δ calculation is independent of geometry effects.

6.4.2 DMTA METHOD IN POLYMER STUDY

DMTA gives the insight information on the cross-linking of polymer and its effect on the mechanical properties. It has the capability to measure transition in a polymer via the time and temperature scan. In temperature scan, the sample is subjected to oscillation at a set frequency whilst being tested over an increasing temperature gradient. In DMA method, the thermal transition in polymer is described in terms of modulus. Figure 6.10 indicates the transition of molecular arrangement in response to temperature scan.

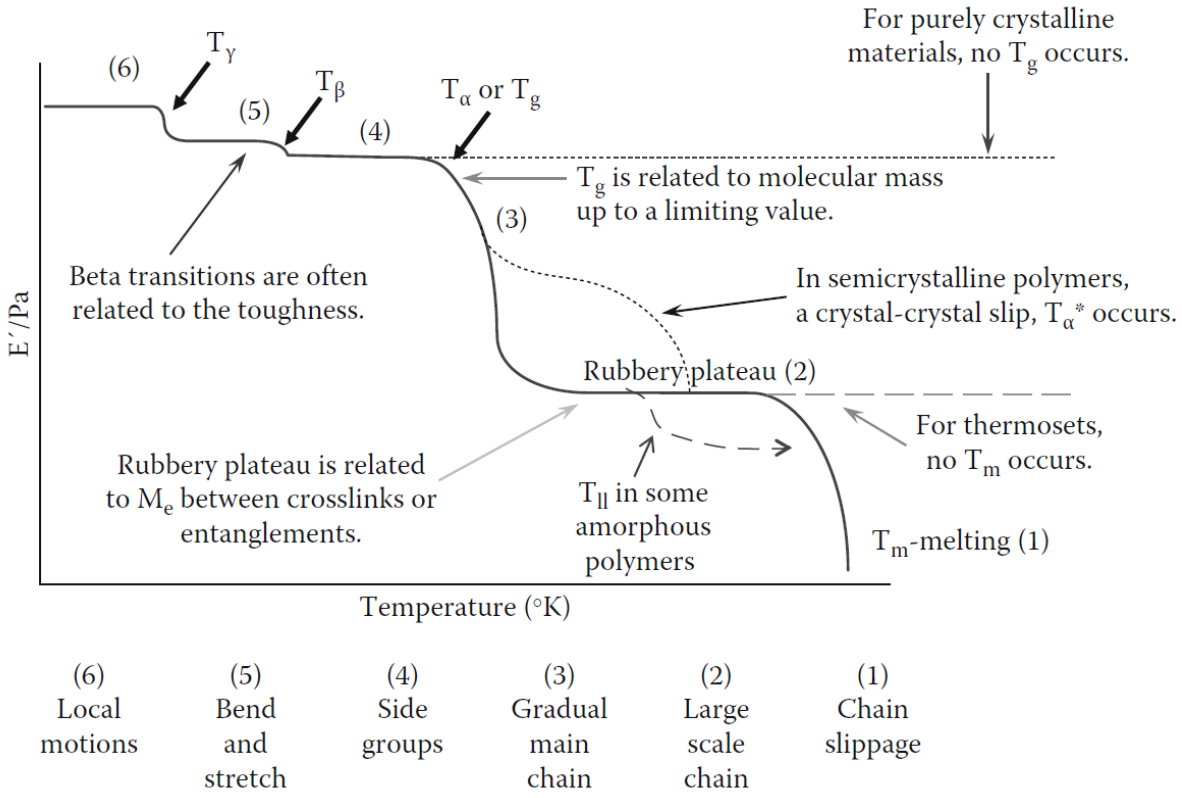

Fig. 6.10 Temperature scan of polymer which exhibits transition of molecular arrangement into six major phases (Menard, 2008)

a) Cross-linking and crystalinity

DMA technique has been extensively used to determine the degree of crosslinking and crystallinity of materials. As the temperature increase during testing, the polymer chains gain enough energy to mobilise and rearrange. This allows major transition where the physical properties of the polymer changes at a critical temperature point. The transitional point is called the glass transition temperature or T_g (T_α). The T_g represent the transitional phase where the material changes from hard glassy to rubbery state. DMA results characterise a material either into highly crystalline, semi-crystalline or amorphous based on the modulus drop which corresponds to the T_g. A highly crystalline and cross-linked material may exhibit almost none transitional phase due to immobility of the polymer chains. Further heating above the Tg may also cause an increase in modulus due to cold crystallisation as indicated in Figure 6.11.

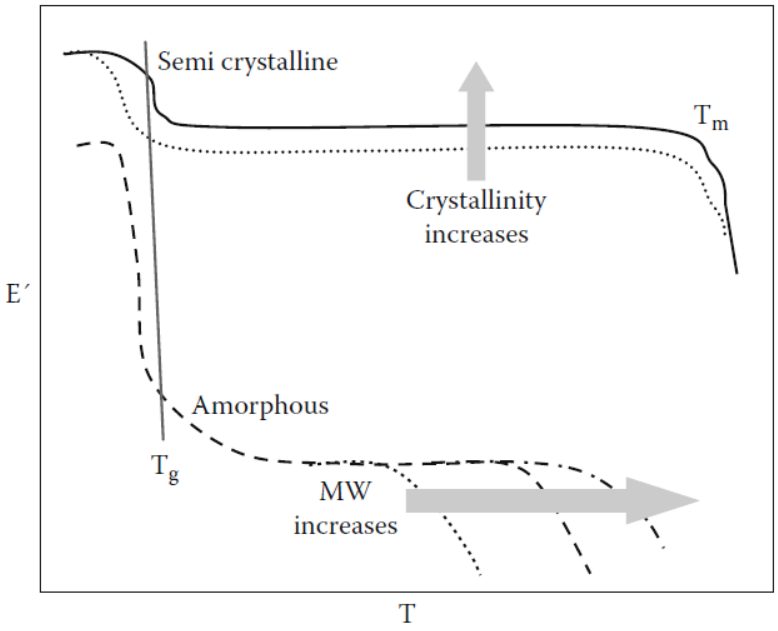

Fig. 6.11 DMA results which indicates the effects of crystallinity and molecular weight (M_w) (Menard, 2008)

The effect of crosslinking or molecular weight between entanglements (M_e) in a polymer can be seen on the lengths of the rubbery plateau (Menard, 2008). As indicated in Figure 6.12, the modulus of plateau is proportionally related to the degree of crosslinking at a specific temperature. Crosslinking may also have an effect of the loss factor peak. The broadening of the loss factor peak is related to the increase of cross-linking within the polymer.

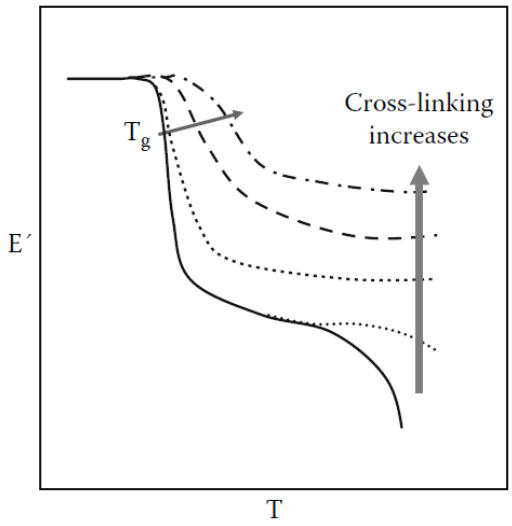

Fig. 6.12 DMA results indicate length of rubbery plateau in relation to degree of crosslinking (Menard 2008).

b) Copolymers and blends

Copolymers and blends are types of polymer which were added to the primary polymer as toughening agent. The addition of secondary or tertiary polymer is either in physical mixture of material (blend) or in mixture of chemical (copolymer). An example on polymer modification via copolymerisation is by adding liquid rubber to brittle polymer. This will give a 'toughening effect' on the polymer. The mechanical properties of this mixture depend on the solubility of the added homopolymers. Menard (2008) indicates that the concentration of the components significantly influences the T_g of the material. Figure 6.13 shows an example on how polymer blending affects the T_g of the material.

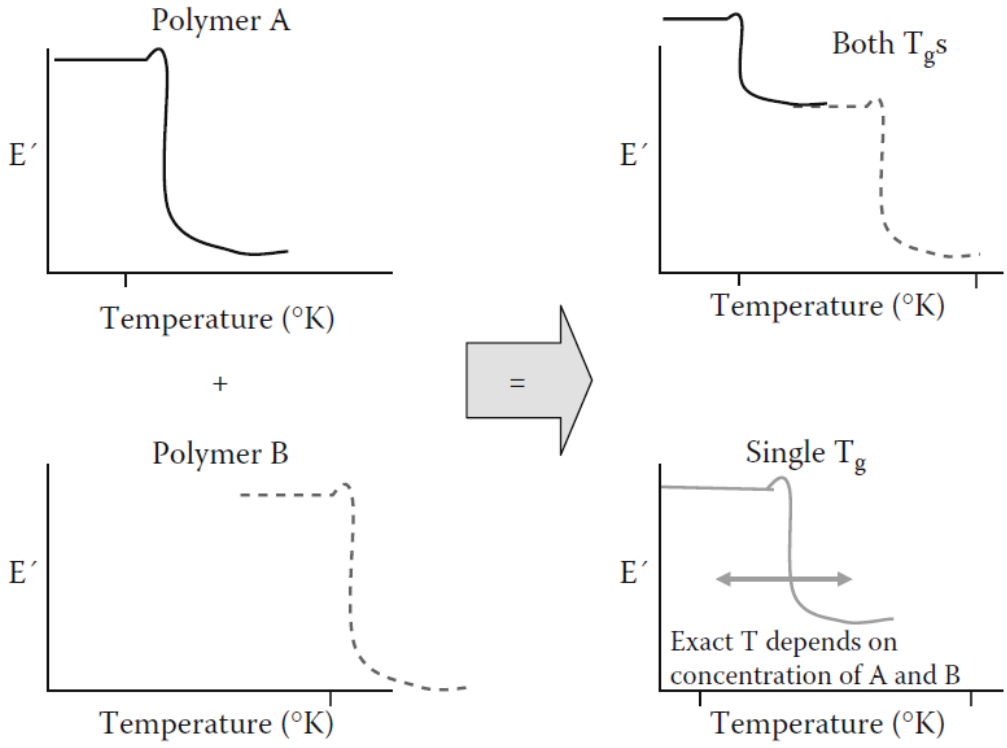

Fig. 6.13 The effect of blends on T_g (Menard, 2008).

Menard (2008) also indicates on the effect of copolymer and blends on tan δ peak. This is supported by a study on liquid rubber-modified epoxy which indicates higher tan δ peak of the blends in comparison to bulk polymer (Kar & Banthia, 2004).

c) Plasticisers and fillers

Plasticisers and fillers are types of materials which were commonly found in commercial polymers. These modifiers served specific function in altering the physical properties of the polymer. The addition of plasticisers, which were commonly of low molecular mass organic materials, is purposely to soften rigid polymers such as PVC. The presence of moisture may also act as plasticising agent in polymer. DMA studies on the presence of plasticiser in a polymer indicate a decrease in storage modulus, low glass transition temperature and broad loss factor peak width (Backman & Lindberg, 2002).

Fillers were added with the purpose to improve the properties of the polymer formulation and to reduce the cost of the compound. An example on the utilisation of filler is by adding calcium silicate and alumina to increase modulus and toughness of epoxy (Wetzel *et. al* 2003) as indicated in Figure 6.14.

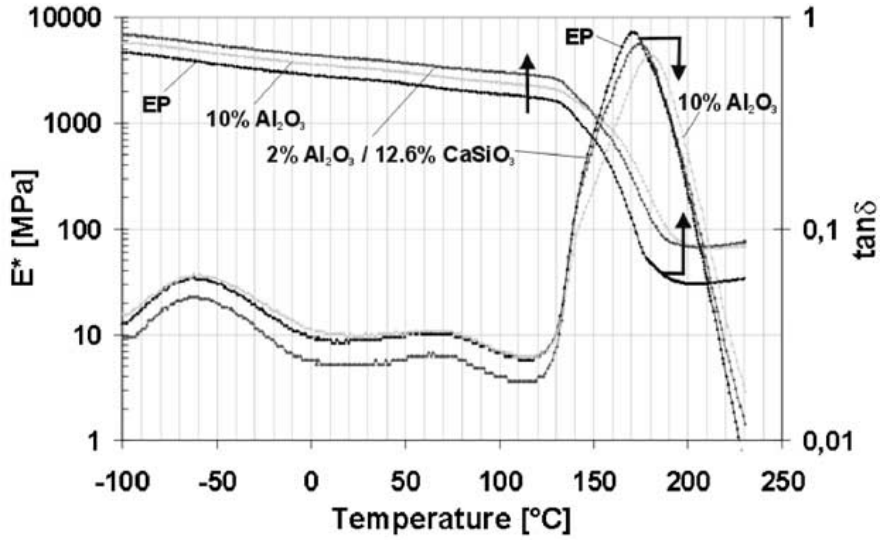

Fig. 6.14 Storage modulus and loss factor (tan δ) of neat epoxy (EP), EP/Al_2O_3 and EP/Al_2O_3/$CaSiO_3$ composites (Wetzel et. al 2003).

d) Secondary transition

Secondary transition or sub-Tg transition (T_β) occurs due to localised molecular movement and much associated to the mechanical properties of the material. As shown by some amorphous polymer, the secondary transition indicates the presence of plasticisers or moistures coupled to polymers. Studies using DMA reported on

the influence of T_β on toughness, flow or creep, acoustic damping and physical aging (Menard, 2008).

6.4.3 MECHANISM OF DMTA

6.4.3.1 Basic principles

The most important part in a DMA apparatus is the linear variable differential transformer (LVDT), which main function is to measure linear displacement. The LVDT measures the displacement through sensing changes in voltage in reaction to the movement of the probe. The probe is connected to a core rod which is enclosed within a temperature control system or furnace. A liner drive motor with a drive shaft support and guidance system provides the load for the applied force. The oscillatory force supplied by the DMA apparatus causes sinusoidal stress and generates strain on to the sample. The schematic diagram of a DMA apparatus is as shown in Figure 6.15.

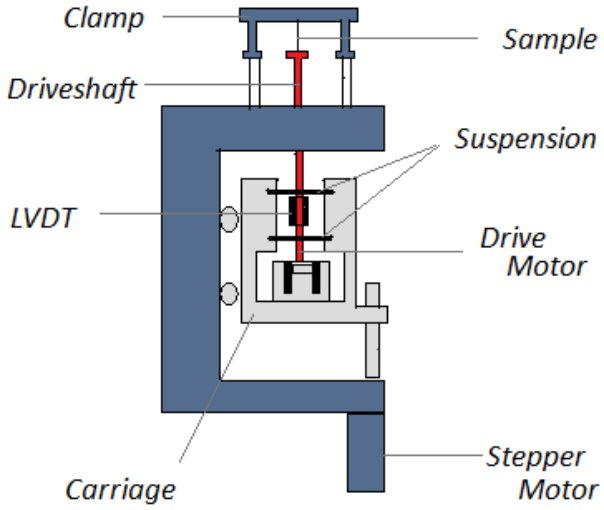

Fig. 6.15 A schematic diagram of Dynamic Mechanical Analysis (DMA) apparatus showing the motor, Linear Variable Differential Transformer (LVDT) and sample compartment (Vincent, 2012)

Two types of analyser which are commonly used currently are forced resonance analyser and free resonance analyser. Force resonance analyser is designed specifically to force the sample to oscillate at a certain frequency. This analyser is most suitable for temperature sweep test. This is due to its robust design which consists of controlling parts for deformation, temperature, sample geometry and

sample environment (Menard, 2008). Figure 6.16 shows an example of force resonance type analyser as produced by Perkin-Elmer.

Fig. 6.16 A PerkinElmer DMA 8000 with fluid bath (PerkinElmer, 2013)

The measurement of free resonance analyser is made through suspending a sample and allows it to swing freely. The measurement on the dampening of oscillation gives a series of sine wave. The decay of amplitude and frequencies were then calculated to generate the period and logarithmic decrement. Samples which can be tested using free resonance analyser is only limited to rod or rectangular-shaped.

DMA analysers can also be characterised according to strain (displacement) or stress (force) control. In strain-controlled analyser, the probe is subjected to a set displacement value. The resultant stress is then measured by the load cell or force balance transducer. For this function, the equipment requires a separate shaft and larger drive motor. The advantage of strain-controlled analyser is its capability to measure low viscosity material in shorter time. It is also ideal for stress-relaxation experiment. In the stress-controlled analyser, a set of force is applied to the sample and tested under variety conditions (temperature, time and frequency) (Menard, 2008).

6.4.3.2 Testing fixture and sample geometries

Dynamic study is a method to evaluate viscoelasticity which allows flexibility in testing conditions. Dynamic testing can be conducted under various sample

geometry. This is a topic of importance since sample geometry has a large influence on stress and strain values (Menard, 2008). The applicable geometries conform to a set of equation on stress and strain as a result from the applied force and deformation. The geometric factor equation is significant to determine the amount of error in the modulus due to inaccuracies of sample measurement.

The DMA measurement can be made under various types of loading. Figure 6.17 indicates various commercially available fixtures for dynamic testing. The loading is usually applied vertically as designed on most types of DMA apparatus.

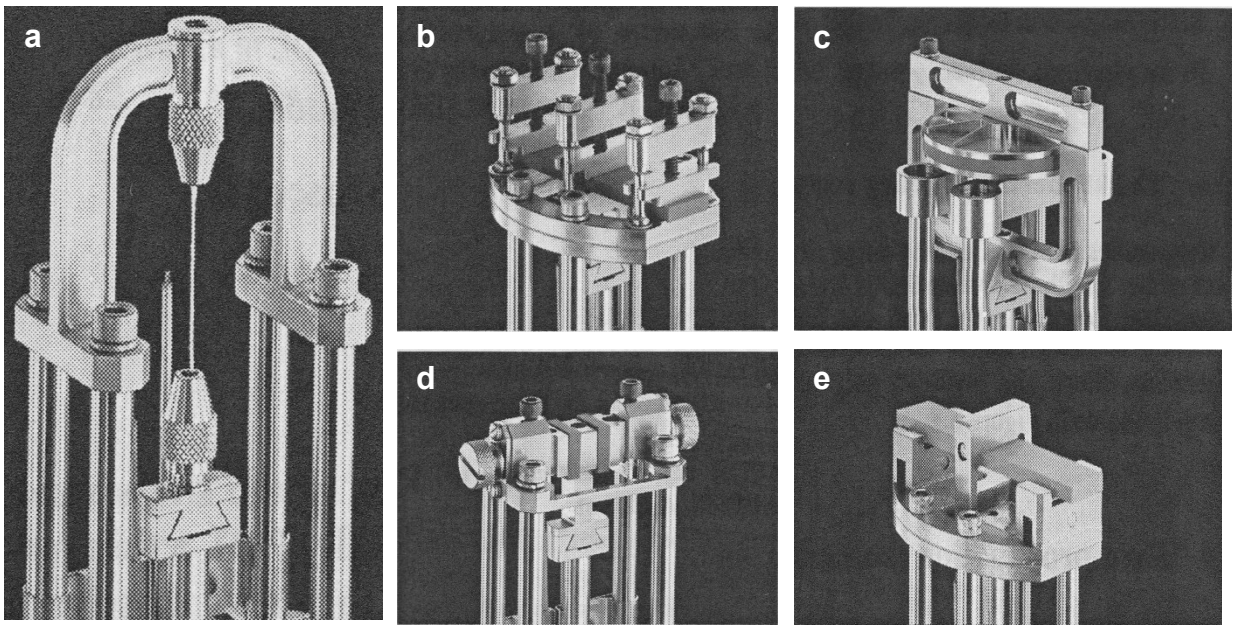

Fig. 6.17 DMA testing configuration which includes (a) tension (b) dual-cantilever (c) compression (d) shear sandwich (e) three-point bend (Ward & Sweeney, 2004)

Three-point or four point bending is one of the common methods in dynamic testing. In this test, the load is applied at a midpoint (three-point bending) or on two-point (four-point bending). The applied stress distribution for four-point bending is better than three-point test. In both cases, the ends of the sample are freely supported. This requires the sample to be 10% longer on each end of the beam. The length to thickness ratio of the sample is a crucial point since a short sample will induce inter-laminar shear stress in the midpoint plane. This arrangement is most suitable for dynamic testing of stiff material (eg. ceramic, metal and composites) and unsuitable for amorphous material due to excessive softening above the glass transition temperature. It is difficult to interpret pure

deformation owing to the existence of tensile and compression strain. This test is useful in determining temperature of transition relaxation.

In dual and single cantilever testing, both or either one of the sample's end is firmly clamped. As both end of the sample being clamped to the support, the midpoint is clamped to the push-rod. This induced a shearing component to the distortion which makes the sample difficult to deform. This arrangement makes it possible to test amorphous material that softens above T_g. The dual cantilever also gives 10-20% higher moduli compared to three-point bending testing. The cantilever mode is ideal for testing amorphous thermoplastic material such as reinforced thermoset, thermoplastic and elastomer. A material which is subjected to expansion due to heat may distort in a constrained arrangement. Single cantilever fixture is best suited for this type of material due to its less constrained arrangement.

In extension or tensile testing, the sample is placed between top and bottom clamp and loaded under tension mode. Adjustment is crucial since this configuration is most sensitive to loading and positioning compared to other geometries. Upon loading, the sample is subjected to pre-stress to prevent buckling during dynamic testing. This arrangement is suitable for testing of thin film or fibre in extension.

Other types of test configuration includes compression and shear mode. Under the compression mode the sample is positioned between two metal plates and subjected to uniaxial loading. Shear sample is commonly tested in sandwich arrangement where the samples were positioned between two sliding plates. Both compression and shear mode are most suitable for dynamic testing of soft rubbers and elastomers.

6.5 CONCLUDING REMARKS

There are many ways to describe the viscoelastic properties of a material. Theoretical approaches may include numerical analysis such presented by Boltzman, Maxwell and Kelvin-Voigt method. Recent development on the Dynamic Mechanical Analysis (DMA) technique which has been widely used gives a more

holistic approach on characterising the viscoelastic behaviour of materials. The thesis will describe the application of DMA for the evaluation of Tg and viscoelastic properties of modified epoxies in creep. The Kelvin-Voigt model will be employed to model creep deformation.

CHAPTER 7 : MICROSCOPIC ANALYSIS OF ADHESIVES

7.1 INTRODUCTION

Electron microscopy (SEM and TEM) was employed to characterise the composition of the adhesives. Five types of adhesive were studied, namely Rotafix Structural Adhesive (RSA), Engineered Adhesive (EA), Albipox, Timberset and Sikadur. The characterisation focussed on the identification of silica-dominated regions of the adhesive microstructure, in the form of silica agglomerate regions and inter-agglomerate regions. Other macro-sized particles and air voids were also detected. EA compositions were imaged with three percentages of CTBN rubber to study the effect of composition on the distribution of silica fume. Albipox was examined to determine whether rubber particles had phase-separated in the epoxy adhesive matrix

7.2 MATERIALS AND METHODS

7.2.1 ADHESIVES BACKGROUND

The selection of adhesives was based on the types of epoxy adhesive available for structural timber bonding. These adhesives were formulated according to their end use and the resin base and fillers were modified to alter the properties of the adhesive system including the glass transition temperature and the elastic modulus.
The principal study of the properties of ambient-temperature curing epoxy system was made on Rotafix Structural Adhesive (RSA). This structural adhesive has been used widely for timber repair and upgrading of glue-laminated components. RSA is a two-part adhesive system with gap filling properties achievable in the range 2-12mm and it has a reputation for forming strong bonds with glass fibre (GFRP) pultrusions and carbon fibre (CFRP) pultruded rods and plates. The resin base of this system was A diglycidylether of bisphenol-A or bisphenol-F (DGEBA/F). The system was modified with the addition of reactive diluents containing rigid particles of nano-sized silica fume. The silica fume was surface treated to improve the filler-matrix distribution. The nano-silica fume also contributed to the shear-thinning properties (thixotropy) of the system. The curing agent used for this formulation was a polyetheramine with the addition of a rheology modifier.

Engineering Adhesive (EA) is very similar to RSA but the reactive diluents are modified with carboxyl-terminated butadiene acronitrile (CTBN) rubber and silica fume nanoparticles. The modification was made to increase the glass-transition temperature (Tg) and toughness.

The third system investigated was Timberset which is also a variant of RSA. Timberset is formulated with the addition of a high proportion of micro-sized ceramic particles (mica, bentonite and silica). Several varieties of EA with altered rubber compositions were also investigated the possibility of phase separation of the rubber. The standard EA sample contained approximately 2.5% of CTBN whilst the specially formulated EA contained 6.5% and 12.5% respectively.

A fourth adhesive systems, Albipox 3001, did not contains silica fume but contained a higher proportion of CTBN (15 wt%). These four adhesives systems were manufactured by Rotafix (Northern) Ltd of Abercraf, South Wales, UK and the proportions of reactive diluent, silica fume and CTBN are summarised in Table 7.1.

Table 7.1. Proportions of reactive diluents, silica fume and CTBN as percentage weight of the adhesive formulations for Rotafix adhesives.

Adhesives	Reactive diluents (%wt)	Silica fume (%wt)	CTBN (%wt)
Rotafix Structural Adhesive (RSA)	25	7.45	None
Engineering Adhesive (EA) – Standard	4.53	7.45	2.5
Engineering Adhesive – Special formulation 1 (EA1)	4.53	7.45	6.5
Engineering Adhesive – Special formulation 2 (EA2)	4.53	7.45	12.5
Albipox 3001	N/A	None	15
Timberset	N/A	None	None

The Rotafix adhesives were compared with a fifth epoxy system, manufactured by Sika and marketed as Sikadur-31. Sikadur is a thixotropic two-part structural adhesive system used for mortar repairs, void and crack filling and consolidation of joints. It is designed for use at temperatures between 10°C and 30°C. The composition of the fillers for this heavily-filled epoxy system was not determined.

7.2.2 ADHESIVE MOULDING

The two-part adhesive systems were hand mixed carefully to avoid the formation of voids. Films of pure adhesive were cast in between two metal plates treated with release agent prior to casting and spaced 3mm apart. The films were left to cure in the mould for 5 days at room temperature and then removed and left to cure for another 15 days prior to observation. A thickness of 3 mm was achieved after the final curing process.

7.2.3 SAMPLE PREPARATION AND OBSERVATION

7.2.3.1 Preparation of sections

Prior to SEM observation, the hardened epoxy samples were embedded in epoxy resin (cold mounting) and subjected to several stages of polishing. Cured epoxy films were reduced to smaller size samples (approximately 15mm x 10mm x 3mm). The samples were potted using the Buehler Epoxicure System, allowing cross sections to be prepared. The Epoxicure system consists of Buehler Epothin®Epoxy resin and Buehler Epothin®Epoxy hardener. Each pot requires a mixture of 12.5g resin and 4.9g of hardener which has to be pre-heated in an oven at 40°C for 5 minutes before mixing. Each pot was labelled and cured at room temperature for 24 hours (Figure 7.1). Hardened embedded samples were then polished using a Buehler Metaserv Grinder and Polisher. The polishing schedule is as indicated in Table 7.2. Cured epoxy embedded samples retained the cylindrical shape of the pot (Figure 7.2).

Table 7.2. Polishing schedule of epoxy embedded sample

Polishing material	Polishing speed (RPM)	Polishing force (lbs)	Time (min)
SiC disc (320grit – 1200grit)	150 rpm	5 lbs	Until plane
RAM cloth (1µm diamond)	200 rpm	5 lbs	4 minutes
Chemomet (0.02µm col silica)	80 rpm	3 lbs	3 minutes

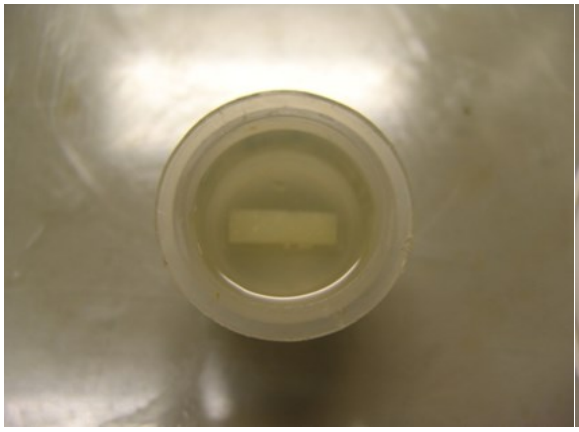

Fig. 7.1 Potted and labelled sample.

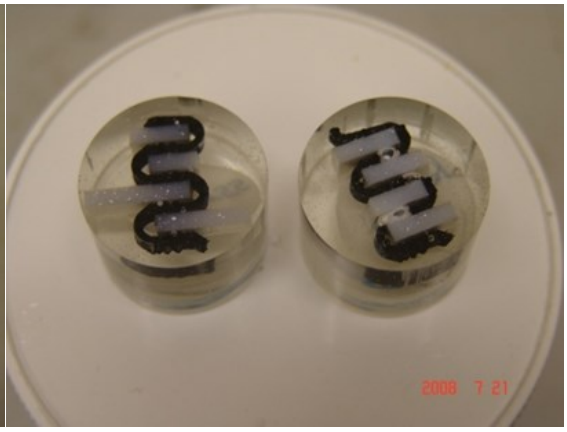

Fig. 7.2 Cured and polished embedded samples supported by plastic clips.

7.2.3.2 Scanning Electron Microscopy (SEM)

Adhesive samples were attached to a stub using either colloidal silver paste or double-sided conductive sticky tape. Coating is carried out to discharge the electron beam to earth (Watt, 1997) and samples were double coated due to the porosity of the adhesive surface. They were first coated with a thin layer of atomic gold using an Edwards Sputter Coater S150B. The gold coated surface was re-polished before applying a second 25µm thick coating of carbon. The coated samples were observed using a JEOL JSN6310 SEM (Figure 7.3) equipped with an Energy Dispersive X-ray Spectrometer (EDS) and using secondary electron imaging (SEI).

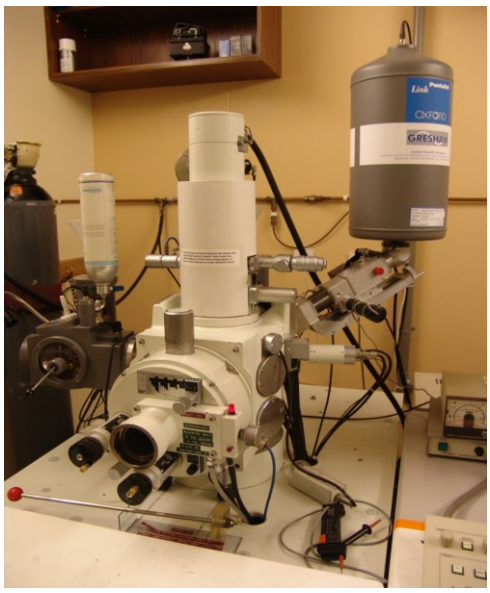

Fig. 7.3 JEOL JSM6310 Scanning Electron Microscope

7.2.3.3 Preparation of thin sections by microtoming.

Small blocks of epoxy samples were held in chucks which were fitted into a slot on a Reichert-Jung ultramicrotome (Figures 7.4 and 7.5). By observing the sample with the microscope attached to the ultramicrotome, the surfaces of the sample were levelled manually with a razor blade. The size of the surface was then reduced by forming it into a trapezoidal shape

Fig. 7.4 Reichert-Jung ultramicrotome

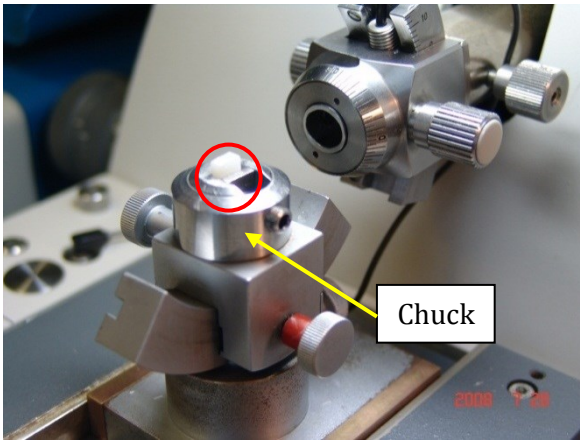

Fig. 7.5 Sample (encircled) held by chucks fitted to the ultramicrotome

A portion of the surface was levelled and smoothed again using a glass knife (Figure 7.6). An LKB 7800 Knifemaker was used to produce a triangular shaped glass knife with a razor sharp edge (Figure 7.7). Vertical movement of the sample in the chuck will slice against the stationary edge of the glass knife. The cut sample surface appeared shinier and smoother than the original sample.

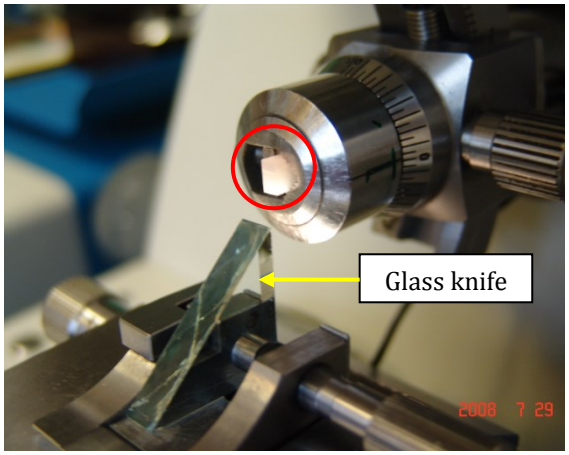

Fig. 7.6 Slicing of sample using a glass knife

Fig. 7.7 LKB 7800 Knifemaker

To ensure proper slicing of the sample, a Diatome diamond knife was used to obtain the required thickness of 1 µm. The diamond knife was used due to its ability to cut hard samples to produce slices of consistent thickness. Thin continuous films of samples were produced by vertically slicing the sample surface with the stationary diamond knife. Cut samples were produced in long thin films and suspended on the surface of water (Figure 7.8). Alcohol fumes were used to stretch out the suspended slices (Figure 7.9). The slices were then carefully picked up using a normal plain mesh 3.05mm diameter support grid made of nickel (Figure 7.10). These grids were dried using a hairdryer and kept in a grid box until observation.

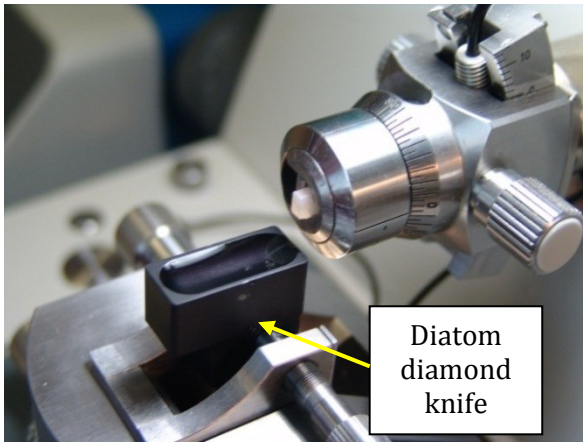

Fig. 7.8 Thin films of sample suspended on the surface of water

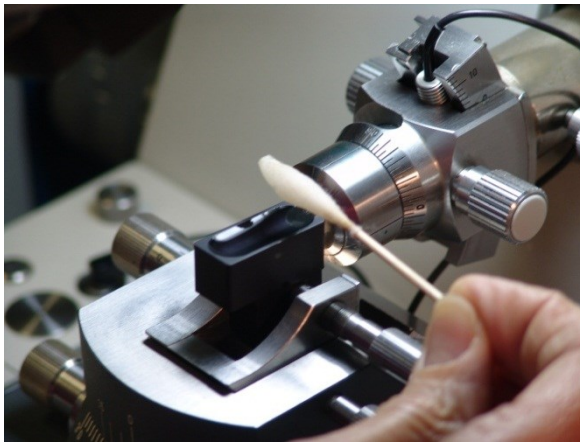

Fig. 7.9 Cotton dipped in alcohol to produce fume to stretch sample

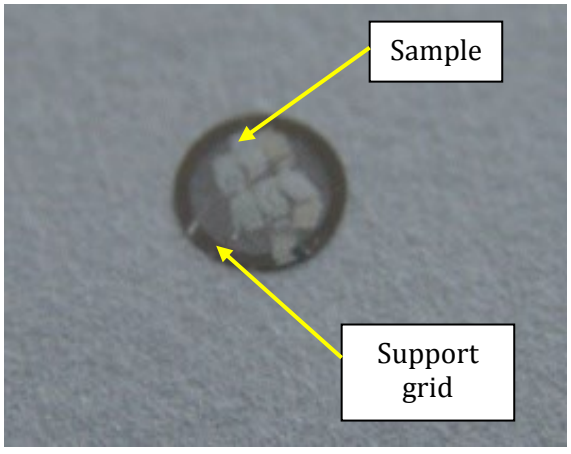

Fig. 7.10 A nickel plain mesh support grid which contains sliced samples

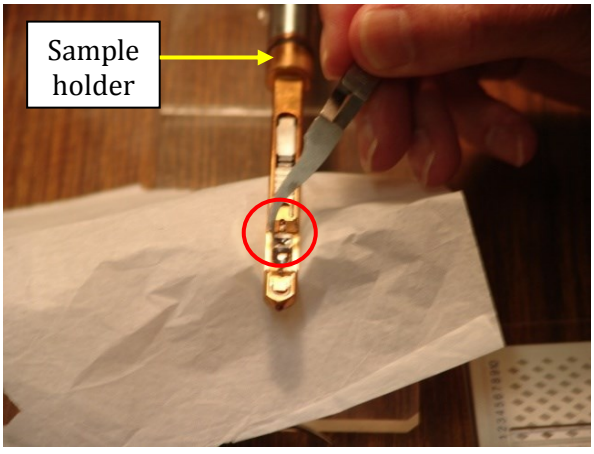

Fig. 7.11 Sample containing support grid (encircled) is being fitted to the sample holder

7.2.3.4 Transmission Electron Microscopy (TEM)

Thin sections were imaged using a Transmission Electron Microscopy (JEOL JEM1200 TEM) equipped with an x-ray spectrometer. The support grid which contains thin epoxy films was fitted to the sample holder prior insertion into the TEM (Figure 7.11). Insertion into the TEM column was made through the side entry part of the sample chamber (Figure 7.12). The sample was set to the required tilt and illuminated by the electron beam. The final image was screened on the electron-fluorescent layer in the viewing screen (Figure 7.13). The TEM is seen in Figure 7.14.

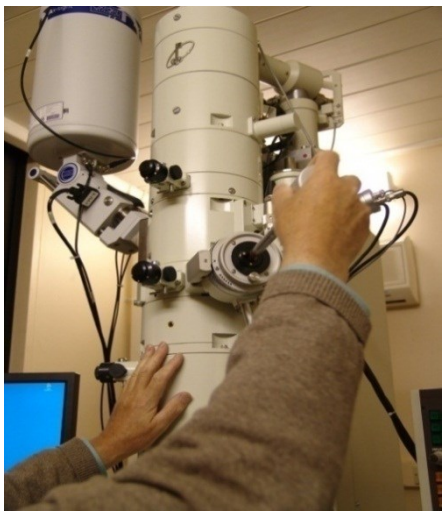

Fig. 7.12 Insertion of sample holder into the sample chamber

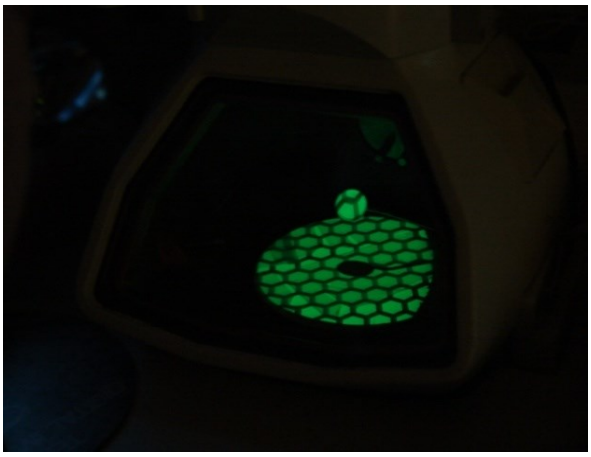

Fig. 7.13 A viewing screen lined by florescent material sheet

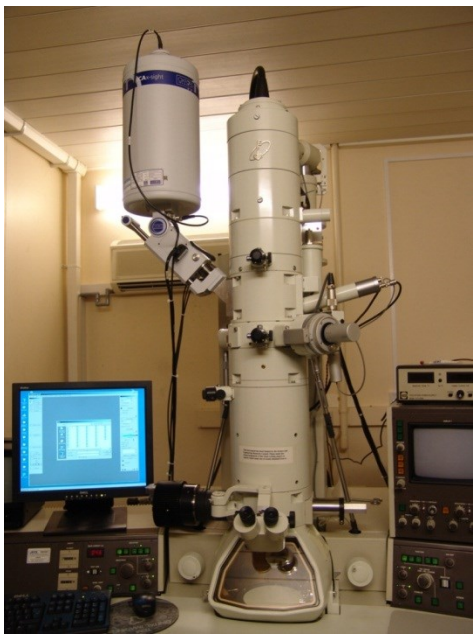

Fig. 7.14 Transmission electron microscope (JEOL JEM1200 TEM)

7.3 RESULTS AND DISCUSSIONS

7.3.1 SEM MICROSTRUCTURE OF EPOXY ADHESIVES

The SEM microstructures of four types of epoxies investigated in this study were presented in Figure 7.15. An overview of the microstructure that was taken at the lowest magnification indicates that all samples were porous with numerous air voids. It is noted that these air voids could probably be eliminated by degassing procedure before casting the adhesive film. However, that practice would produce a material which is not representative to the true nature of the material during application. At 20x magnification, very faint marks of agglomerates of filler embedded within the resin matrix were observed particularly for RSA and EA (Fig. 7.15a and 7.15b). As for Timberset and Sikadur, the rigid micro particulate embedded within the resin matrix was more defined due to its large size and density. The micro-sized rigid particulate of Sikadur is more closely packed than Timberset as indicated in Figure 7.15d suggests Sikadur as a highly-filled adhesive system.

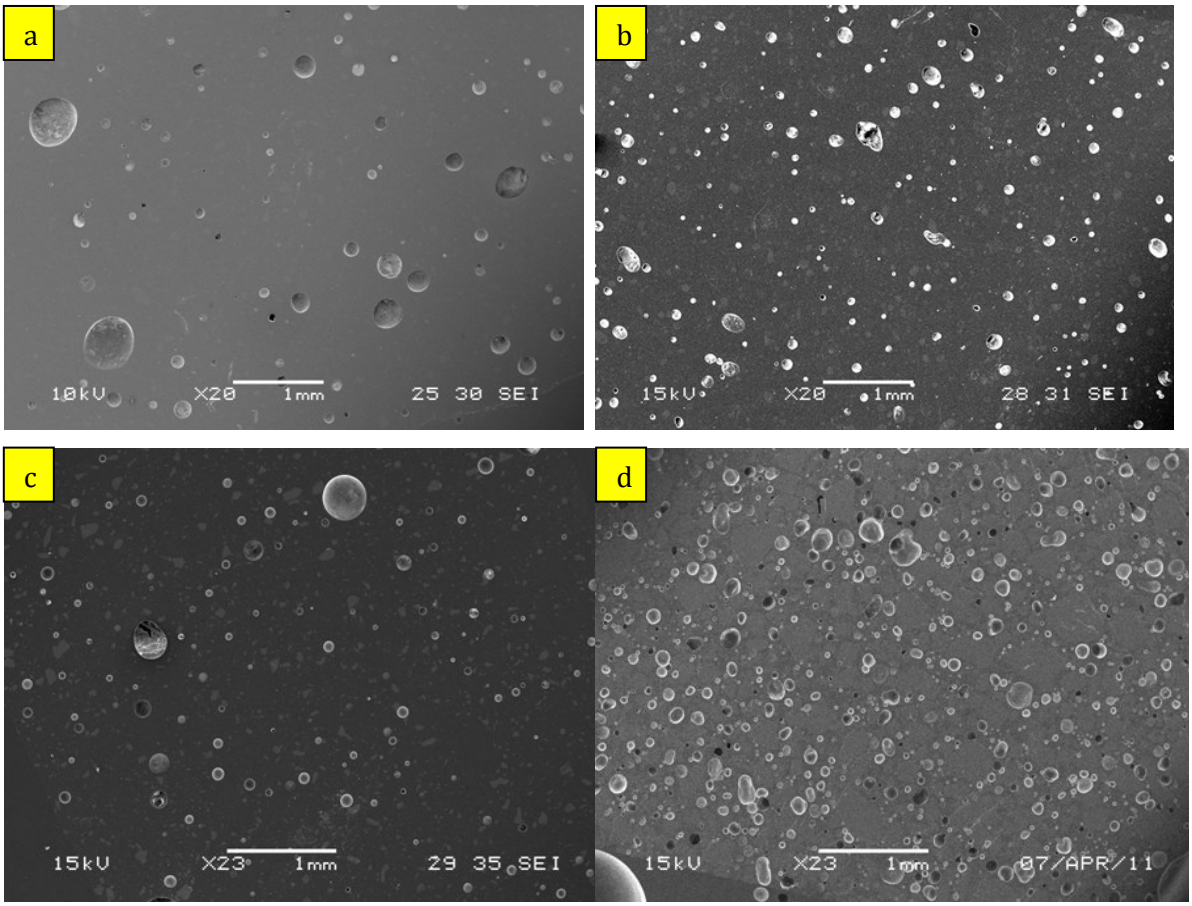

Fig. 7.15 SEM Micrographs of (a) RSA (b) EA (c) Timberset and (d) Sikadur at various magnifications.

Figure 7.16 and 7.17 depicts the micrographs of RSA and standard EA at 600x magnification. Bright patches indicating areas with higher density of silica is marked throughout the surface of material. The rounded-edge patches are the evidence of silica agglomerates within the more evenly distributed nano-silica region. The agglomerates were mainly of individual particles of nano-size silica fume which has been clumped together during the process of curing. The size of the agglomerates of silica is in a range of 10 µm to 40 µm in diameter. As for Timberset and Sikadur (Figure 7.18 and 7.19), the edges of the particles were mainly sharper and more defined. These are mainly of fragments of individual micro-sized particles which were embedded within the resin matrix. Size of these particles ranges between 5 µm to more than 60 µm in length. The perimeter of these particles indicates that it is not as integrated into the resin matrix as the nano-size particles of RSA and EA. Figure 7.19a and 7.19b which indicate the micrography of Sikadur showed cracks along the perimeter between the high-density filler particles and lower density resin matrix. The formation of cracks suggests the evident of residual stress due to external force or heat gradient and differences in the thermal expansion coefficient of the micro-particles and the adhesive matrix.

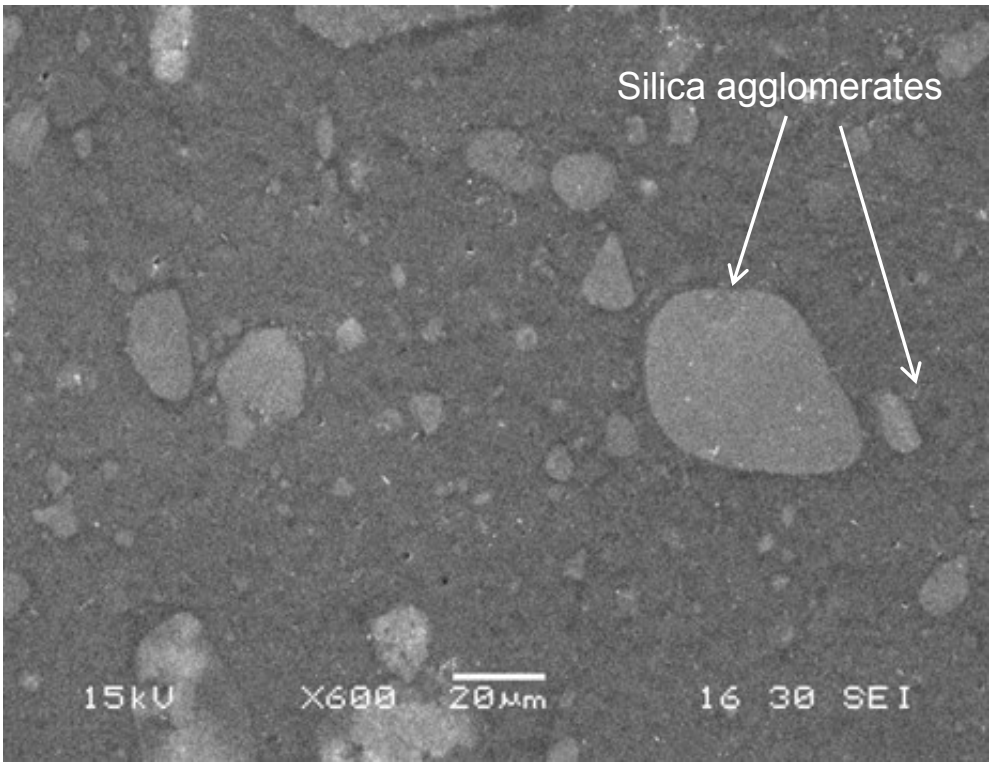

Fig. 7.16 SEM of RSA at 600x magnification indicating silica agglomerate regions

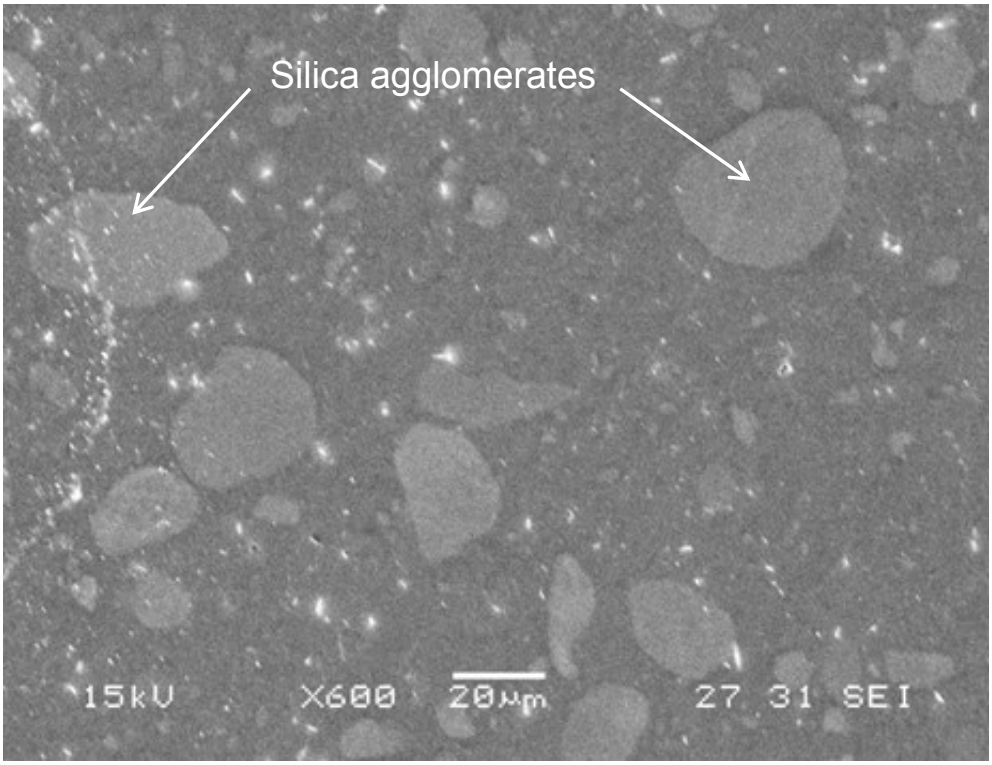

Fig. 7.17 SEM micrograph of EA indicating silica agglomerates

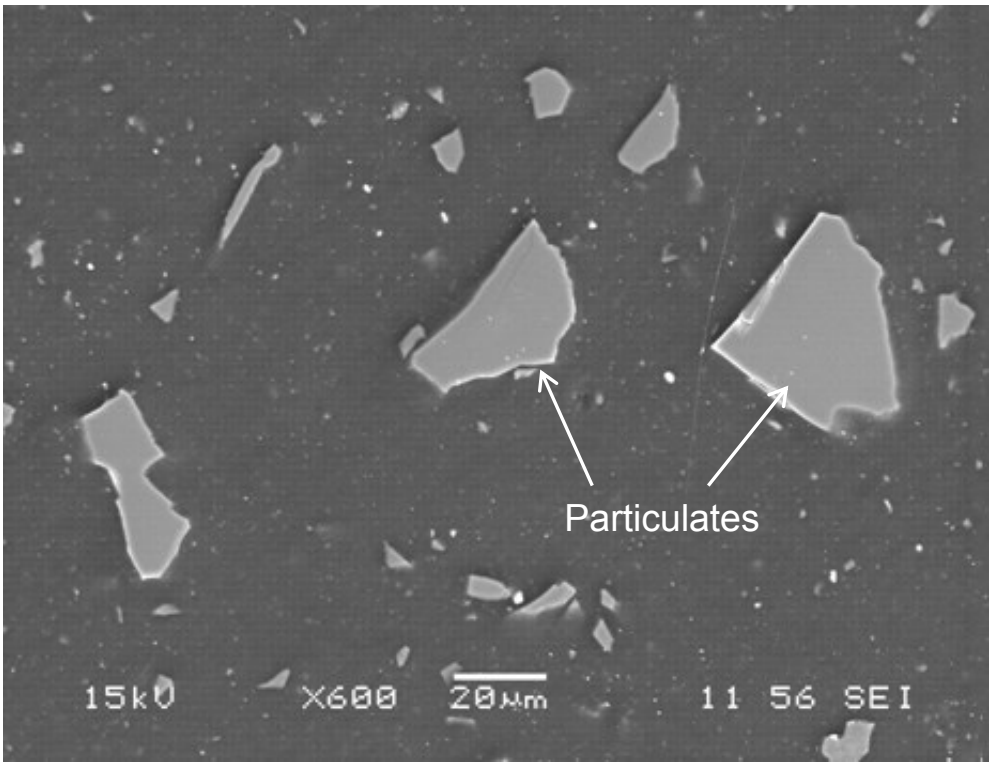

Fig. 7.18 SEM micrograph of Timberset indicating rigid micro-sized particulates

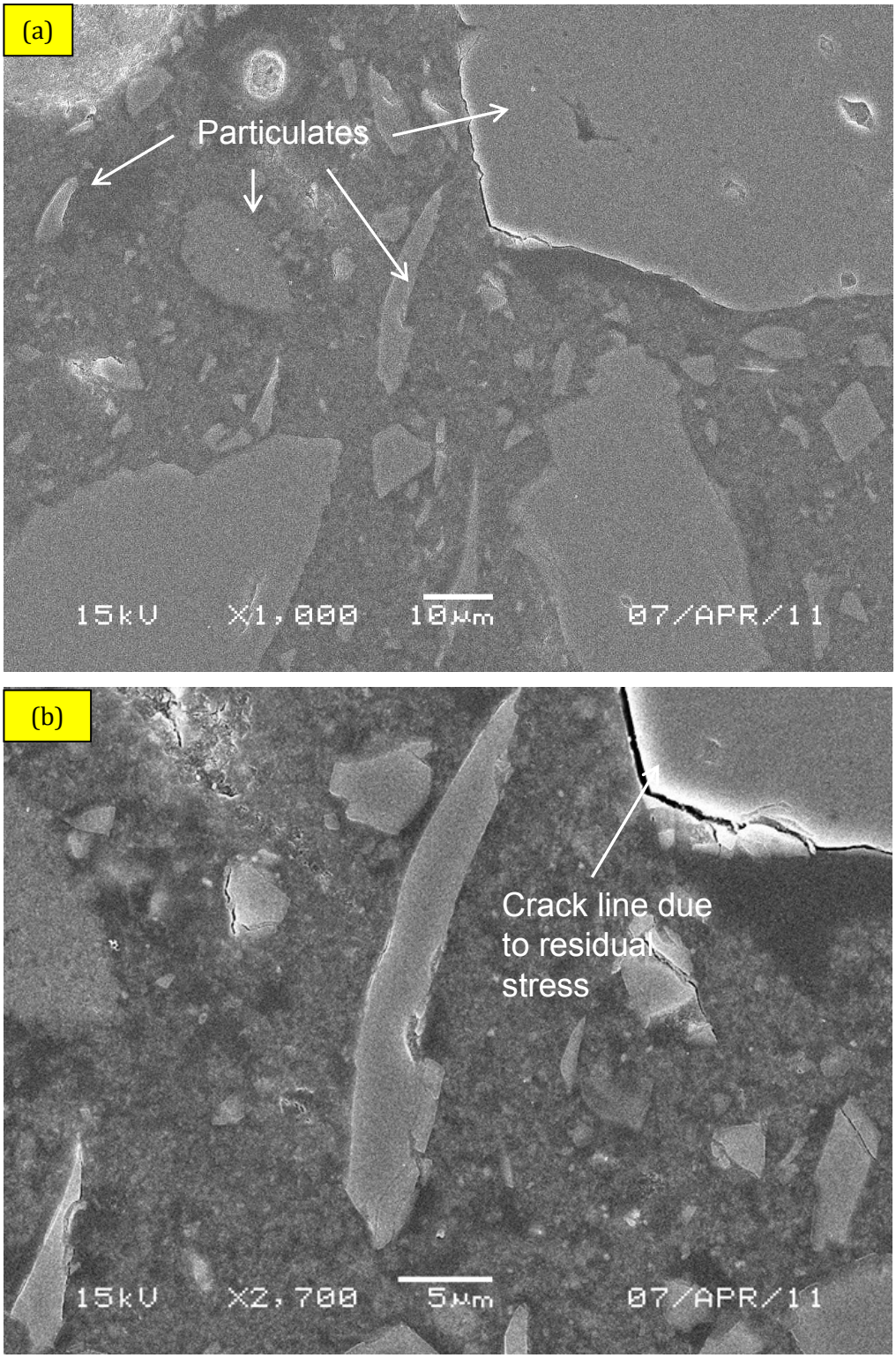

Fig. 7.19 Crack line due to residual stress between high density filler and lower density filler area within Sikadur.

To determine the element composition of the sample, a method called energy dispersive spectroscopy was adopted. Some of the absorbed energy during the SEM process causes ionisation. The ionisation later stimulates the emission of characteristic X-rays from each element. The energy of these photons was then measured as it interacts with the detector. Spectrum of counts over an energy range can be derived to determine elemental composition. For each adhesives understudy, the images of qualitative and quantitative map on different elemental composition were presented. The quantitative mapping was analysed based on peak area. Using the INCA software each element can be accurately mapped or analysed at high count rates. The application of double coating technique (gold and carbon) in this study was to identify areas which contain voids and to characterise surface topography of the sample.

Figure 7.20 indicates the spectrum images collected from RSA which contains silica nano-particles. Electron micron image of RSA indicates quantitative mapping of the sample which included a spherical void area (bottom left hand side). Areas which were previously identified as silica agglomerates were confirmed to be region of high Silicon (Si) density. In this figure, regions of high silica concentration were marked with bright green and red. In addition to silica, other element such as Oxygen (O) is detected, coinciding with the area which contains high silica density. Traces amount of Chlorine (Cl) was also detected. Since the resin base of RSA is synthesized from diglycidyl ether of bisphenol-A/ or bisphenol-F and epichlorohydrin, the presence of chloride ions is expected. It is a desirable trait for an adhesive system to achieve trace amount of chlorine since it would affect the wettability of resin matrix to the particle filler. High concentration of gold within the spherical region indicates void area. Carbon element was presented as qualitative map since the sample was previously carbon coated. The image indicates lesser intensity of carbon within the area which coincides with high silica regions.

Figure 7.21 indicated that the most common elements present in EA sample were Carbon (C), Oxygen (O), Silicon (Si), and Gold (Au). It is assumed that there would be higher content of carbon in EA as compared to RSA due to the inclusion of liquid rubber. The qualitative map image presented for Carbon element indicates the intensity of the element within the sample. The spectrum image of Silicon also indicates regions of high and low

intensity area. In addition to these elements there was also a trace of Chlorine (Cl) which is most likely from the resin matrix. The presence of the Gold of high intensity within the void region is expected due to the application of the sputter coating with the remaining elements part of the adhesive system.

Spectrum images collected from Timberset sample containing macro size rigid particulates is presented in Figure 7.22. Similar element contents of Carbon (C), Oxygen (O), Silicon (Si), and Gold (Au) were detected by the spectrum. The evidence from Figure 7.22 also suggested the presence of high intensity of silica within the micro-sized particulates. In between these micro particles were region of lower silicon intensity which might be attributed to the presence of nano-size silica particles. Traces of gold were expected due to the application of the first layer of coating. It is assumed that the topography of Timberset is not as flat as RSA and EA due to the thickness of the macro particulates which is marked by the presence of gold.

X-ray mapping Sikadur provides quantitative data which indicates that the highest silica intensity was mainly of the macro-size particulates (Figure 7.23). Elements of Carbon, Oxygen, Silicon and trace amount of Chlorine were also detected. An additional element of Calcium was also detected for this sample. It is noted that high intensity of calcium element was observed within the area surrounding the silicon-rich micro particulates.

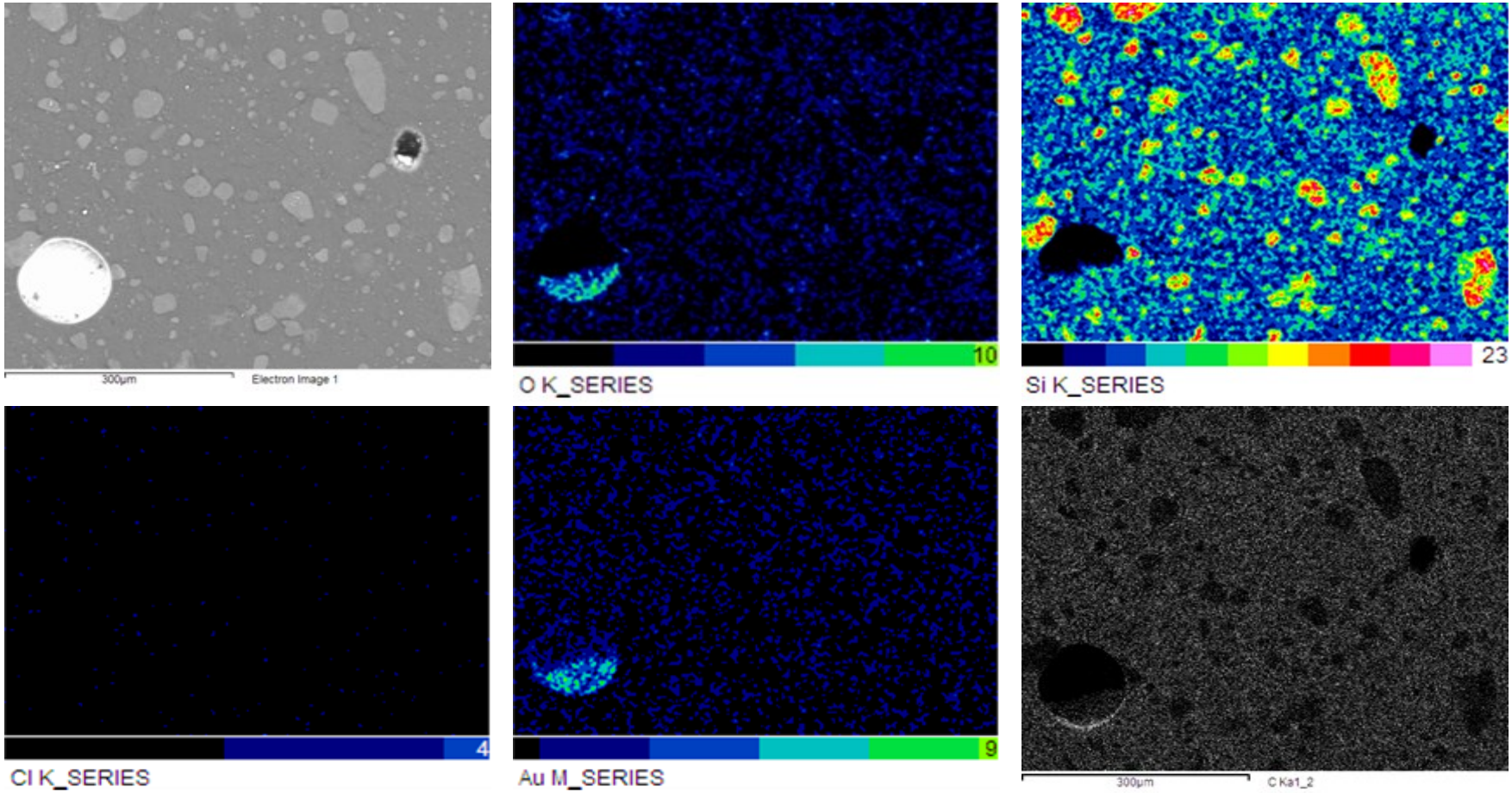

Fig. 7.20 Qualitative and quantitative mapping of Rotafix Structural Adhesive (RSA)

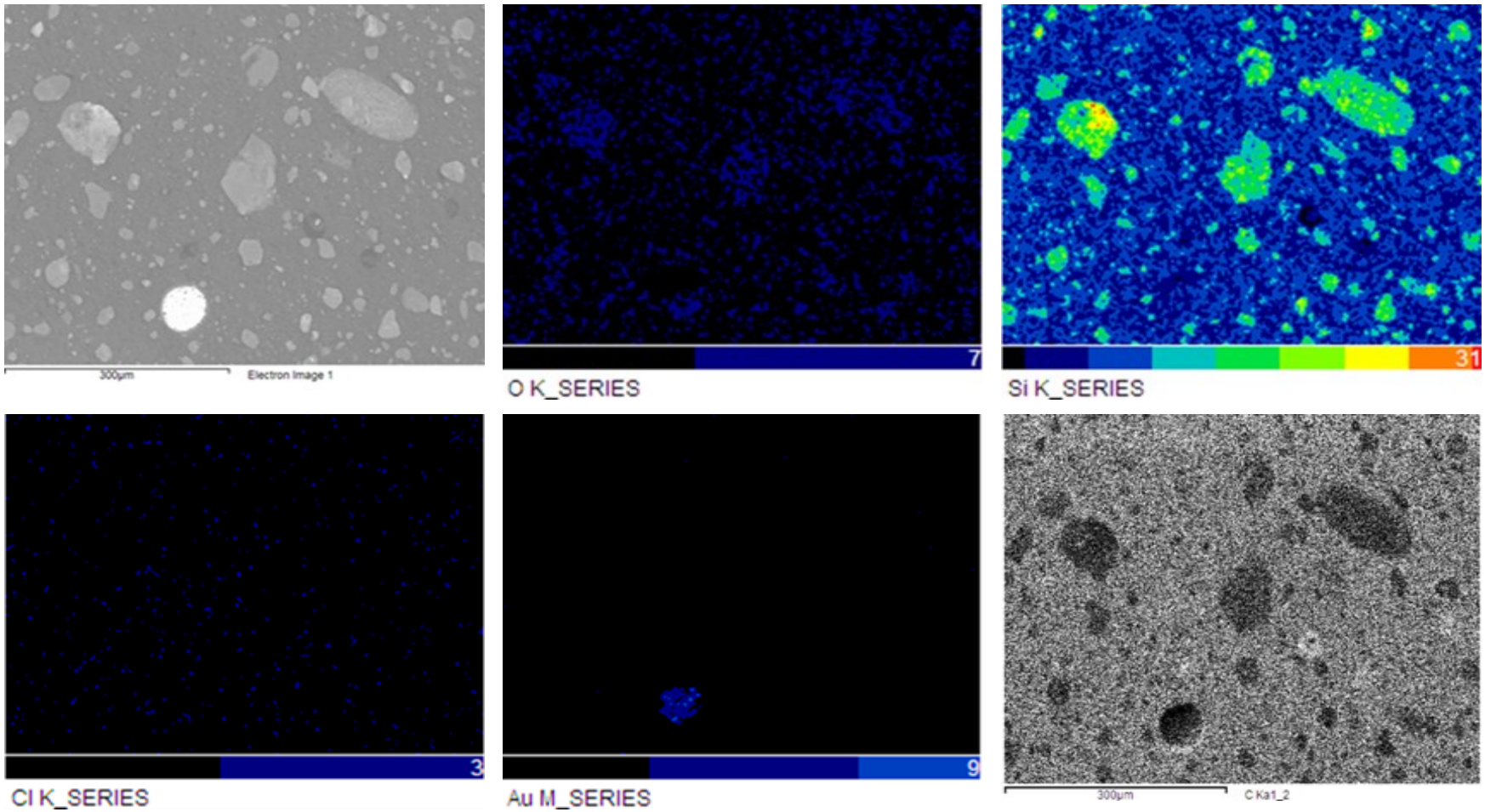

Fig. 7.21 Qualitative and quantitative mapping of Engineering Adhesive (EA)

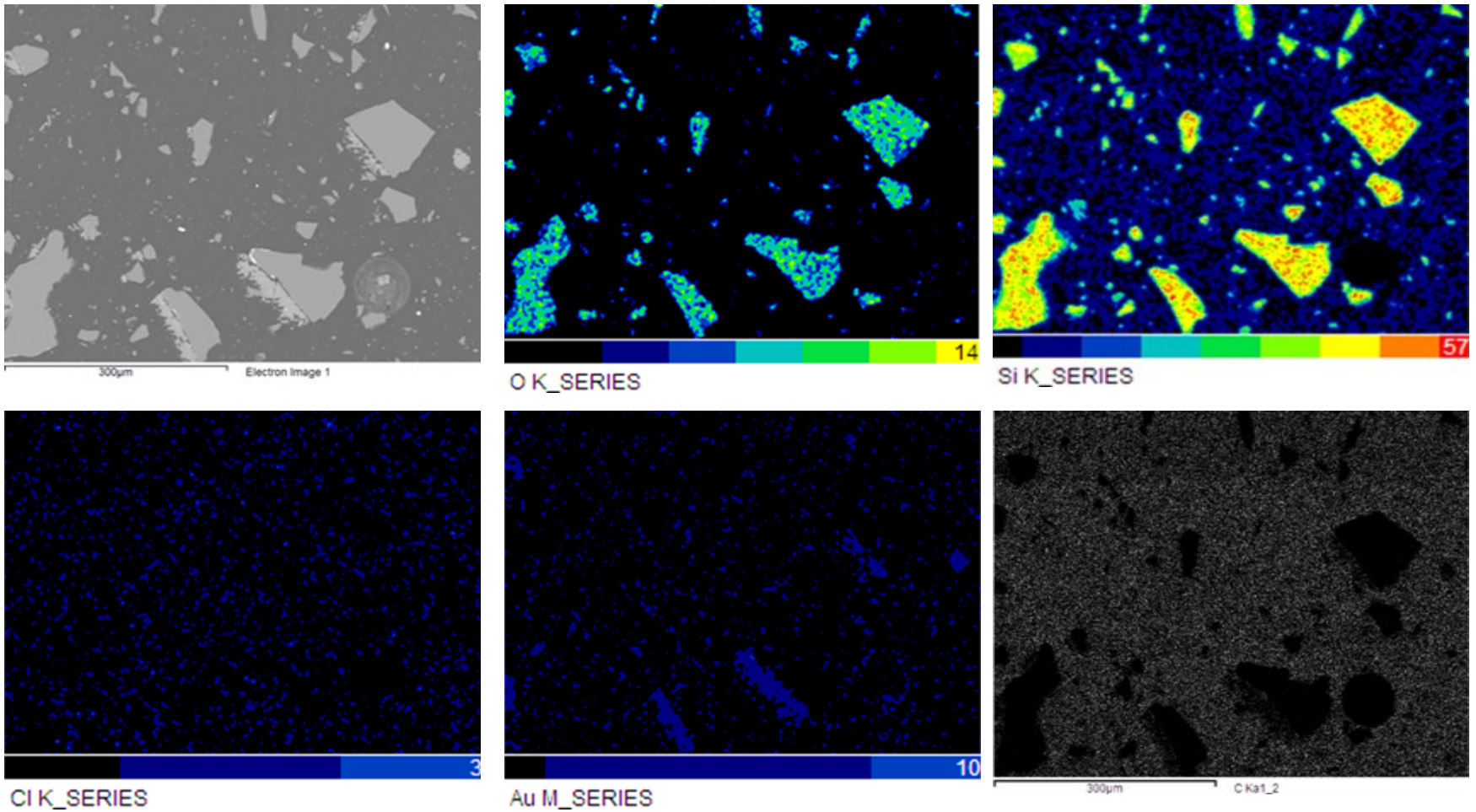

Fig. 7.22 Qualitative and quantitative mapping of Timberset

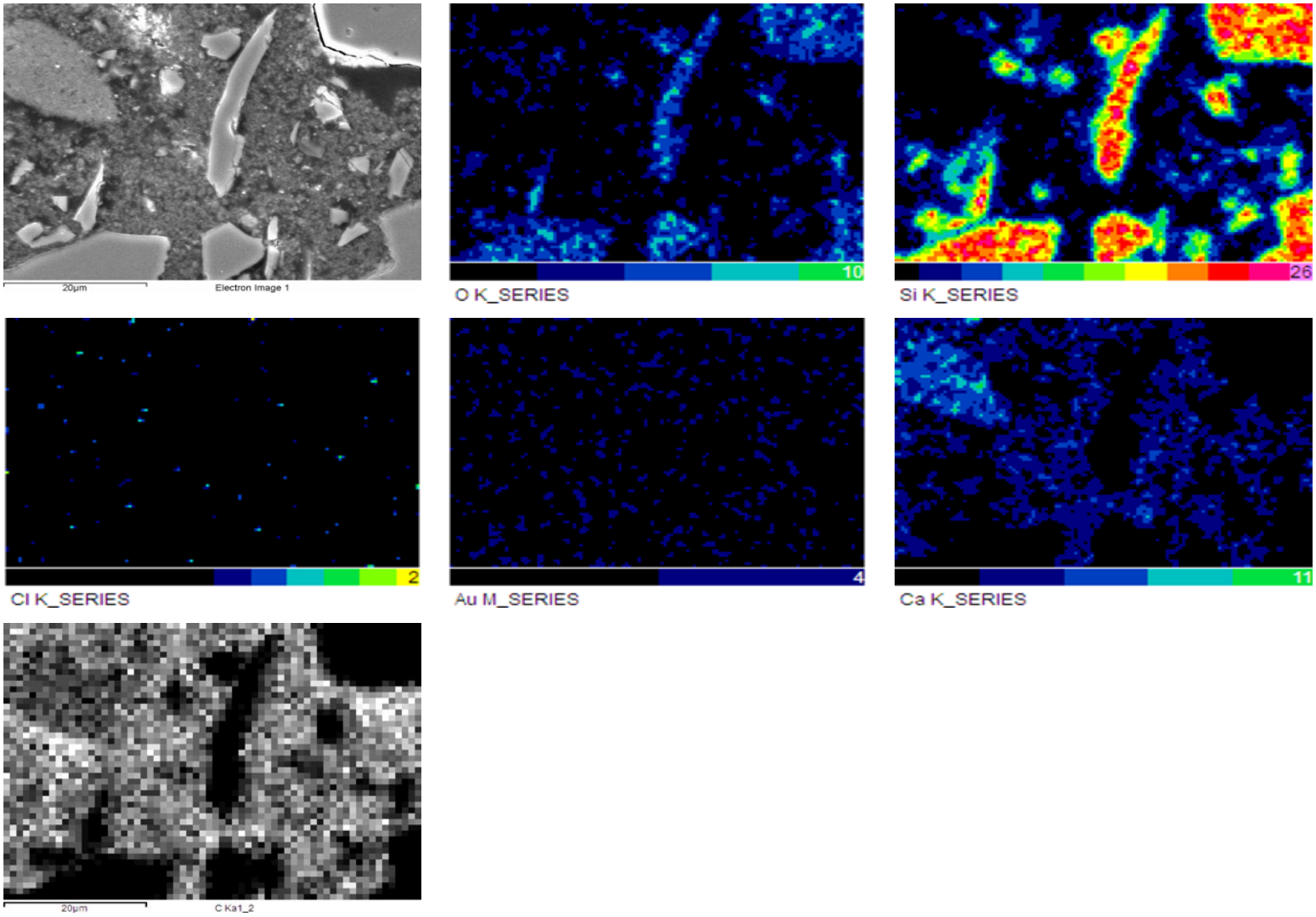

Fig. 7.23 Qualitative and quantitative mapping of Sikadur

7.3.2 TEM MICROSTRUCTURE OF EPOXY ADHESIVE

The microstructure of Rotafix Structural Adhesive (RSA), Engineering Adhesive (EA) and Albipox 3001 has also been observed using Transmission Electron Microscope (TEM). The microstructure of RSA and EA are similar due to the presence of silica fume. Referring to Figure 7.24, the RSA and EA are characterised as a matrix resin with a semi-diffused distribution of silica fume particles. Uneven shaped silica agglomerates defined as highly-dense area of silica were identified throughout the sample. The shape and size of agglomerates for both of the formulations were rather inconsistent without any specific patterns or size range. One distinctive features of silica agglomerate region of RSA is the boundaries are more clearly defined. Boundary of EA's agglomerate regions was more diffuse. The reason for this was detailed later in the report. Between these patches of silica agglomerates were inter agglomerates region where the silica fume is considered less dense and more evenly distributed.

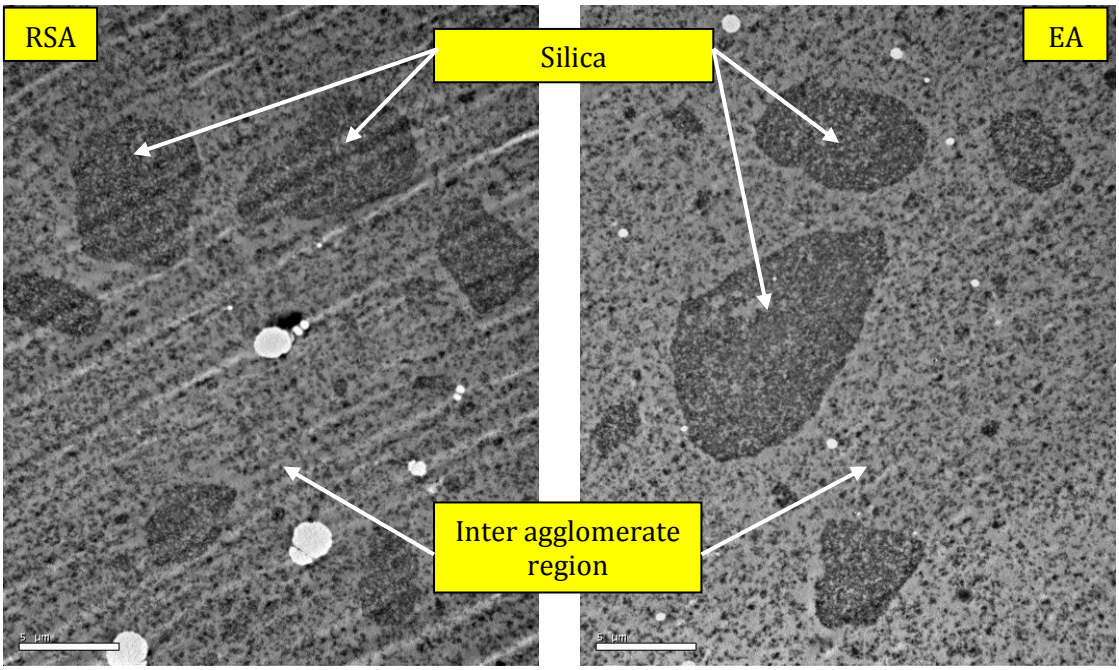

Fig. 7.24 Microcharacterisation of Rotafix Structural Adhesive and Engineering Adhesive which indicates silica agglomerates and inter agglomerate region (TEM micrographs at 5μm).

The agglomerates and inter agglomerate regions are confirmed to contain silica by x-ray analysis. Figure 7.25 show that the agglomerates contain higher density of silica than the inter-agglomerate regions.

Occurrence of silica agglomerates and inter agglomerate region has proven that there is less homogeneity within the modified polymer. During the mixing process, the silica fume is in dry powder state which is then mixed with the resin. The nanoparticle of silica fume has the tendency to stick together due to inter-particle attraction caused by 'van der Waals' forces which originated from the particle's surface energy. As indicated by Rong *et al*. (2001), it is important to obtain a homogenous microstructure since the distribution of particle will determine wear performance of the modified polymer. A study by Wetzel *et al*. (2003) has reported that large agglomerates within the polymer will induce failure since the propagating crack would encounter stress concentration and localisation. This will lead to the initiation of matrix failure. Homogenous distribution of nanoparticles can be achieved through proper particle mixing techniques**.** One of the most established method is using chemical via sol-gel technique. The particles undergo surface modification to produce agglomerate-free colloidal dispersion of nanoparticle in the resin. Other techniques include mechanical mixing such as dissolver technology (rotating disc), rotorstator-system or grinding effect of ceramic balls. The mechanical techniques apply high shear forces that will break up the agglomerates.

Higher magnification TEM on nano sized particles of silica has shown them to be spherical in shape (Figure 7.26). Similar findings have been reported by Imanaka*et al*. (2001), Kwon *et al*. (2008b) and Zhang *et al*. (2008). The nanosilica had a diameter of 20 nm to 25 nm as indicated in Figure 7.26c. Nanoparticles are proven to have superior properties in terms of mechanical strength and stiffness due to its high interface area that is in contact with the matrix as compared to the micro or macro size particles. A variety of tones of particle colours has indicated that the distribution of nanospheres is multilayered which indicates an uneven distribution of particle. The shape and size of a single particle was of a lighter colour tone. A lengthy discussion on the silica fume has been made due to its predominance within the matrix resin. The presence of rubber particles within EA resin was observed to be non-existent. The presence of rubber particle can only be observed if there is more than 3% by weight basis within the resin.

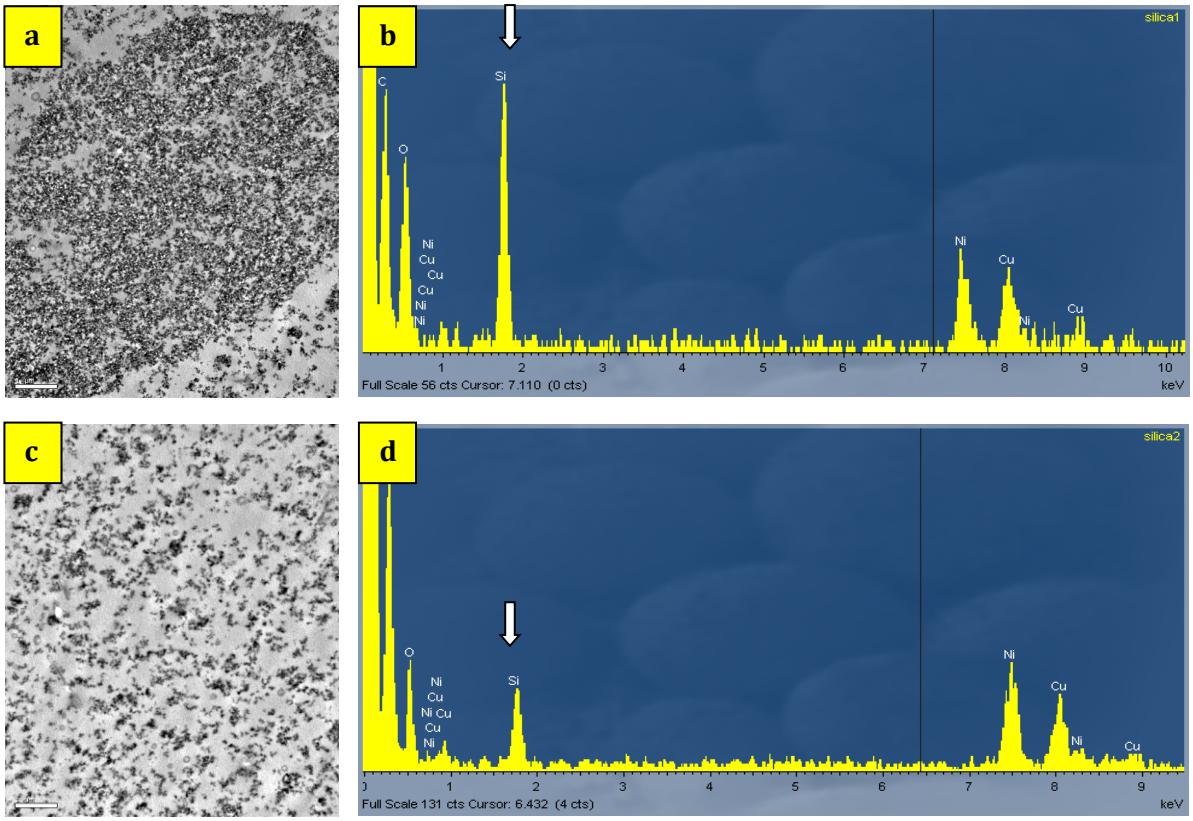

Fig. 7.25 X-ray spectrum of RSA silica-containing regions : (a) silica agglomerates (1µm), (b) x-ray spectrum of a silica agglomerate region, (c) inter-agglomerate region (1µm) and(d) the spectrum of inter agglomerate region. Silica peaks for both of the spectraare marked with arrow.

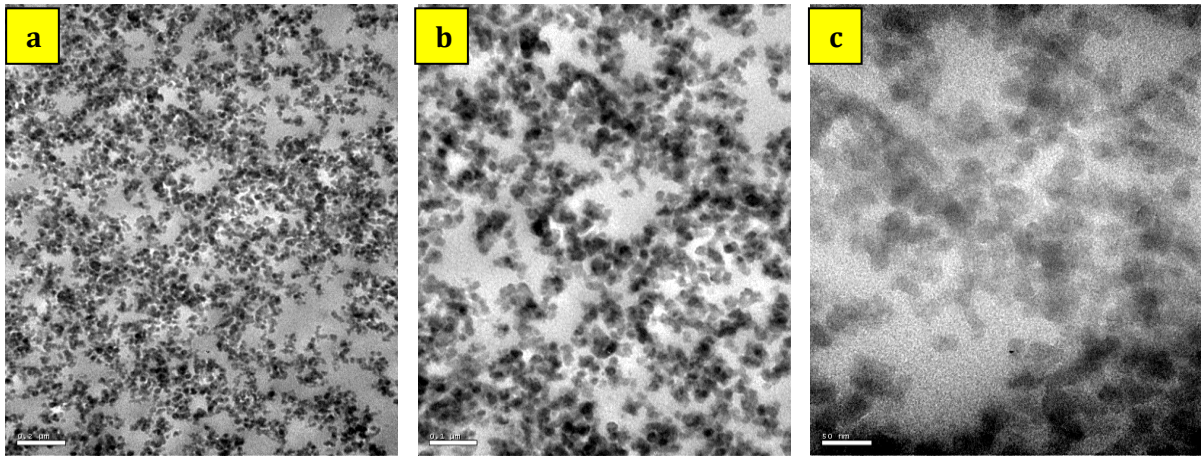

Fig. 7.26 Various magnifications of RSA silica fume at (a) 0.1µm, (b) 0.2µm and (c) 50nm. Darker coloured particles indicate multi-layered particles.

Albipox is mainly characterised by matrix resin (epoxy) and rubber particles (Fig. 7.27). The rubber particles are identified as spherical domain within the matrix resin and similar findings have been reported in various studies (Chen and Jan, 1992, Arias *et al*., 2003, Russell and Chartoff, 2005). The spherical domain is a rubber-rich phase. Due to

the phase separation between rubber (CTBN) and epoxy during curing of the resin, globular particles of rubber were formed. Rubber particles could be observed by using a TEM. The diameter of particles is between 2 μm to 5 μm. As indicated by Manzione and Gillham (1980), phase separation is likely to begin at cloud point and completes at gel point. During phase separation, the rubber particles will coalesce to a form larger particle before reaching gelation stage as occurred in the Figure 7.27a. Due to absence of silica fume, rubber particle is clearly visible. For phase separation to occur there must be a sufficiently high concentration of CTBN. At lower concentration the CTBN is held in solution.

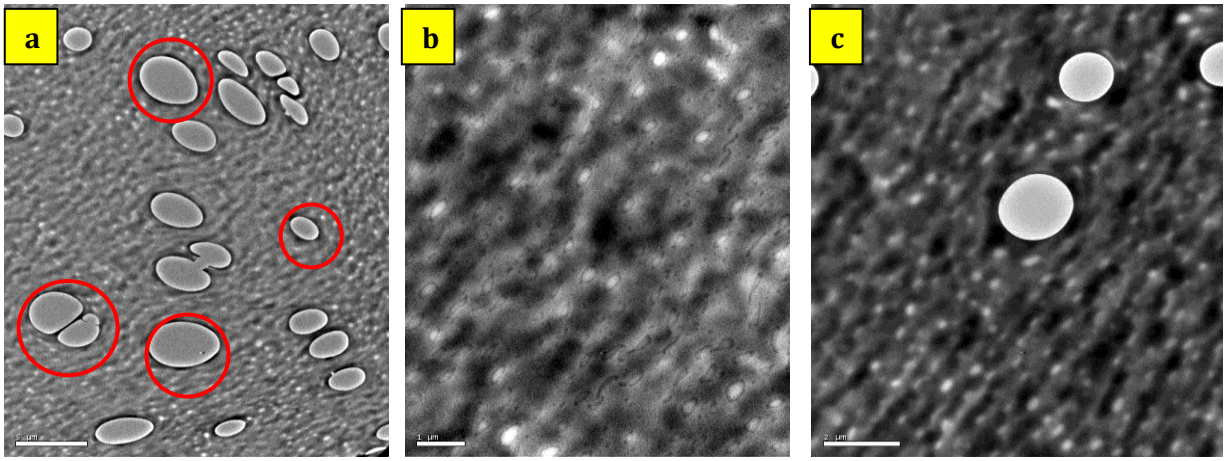

Fig. 7.27 Phase separation in Albipox 3001 resin between CTBN and epoxy resulting globular particles of rubber (encircled) at various magnifications (a) 5μm, (b) 1μm and (c) 2μm.

7.3.3 DISTRIBUTION OF SILICA FUME AND RUBBER CONTENT

In this study, two other types of Engineering Adhesive (EA) were prepared as to be compared with the standard formulation. The differences between these formulations were the amount of CTBN content within the resin. The CTBN content of the standard formulation was 2.5% (EA) but special formulations were produced with and an increased content of CTBN of 6.5% (EA S1) and 12.5% (EA S2) respectively. Overall, the microstructure of the resin appeared similar. Silica agglomerates were visible but a more diffuse distribution of silica was observed within the inter-agglomerate region. Phase separation was not observed.

Focus was given on the boundary region of the silica agglomerates. As referred to Figure 28, the boundary region of standard EA appeared more defined. At higher content of CTBN, the boundary was less visible with silica in some parts appeared partly diffused. At 12.5%, the distribution of silica fumes between agglomerate and inter agglomerate region is more diffused. As depicted in the far right image of Figure 7.28, the region of silica agglomerate (lower right corner) and inter agglomerate region (upper left corner) is almost indistinguishable.

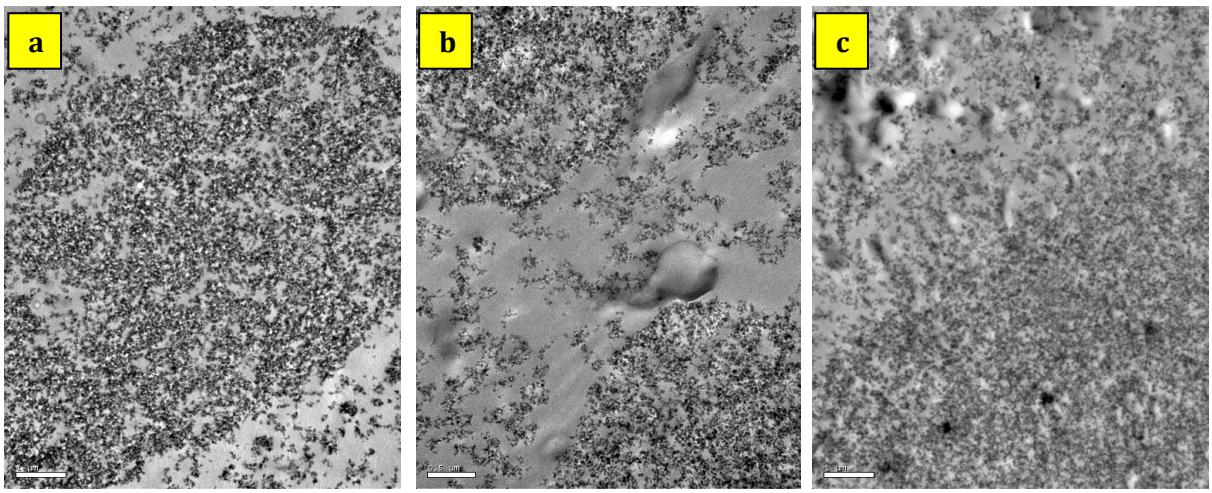

Fig. 7.28 TEM images of various composition of CTBN within EA : 2.5% (a), 6.5% (b) and 12.5% (c). Magnifications : (a) 1µm, (b) 0.5µm and (c) 1µm.

7.4 CONCLUDING REMARKS

Experimental study on the microstructure of epoxy based adhesive was performed and presented in this chapter. Scanning Electron Microscopy and Transmission Electron Microscopy was used extensively to characterise the adhesive. Further investigation using X-ray mapping technique in evaluating the element compositions of the adhesives was also used in this study. These investigations have enables the following conclusion to be drawn for each adhesive under study as presented below:

Rotafix Structural Adhesive (RSA):

- SEM study indicates that RSA contains patches of silica rich region surrounded by more evenly distributed silica region. This is caused by uneven mixing method and the tendency of the nano-silica particle to clump together due to Van de Walls attraction.

- Element composition study as indicated by quantitative and qualitative X-ray mapping exhibited traces of Silicon, Oxygen, Chlorine and Carbon.
- TEM study indicates nanoparticles silica as a spherical shaped object with a diameter between 20nm to 25nm.

Engineering Adhesives (EA):

- Similar microstructural properties to RSA. SEM micrographs indicate the coexistence of silica agglomerates and evenly silica distributed regions. Rubber phase separation is not visible by SEM method.
- TEM investigation indicates presences of spherical shaped nano-silica. Phase separation was not visible on all EA samples under investigation (standard and CTBN content modified) due to the presence of nano-silica fume. Phase separation is only visible on Albipox 3001 sample which contains 15% liquid rubber CTBN due to the absence of silica nanoparticles and higher amount of CTBN.
- X-ray mapping indicates high content of Carbon element due to presence of liquid rubber. Other elements such as Silicon, Chlorine and Oxygen were also present.

Timberset

- SEM micrography of Timberset indicates presence of macro-size rigid particulates with individual size of 5μm to more than 60 μm in length.
- Quantitative and qualitative mapping of Timberset shows that the samples contains element of Carbon, Silicon and Oxygen.

Sikadur

- SEM study indicates that Sikadur is made of high-density micro particles.
- Element composition such as Carbon, Silicon, Calcium and Oxygen were detected in the X-ray quantitative and qualitative mapping study.

CHAPTER 8 : MECHANICAL PROPERTIES OF ADHESIVES

8.1 INTRODUCTION

The mechanical properties of four epoxy adhesives are evaluated in this chapter. The three-point flexural test (BS EN ISO 178), inter-laminar shear (ILS) test (EN 658-5:2002 (E)) and single edge notch bend (SENB) test (ASTM D 5045) were used to assess the mechanical properties of the adhesives in bending, shear and fracture modes. These tests employed the application of a 3-point bending load. For three-point bending a minimum span to thickness ratio of 16 was used in order to minimise shear but for the ILS test a ratio of 5 was used in order to maximise the shear stress in the central region of the tested sample. The SENB test sample has a starter crack machined into the lower face of the specimen below the central roller so that the critical stress intensity factor (K_{IC}) can be evaluated. The adhesive specimens were also tested in tension to measure Young's modulus and strength. The effect of post curing on mechanical properties was measured in a continuation of Ahmad's (2008) study where an improvement in mechanical strength was reported following 7, 10, 20, 30 and 40 days of cure. The study suggested that cross-linking in these adhesives is incomplete and continues after the initial 7 days of curing. In the current study the adhesives were exposed to high temperatures (50ºC and 70ºC) for 24hours to promote further cross-linking of the polymer and to shorten the time required to achieve the optimum fully cured state.

8.2 FLEXURAL PROPERTIES

8.2.1 METHODOLOGY

8.2.1.1 Preparation of adhesives

Four epoxy resins were used in this study namely Rotafix Structural Adhesive (RSA), Engineering Adhesive (EA) and Timberset, provided by Rotafix, and Sikadur, marketed by Sika. The epoxies were supplied in two separate containers which contained the resin base and hardener.

The resin base and hardener were hand mixed and a special folding technique was employed to ensure that the two components blended evenly. This technique also

reduced the risk of producing air pockets which would adversely affect the mechanical and structural properties of the prepared samples.

Films of epoxy resin were prepared by compressing the mixture between two metal plates, each with the dimensions of 35cm x 35cm x 4mm. The mixed resin was poured on top of the first metal plate that was earlier treated with release agent. Four small stoppers with the size of 20mm x 20mm x 3mm were placed at the four corners of the lower metal plate before placing the second metal plate on top of it. Stoppers were used to mould the epoxy resin to the required thickness. Pressure was applied by placing weights on top of the metal plates and the resin was left for 7 days to cure.

The epoxy adhesive films were reduced to the required sample size using a band saw. Dimensions of samples complied with British Standards BS EN ISO 178 (Plastics. Determination of flexural properties) as indicated in Figure 8.1.

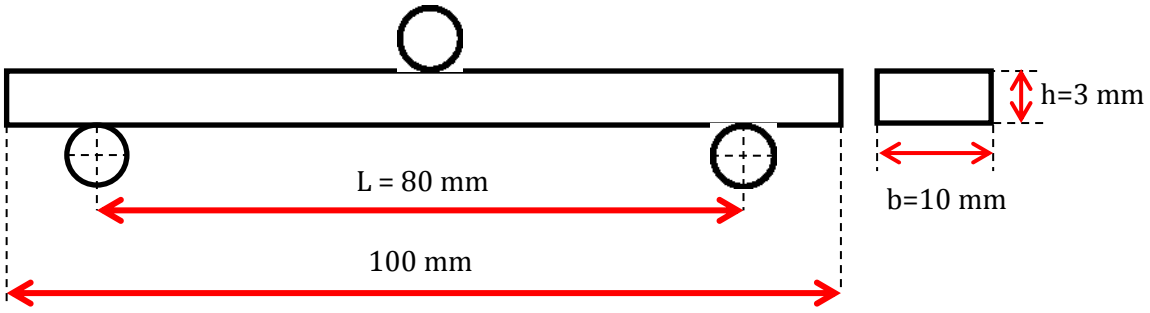

Fig. 8.1 Dimension of flexural sample according to BS EN ISO 178

All samples were left to cure for a further 20 days after the initial seven days. This was to ensure that the resin had fully cured. The RSA samples were also subjected to post curing treatment at 50ºC and 70ºC. The aim was to increase the degree of cross-linking in order to modify Tg and enhance mechanical properties. The treatment matrix indicated in Table 8.1 also applied to samples tested in tension, shear and fracture. Ten samples were prepared for each of the tests.

Table 8.1 Treatment matrix of the adhesives

Sample label		Treatment
Rotafix Structural Adhesive (RSA)	A	20 days curing at temperature 20 ± 3°C
	B	20 days curing at temperature 20 ± 3°C + 50°C post curing for 24 hours
	C	20 days curing at temperature 20 ± 3°C + 70°C post curing for 24 hours
Engineering Adhesive (EA)		20 days curing at temperature 20 ± 3°C
Timberset		20 days curing at temperature 20 ± 3°C
Sikadur		20 days curing at temperature 20 ± 3°C

8.2.1.2 Test configuration

The three point bend tests were conducted using an Instron 3369 Universal Testing Instrument with a 50kN load cell (Figures 8.2 and 8.3). The crosshead speed was set at 1mm/min and the test span was set at 80mm. Data obtained were analysed with Instron Bluehill 2 software. All tests were conducted at a temperature of 20 ± 3°C.

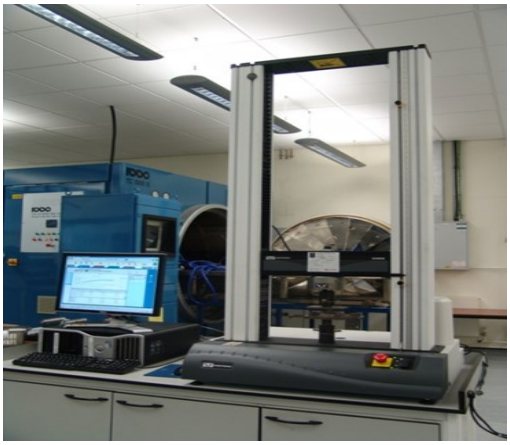

Fig. 8.2 Instron 3369 Universal Testing Instrument

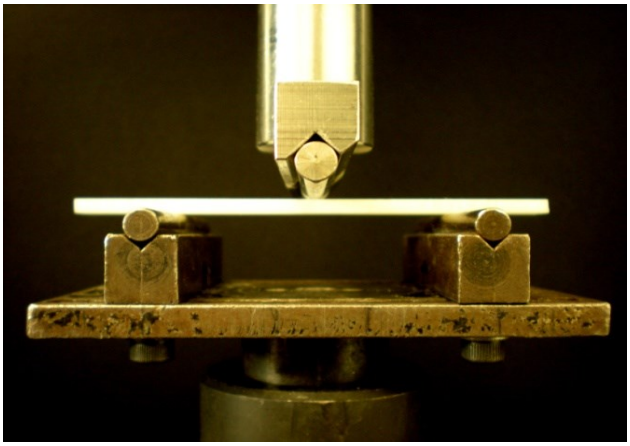

Fig. 8.3 Flexural bending sample under load

The modulus of rupture (MOR) (or flexural strength) and modulus of elasticity (MOE) were calculated using the following equations:

$$\text{Modulus of Rupture (MOR)} = \frac{3\,FL}{2bh^2} \qquad \text{(Eq. 8.1)}$$

$$\text{Modulus of Elasticity (MOE)} = \frac{L^3 m}{4bh^3} \qquad \text{(Eq. 8.2)}$$

where,

F = failure force (maximum flexure load – N)

L = length of sample between the supporting rollers (m)

b = sample width (m)

h = sample thickness (m)

m = slope of load displacement graph (N/m)

MOR and MOE were calculated in MPa.

8.2.1.3 Statistical analysis

Statistical inferences of experiments with more than two levels of a single factor were made using analysis of variance (ANOVA) using SPSS version 19.0. Statistical tests were conducted to differentiate between the mean properties of the adhesives used in the study and also the effect of post curing on the mechanical performance of RSA. ANOVA was calculated assuming that the variances of the groups are homogenous. Before the analysis, the data were subjected to the Levene homogeneity of variance test. Hypothesis testing procedures were as follows:

a. Parameter of interest: The parameter of interest are the mean of mechanical properties ,τ_1, τ_2 and $\tau_3$for RSA post cured sample
b. Null hypothesis, H_0: $\tau_1 = \tau_2 = \tau_3 = 0$, which indicates that all means are indifferent and changing the levels of factor would not affect on the response of means.
c. Alternative hypothesis, H1: $\tau_i \neq 0$ for at least one i
d. Test statistics:

$$f_0 = \frac{MS_{Treatments}}{MS_E} \quad \text{(Eq. 8.3)}$$

where,

$$MS_{Treatments} = \frac{SS_{Treatments}}{a - 1} \quad \text{(Eq. 8.4)}$$

$* a$ is denoted as level or factor (or treatment)

$SS_{Treatment}$ (treatment sum of squares) is verified as:

$$SS_{Treatments} = n \sum_{i=1}^{a} (\bar{y}_{i.} - \bar{y}_{..})^2 \quad \text{(Eq. 8.5)}$$

MS_E (mean square error) is denoted as:

$$MS_E = \frac{SS_E}{a(n-1)} \quad \text{(Eq. 8.6)}$$

where,

SS_E (error sum of squares) is calculated by:

$$SS_E = \sum_{i=1}^{a}\sum_{j=1}^{n}(y_{ij} - \bar{y}_{i\cdot})^2 \quad \text{(Eq. 8.7)}$$

8.2.2 RESULTS AND DISCUSSIONS

8.2.2.1 The effect of types of fillers on flexural properties

Three-point bending of the samples resulted in elastic/plastic deformation of ductile adhesives and elastic fracture of brittle adhesives. During the 3-point bend test samples of RSA-A, EA and Timberset remained bent into a 'v' shape until the samples nearly reached the bottom of the plate due to plastic deformation.

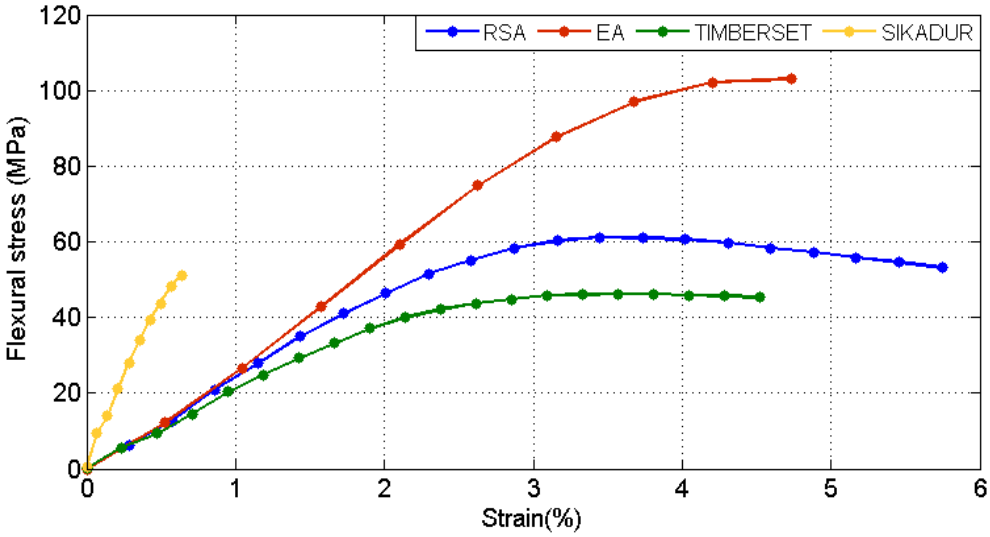

Fig. 8.4 Stress-strain curve of bending tested adhesives.

The stress-strain curve for all four adhesives is presented in Figure 8.4. At the beginning of the test, the curves indicate linearity between stress and strain in the linear elastic region. The proportional limits for the adhesives were EA (~78MPa), Sikadur (~50MPa), RSA (~40MPa) and Timberset (~39MPa). Beyond the proportional limit the peak of the curve is known as ultimate stress and further loading resulted in a reduction in flexural stress before fracture occurred. The adhesives are capable of absorbing large

amounts of strain energy and undergo large permanent strains before fracture as reported by Gere (2006). The behaviour of the Sikadur adhesive can be described as brittle.

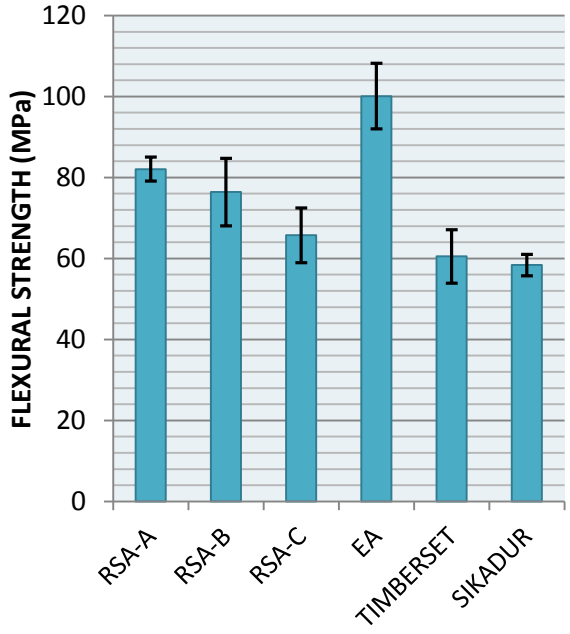

Fig. 8.5 Average bending strength and standard deviations of the adhesives.

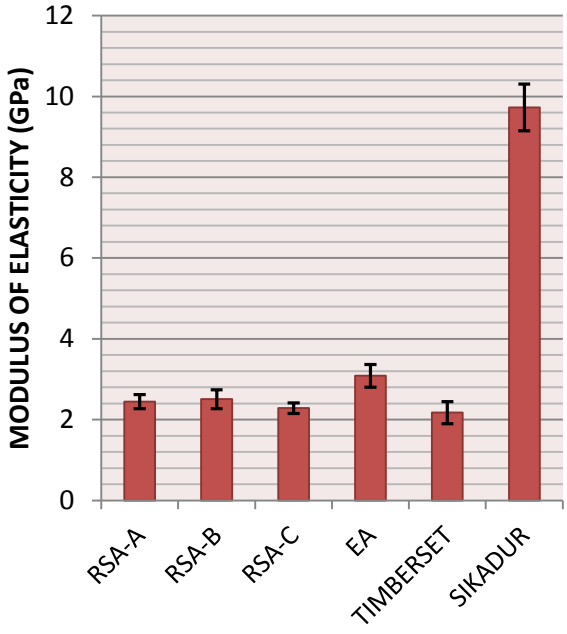

Fig. 8.6 Average modulus of elasticity and standard deviation of the adhesives

The results summarised in Figures 8.5 and 8.6 illustrate the effect of fillers on the flexural strength and modulus elasticity of the adhesives. As indicated in Table 2, the inclusion of nano silica and rubber within EA has resulted in an improvement of 18% in flexural strength as compared to the standard nano-silica containing adhesive (RSA). The positive effect of liquid rubbers on the flexural strength and toughness of epoxy resins has been confirmed in numerous studies (Bussi and Ishida 1994, Nigam *et al*. 1999). Sikadur possessed the lowest flexural strength due to the brittle nature of the material which contains micro-particles but the modulus of elasticity is by far the highest as expected. The flexural modulus of EA is ~20% higher than RSA. This contradicts the work of Ozturk *et al*. (2001) where the rubber modification of diglycidyl ether of bisphenol-A based epoxy resin led to a decrease in elastic modulus.

Table 8.2 Flexural properties of epoxy adhesives

Adhesive	No. of samples	Flexural strength		MOE	
		Mean (MPa)	COV (%)	Mean (GPa)	COV(%)
RSA-A	10	81.85	7.36	2.45	7.13
RSA-B	10	76.40	10.30	2.51	8.23
RSA-C	10	65.74	10.2	2.28	5.65
EA	10	100.01	9.06	3.08	6.06
TIMBERSET	10	60.50	8.91	2.17	10.57
SIKADUR	10	58.37	4.58	9.73	5.94

An analysis of variance at the 0.05% probability level ($p<0.00$) was performed on the MOR and MOE of the different adhesives (Table 8.3). Further analysis by Duncan multiple comparisons in Table 8.4 reveal that there are no significant difference between the flexural strengths of Sikadur and Timberset; but each of these is significantly different to both RSA-A and EA. As indicated in Table 8.5, there is no significant difference between the value of MOE for RSA-A and Timberset.

Table 8.3 ANOVA of flexural properties of untreated adhesives

Flexural properties	F value	p- value
Flexural strength	124.94	0.00
MOE	1117.131	0.00

Table 8.4 Duncan multiple comparison of flexural strength for various adhesives

Adhesive	Subset for alpha = 0.05		
	1	2	3
SIKADUR	58.37		
TIMBERSET	60.37		
RSA-A		81.85	
EA			100.01

Table 8.5 Duncan multiple comparison of flexural MOE for various adhesives

Adhesive	Subset for alpha = 0.05		
	1	2	3
RSA-A	2.45		
TIMBERSET	2.17		
EA		3.08	
SIKADUR			9.73

8.2.2.2 The effect of post-curing on flexural properties

Figure 8.7 plots the flexural stress versus strain (%) of the control RSA and post-cured RSA. In general, the control samples (RSA-A) and post cured samples (RSA-B and RSA-C) deformed in a ductile mode. As indicated in Table 8.2, there was a small reduction in flexural strength of 6.7% for RSA-B and 19.7% for RSA-C compared to RSA-A. The MOE of samples post-cured at 50°C increased by 2.4%. Post-curing of RSA at 70°C which is well beyond Tg, resulted in a reduction of MOE of 6.9%. Analysis of variance (Table 8.6) shows that there are insignificant differences between all mean MOR and MOE values for post-cured and control RSA samples. This study has also shown that prolonged post-curing at temperatures higher than the Tg value of the adhesive will result in the degradation of the polymer correlating well with the results of Ahmad (2008).

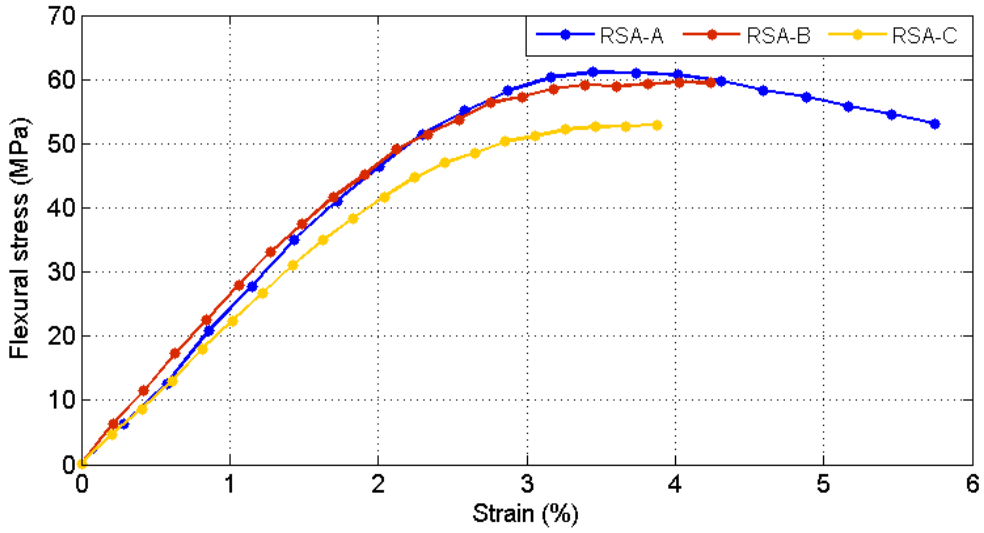

Fig. 8.7 Stress-strain curve of bending tested control and post-cured RSA.

Table 8.6 ANOVA of flexural properties of RSA post-curing treatments

Flexural properties	F value	p- value
Flexural strength	5.15	0.11
MOE	5.72	0.07

8.3.1 METHODOLOGY

8.3.1.1 Sample dimension and test configuration

The adhesive shear test samples prepared according to EN 658-5:2002 (E) have a span to thickness ratio of 5 to 1 (Figure 8.8) in order to promote shear yield. The test is similar to the flexural test except for the span length used which was set at 15 mm (Figure 8.9). The crosshead speed of the Instron 3369 Universal Testing Instrument was maintained at 1 mm/min. All data were analysed with Bluehill2 software and testing was conducted at a temperature of 20 ± 3°C.

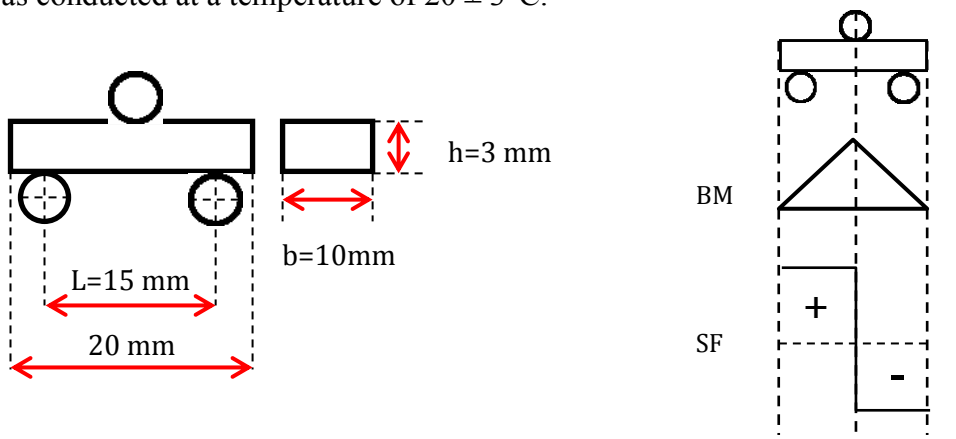

Fig. 8.8 Dimension of ILSS sample according to EN 658-5:2002 (E)

Fig. 8.9 Sample of inter-laminar shear under load

8.3.1.2 Results Analysis

The value of inter-laminar shear strength, ILS, was obtained as follows:

$$\text{Inter} - \text{ laminar shear strength (ILS)} = \frac{3F}{4bh} \qquad \text{(Eq. 8.8)}$$

where,

F = shear failure force (N)

b = sample width (m)

h = sample thickness (m)

8.3.2 RESULTS AND DISCUSSIONS

8.3.2.1 The effect of filler on shear strength

The study of the effect of microstrucure on the inter-laminar shear properties of adhesive was evaluated. RSA samples did not break during the test and continued to bend until they reached the bottom level of the test plate and cracking and stress-whitening was observed on the tensile surface of the samples. EA, Timberset and Sikadur adhesives all fractured as soon as they reached the maximum bending load which resulting in a sharp drop in the load-displacement curve. The results of the ILS tests are summarised in Figure 8.10 and Table 8.7.

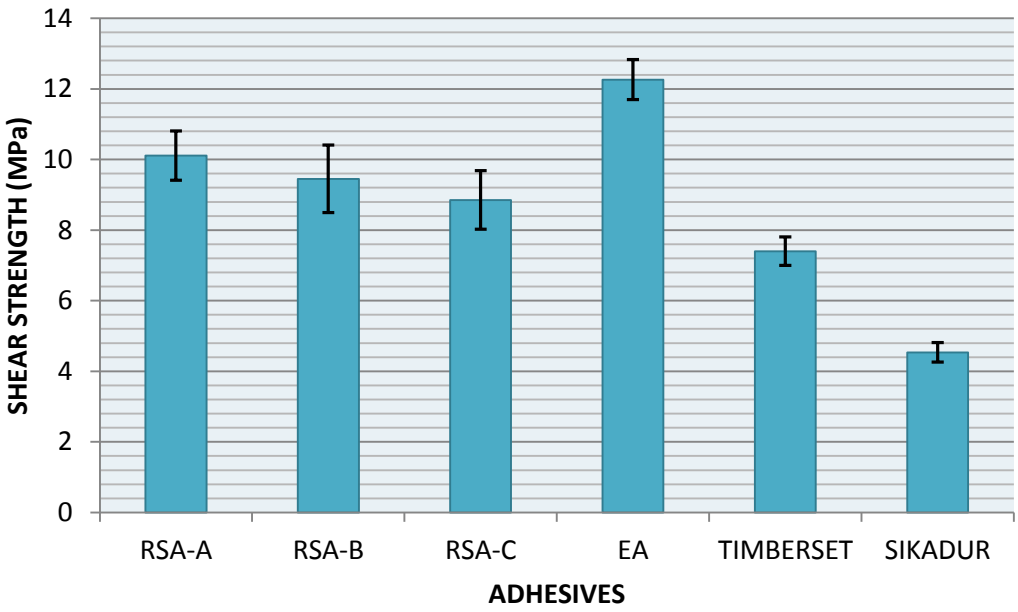

Fig. 8.10 Average shear strength of various adhesives

The rubber particle modification of the epoxy adhesive (EA) has led to an increase of shear strength properties by 17.5% compared to RSA-A. Two epoxy systems (RSA and EA) containing nano-particles possessed the highest shear strength values whilst both the micro particle filled systems (Timberset and Sikadur) exhibited the lowest values.

Table 8.7 Inter laminar shear strength of various epoxy-based adhesive

Adhesive	No. of samples	Inter-Laminar Shear Strength	
		Mean (MPa)	COV(%)
RSA-A	10	10.11	4.22
RSA-B	10	9.45	12.26
RSA-C	10	8.85	9.35
EA	10	12.26	5.53
TIMBERSET	10	7.40	5.50
SIKADUR	10	4.54	6.14

Analysis of variance (Table 8) indicated significant differences (*p-value* <0.05) between the results presented in this study, further supported by Duncan multiple comparison (Table 9) which suggested significant pairwise differences for all the epoxies tested.

Table 8.8 ANOVA of inter-laminar shear strength of various types of fillers

ILSS properties	F value	p-value
Inter laminar shear strength	388.95	0.000

Table 8.9 Duncan multiple comparison of various types of fillers

Adhesives	Subset for alpha = 0.05			
	1	2	3	4
SIKADUR	4.54			
TIMBERSET		7.40		
RSA-A			10.11	
EA				12.26

In understanding these observations, the internal characteristics of composites should be considered. The ILS strength of particulate composite depends on the efficiency of transfer of stress between the matrixes to filler. The filler-matrix interaction is particularly important for nano-filled composites (Wetzel *et al.*, 2003). Large micro-particulate agglomerates within the adhesive result in an uneven dispersion of the filler particles which act as stress concentration sites and initiate crack propagation and failure within adhesives. This study shows that adhesives containing micro-size particules performed poorly in ILS compared to adhesives modified with nano-size particles which impart efficient stress transfer due to the large contact area. Propagating cracks have to interact with nanoparticles before deformation occurs. The addition of liquid rubber CTBN to nano-silica filled RSA adhesive (EA) contributes to enhanced shear strength due to the presence of the dispersed rubber phase. The toughening effect

is due to flexibility of the matrix which promotes shear yielding at low stresses. Similar observations of the enhanced shear strength of rubber-modified epoxies have also been reported by Ratna & Banthia (2000) and Kar & Banthia (2004).

8.3.2.2 The effect of post curing on shear strength

A summary of the ILS strength of the adhesives is presented in Figure 8.10 and Table 8.7. As expected, the samples which were post-cured at 50°C and 70°C prior to testing underperformed considerably compared to control samples. The shear strengths following post-curing at 50°C and 70°C decreased by 6.5% and 12.5% respectively. There were significant differences in shear strength between the treatments (p-value<0.05) based on the statistical analysis summarised in Tables 8.10 and 8.11.

Table 8.10 ANOVA of interlaminar shear strength of RSA post-cured epoxy adhesives

ILSS properties	F value	p- value
Inter laminar shear strength	6.569	0.004

Table 8.11 Duncan multiple comparison of RSA post-cured epoxy adhesive

Adhesives	Subset for alpha = 0.05	
	1	2
RSA - C	8.85	
RSA - B	9.45	
RSA - A		10.11

8.4 TENSILE PROPERTIES

8.4.1 METHODOLOGY

8.4.1.1 Sample Fabrication

The dumbbell-shaped samples for tensile tests were fabricated according to the specification of ASTM D638 (1991). Aluminium moulds coated with release agent (Figure 11) were used to mould the samples which were compressed between 5 mm thick glass plates with weights to the required thickness. The samples were left in the mould for curing at ambient temperature for 7 days. The samples were moulded to a final thickness of 5 mm and width of 10 mm. After the initial 7 days curing, the samples were rigid enough to be removed from the mould. The samples were then subjected to further curing at ambient temperature before tensile testing on the twentieth day. For the tensile test, none of the samples were subjected to the post-curing treatment applied to the flexural and inter-laminar shear test samples.

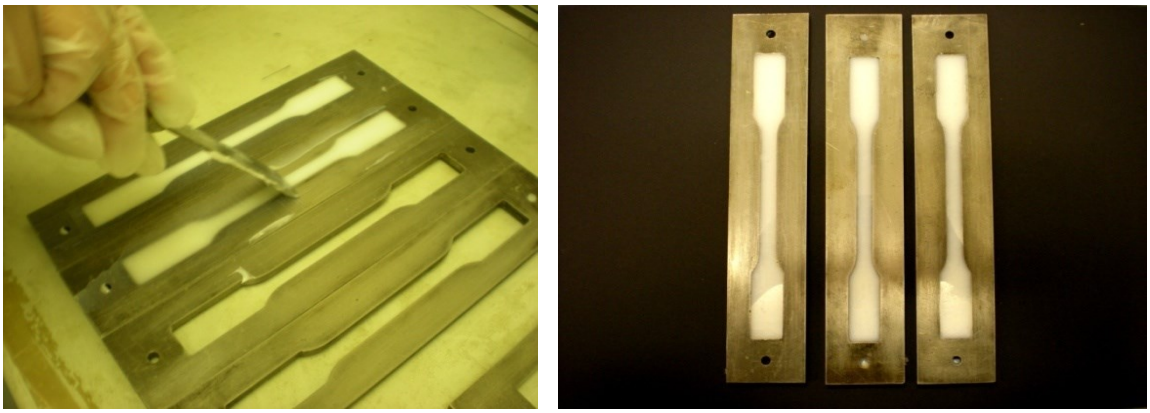

Fig. 8.11 Fabrication of dumbbell-shaped tensile sample

8.4.1.2 Test configuration

The tensile test was performed using an Instron 3369 Universal Testing Instrument equipped with a load cell on 50kN. Strain measurement was made by attaching an Instron extensometer 2630-111 (50 mm) to the mid-span of the dumbbell-shaped sample. The results were recorded and analysed by Bluehill software. Figure 12 shows the test configuration with a sample secured in the wedge grips and fitted with an extensometer. The cross-head speed was kept constant at 5 mm/min until it reached the maximum load. Testing was undertaken at a temperature in the range 20 ± 3°C.

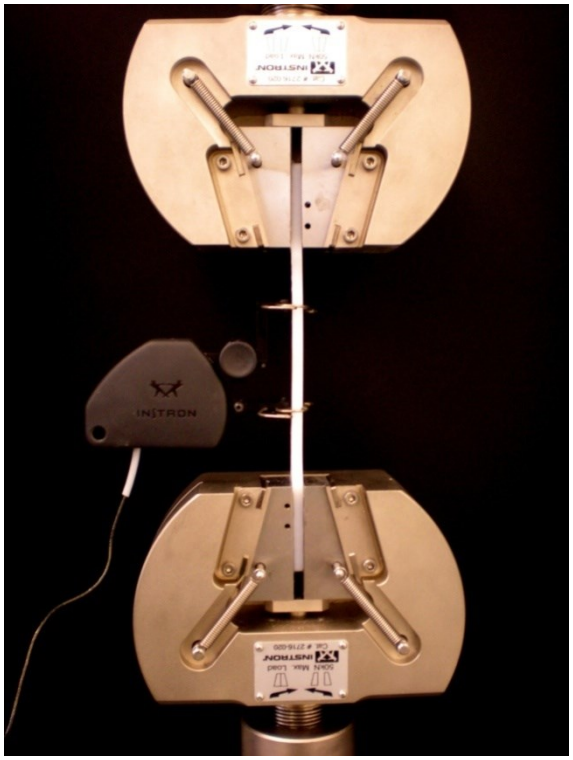

Fig. 8.12 Tensile test configuration

8.4.1.3 Results analysis

The ultimate tensile stress (UTS) and tensile modulus of elasticity (TMOE) were derived from the formulae:

$$\mathrm{UTS} = \frac{\mathrm{P}}{\mathrm{bh}} \qquad \text{(Eq. 8.9)}$$

where

P = Maximum load (N)

b = width of sample (mm)

h = thickness of sample (mm)

and

$$\mathrm{TMOE} = \frac{\Delta\delta}{\Delta\varepsilon} \qquad \text{(Eq. 8.10)}$$

where,

$\Delta\delta$ is the increment of stress

$\Delta\varepsilon$ is the increment of strain

in the linear elastic part of the stress-strain characteristic.

8.4.2 RESULTS AND DISCUSSION

8.4.2.1 The effect of filler on tensile properties

The results from the tensile measurements of RSA, EA, Timberset and Sikadur are plotted as tensile stress versus strain (%) in Figure 8.13. RSA exhibited a linear response up to ~17 MPa which was followed by non-linearity until ductile fracture occurred. Timberset also exhibited similar behaviour before failing at lower stress and strain than RSA. The highest tensile stress was achieved by EA with an almost linear response before breaking at 38.1 MPa. Sikadur exhibited brittle failure at 21.4 MPa.

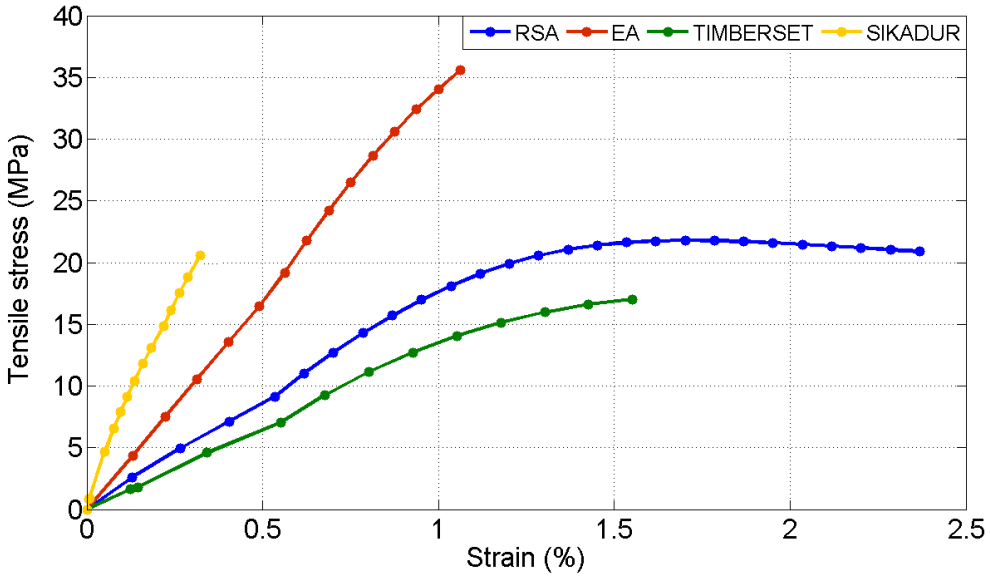

Fig. 8.13 Stress-strain curve of tensile tested adhesives

The values of ultimate tensile strength (UTS) and tensile modulus of elasticity (TMOE) of RSA, EA, Timberset and Sikadur are presented in Figure 8.14, 8.15 and Table 8.12.

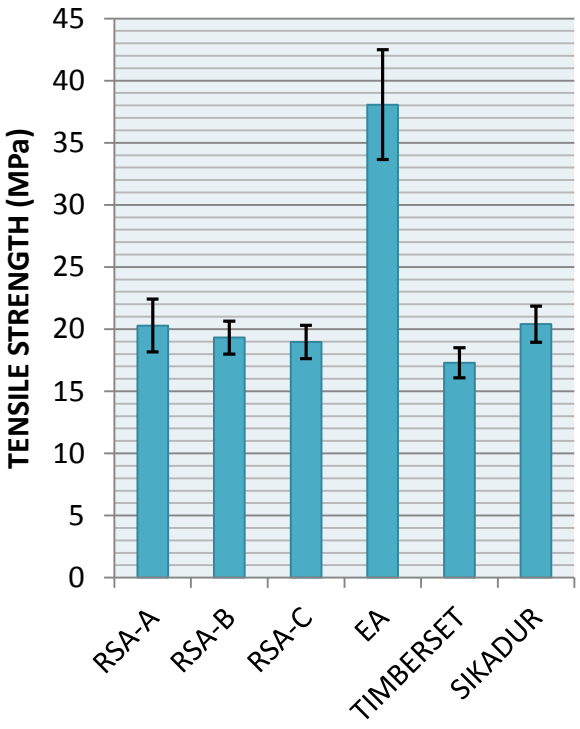

Fig. 8.14 Average tensile strength and standard deviation of adhesives

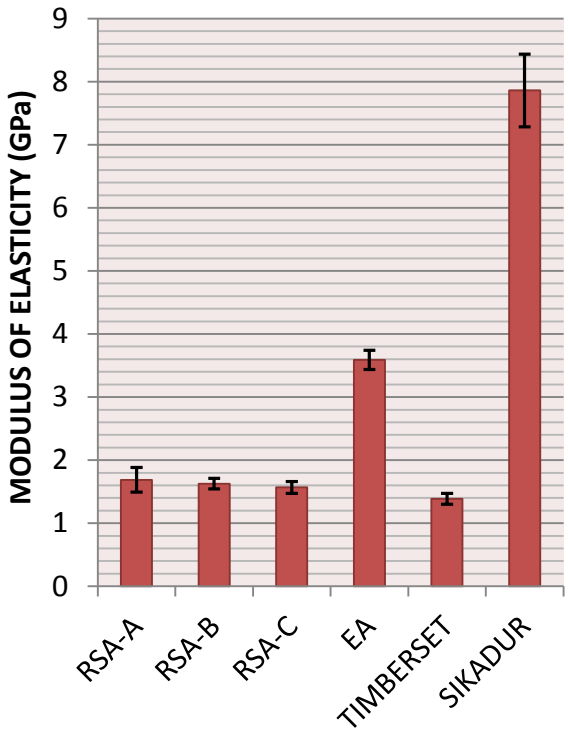

Fig. 8.15 Average modulus of elasticity and standard deviation of adhesives

Table 8.12 Tensile properties of various epoxy based adhesive

Adhesive	No. of samples	UTS		TMOE	
		Mean (MPa)	COV (%)	Mean (GPa)	COV(%)
RSA-A	10	20.29	10.51	1.69	11.57
RSA-B	10	19.31	6.81	1.62	5.08
RSA-C	10	17.97	7.03	1.56	6.03
EA	10	38.07	11.62	3.59	4.29
TIMBERSET	10	17.29	7.05	1.39	6.26
SIKADUR	10	21.40	7.17	6.38	6.25

The rubber-nanosilica hybrid modified epoxy (EA) exhibited improvement in both tensile strength and tensile modulus compared to RSA-A. The UTS of micro particle filled Sikadur is only 5% higher than RSA-A and insignificantly different. Table 8.12 indicates that there is a significant difference between the UTS value of RSA-A and Timberset of 14.8%. The highest tensile modulus (TMOE) is exhibited by the micro-particle filled epoxy Sikadur with a value 73.5% higher than RSA-A. Timberset possessed the lowest tensile modulus despite being filled with rigid micro-particles. The ductile behaviour agreed with the results of the flexural test. Statistical ANOVA

revealed that there is a highly significance difference in both UTS and TMOE for all the tested epoxies (p-value<0.05) as shown in Table 8.13.

Table 8.13 ANOVA of tensile properties of various epoxy adhesives

Tensile properties	F value	p- value
Ultimate tensile strength	114.76	0.00
TMOE	242.41	0.00

The inclusion of rigid microfillers may contribute to the stiffness of the adhesive in agreement with other studies by Wetzel *et al*. (2003), Wang *et al*. (2002), Imanaka *et al.* (2001) and Smith *et al.* (1991). The inclusion of micro particles increases the TMOE of Sikadur but in contrast Timberset exhibits ductile behaviour and a lower modulus even than RSA-A. This result provides evidence of poor filler-matrix interaction as confirmed by Wetzel *et al.* (2003). Weak interfacial bonding can be resolved with silane-treament of the particles to ensure good filler to matrix bonding. The percentage of micro-filler content will also influence the TMOE.

This study indicates improvement in both UTS and TMOE through the incorporation of liquid rubber in the nanosilica composite, confirming the findings of Ozturk *et al*. (2001) and Chikhi *et al.* (2002) which conclude that improvement in tensile properties is dependent on the rubber content. It is also worth noting that, the mechanical performance of modified epoxies depends on the filler, the type of matrix and also chemical and physical interaction at the interface. As mentioned by Wang *et al.* (2002), the interface region may consist of a diffusion zone, a nucleation zone and a chemical reaction zone. The enhanced performance of liquid rubber filled nanocomposites suggest good bonding between filler and matrix enabling efficient stress transfer via the interface. The even dispersion of the nanoparticles is important reducing stress concentrations within the composite. Haupert and Wetzel (2005) state that failure of a composite can occur either by interfacial debonding or cohesive failure within the matrix. Failure in a heavily filled micro particle adhesive such as Sikadur occurs at the filler-matrix interface but failure in a nanoparticle-filled adhesive such as EA may occur by both particle debonding and cohesive failure of the epoxy.

Tensile properties (Table 8.12) reflect the flexural properties (Table 8.2) although the flexural moduli are higher than the tensile moduli. The differences are mainly attributed to the mode of testing. The flexural modulus is measured in a 3-point bend configuration where the sample is supported on two rollers with the maximum fibre stress at the outer surface of the sample only.

8.4.2.2 Effect of post-curing on tensile properties

The effect of post-curing on the tensile properties of the adhesives also reflects the results obtained in the flexural and shear studies. Stress versus strain characteristics for representative control and samples heat treated at 50°C and 70°C for 24 hour are depicted in Figure 8.16. Temperature degrades the tensile strength and stiffness of the composite although the curves show that the adhesive still retains ductility after being exposed to temperatures greater than the glass transition temperature. There is a slight increase in failure strain following exposure at 50°C. As is evident in Table 8.12, the UTS of samples treated at 50°C and 70°C was reduced by 4.8% and 11.43% respectively and the TMOE was degraded by 4.1% and 7.6% respectively. Statistical analysis of the means indicates insignificant differences.

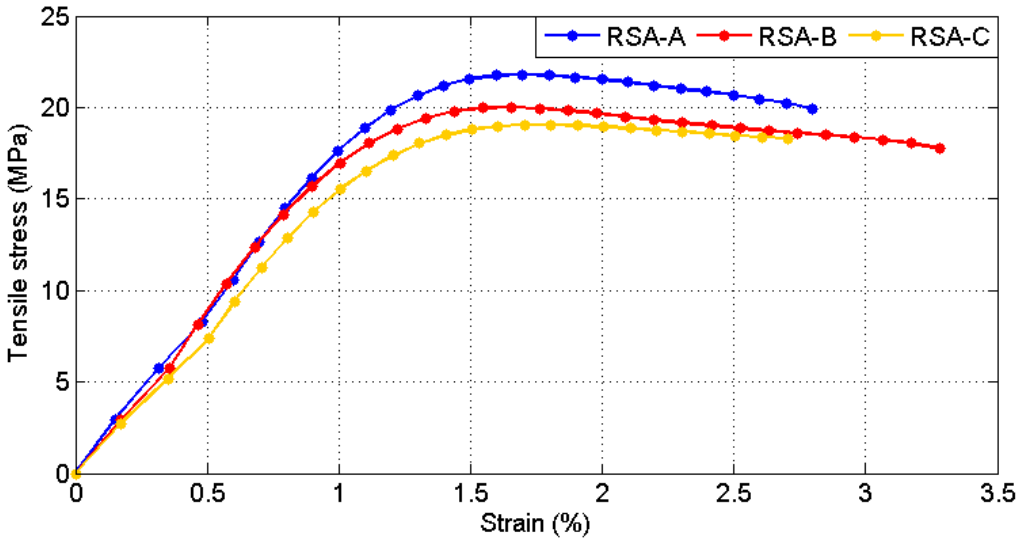

Fig. 8.16 Stress-strain curve of tensile tested control and heat treated RSA adhesive

8.5.1 METHODOLOGY

8.5.1.1 Adhesive preparation and sample dimension

The epoxy resin and hardener were mixed thoroughly before curing between two metal plates to produce a flat sheet. The thickness of the sample was set at 4mm and it was cured at ambient temperature for 20 days. The effect of post-curing on fracture toughness was also investigated after the initial 20 days of curing at room temperature. The objective of the study was to measure the critical stress intensity factor (K_{IC}) and critical strain energy release rate (G_{IC}) and the influence of heat treatments on both of these properties. Samples were cut from the sheet using a band saw (De Walt 3501). The dimension of single edge notched sample was based on the requirements of ASTM D 5045 and dimensions are shown in Figure 8.17.

Two types of notches were made in the sample. The initial notch of 4 mm depth was made by using a handsaw. A much thinner pre-crack was initiated by using a single edge razor blade. By using a rubber mallet, the edge of the razor blade was tapped into the bottom of the notch produced earlier with a handsaw.

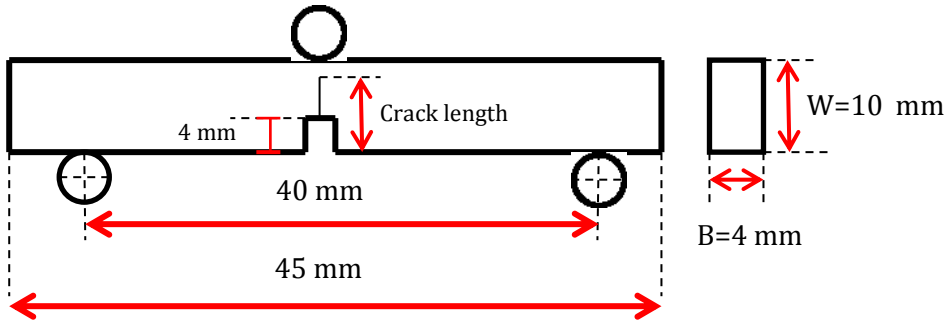

Fig. 8.17 Dimension of single edge notch sample according to ASTM D 5045 standard

The length of the fine crack line was then measured using an inverted microscope (Leica DM IL) at x5, x10 and x20 magnification (Figure 8.18). The total crack length was obtained by adding the measured length of the fine crack line to the depth of the notch (4 mm). Samples were subjected to 20 days curing at ambient temperature. Batches B and C were also heat treated at 50^{o}C and 70^{o}C for 24 hours in an oven.

Fig. 8.18: Leica DM IL

8.5.1.2 Single notched-edge bend (SENB) testing

The mode I single edge notched test was performed using an Instron 3369 Universal Testing Machine with a 50kN capacity load cell as indicated in Figure 19 at a ramp rate of 10 mm/min. Ten samples were tested for each batch and all tests were conducted at room temperature. During the test, the load and displacement were recorded by computer controlled data acquisition software Bluehill2.

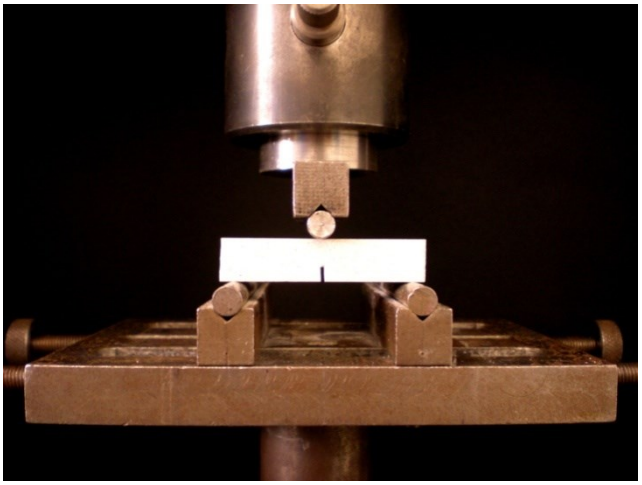

Fig. 8.19 Test configuration of SENB

8.5.1.3 Test evaluation and statistical analysis

The load versus displacement curves are linear before reaching breaking point. The critical stress intensity factor (K_{Ic}) or fracture toughness can be calculated according to linear elastic fracture mechanics. The critical stress intensity factor,

$$K_{Ic} = \frac{6\,\xi P_{max}}{BW^{1/2}} \qquad \text{(Eq. 8.11)}$$

Where P_{max} is the maximum load before initiation of crack (kN), B is the thickness of the sample and W is width of the sample. The geometrical correction factor, ξ is given as :

$$\xi = 1.93\left(\frac{a}{w}\right)^{\frac{1}{2}} - 3.07\left(\frac{a}{w}\right)^{\frac{3}{2}} + 14.53\left(\frac{a}{w}\right)^{\frac{5}{2}} - 25.11\left(\frac{a}{w}\right)^{\frac{7}{2}} + 25.80\left(\frac{a}{w}\right)^{\frac{9}{2}} \qquad \text{(Eq. 8.12)}$$

Where a/W is the ratio between crack length (a) and width (W). The unit of critical stress intensity factor is $MPam^{1/2}$.

The critical strain energy release rate (G_{Ic}) was calculated from the relationship:

$$G_{Ic} = \frac{K_{Ic}^2}{E} \qquad \text{(Eq. 8.13)}$$

The value of E was taken to be the TMOE. The unit for critical strain energy release rate is kJm^{-2}.

8.5.2 RESULTS AND DISCUSSIONS

8.5.2.1 The effect of types of filler on fracture toughness

Figures 8.20 and 8.21 show that both critical stress intensity factor (K_{Ic}) and critical strain energy release rate (G_{Ic}) of polymer composite depend on microstructure.

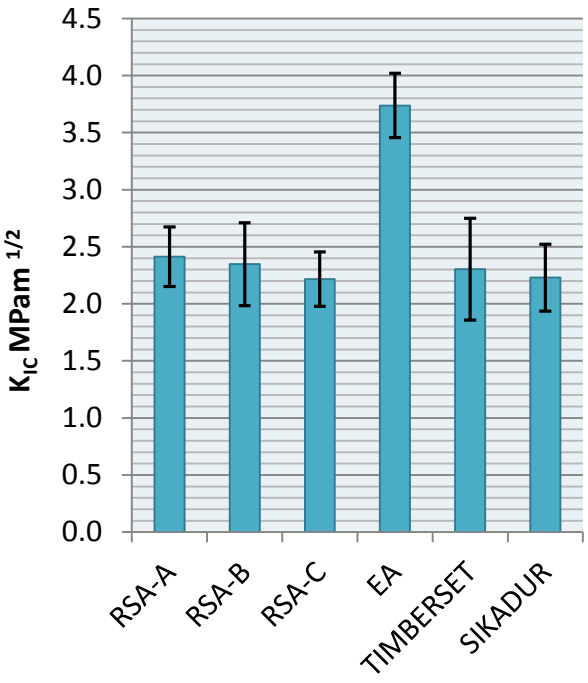

Fig. 8.20 Average critical stress intensity factor of adhesives and standard deviation

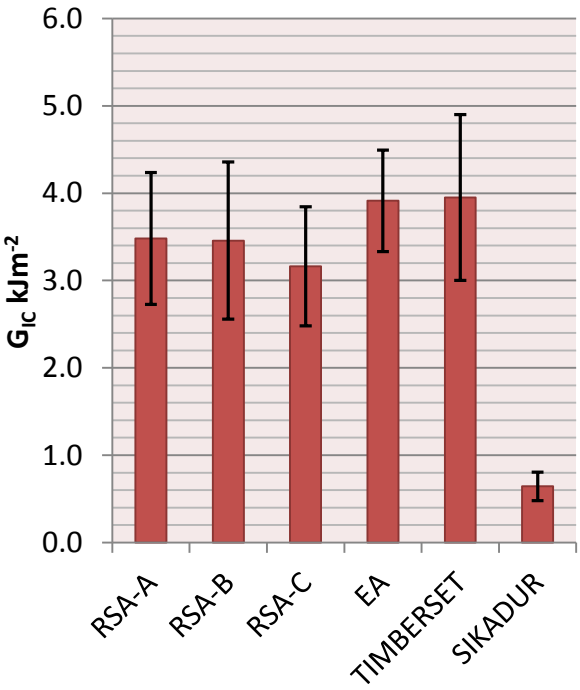

Fig. 8.21 Average critical strain energy release of adhesives and standard deviation

SENB samples behaved in a brittle fashion such that the load would increase linearly, followed by a sudden drop as the crack propagated. The values of both K_{Ic} and G_{Ic}, including their coefficients of variation, are presented in Table 8.14.

Table 8.14 Fracture toughness of epoxy adhesives

Adhesive	No. of samples	K_{IC} (MPam^{½})		G_{IC} (kJm^{-2})	
		Mean (MPa)	COV (%)	Mean (GPa)	COV(%)
RSA-A	10	2.41	4.6	3.48	8.9
EA	10	3.74	5.7	3.91	10.6
TIMBERSET	10	2.30	5.9	3.95	10.8
SIKADUR	10	2.23	6.2	0.64	12.4

The adhesives containing nano-particles significantly outperformed the adhesives containing micro-particles in terms of K_{Ic} values as indicated in Table 8.15.

Table 8.15 ANOVA of fracture toughness properties of epoxy adhesives

Fracture toughness properties	F value	p- value
K_{IC}MPam$^{1/2}$	57.96	0.00
G_{IC} kJm^{-2}	36.46	0.00

Adachi *et al*. (2008) reported on fracture toughness improvements in epoxy resins as the diameter of the particle content decreased. EA has the greatest values of K_{Ic} which indicates that the toughness of the hybrid-particulate composite increases with the addition of liquid rubber CTBN. The fracture toughening effect of CTBN additions is supported in numerous studies by Kinloch *et al*. (1985a, 1985b and 2005). The addition of rubber significantly raises the fracture energy of EA by 11% compared to RSA. Young (1986) mentioned that the improvement in toughness can be achieved with the inclusion of rubber and rigid particulates. His study indicates that both rubber and rigid-particulates act as initiation sites for shear yielding and deformation in an epoxy resin matrix. These particulates are responsible for crack pinning and localised plastic deformation. During crack propagation, the crack becomes pinned and deviates to produce secondary cracks. The formation of new surfaces requires energy thus contributing to the high value of G_{Ic} for EA. One interesting finding from this study is the magnitude of the difference between the value of K_{Ic} and G_{Ic} for Sikadur. Compared to the other nano- and micro-particulate filled systems, the fracture toughness result indicates that Sikadur has the lowest value of G_{Ic}. Young (1986) states that K_{Ic} is very much influenced by the volume fraction of the filler, whilst G_{Ic} is more dependent on the size of the particles.

8.5.2.2 The effect of post curing on fracture toughness

Tables 8.16 and 8.17 show that both K_{Ic} and G_{Ic} of RSA are not significant influenced by the post curing treatment. It can be seen that K_{Ic} of RSA-B and RSA-C decreases by only 2.5% and 7.9% respectively compared to RSA-A. Treatment at 70°C demonstrated a lower value of 2.37 GPa, which is 19.1% less than RSA-A. The mode of crack propagation was observed to be stable and ductile. The influence of the post curing was not significant since the test was conducted at room temperature. However, a significant decrease in fracture toughness would most likely have been observed had the test been conducted at 50°C or 70°C due to the increase in epoxy ductility.

Table 8.16 Fracture toughness of RSA post-cured adhesives

Adhesives	No. of samples	K_{IC} (MPam^{½})		G_{IC} (kJm^{-2})	
		Mean (MPa)	COV (%)	Mean (GPa)	COV(%)
RSA-A	10	2.41	5.8	3.48	10.66
RSA-B	10	2.35	6.46	3.29	12.42
RSA-C	10	2.22	5.81	2.37	10.54

Table 8.17 ANOVA of fracture toughness of RSA post-cured adhesives

Fracture toughness properties	F value	p- value
K_{IC}MPam$^{1/2}$	6.86	0.003
G_{IC} kJm^{-2}	4.767	0.014

8.6 SUMMARY OF PROPERTIES

A summary on the mechanical tests conducted on RSA, EA, Timberset and Sikadur is as stated below:

Table 8.18 Summary of mechanical properties

Property	RSA	EA	Timberset	Sikadur
Tensile Modulus (GPa)	1.69	3.59	1.39	6.38
Inter Laminar Shear Strength (MPa)	10.11	12.26	7.40	4.54
Tensile strength (MPa)	20.29	38.07	17.29	21.40
Fracture toughness K_{IC} (MPam$^{1/2}$) G_{IC} (kJm^{-2})	 2.41 3.48	 3.74 3.91	 2.30 3.95	 2.23 0.64

8.7 CONCLUDING REMARKS

Three- point bending (flexural), inter-laminar shear, tensile and fracture toughness tests were performed on four types of epoxy-based adhesives. The adhesives used varied in terms of nano- and micro-sized additions. One of the nano-particle containing adhesives was selected for a post-curing study. The following conclusion can be drawn from each of the mechanical tests:

a) Flexural test:

- Incorporation of nanorubber particles within the EA adhesive improved the MOR and MOE compared to RSA. Micro particulate fillers resulted in a high modulus of elasticity in Sikadur but lower flexural strength.

- Samples of RSA, EA and Timberset deformed plastically whilst the Sikadur behaved in a brittle fashion.
- There was no significant difference in the MOR and MOE of post-cured and control RSA samples.

b) Inter-laminar shear test
   - There was a significant increase in the ILS strength of the nano-rubber particle modified epoxy adhesive (EA) compared to RSA by a factor of 17.5%. The micro particle filled systems (Timberset and Sikadur) exhibited lower values of shear strength than RSA.
   - The ILS strength of 50°C and 70°C heat treated samples decreased by 6.5% and 12.5% compared to control RSA samples probably due to thermal degradation.

c) Tensile test
   - The addition of nano-rubber particles significantly improved the UTS and TMOE of nano-silica containing epoxy adhesives. Reinforcement of epoxy resin with rigid micro-particles resulted in superior TMOE compared to adhesives incorporating nano-particles.
   - The tensile test indicates that high temperature had the capacity to degrade the strength and stiffness of adhesives incorporating nano-particles.

d) Fracture toughness test
   - The reinforcement of adhesives incorporating nano-particles with nano-rubber significantly increased the fracture toughness. The addition of rigid micro fillers also improved the fracture toughness.
   - Post-curing treatments did not contribute significant difference to the fracture toughness of adhesives incorporating nano-silica.

CHAPTER 9: CREEP STUDY USING DYNAMIC MECHANICAL ANALYSER (DMTA)

9.1 INTRODUCTION

This chapter reviews the investigation of bulk epoxy under constant load. Using Dynamic Mechanical Thermal Analysis (DMTA) method, the creep properties of RSA, EA, Timberset and Sikadur were evaluated based on response to various temperature and stress level. The creep test via DMTA was conducted in tension and shear mode. These results were then depicted in composition of curves according to corresponding stress level. The data from creep in tension at 360 dwell time is presented based on creep equation according to the Kelvin-Voigt model.

9.2 METHODOLOGY

9.2.1 RESIN

All four commercial epoxy-based adhesives used in previous studies were selected for the DMTA creep study. The first three adhesives namely Rotafix Structural Adhesive (RSA), Engineering Adhesive (EA) and Timberset were produced from the same manufacturer Rotafix (Northern) Ltd of Abercraft. The fourth adhesive was manufactured by Sika Ltd and marketed as Sikadur-31. All adhesives were two part base-hardener and required thorough mixing before casting.

9.2.2 SAMPLE PREPARATION AND FABRICATION

Two types of samples were produced for the DMTA creep study. The first type was made of films of bulk adhesive. The films were cast in between two metal plates. The metal plates were treated with releasing agent prior casting. The films were left to cure in the mould for 5 days at room temperature. The films were then removed and left to cure for another 15 days. Thickness of 3 mm was obtained after the final curing process. Prior DMTA testing, the films were reduced to size 20 mm in length and 5 mm in width. The diagram on the preparation of bulk adhesive is presented in Figure 9.1. The bulk adhesive was used for creep testing in tension mode.

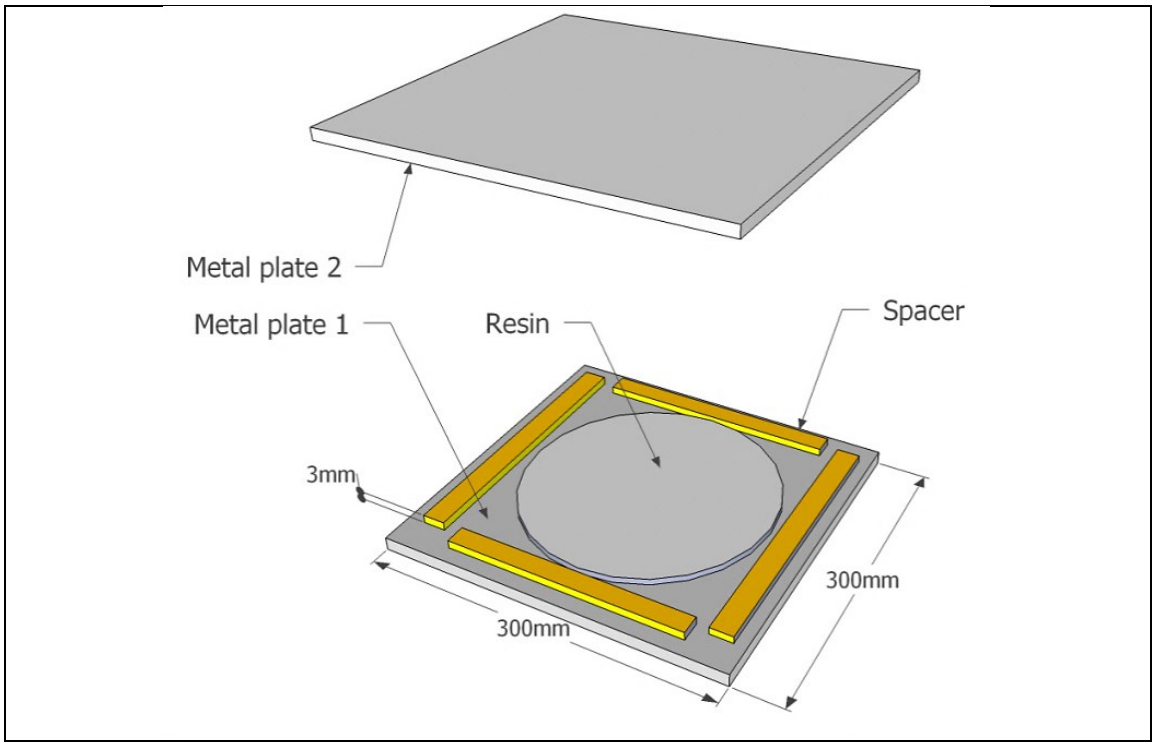

Fig. 9.1. Diagram of the metal plates and spacers used for adhesive film moulding.

The second sample was fabricated in between layers of beech veneer. The layout of the sample is presented in Figure 9.2. The sample preparation in terms of casting and room temperature curing process is similar to the preparation of bulk adhesive. Sandwich DMTA samples were approximately 20 mm in length, 5 mm in width and 3 mm in thickness. Minus the veneer layer, the thickness of adhesive layer is approximately 2 mm. Two cuts were made on the sandwich layer as to resemble a lap joint. The objective of the sample configuration was to demonstrate shear creep via DMTA apparatus. The actual figure of shear creep sandwich sample including its dimension as is presented in Figure 9.3.

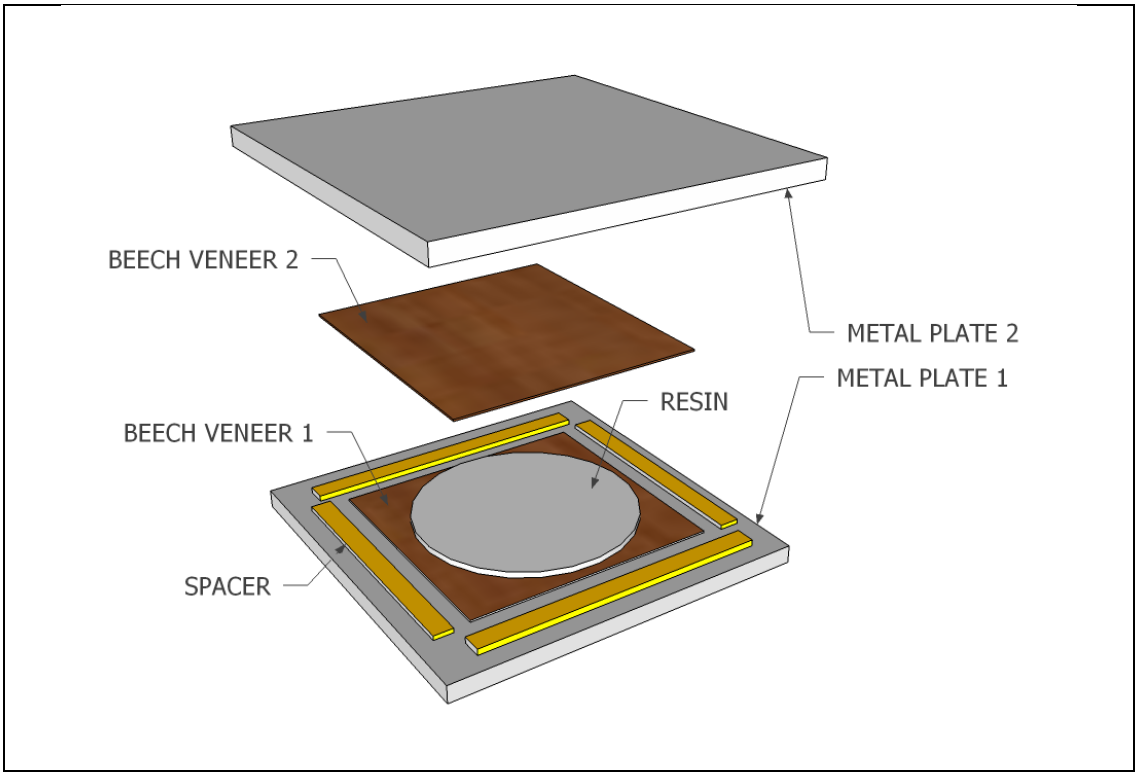

Fig. 9.2. Lay-up of wood-adhesive-wood sample pressed in between two metal plates

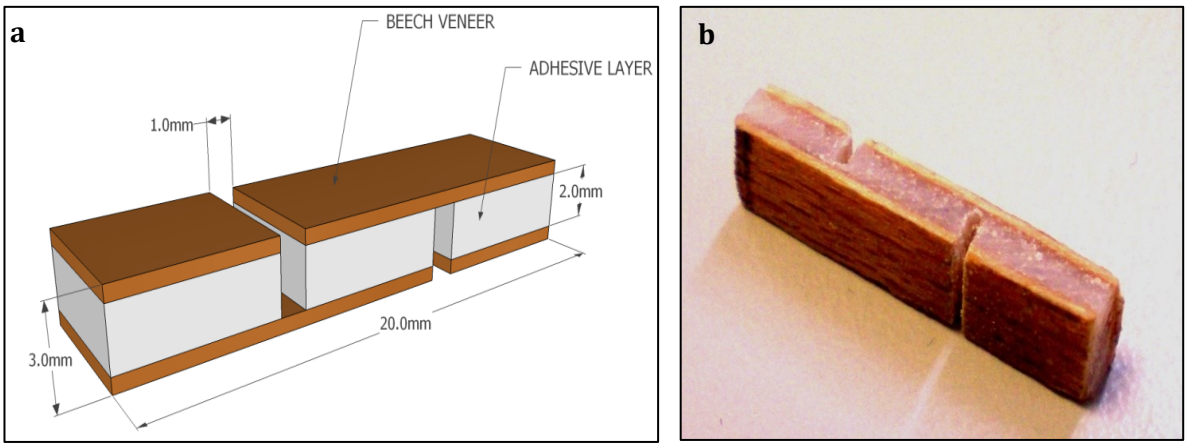

Fig. 9.3. Dimension of wood-adhesive-wood sample (a) and figure of the actual sample (b)

9.2.3 DYNAMIC MECHANICAL ANALYZER TEST CONFIGURATION

9.2.3.1 Temperature sweep for determination of glass transition temperature

Dynamic force testing is a method to characterise visco-elastic property of materials. In this study, the test was conducted onto bulk adhesives samples by applying sinusoidal vibration at a fixed frequency. The test was performed using a Tritec 2000 Dynamic Mechanical Thermal Analyzer (DMTA) manufactured by Triton Technology of

Keyworth, Nottinghamshire, UK (Figure 9.4). The objective of the test was to determine the temperature of transition from glassy state to rubbery phase by measuring storage modulus (E'), loss modulus (E") and the loss tangent (tan δ) as a function of temperature. In dynamic testing, the storage modulus (*E'*) represents elastic property of the material while loss modulus (*E"*) illustrates the viscous characteristic of the material. Damping characteristic is determined by tan delta (*tan δ = E'/E"*). During transition from glassy to rubbery, a significant drop (relaxation) in dynamic modulus (storage modulus, *E'*) was observed. The result on the glass transition of materials may influenced by the frequency used during the test.

Testing was conducted at a range of temperature -50°C to 100°C with a ramp rate of 2°C/min using liquid nitrogen as the cryogenic coolant. The test to determine Tg properties was conducted in single cantilever mode as indicated in Figure 9.5. There are 5 different ways to determine the T_g. In this study, the T_g was determined by interpolating the tangent between the elastic and viscoelastic phase. The T_g value was measured as the temperature at the point of intersection.

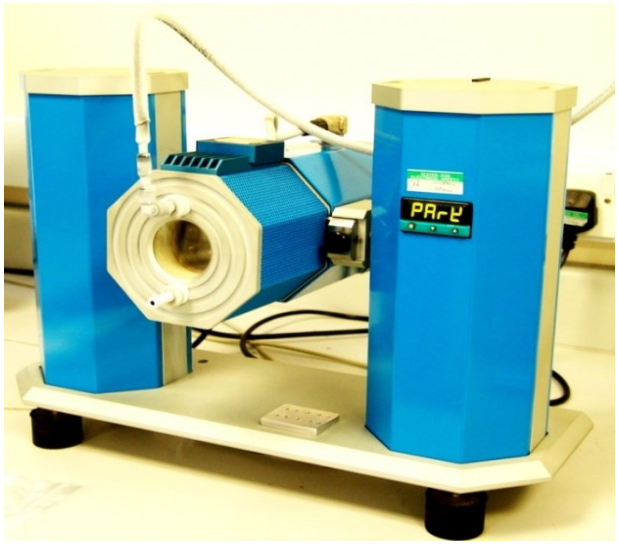

Fig. 9.4. Tritec 2000 Dynamic Mechanical Thermal Analyzer (DMTA).

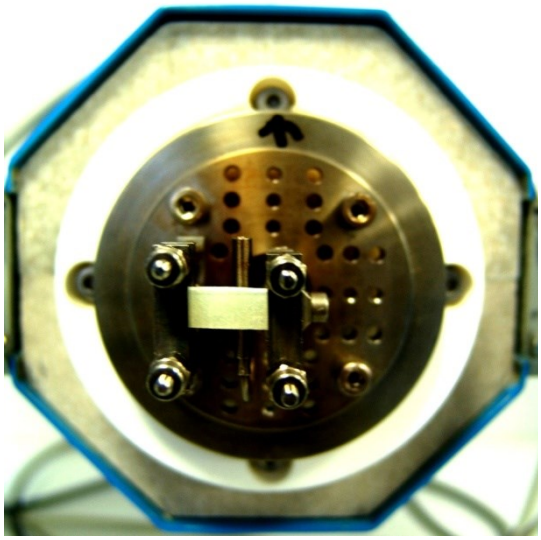

Fig. 9.5 Test rig in single cantilever mode

9.2.3.2 Creep test in tension and shear

This test was performed on sample of bulk adhesive and sandwich samples made from the four types of epoxy adhesives as described earlier. The aim of the test was to

measure creep by measuring displacement under constant loading. The tensile test was performed at the temperature range of 20°C to 80°C. For both bulk adhesive and sandwich sample, creep tests were conducted in direct force tension. The test configuration and testing mode is as presented in Figure 9.6. Creep measurement was made by employing a creep/TMA application as designed by Tritec. Under creep mode via DMTA, static force is applied onto the tension loaded sample instead of dynamic force under normal temperature sweep mode. Data collection was made at 30, 120 and 360 minutes dwell time for every step of 5°C intervals. A minimum of 3 measurements were made on each dwell time and types of adhesive. Runs were made at 2N, 6N and 10N load. Thinner sample was used to increase the stress applied since DMTA machine only has the capability to impose load up to 10N. The thickness of the samples was reduced from the original 3mm to 1mm thick by gentle sanding. A pre-load of 1N was employed to prevent the sample from buckling after loading.

Data logging was made possible using specialised software developed by Tritec technology. In static test, the relevant data is static displacement and static force and it is plotted in isotherms of curves according to time and temperature steps. This data were then calculated into normal strain or shear strain and plotted against time and temperature.

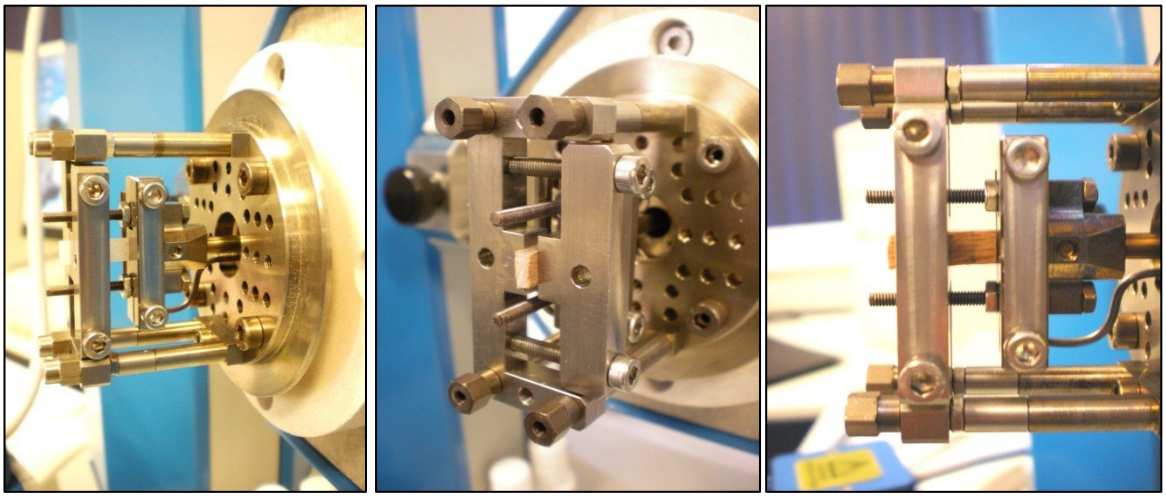

Fig. 9.6. DMTA test rig in tension mode testing bulk adhesive (a) and shear sample (b and c)

9.2.3.3 Thermal expansion study

The purpose of the study was to employ DMTA to measure thermal expansion of material. The concept of a DMTA machine is somewhat similar to a dilatometer. The principal of both of the apparatus is LVDT, therefore the DMTA also has capability in measuring displacement due to temperature changes. The DMTA, however, has extra function with its capability to apply dynamic and static force.

In this study, two methods were used and data obtained from both of the methods was compared to the data obtained from a dilatometer. The thermal expansion function can either be obtained using the temperature sweep or the Creep/TMA mode. Using the temperature sweep mode, a frequency of 1Hz was employed to perform thermal scan from 20°C to 100°C. A minimal displacement value of 0.001 mm was set for the tests. As for creep/TMA method, the displacement was set at 0.000 mm with a minimal load of 0.002N. Since this is a static test, load needs to be determined to avoid error. Testing temperature range was limited to 20°C to 60°C since creep/TMA function only allows for 40 temperature steps. Ramp rate was set at 1°C/min with a soaking time and interval temperature of 1min and 2°C respectively.

As to measure the rate of thermal strain per degree to temperature change, the linear thermal expansion coefficient, α is given by Equation 9.1:

$$\alpha = \frac{1}{L} \cdot \frac{\delta L}{\delta T} \qquad \text{(Eqn. 9.1)}$$

where,
L = linear dimension of the material.
T = temperature

The units of α is microstrain/C.

9.2.4 DATA ANALYSIS AND CURVE FITTING

Raw data from DMTA were plotted in displacement and force against time and temperature by Tritec data logging software. These data were then translated into tensile

strain or shear strain versus time and temperature using MATLAB. In tension mode, the tensile strain (ε) or elongation per unit length is given by the Equation 9.2 and depicted graphically in Figure 9.7.

$$Tensile\ strain, \varepsilon = \frac{\delta L}{L_o} \qquad \text{(Eqn. 9.2)}$$

where,

δL = total elongation, (L – Lo)

Lo = original length

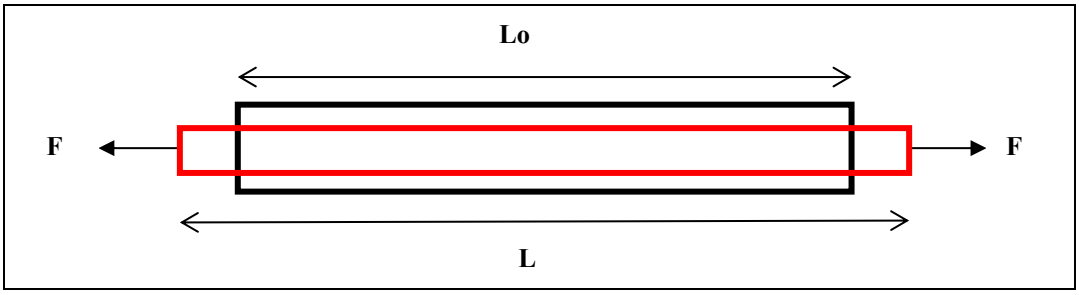

Fig. 9.7. Element under tensile loading

For an element which is subjected to shear deformation, the distance of shear (*w*) is taken into consideration when calculating shear strain (γ). Shearing strain (γ) is defined as an angle formed when the element is subjected to shearing force. The angle is measured between the vertical line (thickness of the element) and the oblique surface of the deformed element. The angle of shear strain is nominal and can be expressed in radians by Equation 9.3 as shown in Figure 9.8.

$$Shear\ strain, \gamma \approx \tan\gamma = \frac{w}{L_o} \qquad \text{(Eqn. 9.3)}$$

where,

w = distance due to shearing

Lo = original length

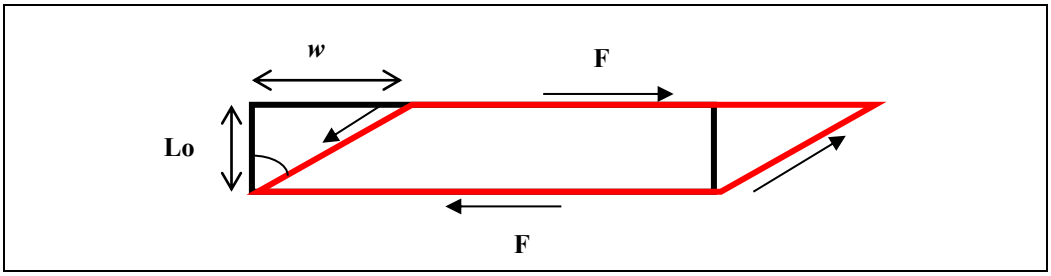

Fig. 9.8. Element under shear loading

Data on tensile strain (ε) were plotted against time and temperature using MATLAB. The creep data were analysed and fitted according to viscoelastic model as proposed by Kelvin-Voight. The model represents the time dependant component of creep through elements of Newtonian damper (dashpot) and Hookean elastic spring arranged in parallel configuration. A schematic diagram of the model is presented in Figure 9.9.

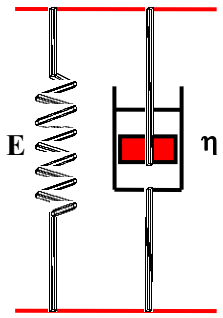

Fig. 9.9. The Kelvin-Voigt unit

At a constant stress the retardation of time is being characterised by dashpot as it delays the instantaneous extension represented by the spring. The model described creep strain as a function of time, ε(*t*) under constant creep stress (σ_o) as indicated in the Equation 9.4:

$$\varepsilon\,(t) \;=\; \frac{\sigma_O}{E}\cdot\left[1-\exp\left(-\frac{t}{\tau}\right)\right] \qquad \text{(Eqn. 9.4)}$$

where *E* is the spring elastic modulus and τ is the characteristic retardation time respectively.

To demonstrate a goodness of fit to exponential response in creep an array of parallel and series of Kelvin-Voight model was proposed to improve the model over the

complete range of temperature. The series of double exponential model is graphically presented in Figure 9.10 and Equation 9.5:

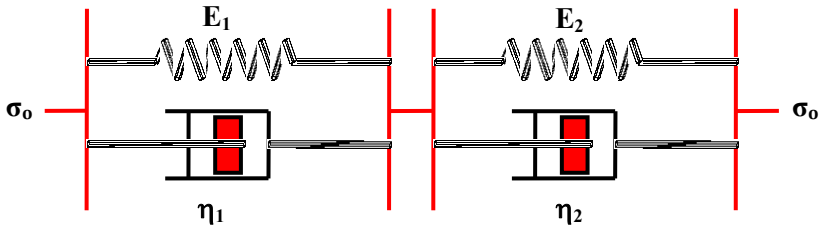

Fig. 9.10. Kelvin-Voigt units in series for creep simulation

$$\varepsilon(t) = \frac{\sigma_O}{E_1} \cdot \left[1 - \exp\left(-\frac{t}{\tau_1}\right)\right] + \frac{\sigma_O}{E_2} \cdot \left[1 - \exp\left(-\frac{t}{\tau_2}\right)\right] \qquad \text{(Eqn. 9.5)}$$

9.3 RESULTS AND DISCUSSIONS

9.3.1 THERMO MECHANICAL PROPERTIES OF EPOXY IN TENSION

The thermal properties of RSA, EA, Timberset and Sikadur are presented in Figure 9.11, 9.12 and 9.13 which consists of individual figures of storage modulus (E'), loss modulus (E") and loss factor (tan δ). All adhesives under investigation show one transition peak. The values of storage modulus (E') at 20C, tan δ_{max} and tan δ peak temperature are as presented in Table 9.1.

The effect of particle size and liquid rubber modification on high-temperature relaxation peak shown in Figure 9.11 depicts the storage modulus (E') plot against temperature for the studied adhesives. The storage or elastic modulus (E') represents the elastic properties of the material. The dynamic mechanical spectra of the adhesive resemble a generic amorphous polymer. The tensile storage moduli of micro- and nano-particulate modified epoxy at ambient temperature (20°C) vary from 1.25GPa to 2.25GPa. It is found that the storage modulus is strongly

influenced by the size of particulate and the presence of liquid rubber within the epoxy matrix. Of all adhesive tested, the heavily-filled micro particulate Sikadur exhibited the highest modulus which is a reflection of high molecular weight. The high crosslink density of Sikadur is also represented by large storage modulus within the rubbery plateau region which agrees well with the result on tensile test as mentioned in Chapter 8. Comparisons are made between the result in tensile modulus (Table 8.18) and the value of storage modulus at 20°C. According to Figure 9.11, the values for RSA, EA, Timberset and Sikadur are 1.3, 1.6, 1.2 and 2.2 GPa respectively. Although the DMA values of E' are smaller than TMOE, the sequence are in exactly the same order. The incorporation of liquid-rubber within EA epoxy improves the storage modulus of nano-silica composite at 20°C by 34% as compared to unmodified nano-silica epoxy (RSA). The improvement in storage tensile modulus indicates on the presence of reinforcing action of nano-silica within the network structure of EA adhesive. This is further supported by the storage modulus values at higher temperature such indicated at 50°C. The storage modulus of unmodified nano composite reduces significantly with the increase of temperature. At this point, the CTBN-nanosilica hybrid exhibits only a slight decrease in modulus. The differences between these values are highest within the range of 50 to 60°C. It is also evident that within the rubbery plateau, the storage modulus decreases according to the configuration Sikadur> EA > Timberset > RSA. The extent of plateau modulus is dependent upon the molecular weight between crosslinks. Crosslink density has an inverted effect on the chain mobility. As indicated by Pocious (2002), an increase in molecular weight would also increase the temperature at which the thermoset flows.

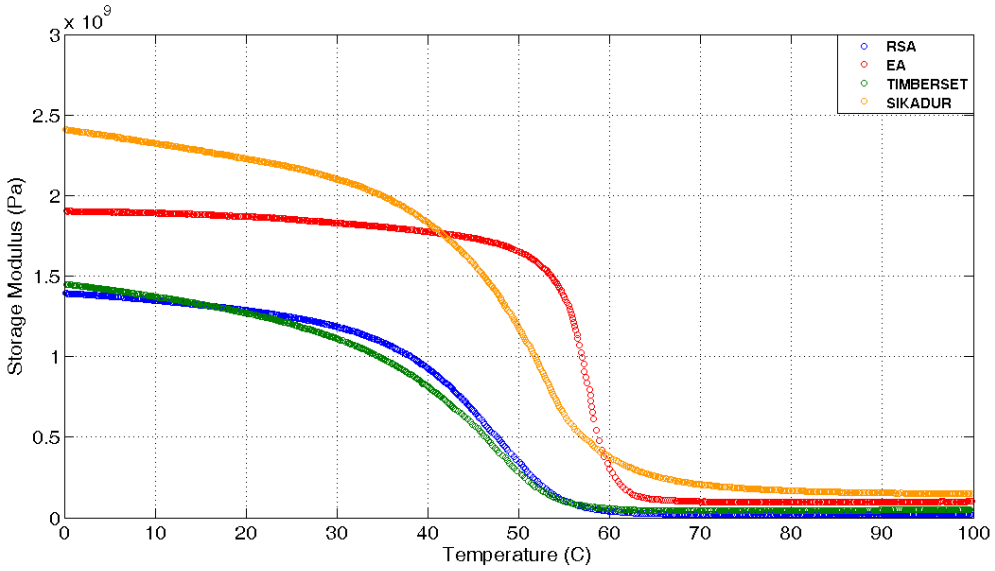

Fig. 9.11. Storage modulus of adhesives

Thermal property of a polymer is best characterised using the glass transition temperature or Tg. In this investigation, Tg was determined based on three methods. The first method uses the "onset Tg" as proposed by standard DIN 65583. The point of intersection between two tangents of the storage modulus (E') was taken as the temperature where the glass transition takes place. Within this phase, the polymer changes from a relatively hard and glass like material to soft rubber like material. The degree of relaxation within a polymer matrix is much associated with crystallinity. Amorphous polymer in relaxation phase exhibit severe drop in storage modulus at Tg temperature. For highly cross linked material, the covalent bond formed between polymer chains brings the molecules closer together. As for lightly cross-linked materials, the storage modulus decreases with temperature increase and a substantial drop within the Tg temperature region. This observation is evident on all tested epoxy composite. This behaviour study conforms to the elastic rubbery characteristics of the tested epoxies.

The second method in determining Tg as proposed by ASTM D 4065 employs the maximum peak in the loss modulus. Values of Tg according to both standards are as summarised in Table 9.1. The loss modulus which represents the loss of energy due to viscous deformation (frictional or internal motions) is depicted in Figure 9.12. Broadening of loss factor peak is an indication of highly cross link material which is most evident on Sikadur.

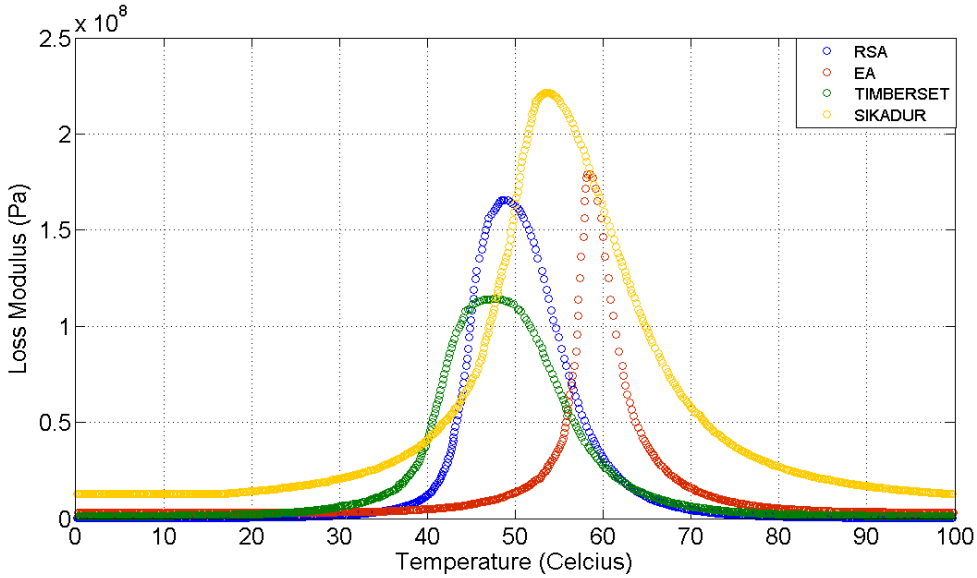

Fig. 9.12. Loss modulus of adhesives

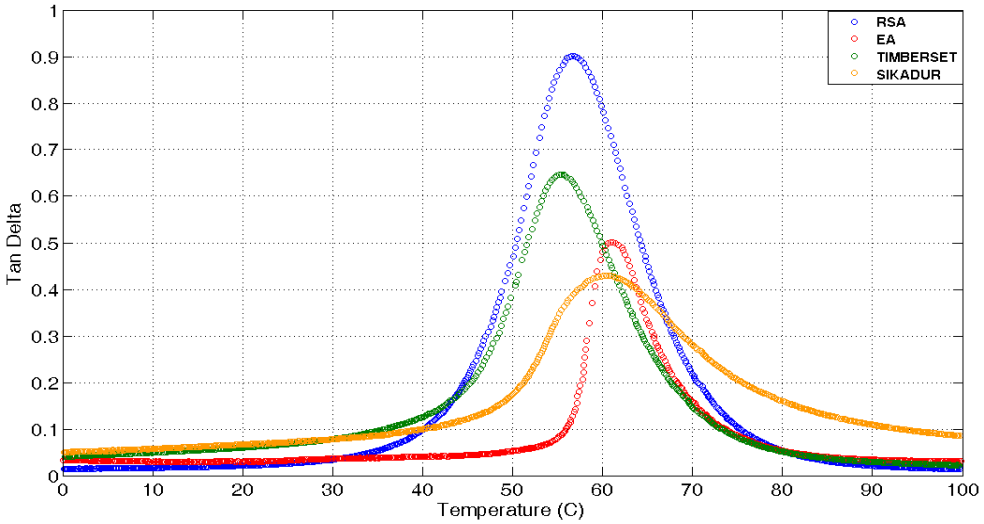

Fig. 9.13. Tan delta of adhesives

The tan δ plots of the tested epoxy composites are presented in Fig 9.13. It is evident that the peak gradually reduces and broadens with the increase of Tg. The plot indicates the value of tan δ peak height according to sequence: RSA > Timberset > EA > Sikadur. It is also noted that the gradual shift of tan δ peak towards higher temperature is consistent with the point that the storage modulus exhibit maximum change in slope. The indication of high Tg for sample Sikadur indicates a broader chain length distribution. This is reflected qualitatively by its broader tan δ peak.

The summary on all three techniques used to determine the values of Tg is shown in Table 9.1. Tan δ produces the highest values of Tg compared to other techniques. Various studies (Qiao and Easteal 2001 and Pervin *et al*. 2005) have also quoted from the peak tan δ as Tg values. As mentioned by Menard (1999), tan δ is an indicator of how efficiently the material loses energy to molecular arrangements and internal friction. Tan δ is also independent of geometry effect which means that any changes on sample size would likely affect the value of storage modulus and loss modulus. However, the values of Tg based on peak tan δ are always higher than those determined by the evaluation of storage modulus and beyond the service temperature of the composite (Wolfrum *et al.* 2000). Based on this assumption, it is best to use the storage modulus to determine the Tg of the epoxy composites. The Tg values as indicated by onset E' values are in the subsequent order: EA> Sikadur > RSA > Timberset

Table 9.1. The result of Tg determination

Adhesives	Onset E' curve (°C)	Peak E" curve (°C)	Peak tan δ (°C)
RSA	36.8	48.7	56.6
EA	53.4	58.7	60.9
Timberset	35.4	47.1	55.4
Sikadur	42.5	52.5	60.4

From the observation on the thermal properties of all adhesive tested it is found that the utilisation of high proportion of macro and nano-size particles embedded in a matrix produces high cohesive strength and creep resistance composite.

9.3.2 MULTI-STAGE CREEP IN TENSION

9.3.2.1 Multi-stage creep in tension at 30 minutes

The purpose of this investigation was to describe the viscoelastic behaviour and deformation characteristics of epoxy adhesive. It is likely that all materials investigated in this study deform according to the classic behaviour of elastic solids and viscous fluids. The multi-step temperature programme was designed based on Boltzman's superposition principle which applies multi-step loading programme. According to Boltzman's method, step change in stress resulted in time-dependant creep behaviour which was subject to its past loading history. Based on the test, the strain reacted in proportion to the magnitude of applied stress. The final deformation is the sum of the independent contributions of each loading step. Since the multi-step loading programme

could not be used in the DMTA (due to the limitation of the equipment), a multi-step temperature programme was proposed. Similar investigations using DMTA has not been reported elsewhere. The concept of both of the multi-step programmes appeared somewhat similar, although the reactions at molecular levels are different. A material in the glassy phase or rubbery phase will exhibit a different retardation time (τ). Incremental increases in temperature will increase the frequency of molecular rearrangement thus reducing the τ value. It is noted that changing the temperature would also result in changes in the time scale.

In this initial investigation on creep using DMTA, the sample of RSA pure adhesive was subjected to static force of 1.75N (calculated stress of 0.12 MPa). Testing was conducted in tension mode with a pre-load of 1N to prevent sample buckling. The test temperature ranges from 25°C to 80°C at 5°C steps. Dwelling time for every step was set at 30 minutes with a total time of 430 minutes. Figure 9.14 shows the time dependant behaviour of the material which increases in strain following step change in temperature. As a whole, the curve resembles a master curve of creep strain made up of smaller creep strain and corresponded to temperature increase. The test might have taken a very long time if the test was conducted at a constant temperature. The time scale was shortened by testing the material at increased temperature.

It was observed that within temperature range of 25°C to 30°C, the strain as resulted by constant load was very minimal. The shape of strain increment during 25°C to 30°C was somewhat less exponential. The exponential form starts to take shape as the temperature reaches 30°C with notable strain increase. The strain of the material starts to show significant acceleration in creep rate at 40°C (Figure 9.15). Plausible explanation can be done by referring to the temperature sweep data of RSA. According to the storage modulus (E'), the calculated glass transition temperature, Tg, of RSA is 34.5°C. At this point (35°C to 40°C), the material is behaving viscoelastically, which signifies the transition from the glassy to the rubbery state.

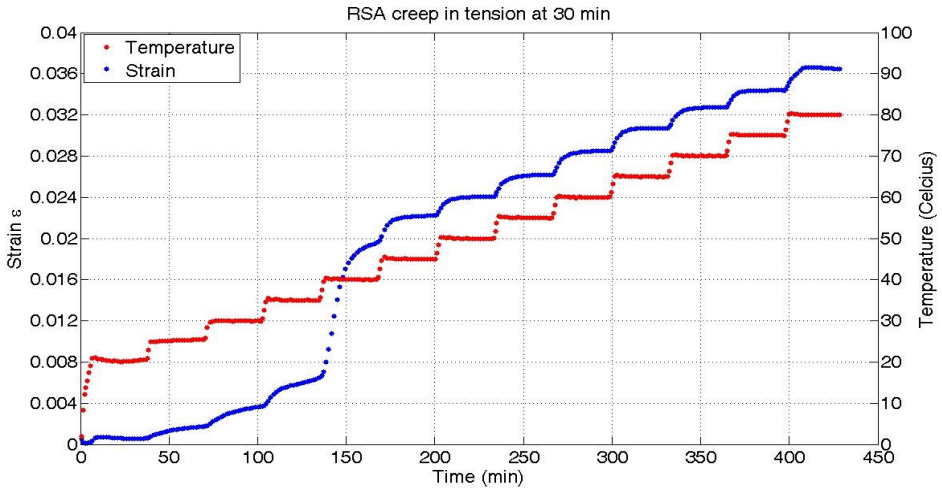

Fig 9.14. DMTA thermal scan for RSA in tension with 30 minutes dwell time

Figure 9.15 and 9.16 shows the magnification of strain increment above 40°C. At 45°C and as creep strain of other temperature steps above it, a small increase in strain was observed. The classical exponential creep form was observed within these phase. Focusing on a creep strain of a single temperature step, the strain rate appears to increase proportionally with time until up to a certain point where it finally diminishes to an almost constant strain value. An initial expectation that large strain in creep would be continually observed after 40°C was proven wrong. The strain instead continues in smaller steps with the sample kept intact without failing at 80°C. It is calculated that the strain in RSA increases by approximately 0.2% for every 5°C steps. In understanding the mechanism of creep strain above 40°C, the influence of thermal expansion was proposed.

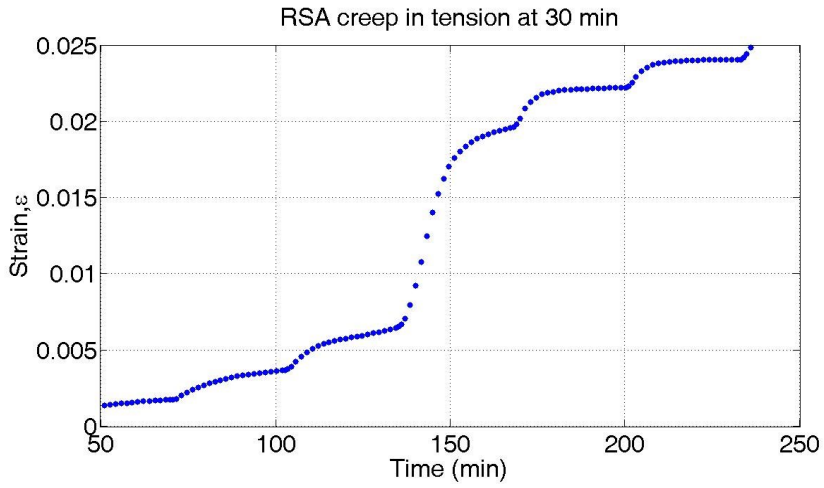

Fig. 9.15. DMTA thermal scan for RSA in tension with 30 minutes dwell times showing creep steps between 30°C and 50°C.

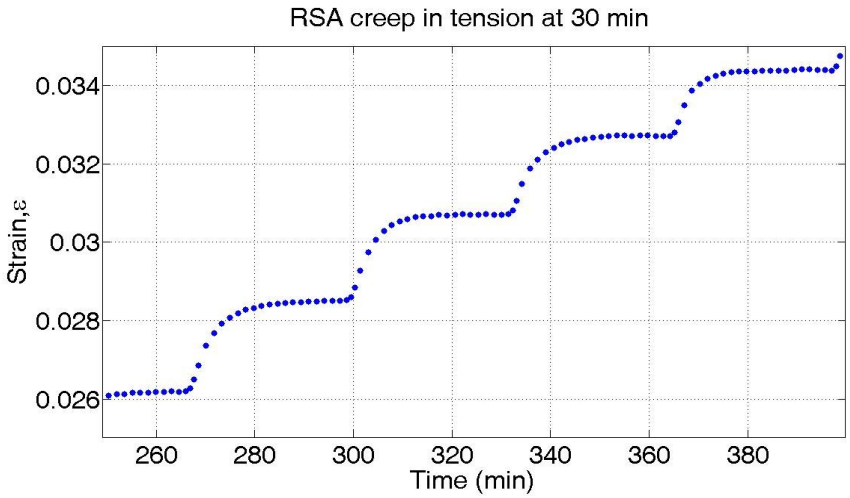

Fig. 9.16. DMTA thermal scan for RSA in tension with 30 minutes dwell times showing creep steps between 55°C and 75°C.

An additional study on thermal expansion coefficient,α, was conducted on RSA using DMTA. This approach was proposed as to investigate the probability of using DMTA in determining the α value. The results obtained were then cross examined with α results obtained by using a dilatometer. Two methods were proposed for this study. In the first experiment (method I), the RSA was tested in tension mode with starting temperature of 20°C to 100°C and ramp rate of 1°C per minute. No force was applied on the tested sample. In the second method (method II), a minimal force was applied (0.002N) to stabilise the testing programme. The test was carried out also in tension mode with temperature steps of 1°C per minute. The limitation using this method is that it only allows a maximum of 40 creep steps. Therefore, the experiment was designed to run from 20°C to 60°C. For both methods, the strain is plotted against temperature as shown in Figures 9.17 and 9.18 respectively.

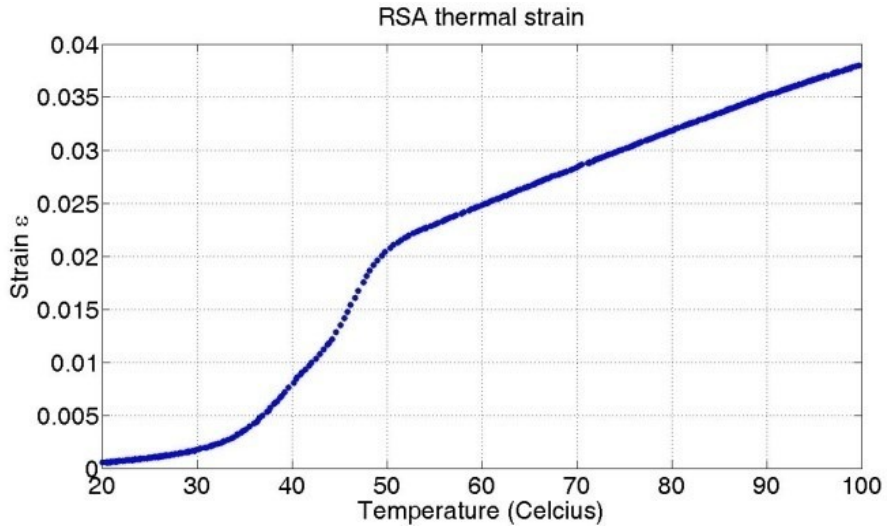

Fig. 9.17. Strain plotted versus temperature for RSA unloaded and clamped in tension mode (method I).

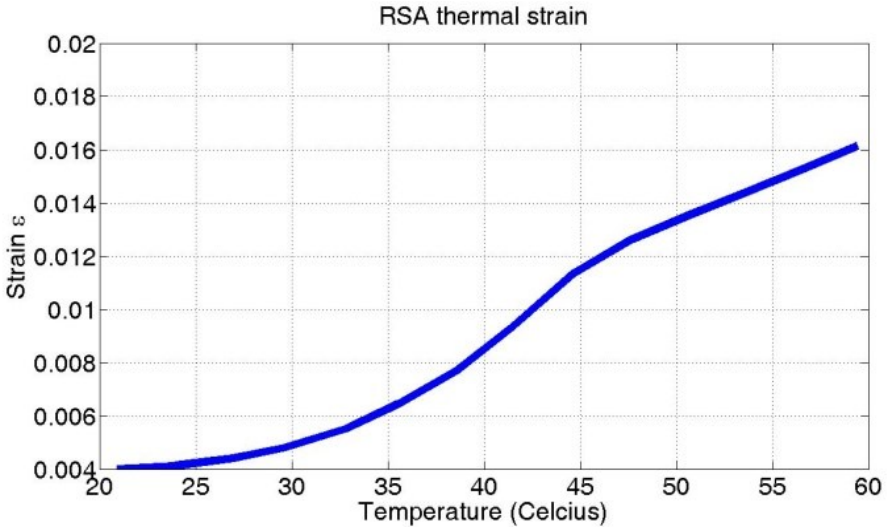

Fig. 9.18. Strain plotted versus temperature for RSA clamped in tension mode using the creep programme (method II).

A similar form of strain was observed on both Fig 9.17 and 9.18 with a significant increase as the test temperature reached 35°C. This behaviour is very similar to the findings of the creep experiment where large strain was observed within the viscoelastic phase. Towards the end of the viscoelastic phase, change in slope gradient was observed. The data in Fig 9.18 is converted into a plot of thermal expansion coefficient versus temperature and a peak value of α occurs at ~42°C as shown in Fig. 9.19.

To further emphasize on the theory of thermal expansion behaviour at (Tg + 15)°C, comparison was made to data in Fig 9.16 which show creep strain at 55°C to 75°C

temperature steps. Focusing on a single temperature step at 60°C, the equilibrium strain was estimated to be 0.0285 (2.85%). From Figure 9.17 and 9.18 the strain were noted as 0.025 (2.5%) using method I and 0.016 (1.6%) using method II respectively. Both of these values conform to the thermal expansion behaviour of the material while the residual strain (0.35% to 1.25%) is noted as the creep strain. The values of creep strain (residual strain) according to the respective methods are calculated by subtracting the value of thermal strain (e.g 0.025 and 0.016) from the value of strain derived from the tension creep experiment at specific temperature (e.g 0.0285 at 60°C). The hypothesis put forward is that thermal expansion has significant effect on the material at Tg and (Tg + 15) °C. The calculated assumption based on the data at temperature step 60°C indicates that thermal expansion contributed up to 56.1% to 87.7% of the total strain. Data on Figure 9.19 indicates on good correlation to the creep strain as plotted in Figure 9.16. Thermal expansion coefficients is calculated and shown in Fig 9.19 for RSA is as function of temperature. Comparison test has empirically proven that the behaviour of RSA after a significant deformation within the viscoelastice zone would dominantly be influenced by its thermal expansion properties.

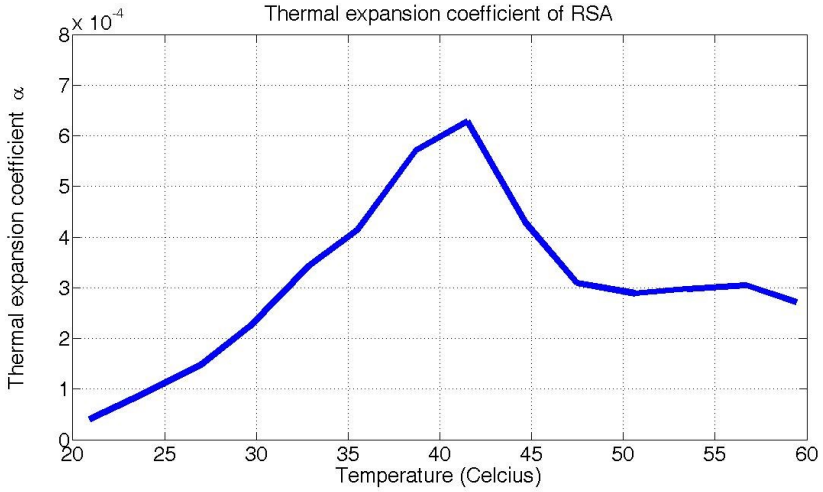

Fig. 9.19. Thermal expansion coefficient plotted versus temperature for RSA based on data from Figure 9.18.

The creep test using multi-step temperature programme has successfully characterised the material in study. Referring to these figures, there is a clear indication of the transition of phase within the material as it is being tested at a constant load. The test indicates on the behaviour of the material in instantaneous (elastic), viscous and rubbery phase. The main question was either to classify RSA as elastic material, a rubber, a partially cross-linked rubber or a viscous polymer.

Application of stress will cause the molecule to change from coiled to extended configuration instantaneously. This causes rubber like elasticity, extension and contraction occurs instantaneously, neglecting permanent deformation. In natural rubber, molecules slide past each other and do not recover completely. Permanent flow is prevented in a highly cross-linked rubber. There are two elements to be taken consideration, stress and heat. Both stress and heat has influence in changing the internal energy and entropy of a polymer. Finding from the study as depicted in Figure 9.14 suggested at temperature below Tg (25°C to 30°C), an almost linear strain/temperature relationship was observed. Significant increase in strain was observed at 35 and 40°C. High strain results in a greatly- reduced entropy. The result obtained also indicates as for creep strain above (Tg + 15) °C, RSA expands as the temperature increases. This proves that RSA is acting like a semi cross-linked rubber. A heated fully cross-linked rubber (e.g polyisoprene) is expected to maximise the entropy which results to the contraction in the configuration of chain. It is decided that further investigation is required to associate the material to a semi rubbery behaviour with partial cross linking structure.

9.3.2.2 Multi-stage creep in tension at 120 minutes

To investigate on the possibility of a semi cross-linked structure, a similar experiment was repeated with a longer dwell time. 5°C steps of temperature from 20°C to 80°C were maintained at 120 minutes. Figure 9.20 shows the creep behaviour of RSA as a function of time and temperature. As a result to a much longer dwell time, it was observed that the exponential shape of the creep strain was more defined. At the end of the step, creep strain reaches equilibrium as the strain reaches almost constant values.

Little deformation was observed during the 20°C to 25°C steps. The evidence of significant deformation was observed during 30°C, 35°C, and 40°C steps. It is likely that the behaviour within these regions associates to the viscoelastic phase. The absence of the classic exponential shape within these deformation dominated region indicates that creep does not occur until later stage. At the end of 40°C steps however, the creep strain settle down and reaches equilibrium.

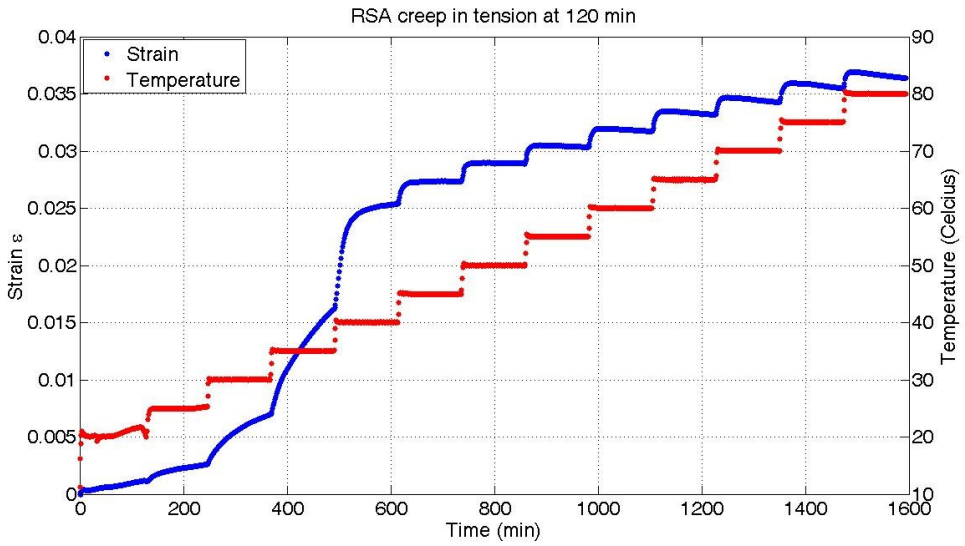

Fig. 9.20. DMTA thermal scan for RSA in tension with 120 min dwell time

Development within the 50°C to 80°C temperature steps helps to define the character of RSA. Based on the past experiment using 30 minutes dwell time, the total strain was dominantly resulted by thermal expansion. Referring to Figure 9.21, at a much longer dwell time (120 minutes), similar exponential shape was observed. At the end of the temperature step, as opposed to diminishing to a constant strain value, the material demonstrated a decrease in strain. The change in the trend of creep strain was due thermal expansion and strain recovery. The behaviour of extension and retraction can be associated with a partially cross-linked, semi rubbery structure. The expanded plot of 60°C to 75°C also indicated that the strain recovery increased in steepness towards 75°C.

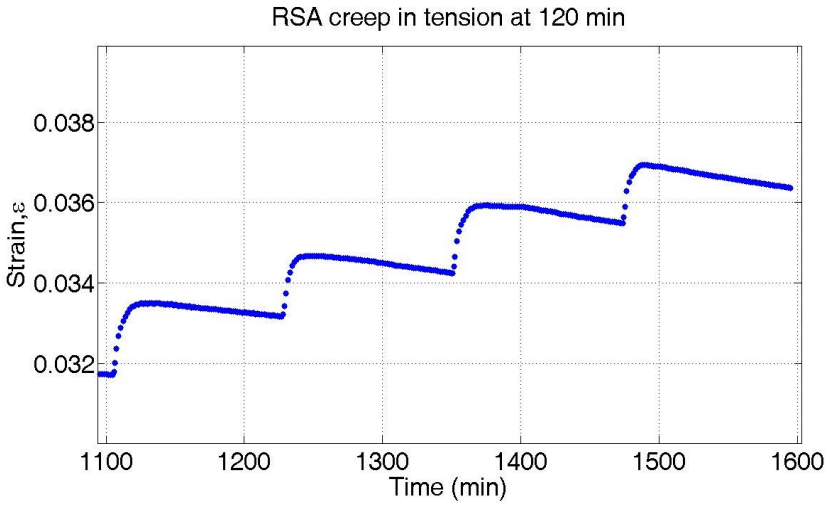

Fig. 9.21. DMTA thermal scan for RSA in tension with 120 min dwell times between 60 and 75°C

The finding on expansion and contraction of RSA at increased temperature and loaded in tension is much related to the entropy theory. Above Tg, rubber is fully amorphous, semi cross-linked polymer. Within a semi cross-linked system, the flow of polymer is restricted by the polymer chain. The chain segments of the polymer however, are free to uncoil and recoil. Under tension loading, the polymer molecule changes formation by experiencing uncoiling. During early stages of the applied stress, rubber conforms to the Hookean behaviour. The linear behaviour between stress and strain only applies up to 1% strain at normal temperature. Since this experiment was conducted at higher than ambient temperature, the threshold for linear stress-strain was probably lower as depicted in Figure 9.21. Due to changes in configuration of entropy, the relationship of force to extension is non-linear when the state of equilibrium was established. The state of equilibrium is reached as the uncoiling is inhibited by the cross-linking of the polymer. The entropy of rubber is reduced by extension and the molecules become less disordered. Heating caused the contraction of rubber in the loading direction due to increase of molecule disorder, thus maximising entropy. It was noted that contraction in creep strain was not observed in the earlier study at 30 minutes dwell time. At longer dwell time (120 minutes) the creep strain is able to reach equilibrium. Extension and contraction are much influenced configurationally by entropy rather than internal energy. A low molecular mass material would increase in internal energy during extension, giving it the characteristic of energy spring. Due to this respond, the semi-crosslink rubbery RSA can be characterise as an entropy spring.

As the temperature increased, the multi-stage creep experiment approaches equilibrium at the end of each step with longer dwell time and corresponds to a force of 2N. Based on the dimension of the sample (3mm in thickness), the stress of the sample which corresponds to the force of 2N is 0.13MPa. Higher level of stress was needed to emulate the level of stress experienced in a bonded-in glue line timber joints. The test was repeated with a force of 6N and 10N at the DMTA actuator. The dimension of the sample was reduced to 1mm to induce higher stress level. The result of multi-stage creep experiment tested according to various stress levels are as presented in the next section.

9.3.2.3 Multi-stage creep in tension of various epoxies

The test on various epoxies was conducted at 120 minutes of dwell time per step with temperature step from 20°C to 80°C. For every stress level, the experiments were repeated three times for consistency and ensuring reproducible results.

All adhesives which have been tested at the lowest stress level of 0.13MPa exhibited thermal stability up to 80°C and lasted for 1600 minutes. The thermal stability was due to the further cross-linking of the semi-crosslinked epoxies during the experimental run. The cross-linking continues during the test whilst still retaining its loosely bound rubbery network. Based on the composition of RSA adhesive, the rubbery network of molecular chain is highly influenced by the combination of reactive diluents and silica nanoparticles employed in the DGEBA/F base adhesive. Referring to the RSA's Tg, the storage modulus which corresponds to the modulus of elasticity was reduced to ~0.01GPa in the rubbery state from ~1.3GPa in the elastic state. Despite that, the adhesive is still capable of transferring stress at elevated temperature which is largely contributed to its increase in ductility and toughness.

Comparison on creep performance of nano-silica modified epoxies (RSA and EA) and micro-particulate filled epoxies (Timberset and Sikadur) are as presented in the following figures. The creep strain behaviour of RSA, EA, Timberset and Sikadur in relation to time, temperature and stress level is as depicted in Figure 9.22, 9.23, 9.24 and 9.25 respectively. Based on the creep behaviour of each studied adhesive, the following observation can be made:

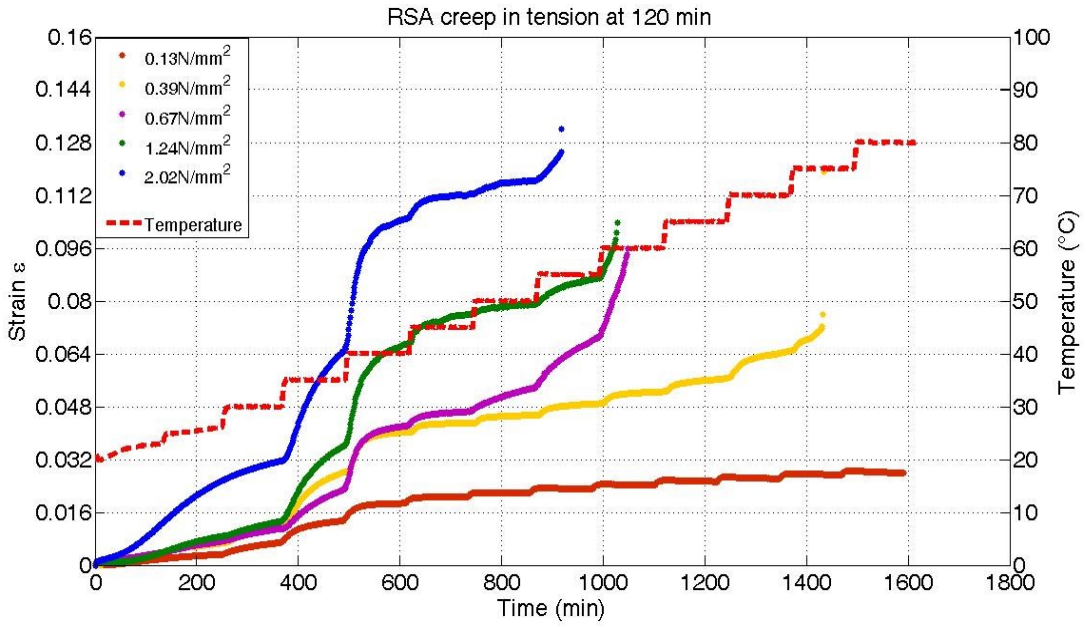

Fig. 9.22. Strain versus time for RSA subjected to temperature increased in 5°C steps for 120 min. Intervals from 20 to 80°C at constant stresses ranging from 0.13 to 2.02Mpa

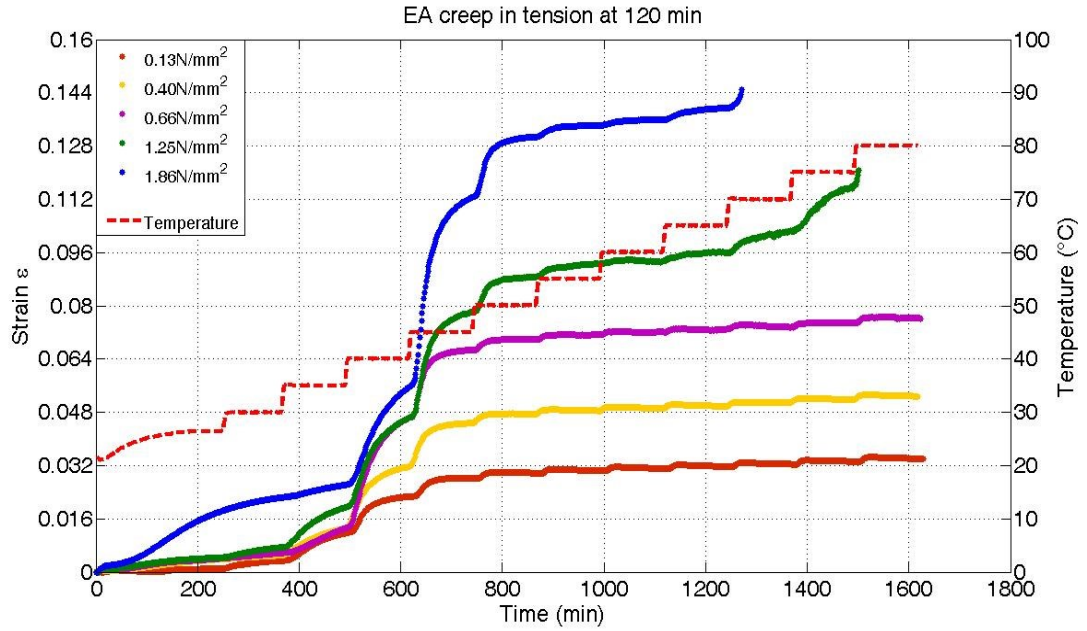

Fig. 9.23. Strain versus time for EA subjected to temperature increased in 5°C steps for 120 min. intervals from 20 to 80°C at constant stresses of 0.13 to 1.86MPa

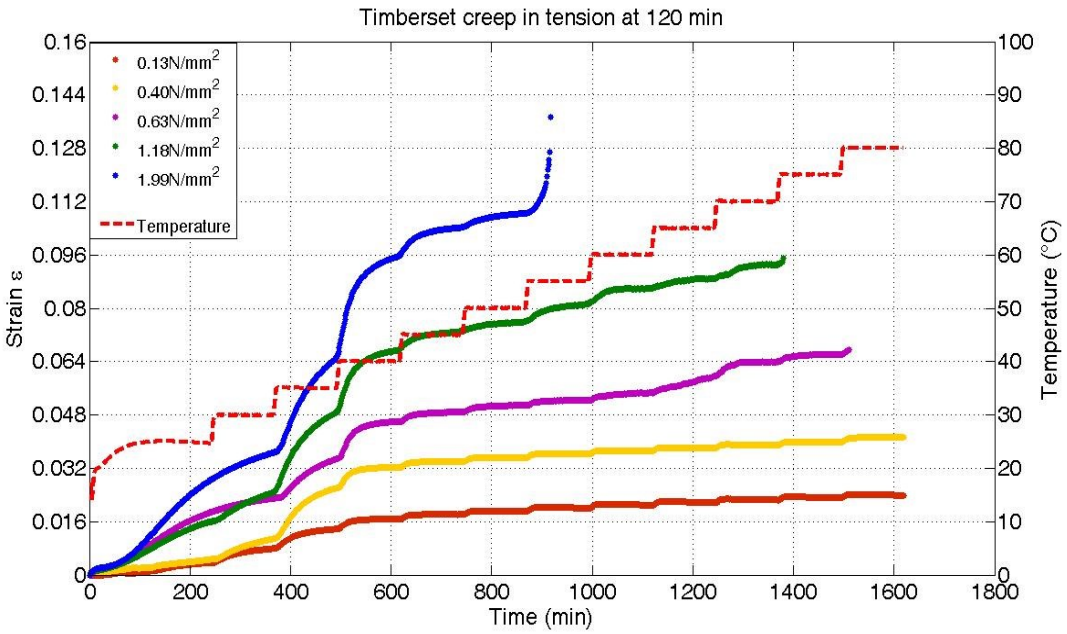

Fig. 9.24. Strain versus time for Timberset subjected to temperature increased in 5°C steps for 120 min. Intervals from 20 to 80°C at constant stresses from 0.13 to 1.99MPa

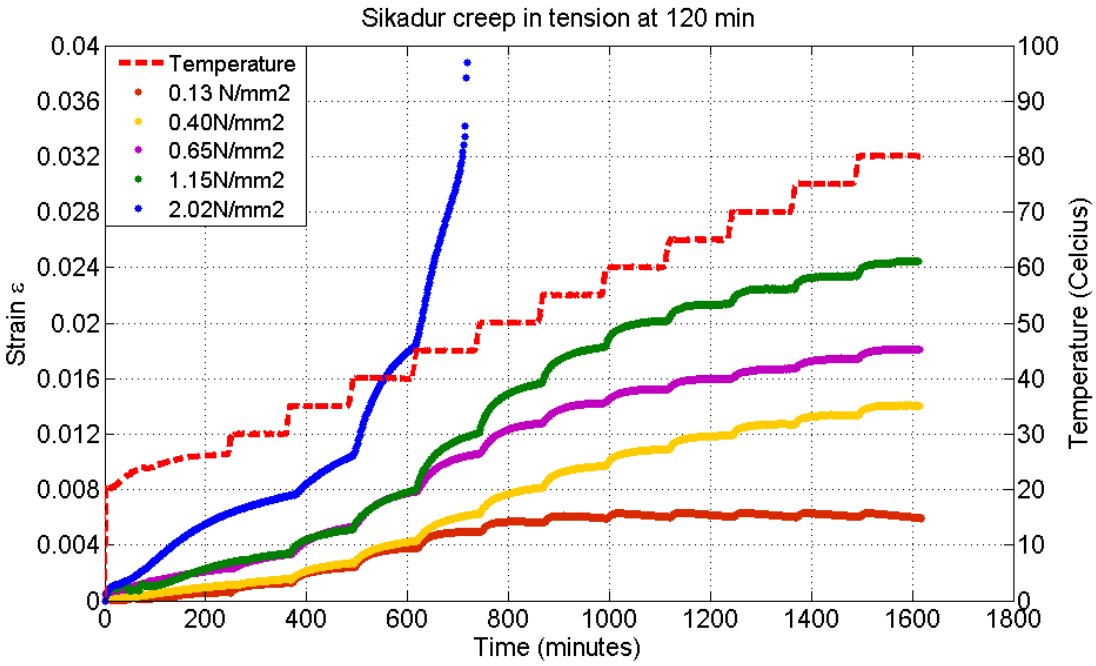

Fig. 9.25. Strain versus time for Sikadur subjected to temperature increased in 5°C steps for 120 min. Intervals from 20 to 80°C at constant stresses from 0.13 to 2.02MPa

a) Increase of creep strain due to the increase of stress level

It is noticeable that, in comparison to the lowest stress level, all test conducted at higher level of applied stress depicted higher creep strain. At stress of 0.13MPa, the behaviour of RSA (Figure 9.22) is as almost similar to the test at 30 minutes dwell time with creep

strain of less than 4%. At the maximum stress of 2.02N, the adhesive is stable up to 55°C and failed at creep strain of 12%. Within the region of 20°C to 30°C, creep strain was kept below 1.6% at 0.13 to 1.24 MPa before experiencing large leap to ~3.2% at maximum stress level (2.02 MPa).

EA, Timberset and Sikadur sample also exhibited similar behaviour to RSA under loading with increasing strain corresponding to the increase in stress level. At the lowest stress level (0.13MPa) EA exhibited ~ 3.2% of creep strain at the end of 1600 minutes testing. The highest stress level shows failure at less than 14% strain. Although it shows higher creep strain that RSA, the EA samples failed at much later than RSA. Referring to Figure 9.22, sample RSA failed at ~900 minutes whilst EA failed at ~1300 minutes as depicted in Figure 9.23. Under maximum stress loading, both micro-filled Timberset (Figure 9.24) and Sikadur (Figure 9.25) exhibited less creep strain at shorter test time. Prolong heating during testing may contribute to further crosslinking of Timberset and Sikadur that leads to the brittleness of the epoxy.

It is noticeable that in comparison to RSA, the EA formulation is more stable. This also indicates that at much higher stress level and high temperature, EA still retain its ductility. The effect of further cross-linking during test has resulted RSA to become more brittle (losing ductility) thus resulting it to become less stable than EA. It is proposed that the stability of EA was contributed by the addition of liquid rubber and variation of reactive diluents.

b) Creep strain at low temperature is less defined

Creep strain steps at lower temperature region (20°C, 25°C and 30°C) becoming less defined with increasing stress level as shown by all adhesives. At lower stress the creep strain curve corresponds to the temperature steps. At higher level of stress, the steps within these regions became almost linear until the temperature reaches the transitional region (T_g). The observation at maximum stress level has indicated that creep strain was less influenced by temperature steps. As indicated in Figure 9.22, during testing period of 20°C to 30°C the curves merged into one large step and equilibrate shortly at the end of 30°C step. Significant creep strain was again observed at 35°C and 40°C before settling to smaller creep steps at 65°C onwards. The onset of a more defined curve of

creep strain only occurs after reaching Tg. The hypothesis put forward is that under high stress condition, creep is more influenced by magnitude of stress than temperature.

(c) Shorter duration of testing time

With an increase in magnitude of stress, the stability of the adhesive which correspond to the level of temperatures will also decrease. This is evident through shorter testing duration obtained from repeated experiments at higher level of applied stress. At 0.13MPa, the tested samples were stable up to the end of the test (80°C) which takes up to 1600 minutes to complete. Except for the lowest stress level, the remaining tests ended before the 1600 minutes duration accordingly with the highest stress level completed at the shortest time. The stability of the adhesive was shortened to ~900minutes (RSA), ~1200minutes (EA), ~900minutes (Timberset) and ~700minutes (Sikadur) when tested at maximum applied stress. The most probable explanation is that there is an increase of cross linking of adhesive due to increase in testing temperature. This have resulted the adhesive to change from ductile to almost brittle behaviour, losing its rubbery behaviour. When imposed to higher stress, the adhesive which acted more brittle rather than ductile will experience shorter test duration. This observation can be related to the flexural testing of pure RSA samples that has been post cured. The test indicates that post curing will produce adhesive of slightly higher modulus and behaves more brittle (hence losing ductility) than un-post cured samples. The un-post cured samples also lasted longer before failing than post cured samples.

The EA formulation also performed better in terms of durability when compared to RSA. Findings from the study indicate duration of testing is longer on EA in particular with samples tested at higher stress. Evidence from Figure 9.24 suggests that samples tested at 0.13, 0.44 and 0.66 MPa completed the test with duration of 1600 minutes. Being compared to previous study, the RSA sample at 0.39 and 0.67 MPa had shorter testing time with ~1450 minutes and ~1050 minutes respectively. This finding suggested that EA formulation is more creep resistant than RSA when tested at higher temperature. Testing at higher stress level indicates that EA sample is still stable at 65°C. Based on this finding, the creep stability of EA formulation has implied that it is suitable for application on glued-in joints at high temperature. It is important, however, the application of glued-in joints conforms to appropriate design load and the stress

does not exceed the limitation of the adhesive under service condition at high temperature and humidity. The effect of temperature and humidity on glued-in joints will be presented in Chapter 12.

(d) Absence of retraction at the end of equilibrium

All figures suggested that strain recovery can be observed at the end of creep increment and this observation is only true for lower stress level. As indicated in Figure 9.22, the curve at 0.67 to 2.02 MPa shows that creep strain will continue to rise corresponding to temperature steps. Towards the end of the test, the creep strain continues to rise without reaching equilibrium before failing. This behaviour resembles the classic secondary and tertiary creep phase before failure occurs.

Following the phase of viscoelastic zone, creep strains of EA sample increases and equilibrate at the end of each temperature steps (50°C onwards). It was observed that retraction of strain occurs at the end of equilibrium stage due to entropy behaviour as depicted in all samples. The retraction is however less prominent for samples tested at higher stress level since all samples at Tg + 15°C does not settle to a constant value and equilibrate. Creep strain for all samples continues to increase gradually indicating second and tertiary creep phase before failing.

9.3.3 MULTI-STAGE CREEP IN SHEAR

Creep experiments in shear within the DMTA are limited by the application of a peak static force of 10N. As a result peak shear stresses are limited to ~0.3MPa. In a bonded-in rod subjected to a design load of from 2 to 3N/mm^2 of rod surface area the shear stress in the adhesively bonded interface could reach 2.4 to 3.5 MPa for a bonded-in depth of 200mm. Shear stress will decrease as the bonded-in depth is increased. The same theory is being applied in this study where the levels of stresses are imposed by varying the sandwich sample overlap length.

Despite the limitation of the applied shear stress available in the DMTA the observed trends in creep response (Figure 9.26) provide a basis for understanding the creep

behaviour of bonded-in connections (GFRP pultrusions in LVL) to be reported in Chapter 12.

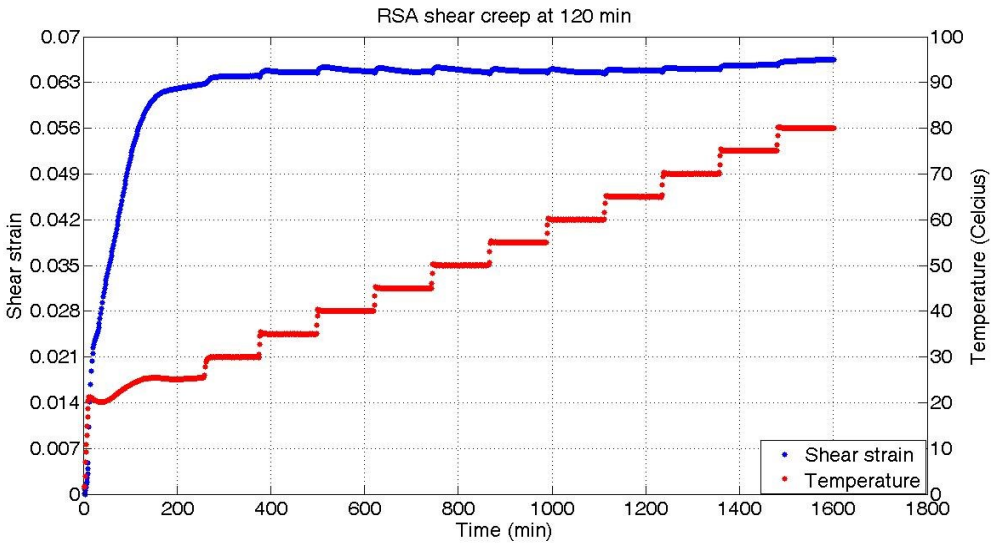

Fig. 9.26. DMTA thermal scan for RSA in shear with 120 min dwell times

The shear characteristic for all adhesive at constant stresses of 0.07, 0.17 and 0.30MPa are as presented in Figure 9.27, 9.28, 9.29 and 9.30 respectively. In shear the adhesives show more strain close to T_g than in tension (Figure 9.27) but at ~45ºC the change in strain as a function of temperature is very modest and the strain versus time characteristics, with incremental change in temperature, are close to linear. The shear modulus of the adhesive is of the order of one third of the tensile modulus hence temperature-induced creep stabilises more quickly than in tension and deformation at higher temperatures is controlled by the rubbery network. In RSA, the largest shear stress applied (0.30MPa) is insufficient to fail the adhesive in shear up to 80ºC.

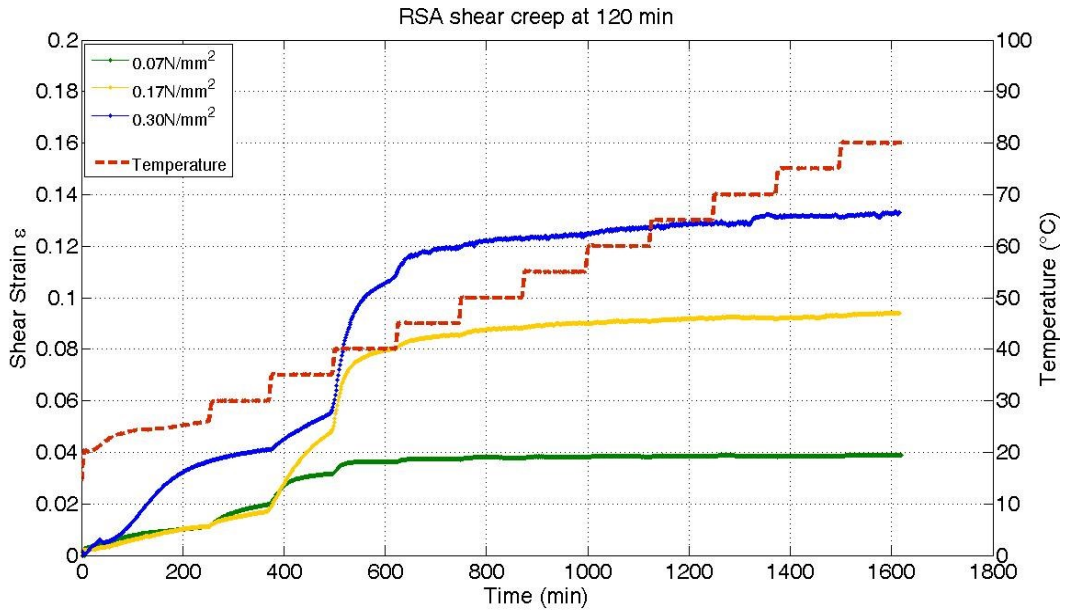

Fig. 9.27. Strain versus time for RSA subjected to temperature increased in 5°C steps for 120 min intervals from 20 to 80°C at constant stresses ranging from 0.07 to 0.30MPa.

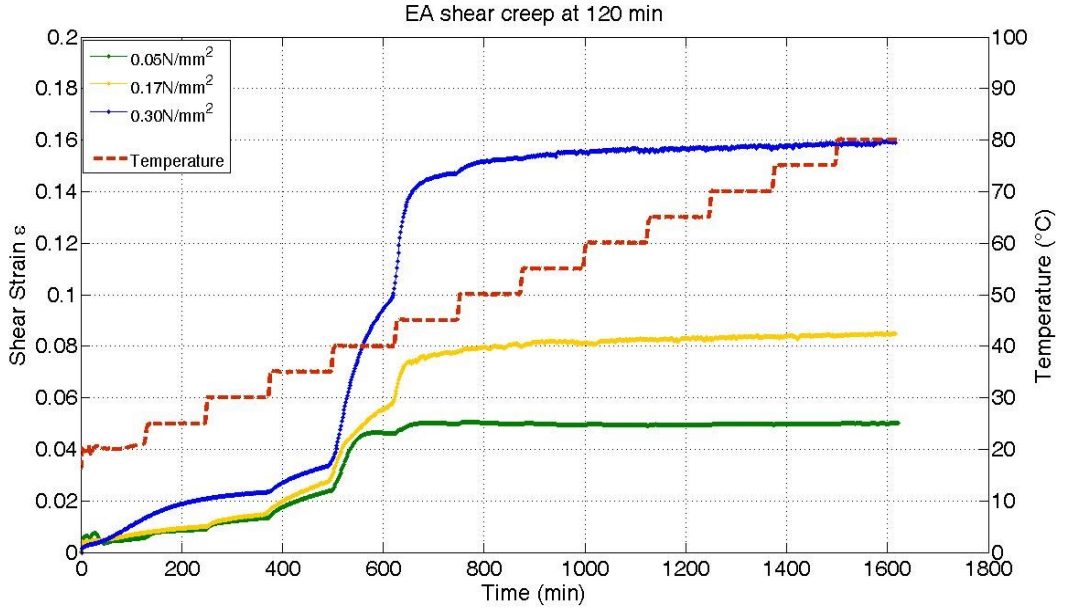

Fig. 9.28. Strain versus time for EA subjected to temperature increased in 5°C steps for 120 min intervals from 20 to 80°C at constant stresses ranging from 0.05 to 0.30MPa.

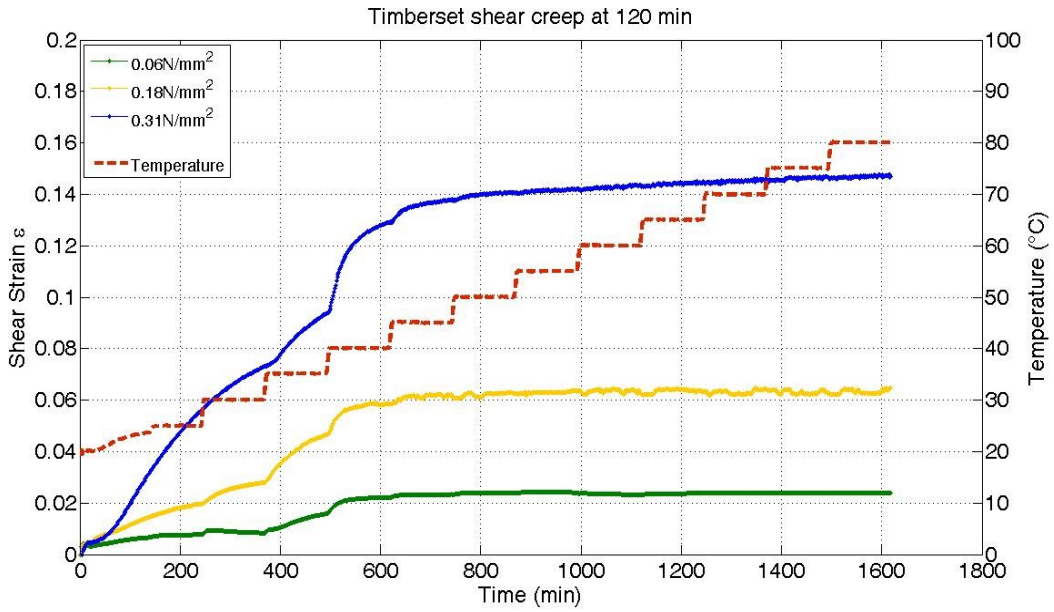

Fig. 9.29. Strain versus time for Timberset subjected to temperature increased in 5°C steps for 120 min intervals from 20 to 80°C at constant stresses ranging from 0.06 to 0.31MPa.

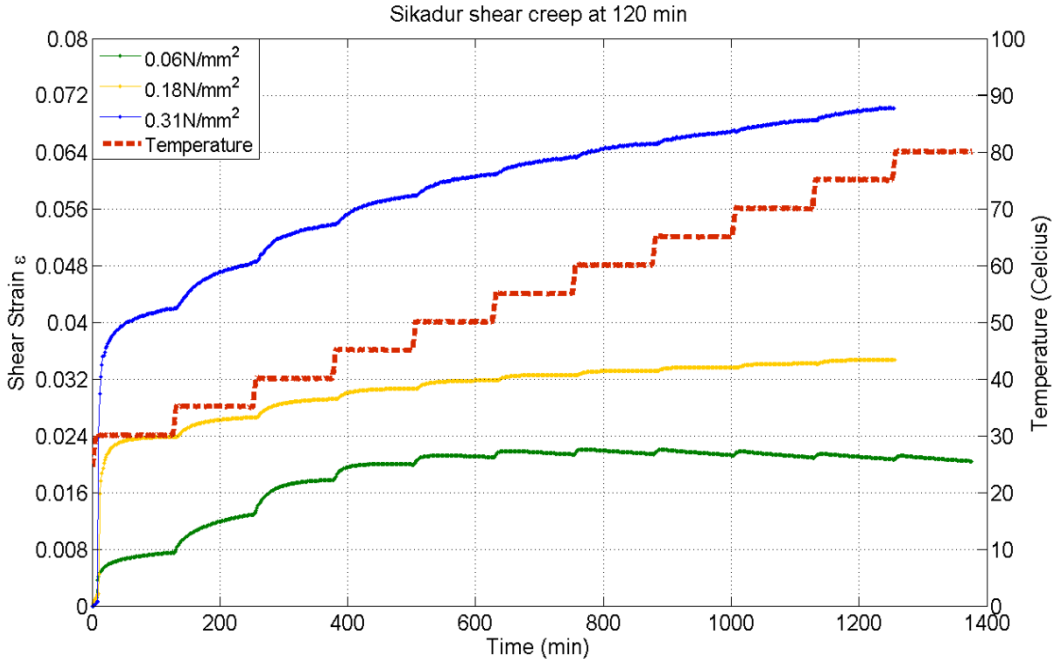

Fig. 9.30. Strain versus time for Sikadur subjected to temperature increased in 5°C steps for 120 min intervals from 20 to 80°C at constant stresses ranging from 0.06 to 0.31MPa.

The EA formulation subjected to creep is shear (Figure 9.28) behaves similarly to RSA although the peak shear strain at 0.30MPa is higher than for the RSA at the same stress level possibly as a result of the liquid rubber content. The likelihood of phase separation

of the rubber content depends on the volume fraction of rubber in the base adhesive. In this case the rubber is evenly dispersed throughout the adhesive and phase separation has not been observed using transmission electron microscopy as indicated in Chapter 7.

As expected, creep strains for EA in shear are much greater than for tensile creep (Figure 9.28) at similar stress levels. The ability of the adhesive to maintain an almost constant creep strain up to 80ºC above the viscoelastic transition indicates the stable behaviour of a rubbery network.

The creep behaviour of Timberset in shear (Figure 9.29) is similar in general form to Figures 9.27 and 9.28 for RSA and EA adhesives respectively. The particle-filled microstructure does not have a marked influence on creep compared to the unfilled adhesives, consistent with behaviour in tensile creep.

The shear creep response of Sikadur (Figure 9.30) marked a different response compared to the behaviour of RSA, EA and Timberset. Sikadur subjected to shear creep under constant stress of 0.06, 0.18 and 0.31MPa failed at 1390 and 1250minutes respectively. At 0.31MPa, Sikadur continues to increase in creep strain, showing classic secondary and tertiary creep response before failing. It is also noted that Sikadur creep at much lesser strain compared to the other adhesive in this study. This gives an insight on the response of brittle (high modulus) epoxy to shear creep in comparison to ductile epoxy. This shows that the type of filler and matrix has a significant influence on the durability of epoxy adhesive under shear load. Low creep strain of polymer is much influenced by restricted polymer chain sliding due to high crosslinking. Sikadur performed better in tension static test (Chapter 7) and creep in tension but exhibited less desirable performance under shear mode.

9.3.4 MATHEMATICAL MODEL FOR CREEP IN TENSION

All four adhesives under investigation appear to exhibit classic viscoelastic creep in the temperature range of Tg to Tg + 15ºC. The Kelvin-Voigt equation for creep strain ε(t) under constant creep stress (σ_0) as given by Equation 9.4:

$$\varepsilon\,(t) \;=\; \frac{\sigma_O}{E}\cdot\left[1-\exp\left(-\frac{t}{\tau}\right)\right] \qquad \text{(Eqn. 9.4)}$$

In order to establish how closely the thixotropic adhesives obey the creep equation of Equation 9.4, tensile creep data for all adhesive were generated in the DMTA for time intervals of 360 minutes at temperatures from 30 to 60ºC with an applied force of 2N equivalent to a stress of 0.4MPa. The data on creep strain versus time for RSA, EA, Timberset and Sikadur are as presented in Figures 9.31, 9.32, 9.33 and 9.34 respectively.

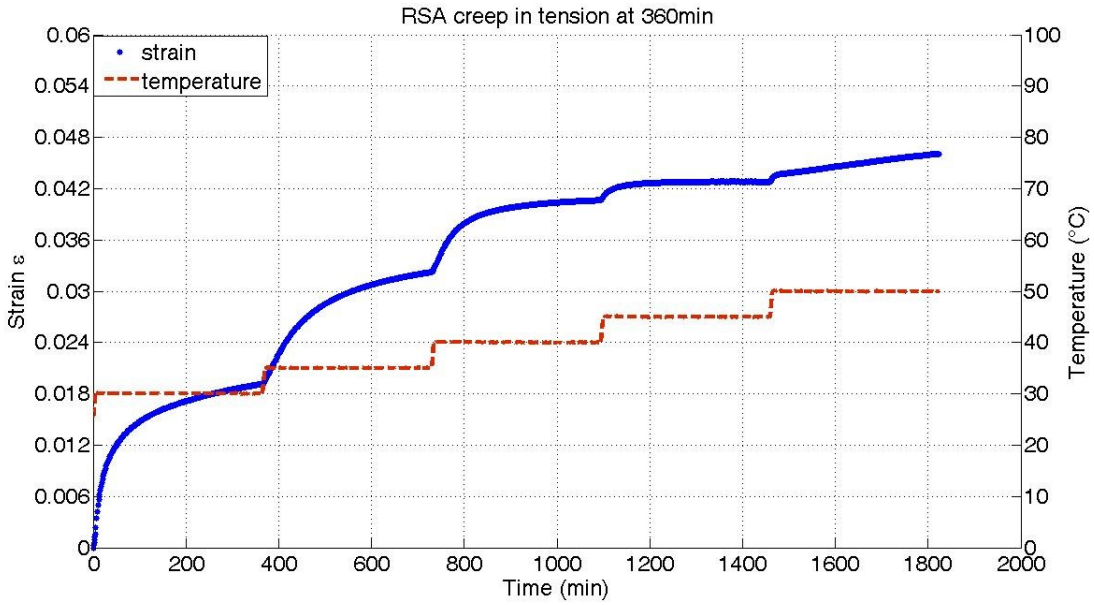

Fig. 9.31. Creep curves for RSA in tension (2N) in the viscoelastic zone from 30 to 50°C with time increments for creep of 360 minutes.

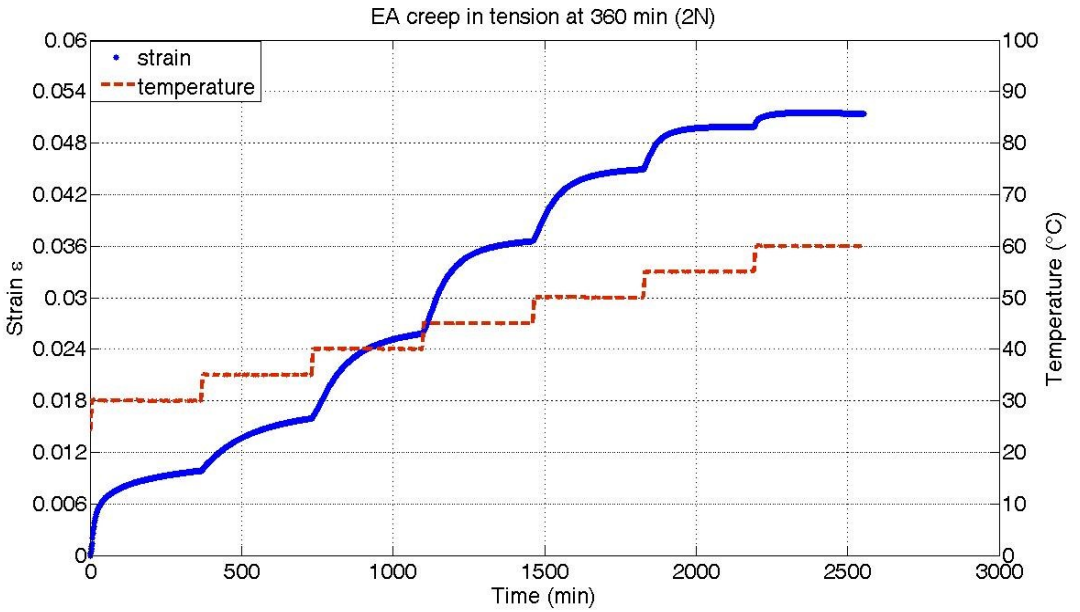

Fig. 9.32. Creep curves for EA in tension (2N) in the viscoelastic zone from 30 to 60°C with time increments for creep of 360 minutes.

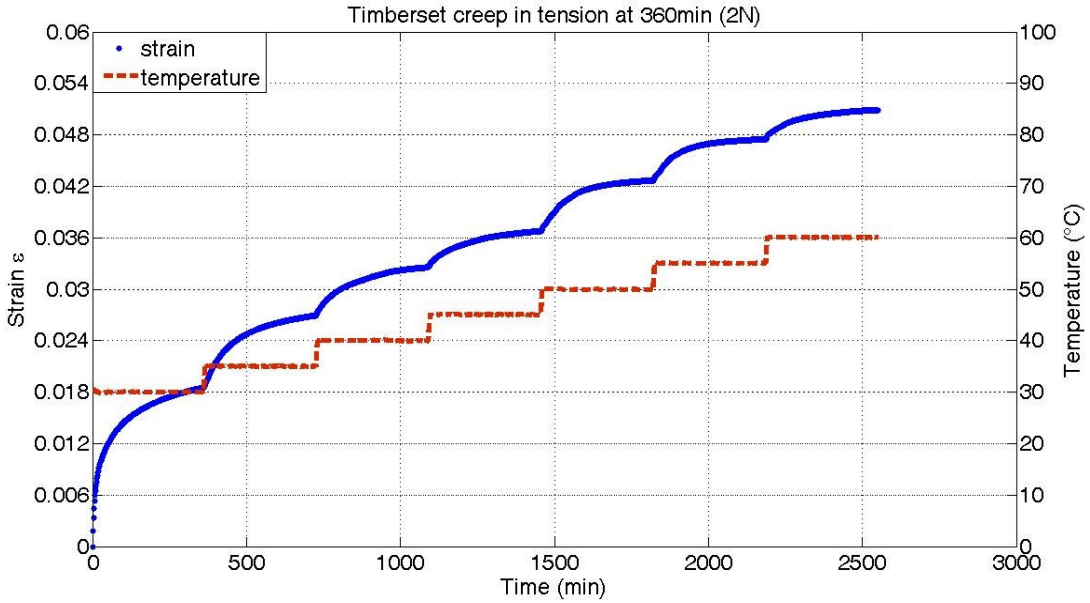

Fig. 9.33. Creep curves for Timberset in tension (2N) in the viscoelastic zone from 30 to 60°C with time increments for creep of 360 minutes.

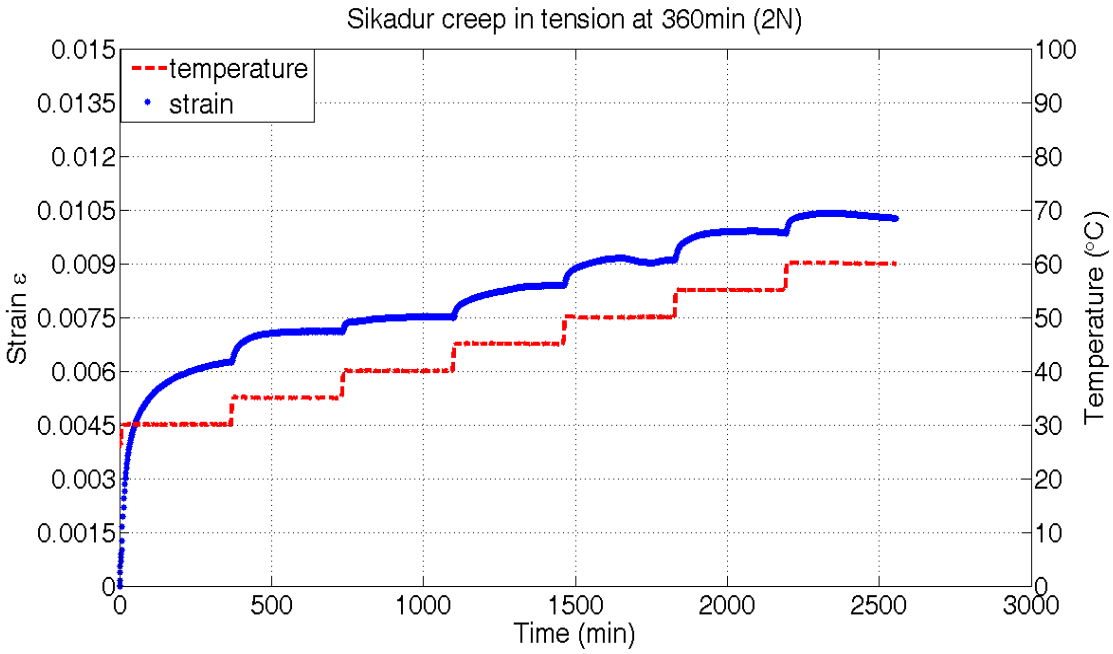

Fig. 9.34. Creep curves for Sikadur in tension (2N) in the viscoelastic zone from 30 to 60°C with time increments for creep of 360 minutes.

Each curve at corresponding temperature was separately analysed with Matlab and the results are presented in Table 9.2 to 9.5 under the heading MODEL1. The creep strain curves are fitted according to the Kelvin-Voight creep equation and are featured in the section Appendix 1 to 4. In the mentioned tables, the parameter *a* is equal to σ_0/E, τ is the characteristic retardation time and the elastic modulus *E* is computed from the predicted strain at equilibrium at the end of each creep stage. For EA, the dashpot viscosity at 45ºC is predicted to be $2.0.10^{11}$Ns.m^{-2}. Between 35 and 55ºC (above Tg) the data fits the equation well and the retardation time at 35ºC (163.8min) drops progressively to 23.9min at 60ºC. However the coefficient of determination (R^2) at 30 and 60ºC demonstrates that the goodness of fit is less ideal. Therefore to improve the model over the complete range of temperature a series two element Kelvin-Voigt model is proposed. Strain as a function of time is given by Equation 9.5:

$$\varepsilon(t) = \frac{\sigma_0}{E_1}\cdot\left[1-\exp\left(-\frac{t}{\tau_1}\right)\right]+\frac{\sigma_0}{E_2}\cdot\left[1-\exp\left(-\frac{t}{\tau_2}\right)\right] \qquad \text{(Eqn. 9.5)}$$

The parameter *a* is equal to σ_0/E_1 and the retardation time τ_1 corresponds to the left hand element. The parameter b is equal to σ_0/E_2 and the retardation time τ_2 corresponds to the right hand element. The results of curve fitting with the two elements MODEL2 are also summarised in Table 9.2 to 9.5. The coefficients of determination are now all very close

to unity. It is proposed that a one or two element Kelvin-Voigt model is suitable for modelling the time-dependent creep behaviour of ambient cure thixotropic adhesives above Tg and that modelling with a spectrum of retardation times is unnecessary. In general, the mentioned tables of creep coefficients indicate that τ_2 is less than τ_1 and thus two creep processes with different time constants take place simultaneously. Creep mechanisms might relate to the realignment of the rubbery network and the more rapid movement of more mobile molecular chains enclosed by that network.

Table 9.2. Modelled creep coefficient for RSA

	MODEL 1				MODEL 2						
T (°C)	σ/E	τ(min)	E(Gpa)	R^2	σ/E	τ_1(min)	E_1(Gpa)	σ/E	τ_2(min)	E_2(Gpa)	R^2
30	0.0180	48.38	0.0223	0.957	0.010	18.88	0.039	0.010	167.400	0.041	0.999
35	0.0140	110.90	0.0301	0.999	0.004	52.55	0.098	0.010	149.100	0.039	0.999
40	0.0082	62.20	0.0492	0.996	0.002	36.65	0.168	0.006	80.140	0.068	0.998
45	0.0020	34.63	0.2313	0.991	0.001	43.27	0.272	0.001	2.494	0.660	0.996
50	Response not viscoelastic										

Table 9.3. Modelled creep coefficient for EA

	MODEL 1				MODEL 2						
T (°C)	σ/E	τ(min)	E(Gpa)	R^2	σ/E	τ_1(min)	E_1(Gpa)	σ/E	τ_2(min)	E_2(Gpa)	R^2
30	0.0092	41.13	0.0435	0.9422	0.0058	169.00	0.0689	0.0045	16.52	0.0884	0.9998
35	0.0068	161.80	0.0589	0.9999	0.0006	162.20	0.6427	0.0068	1.05	0.0589	0.9999
40	0.0106	112.50	0.0379	0.9998	0.0106	112.40	0.0379	0.0011	17.91	0.3484	0.9998
45	0.0115	80.71	0.0348	0.9997	0.0002	84.71	1.6267	0.0113	0.01	0.0354	0.9999
50	0.0086	79.20	0.0464	0.9997	0.0008	80.28	0.5070	0.0086	0.05	0.0466	0.9997
55	0.0050	45.91	0.0800	0.9992	0.0005	142.60	0.8237	0.0046	41.34	0.0864	0.9998
60	0.0011	29.28	0.3518	0.8958	0.0014	0.63	0.2780	0.0003	0.05	1.2630	0.9877

Table 9.4. Modelled creep coefficient for Timberset

	MODEL 1				MODEL 2						
T (°C)	σ/E	τ(min)	E(Gpa)	R^2	σ/E	τ_1(min)	E_1(Gpa)	σ/E	τ_2(min)	E_2(Gpa)	R^2
30	0.0174	47.82	0.0230	0.9180	0.0106	176.90	0.0379	0.0091	20.5100	0.0438	0.9999
35	0.0081	105.30	0.0492	0.9975	0.0057	208.60	0.0703	0.0037	49.4100	0.1080	1.0000
40	0.0052	153.50	0.0770	0.9992	0.0011	166.00	0.3653	0.0051	22.3900	0.0791	0.9995
45	0.0040	155.00	0.1009	0.9997	0.0006	158.10	0.6407	0.0039	14.1000	0.1014	0.9998
50	0.0059	89.54	0.0673	0.9995	0.0060	89.35	0.0672	0.0004	0.0049	1.0793	0.9995
55	0.0046	77.89	0.0863	0.9988	0.0004	78.24	0.9615	0.0046	0.4439	0.0865	0.9988
60	0.0031	111.40	0.1289	0.9983	0.0013	190.00	0.3195	0.0024	42.2700	0.1689	0.9999

Table 9.5. Modelled creep coefficient for Sikadur

	MODEL 1				MODEL 2						
T (°C)	σ/E	τ(min)	E(Gpa)	R^2	σ/E	τ_1(min)	E_1(Gpa)	σ/E	τ_2(min)	E_2(Gpa)	R^2
30	0.0055	41.06	0.0727	0.9727	0.0024	110.10	0.1661	0.0040	17.05	0.0990	0.9987
35	0.0007	39.51	0.5825	0.9896	0.0002	37.73	2.1704	0.0006	3.04	0.6607	0.9991
40	0.0002	105.20	1.8493	0.9598	0.0001	100.40	3.5273	0.0002	3.00	1.9084	0.9771
45	0.0007	119.70	0.5687	0.9853	0.0002	134.20	1.9685	0.0007	6.90	0.5770	0.9980
50	0.0005	38.51	0.7386	0.8489	0.0002	45.93	2.5543	0.0005	3.97	0.8300	0.8685
55	0.0005	48.12	0.7289	0.9741	0.0002	51.41	2.1209	0.0005	3.65	0.7663	0.9857
60	0.0003	21.10	1.2837	0.5812	0.0000	10.86	14.7601	0.0003	0.91	1.1908	0.5214

From these comparisons, it is important to take notice two most influential properties and to distinguish how these entities affect the material differently. The creep experiment was conducted to emulate the behaviour of the adhesive at extreme condition. Creep is a time dependant property that occurs onto a material when load is applied and at low strains (~1%) is recoverable after unloading. The influence of temperature on creep is to accelerate the process, which means that creep will still occur even without the influence of temperature. Thermal expansion on the other hand is activated only by an increase in temperature which is responsible to increase molecular rearrangements and the onset of reaction is not subjected to external load. These aspects are the topics of concern since there have been discussions on the practicability of using low Tg adhesive for structural purposes. Through this study, it was proven empirically that the adhesive will endure high temperatures under load. Suitable structural design in concealing joint locations is recommended, in which the joint is not exposed to extreme temperature and humidity.

Therefore, the following conclusion can be drawn:

- The creep properties of three commercial, thixotropic, shear-thinning timber adhesives have been measured using a static creep programme in a Dynamic Mechanical Thermal Analyser.
- The DMTA has demonstrated that tensile creep strains are a function of temperature and stress, as expected, but above Tg + 15ºC the adhesives behave like rubbers with low elastic moduli. At low stresses the adhesives are stable up to 80ºC but as the stress is increased the rupture stress falls to temperatures as low as 50ºC.
- Creep testing in the DMTA has also been employed to evaluate shear creep in miniature structural sandwiches with a 2mm thick glue line bonded between wood veneers. Shear creep occurs more rapidly than tensile creep but settles down to a constant creep strain once the viscoelastic range of temperature has been exceeded.
- Simple Kelvin-Voigt elements have been used successfully to model creep in the viscoelastic zone. A two element model is sufficient to model creep in thixotropic adhesive

CHAPTER 10 : THICK ADHEREND SHEAR TEST (TAST)

10.1 INTRODUCTION

One of the most destructive adhesive system failures is delamination of the reinforcing layer. The connection between the adhering layers has an essential influence on the mechanical properties of bonded joints. To understand the basic failure mechanism and the interrelation between adhesive and adherend, the Thick Adherend Shear Test (TAST) was employed. The TAST was developed with the objective of obtaining the state of pure shear stress through the removal of non-uniformity in stresses. This test is practically a modification of a typical single lap joint except the substrates used in this test are thicker, which makes it even more rigid. Volkersen (1938) has indicated that one of the factors that can be used to decrease the shear stress concentration in adhesive layer is by increasing the stiffness of the substrates. RSA, EA and Timberset epoxy adhesive were selected for the TAST study. Values of stress-strain exhibit brittle failure for all tested adhesive. The mean shear strength (MPa) is the highest in EA. Elastic finite element analysis (FEA) indicates peak stresses around the end of lap zone. Distribution of stress on wood-adhesive interface and mid-bondline indicates a gradient of stresses in accordance to distance to the edge of lap zone.

10.2METHODOLOGY

10.2.1 SAMPLE FABRICATION

RSA, EA and Timberset were tested for the thick adherend lap joint test. The mechanical properties and microscopic details of the adhesives have been thoroughly discussed in Chapter 7 and 8.

For the adherend of the test samples, five samples with Radiata pine solid wood adherends were prepared with each of three epoxy-based structural adhesive. Shear samples as depicted in Figure 10.1 with a total length of 250mm, 25mm in width and thickness of 2 x 6 mm was used in this study. The overlap length of the joint

was fixed at 5 mm. The dimension of the samples was fabricated based on ISO 11003-2:2001 standard on determination of shear behaviour of structural adhesives. According to the standard, the geometry of the sample was designed to reduce peel effects and to achieve state of pure shear in the adhesive layer.

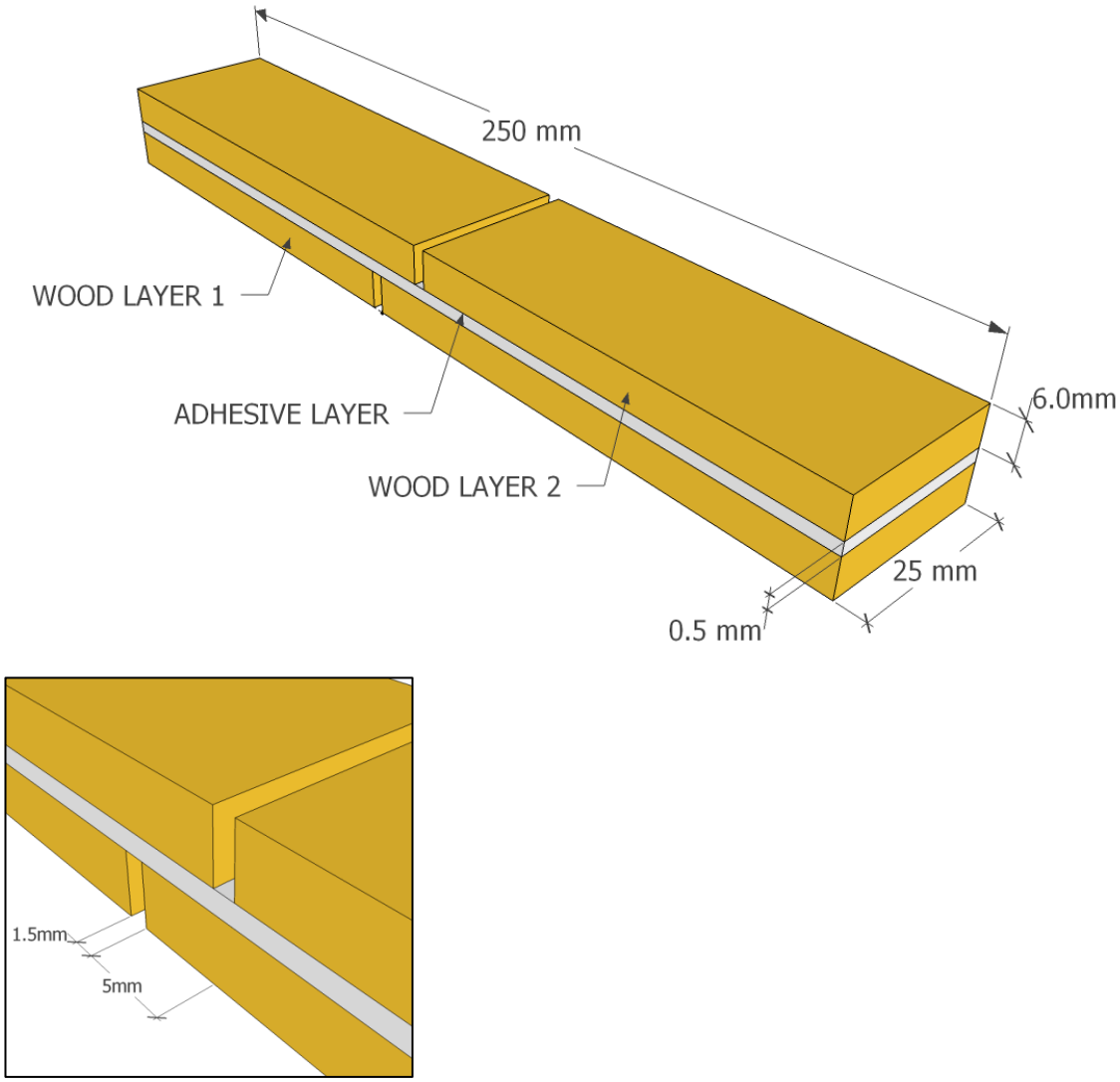

Fig. 10.1. Dimension of thick adherend sample including notch (insert)

The samples were fabricated by bonding two 6 mm thick knife-planed, straight grain Radiata pine wood slats (Figure 10.2). Aluminium spacers were glued in 50 mm interval on the surface to be bonded. The thickness of the aluminium spacers dictates the bondline thickness of the TAST lap joint. Adhesive thickness was fixed at 0.5mm. Gluing was done at a room temperature (20 ± 3°C) and allowed to cure under pressure of 0.1 N/mm^2. The samples were conditioned for 20 days (at 20 ±

3°C) after the initial 48 hours of cold-pressing before testing. The aluminium spacers were removed after the curing of the samples by cutting both sides (lengthwise) of the wood slats. The incision was made using a band saw to direct the notches towards the glue line. The bonded length of the samples was fixed at 5mm as suggested by ISO 11003-2:2001 standard. The measurement of adhesive thickness was done by subtracting the thickness of adherend from the value of overall bonded thickness of the sample. Prior testing the samples were conditioned at 20 ± 3C and 65% relative humidity (RH). The sample dimensions were determined by using a digital micrometer. 15 samples were tested for each glue type under investigation.

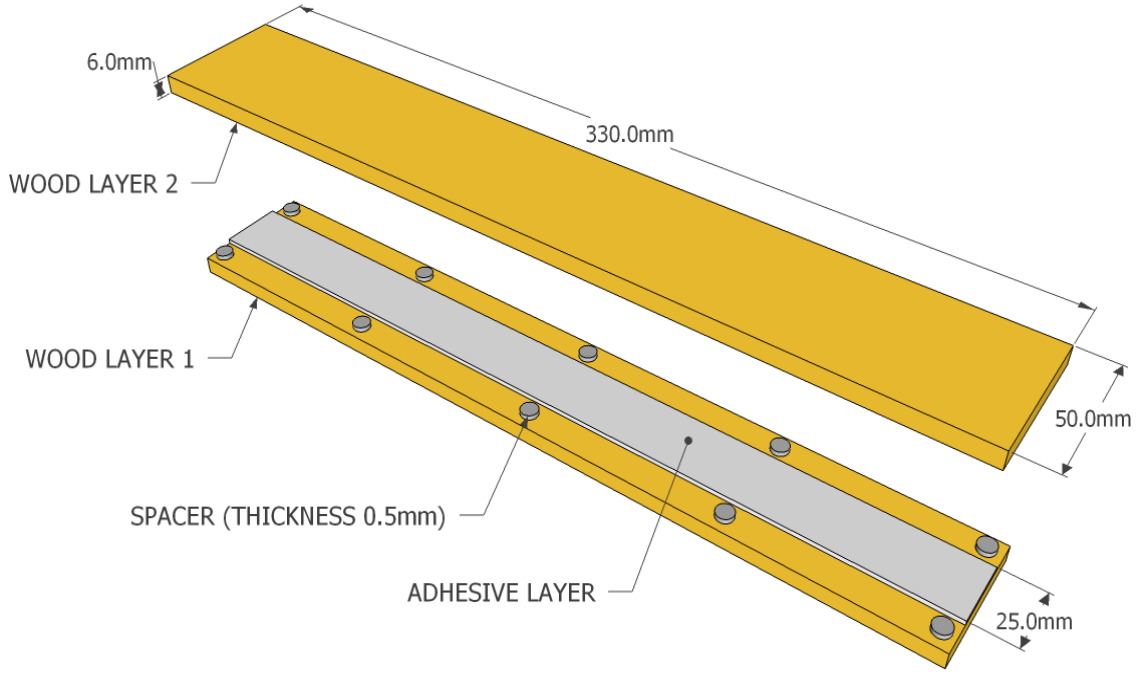

Fig. 10.2. Fabrication of TAST sample using two layer of wood

10.2.2 TESTING CONFIGURATION

The samples were tested to failure using a universal testing machine (Instron 3369) by applying the load at crosshead speed of 1mm/min. The load measurements were made using a computer data acquisition system Bluehill2. The test rig is as depicted in Figure 10.3. Samples were positioned between the grips and tested in pull-pull configuration. A close up on a sample under loading shows the grip length which extended from the edge of the sample until 5mm from the notch (Figure 10.4). All tests were conducted at room temperature (20 ± 3°C).

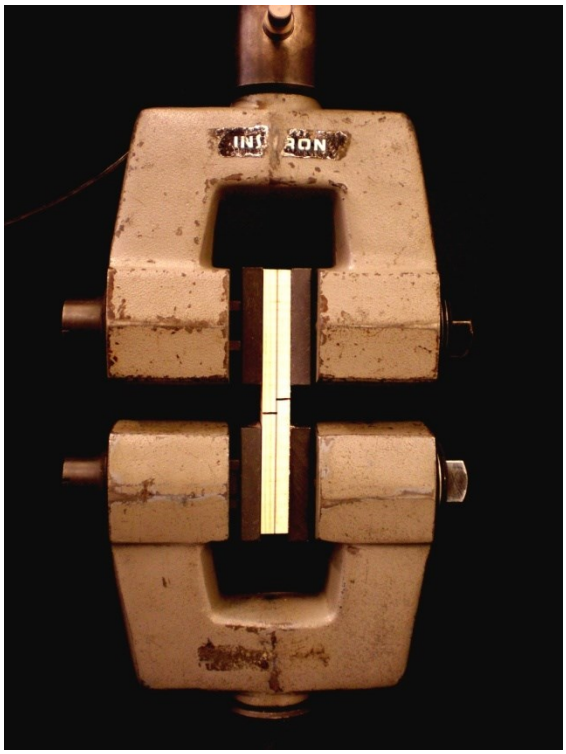

Fig. 10.3. Thick adherend shear sample fitted to the tensile test rig.

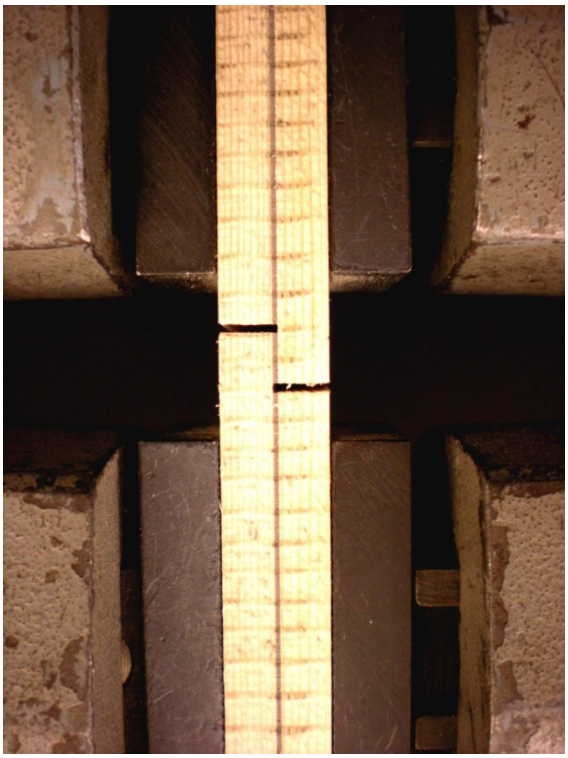

Fig. 10.4. Close-up of a sample fitted to the test rig showing thin glue-line for shear testing.

10.2.3 DATA ANALYSIS

The measurement of shear stress and strain was made based on the assumption that the lap joint is in pure shear condition. Shear stress was assumed to be uniform along the bonded length. The stress-strain curve was plotted based on the calculation of shear strain and average shear stress. The shear strain, γ of a lap joint can be calculated through the relationship:

$$\gamma = \frac{d}{t} \qquad \text{(Eqn. 10.1)}$$

Where, *d* represents the relative shear displacement and *t* denotes the thickness of adhesive layer. Both *d* and *t* were measured in mm.

Average shear stress, τ (MPa) is given by the equation:

$$\tau = \frac{F}{lb} \qquad \text{(Eqn. 10.2)}$$

Where, F is the applied force measured in N. l and b represents the overlap length and width respectively.

10.2.4 FINITE ELEMENT ANALYSIS (FEA)

The model and mesh were built using ANSYS finite element software. 2D modelled mesh with PLANE 182 4-node element was used in this study for the adherend and adhesive. Selection of element was made base on the suitability of the element for modelling irregular mashes. The elastic constants used in the finite element are as shown in Table 10.1. The model was loaded in tension at 1.98 kN, which is the failure load for RSA. The detail mesh of the model and boundary condition is as shown in Figure 10.5 and 10.6 respectively. Results on stresses data were obtained at the mid-bondline and near the interface of the adherend.

Table 10.1. Elastic constants of materials

Properties	Epoxy adhesive (RSA)	Adherend (Radiata pine)
Ex (MPa)	1600	10,000
Ey (MPa)	-	1000
Ez (MPa)	-	1000
Poisson ratio (γ)	0.3	0.35
Gxy (MPa)	-	760
Gyx (MPa)	-	400

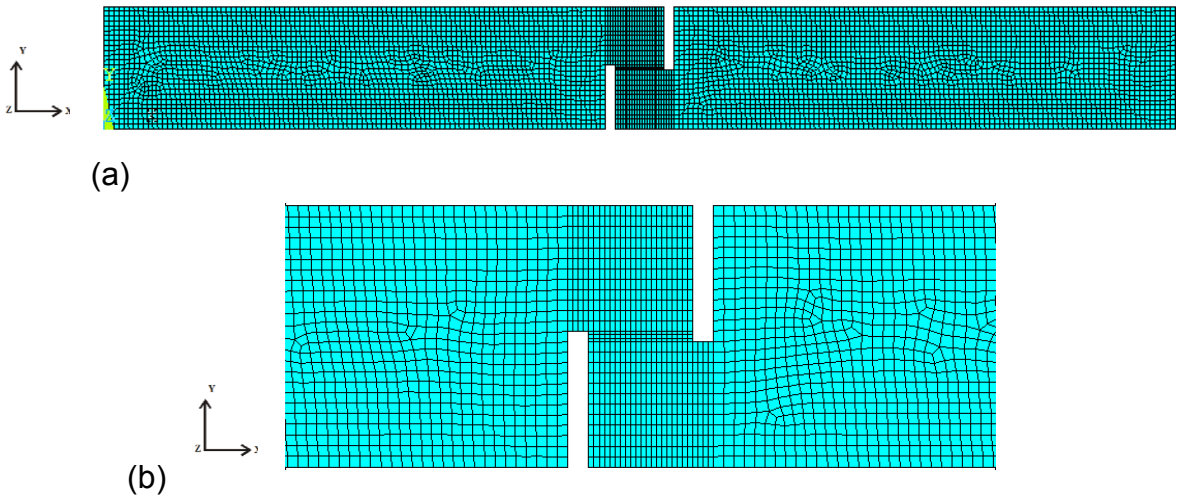

Fig.10.5. Finite element model : (a) mesh of model overall and (b) detail mesh for overlap zone

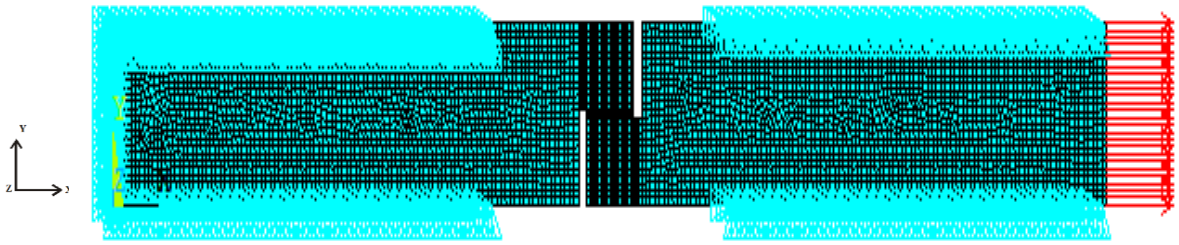

Fig.10.6. Finite element model showing boundary condition

10.3 RESULTS AND DISCUSSIONS

10.3.1 SHEAR STRESS AND STRAIN

The shear stress-strain behaviour of epoxies under investigation was shown in 10.7. Table 10.2 shows the data for adhesives tested for shear test. All adhesive exhibited similar response of brittle failure, which characterise the physical behaviour of a stiff adhesive. None of the shear stress-strain curves levels off before failure. EA adhesive remains linear until 14MPa shear stress before exhibiting non-linearity. Maximum shear strength of EA adhesive is about 18 MPa before failure sets in. The maximum shear strength of RSA was found to be slightly lower than EA. The elastic limit of Timberset reached 12MPa before failure. Generally, the shear-strain curve for all adhesive exhibited linear response reaching to failure.

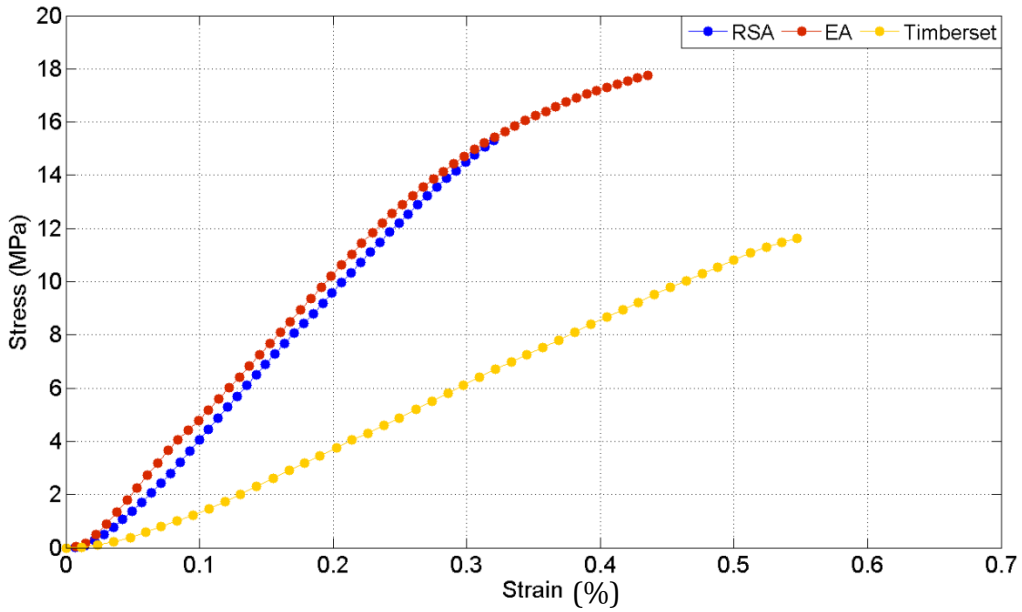

Figure 10.7. Shear stress and strain of various adhesives

10.3.2 MEAN SHEAR STRENGTH

The shear strength data of TAST samples made using RSA, EA and Timberset adhesive illustrated in Figure 10.8. The mean shear strength values and coefficient of variation for each adhesive are given in Table 10.2. Based on the satisfactory performance of the shear strength, it can be concluded that the application of thick adherend lap joint obtained with RSA, EA and Timberset adhesives was successful. As shown in the Figure 10.8, lap joints made of EA adhesive had better shear strength than RSA and Timberset. The performance of these adhesive under shear loading conforms well to the mechanical performance of the bulk adhesive as reported in Chapter 8.

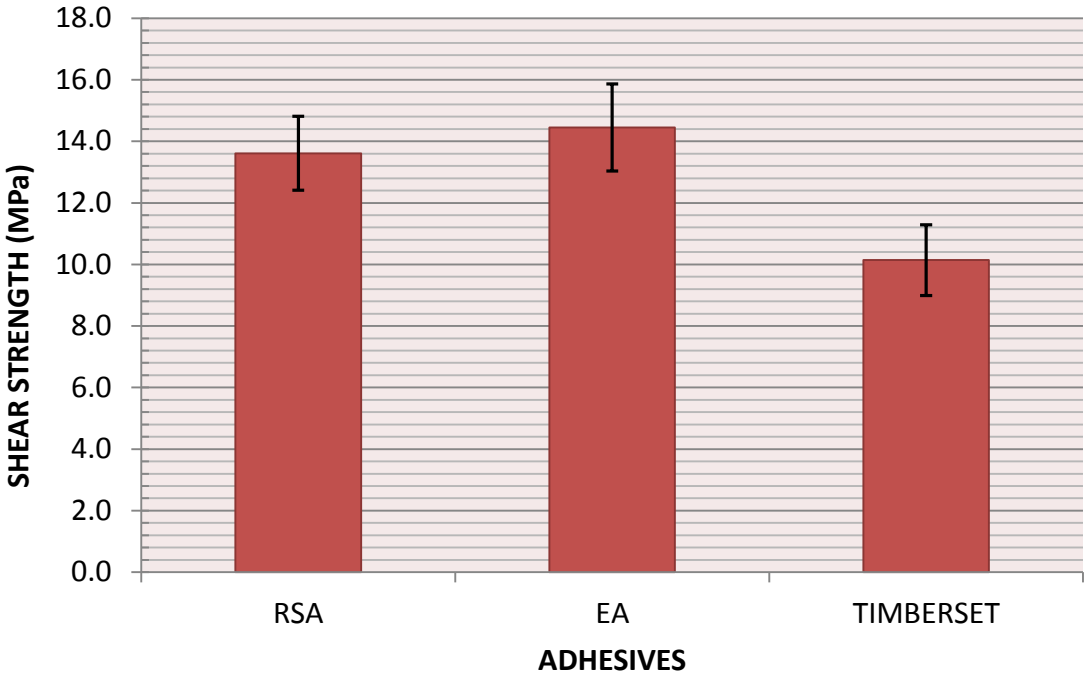

Fig. 10.8. Mean shear strength and standard deviation of TAST tested adhesives

Table 10.2. Mean shear strength of epoxy adhesive joint tested using TAST method

Adhesives	No. of samples	Max. load (kN)	Shear Strength (MPa)	
			Mean (MPa)	COV (%)
RSA	15	1.98	13.61	5.53
EA	15	2.09	14.45	7.71
TIMBERSET	15	1.66	10.14	5.19

The ANOVA results for the TAST test on RSA, EA and Timberset adhesive are shown in Table 10.3. The resulting F-value was significant at 95% probability level. The statistical analysis indicates that the types of adhesive used in the study and the resultant shear strength were significant. Statistical significant differences exist between all adhesive except for adhesive RSA and EA as shown in Figure 10.4.

Table 10.3. ANOVA of shear strength of TAST for various adhesives

TAST	F value	p- value
Shear Strength (MPa)	9.428	0.00

Table 10.4. Duncan multiple comparison of shear strength of TAST for various adhesives

Adhesives	Subset for alpha = 0.05	
	1	2
TIMBERSET	10.14	
RSA		13.61
EA		14.45

10.3.3 FAILURE MODE

The tested samples exhibited three types of failure mode which is wood failure, wood to adhesive failure and adhesive failure. None of the samples failed during testing. Sample failure can be defined as failure which occurred in the region that is not immediate to the high shear region (overlap length). This indicates the design of the TAST sample used in the test in valid. Most failure occurred in the wood as indicated in Figure 10.9, 10.10 and 10.11. These figures show the presence of glueline on the shear region with remaining thin layer of wood. All EA tested samples failed in wood with on 78.5% and 61.5% for RSA and Timberset respectively.

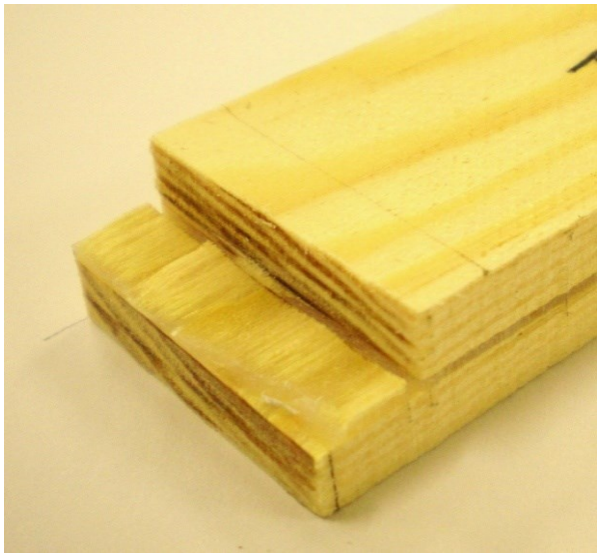

Fig. 10.9. Wood failure of TAST tested RSA samples

Fig. 10.10. Wood failure of EA samples

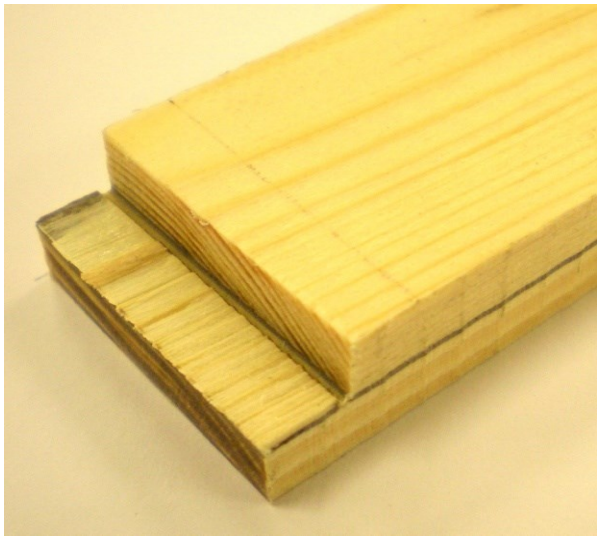

Fig. 10.11. Wood failure of TAST tested Timberset samples

Fig. 10.12. Wood failure of TAST tested Timberset samples with portion of earlywood.

The thickness of wood layer left on the tested sample may depend on the thickness of the growth rings. Close growth rings (Figure 10.13) will result wood failure of almost even thickness whilst wide growth rings (Figure 10.14) resulted otherwise. This is due to high portion of wood failure in earlywood as shown in Figure 10.12. The angle of the growth rings to the bondline is another factor which influences the mode of failure.

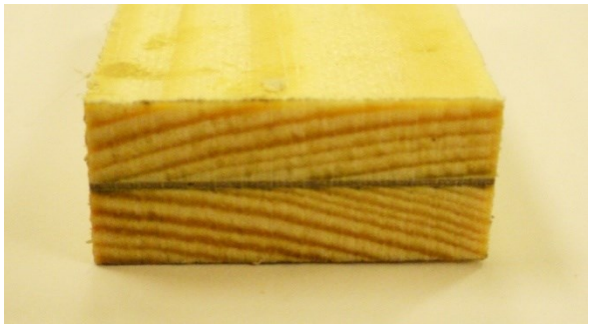

Fig. 10.13. Close growth rings

Fig. 10.14. Wide growth rings (bottom layer)

None of the TAST tested samples failed at wood to adhesive interface. A small percentage of RSA (21.4%) and Timberset (38.5%) samples failed within the adhesive layer. Adhesive failure is defined as failure of more than 50% of the glue layer as indicated in Figure 10.15 and 10.16. These results indicate on good bonding properties of the adhesives to wood substrate.

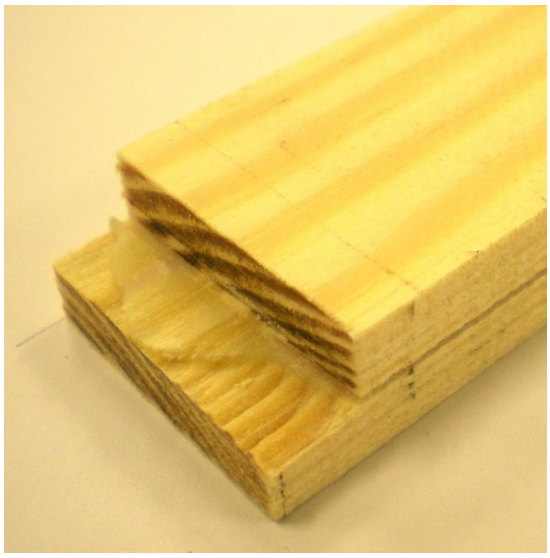

Fig. 10.15. Adhesive failure in TAST tested RSA sample

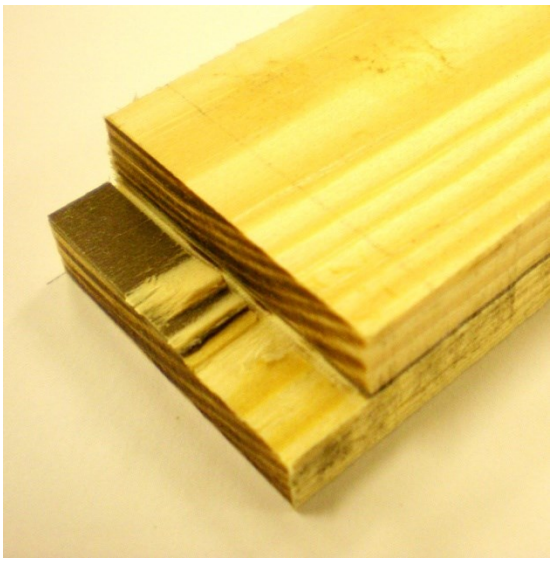

Fig. 10.16. Adhesive failure in TAST tested Timberset sample

10.3.4 FINITE ELEMENT ANALYSIS (FEA)

The tensile load was applied at the left-end of the lap joint sample as shown in Figure 10.6. As depicted in the stress contour plot in Figure 10.17, high stress concentration near the edge of the lap zone can be seen on the upper and lower substrates. The deformed shape of the lap joint shows slight distortion and bending moment, particularly within area which is immediate to the glue-line as shown in Figure 10.18.

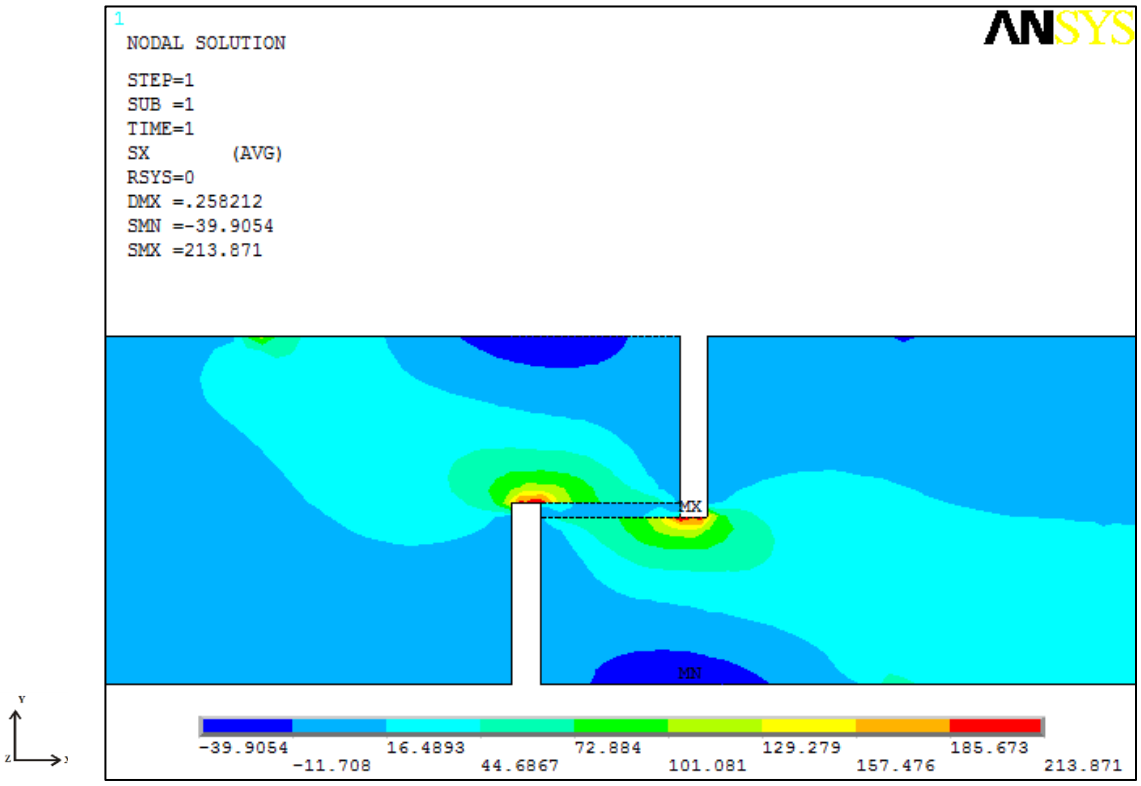

Fig. 10.17. Close up of x-stresses in the lap joint

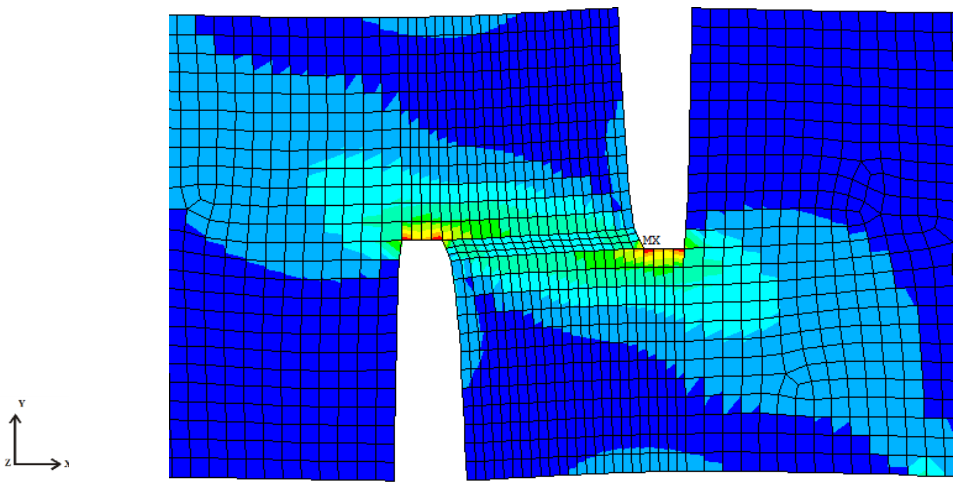

Fig. 10.18. Deformed shape of lap joint showing displacement in the x-direction

Figure 10.19 shows the paths which the stress distribution along the overlap length (5mm) were interpolated and presented in the following graphs. Path A-A' (y = 6.5mm) and C-C' (y = 6.0mm) defines the stress distribution along the wood substrate – adhesive interfaces. The stress distribution of mid-bondline is measured along the B-B' path (y = 6.25mm).

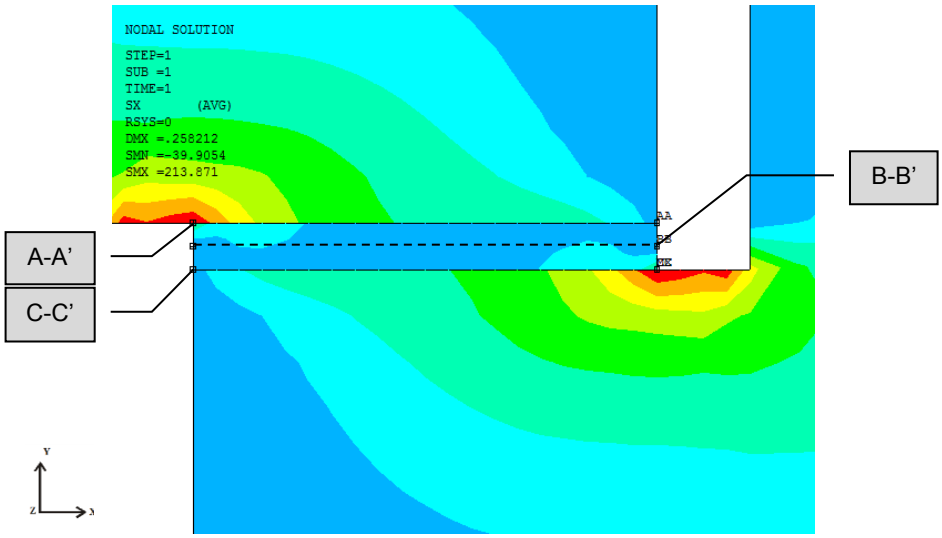

Fig. 10.19. Path for stress-distribution analysis

The distribution of the longitudinal x-stress along section A-A', B-B' and C-C' on the global xy plane are shown in Figure 10.20. It can be seen that the stress peaks towards the end of the overlap. Maximum stress peak is distributed along the gap length. Along the wood-adhesive interface paths (A-A' and B-B'), the peak stresses increases through the adhesive towards the wood substrate (point A and C'). Correspondingly to the longitudinal stress Sx curve at the mid-bondline (B-B'), the overlap length showed lower stresses in the middle portion of the overlap.

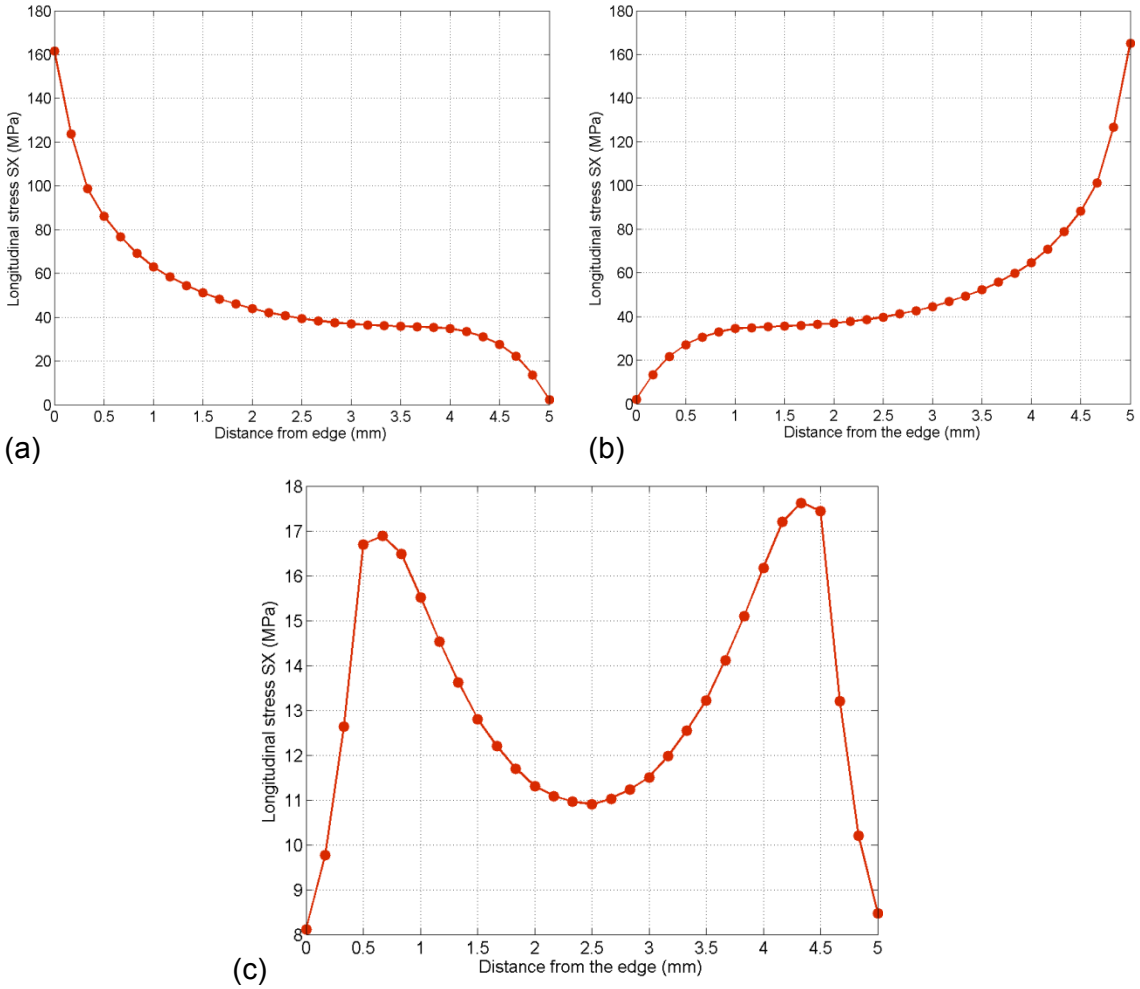

Fig. 10.20. Stress distribution in lap joint: the longitudinal stress Sx in the (a) wood-adhesive interface at y=6.5mm (A-A') (b) wood-adhesive interface at y=6.0mm (C-C') and (c) mid-bondline at y=6.25mm (B-B').

In order to describe the magnitude of stresses on a particular joint, mathematical analysis is essential for the interpretation of experimental data. The geometry of the adhesive joint is one of the key factors in mathematical analysis. According to Volkersen's analysis (1938), adhesive deformation is only affected by shear and the behaviour of the adhesive is assumed to be linear elastic. Calculation of shear stress according to Volkersen is as given by Equation 10.2.

The observation in this study conforms well to Volkersen's theory. Referring to Figure 10.19, the lower substrate which bears the applied tensile load, gradually transmits the stress to the upper substrate through the adhesive layer. The figure also depicts that point C' is the peak value of the stress. The stress gradually decrease to zero as it moved towards point C. As for the upper substrate, the peak value of the stress is at point A

which progressively decreases until it reaches zero stress at point A'. The progression of highest point to lowest point of shear stress occurs for rigid and elastic substrates. Loading in shear will eventually lead to a uniformly sheared parallelogram of adhesive which later on becomes distorted (differential shear) due to the continuity of the adhesive/substrate interface (Kinloch, 1987).

Goland and Reissner (1944) have proposed the existence of bending moments and rotation of the overlap joint due to the eccentricity of the joints under loading as also seen in this study (Figure 10.18). The effect of unevenness in stress distribution within the joint can best be described by expressing it through bending moment factor, *K,* and associated rotation factor, *K**. The geometry of the joint is the most important factor which affects the value of *K* as well as mechanical properties of the substrates and stress applied to the substrates. Bending moments and rotation occur primarily in order to decrease the stress concentration in the joint. For quite flexible substrates such as wood, the value of *K* will diminish towards zero as rotation occurs which eventually shifts the line of action due to applied load closer to centre line of the substrates (Kincloch, 1987).

10.4 CONCLUDING REMARKS

Three commercially available structure adhesives were tested using the thick adherend shear test (TAST). The selection of TAST method was made based on the objective to achieve a uniform shear stress-strain in the bonded area. All tested adhesive show brittle failure and a mean shear strength of 12.7MPa. Elastic FE analysis presented in this chapter explains more about the stress distribution within the lap joint samples. The variation of stresses along the bonded length was presented according to various interfaces and areas of interest. The study shows high concentration of stresses on the edges of the overlap zone.

CHAPTER 11 : PULL-OUT TEST FOR BONDED-IN JOINT

11.1 INTRODUCTION

The pull-out test for bonded-in rods is one of the most widely used methods for evaluating the strength of bonded-in connections. This chapter reports results of testing for a standard geometry single-ended specimen. The pull out test was conducted at room temperature and at 50^{o}C. The pull-out test assesses the influence of adhesive type, rod types and the effect of post cure treatment at different temperatures on the strength and failure of the connection. The adhesives used in this study vary according to type and size of filler, thixotropy and glass transition temperature (T_g). These tests were also used to characterise the strength of bonded-in connection using solid wood and composite lumber such as Laminated Veneer Lumber (LVL). All specimens were bonded parallel to the grain.

11.2 METHODOLOGY

11.2.1 MATERIALS

11.2.1.1 Adhesive

The adhesives used in this study are two-component epoxies which consist of base resin and curing agent. Two of the adhesives (Rotafix Structural Adhesives (RSA) and Engineering Adhesive (EA), supplied by Rotafix Ltd.) are thixotropic adhesives containing nano-size silica fume with good gap filling ability. Timberset (Rotafix) and Sikadur (Sika) are heavily-filled epoxies. The mechanical properties of the adhesives are summarised in Table 11.1.

Table 11.1 Physical and mechanical properties of adhesives.

Property	RSA	EA	Timberset	Sikadur
Tensile Modulus (GPa)	1.69	3.59	1.39	6.38
Inter Laminar Shear Strength (MPa)	10.11	12.26	7.40	4.54
Tensile strength (MPa)	20.29	38.07	17.29	21.40
Coefficient of thermal expansion (10^{-6}°C^{-1})	71.5	55.8	63	37.3
Glass transition temperature (°C)	36.8	53.4	35.4	42.5

11.2.1.2 Types of wood

The specimens were produced by bonding rods into Kerto-S LVL, Accoya® wood, Radiata pine, yellow resak, keruing and resak. Kerto-S LVL has consistent mechanical properties and is made by bonding together veneer plies to the required thickness which distributes defects such as knots evenly, and reduces the tendency to warp, twist, bow and shrink. Accoya® wood is chemically modified by the acetylation process producing a dimensionally stable and durable material due to the presence of hydrophobic acetate group in the acetylated wood. The purpose of testing Accoya® wood was to evaluate the bond strength of a substrate that has been chemically treated. The pull-out strength results for Accoya® wood were compared to results for control specimens fabricated from Radiata pine, yellow resak, keruing and resak which are all heavy hardwoods of Malaysian origin. All three species have been used in the construction of Malaysia's first glulam-based building. The physical and mechanical properties of the wood used in testing are shown in Table 11.2.

Table 11.2 Physical and mechanical properties of wood.

Property	Kerto-S LVL	Accoya ® wood	Radiata pine	Yellow resak	Keruing	Resak
Density (kg/m^3)	490	512	498	873	817	905
Modulus of Elasticity (GPa)	13.8	-	8.23	17.36	19.7	16.25
Bending strength (MPa)	50.0	80.0	85.8	96	112	93
Compression strength (MPa) ∥ to grain ⊥ to grain	 35.0 6.0	 n/a n/a	 36.8 n/a	 53.6 n/a	 59.2 6.8	 51.3 8.2
Shear strength (MPa) ∥ to grain ⊥ to grain	 5.0 n/a	 n/a n/a	 11.6 n/a	 9.7-11.3 n/a	 9.2-12.3 n/a	 9.3-12.6 n/a

11.2.1.3 Types of rod

The effect on the bonded-in strength of using threaded or smooth rods was assessed. Threaded stainless steel rods of grade A2/304 and smooth-surfaced glass fibre pultruded rods (GFRP) were used for bonded-in specimens. The differences between the steel and unidirectionally-reinforced GFRP relate to the surface properties of the rod (in relation to mechanical interlocking and chemical bonding), the ability of steel to yield and the thermal expansion coefficients and Young's moduli of the rods. The mechanical properties of both rods are presented in Table 11.3.

Table 11.3 Physical and mechanical properties of rods.

Properties	Steel rod (grade 304)	GFRP
Density (kg/m3)	8000	1800
Tensile modulus (GPa)	193	40
Shear Modulus (GPa)	n/a	15
Tensile strength (MPa)	800	515
Yield strength 0.2% (MPa)	205	-
Poisson's ratio	0.3	0.3
Coefficient of thermal expansion (10^{-6}°C^{-1})	17.8	10

11.2.2 SAMPLE PREPARATION

The LVL and wood blocks were cut by using a DeWalt radial arm saw into 63mm cubes (Figs. 1a and 2). Central holes were drilled parallel to the grain with a diameter of 12mm through the full thickness of the LVL/wood blocks (Fig. 1b). The hole was 4 mm bigger in diameter than the diameter of the rod, allowing a 2 mm gap for the adhesive around the rod. Thick glue lines are more able to transfer stress thus limiting stress concentrations within the glue line (Felignioni *et al.* 2003) in contrast to thin gluelines (<0.5 mm). The inner surface of the hole was cleaned to remove debris. The moisture content of the material was kept constant at 10-12.5% before testing.

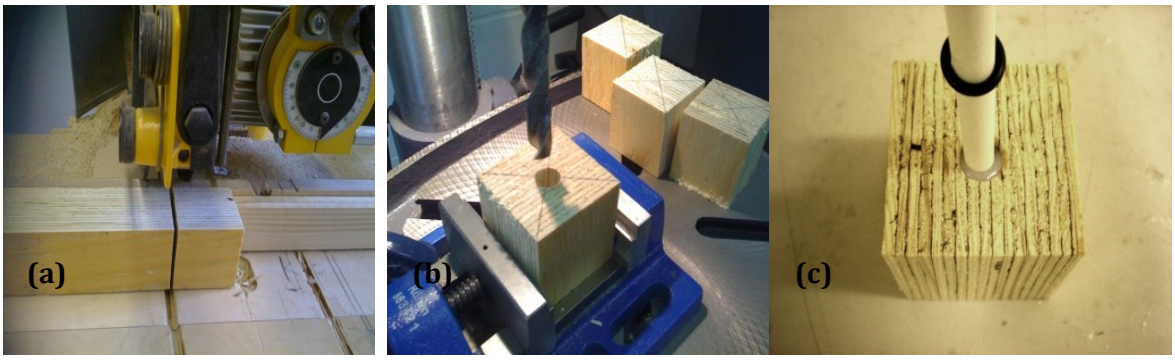

Fig. 11.1 Overview of sample fabrication (a) wood block cutting (b) centre hole drilling (c) rod insertion into adhesive-filled hole.

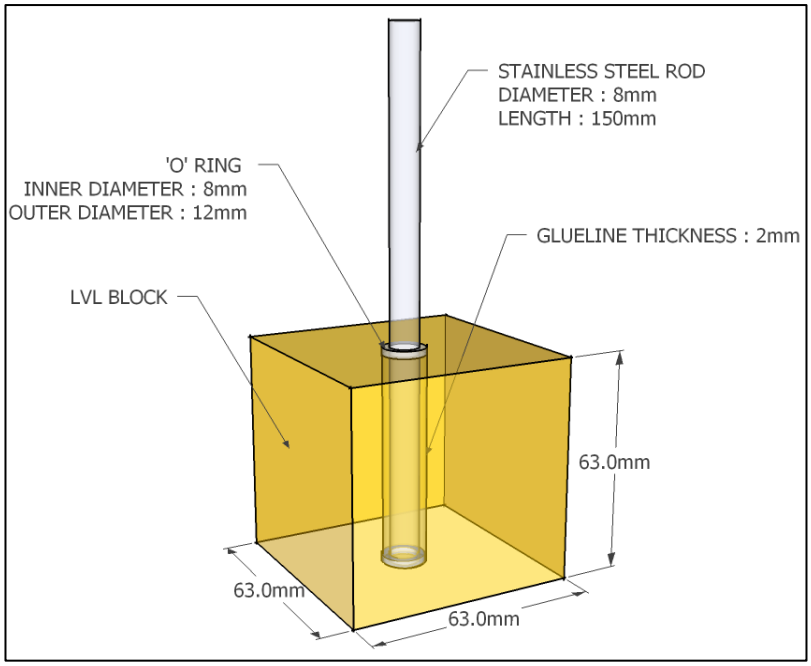

Fig. 11.2 Sample configuration depicting dimension of LVL/wood block, rod and 'o' ring.

Prior to the bonding process, the rods were surface treated to enhance adhesion of the epoxy resin to the rod. Although this method is generally not used during construction, surface preparation improves bonding as reported in many studies (Harvey & Ansell, 2000; Lorenzis *et al*., 2005). The threaded steel rod was wiped with acetone solvent. The smooth surface of GFRP rods was sanded lightly to enhance bonding and then wiped with ethanol to remove grease and release agent which could affect bonding. Both stainless steel and GFRP rods had an outer diameter of 8mm and they were 150mm in length.

Adhesives were mixed according to the manufacturer's recommendation. RSA, EA and Timberset came in batches of 400c resin base and 100cc hardener. Sikadur was mixed in the proportions 2 parts resin and 1 part hardener by weight. Both RSA and EA have a long *working time* due to their shear thinning properties. The resin required constant mixing to ensure a continuous flow during insertion into the drilled hole. Although Sikadur is also marketed as a thixotrophic adhesive it has a shorter *working time* and must be injected into the drilled hole without delay. Timberset is not a thixotropic adhesive and requires instant application after mixing.

Fabrication of the bonded-in rod test piece was made by injecting epoxy into the LVL block using a syringe. The holes were filled up to three quarter full and left to settle before rod insertion. The insertion was made slowly with a downward twisting motion (Figure 11.1c) to ensure thorough epoxy coating along the bonded length of the rod and to avoid the formation of voids. A rubber 'O' ring was used to centralize the position of the rod at each end of the drilled hole. The bonded-in samples were left for 20 days at 65% RH in a humidity chamber for further curing (Figure 11.3)

Fig.11.3 Threaded steel rods bonded into LVL and wood with different adhesives.

11.2.3 EQUIPMENT AND TEST CONFIGURATION

11.2.3.1 Room temperature testing

As mentioned in the chapter's introduction, this study conducted in two testing condition. This study which was tested at room temperature investigates the influence of adhesive and wood type on the pull-out strength of the joint. Samples which were made of LVL were bonded using RSA, EA, Timberset and Sikadur. Accoya® wood, Radiata Pine, Resak, Yellow resak and Keruing were also bonded using RSA. The test matrix for this study is presented in Table 11.4.

Table 11.4 Test matrix for room temperature testing

Sample code	Types of wood	Types of Adhesive	Rod	No. of samples	Test temp.
RSA	LVL	RSA	Steel	10	20 ± 3°C
EA	LVL	EA	Steel	10	20 ± 3°C
Timb	LVL	Timberset	Steel	10	20 ± 3°C
Sika	LVL	Sikadur	Steel	10	20 ± 3°C
AC	Accoya®wood	RSA	Steel	10	20 ± 3°C
AC-UT	Radiata Pine	RSA	Steel	10	20 ± 3°C
RS	Resak	RSA	Steel	10	20 ± 3°C
YR	Yellow Resak	RSA	Steel	10	20 ± 3°C
KR	Keruing	RSA	Steel	10	20 ± 3°C

A total of 90 samples were tested in pull-pull configurations at room temperature. The test was conducted using a universal testing machine (Instron 3369) and was fitted with a 50-kN load cell. A special testing jig was fabricated using 10mm thick aluminium plates and M8 threaded stainless steel rods for this study. The wood block was fitted into the testing jig by placing the bonded rod through the bottom base plate and attached to the lower grip (Fig.4). The bottom plate acts as reaction plate as the block being pulled in tension during testing. The pull-out test was held at a constant cross-head displacement rate of 2 mm/min.

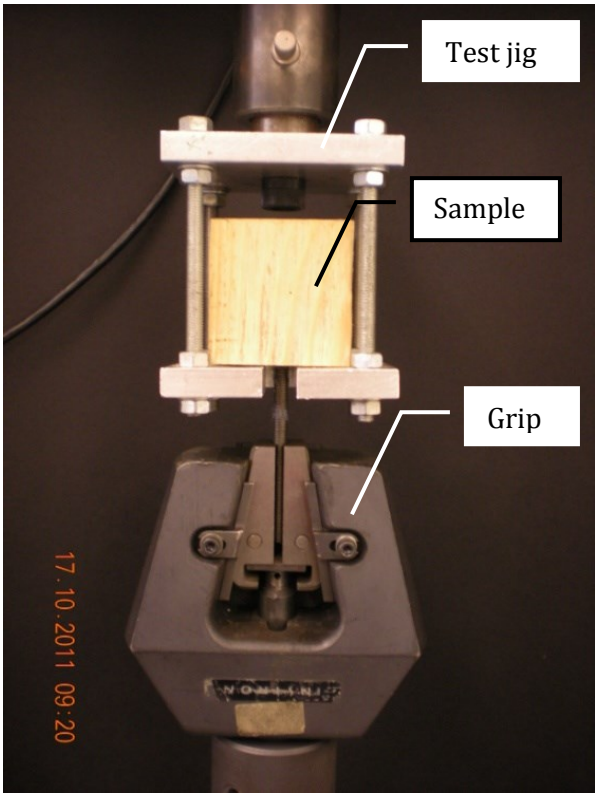

Fig. 11.4 Test configuration of static pull-out test conducted at room temperature.

11.2.3.2 HIGH TEMPERATURE TESTING

The study also investigated the effect of post curing on the pull-out strength of LVL samples bonded using Rotafix Structural Adhesive. The test matrix for determining the effect of various treatments on shear strength is presented in Table 11.5 according to the post curing treatment, type of rod and test temperature.

The samples were tested in tension with an Instron 3369 universal testing machine at 21ºC or 50ºC. The Instron machine was fitted with an oven (Instron 3111) to enable the test to be conducted at 50^{o}C (Figure 11.5a). A rigid connecting rod made the connection between the shear fixture inside the oven and the load cell. Prior to the pull-out test at 50^{o}C, the samples were pre-conditioned in the oven at 70^{o}C for an hour. The test jig resembles a cage which holds the LVL cube in position for tensile testing (Figure 11.5b). The rod of the single ended bonded-in rod was then secured in the lower grip of the testing machine.

Table 11.5 The experimental matrix of bonded-in shear strengths test

	Sample Code	Description	Rod Material	Total Sample	Test temperature
1	A1	RT* curing for 20 days	GFRP	11	20 ± 3°C
2	B1	RT* curing for 20 days + post curing at 50°C for 24 hours	GFRP	11	20 ± 3°C
3	C1	RT* curing for 20 days + post curing at 70°C for 24 hours	GFRP	11	20 ± 3°C
4	D1	RT* curing for 20 days + post curing at 70°C for 24 hours	GFRP	11	50°C
5	A2	RT* curing for 20 days	Steel	11	20 ± 3°C
6	B2	RT* curing for 20 days + post curing at 50°C for 24 hours	Steel	11	20 ± 3°C
7	C2	RT* curing for 20 days + post curing at 70°C for 24 hours	Steel	11	20 ± 3°C
8	D2	RT* curing for 20 days + post curing at 70°C for 24 hours	Steel	11	50°C

**RT= Room Temperature*

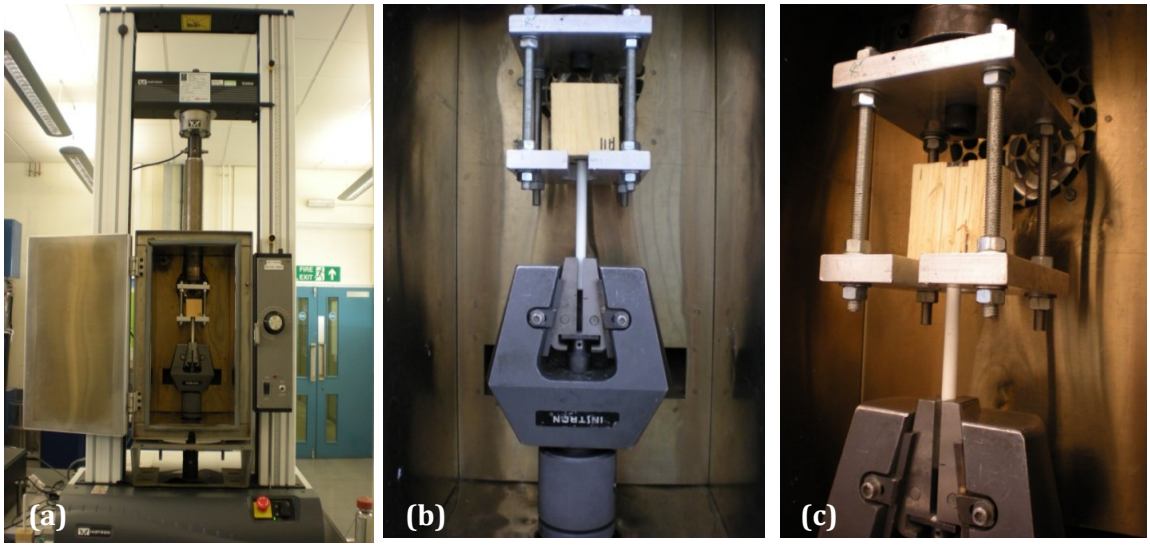

Fig. 11.5 Instron 3369 universal testing machine with oven (Instron 3111) (b) test rig fitted to the testing machine and grip to hold the rod (c) a sample tested to failure.

Test data was then encoded using Bluehill2© software where failures were depicted in load-deformation curves. In order to check the temperature of the bond-line during testing, a bonded-in rod sample was fitted with a thermocouple and placed near the test rig (Figure 11.6). The failure mode of each sample was recorded manually.

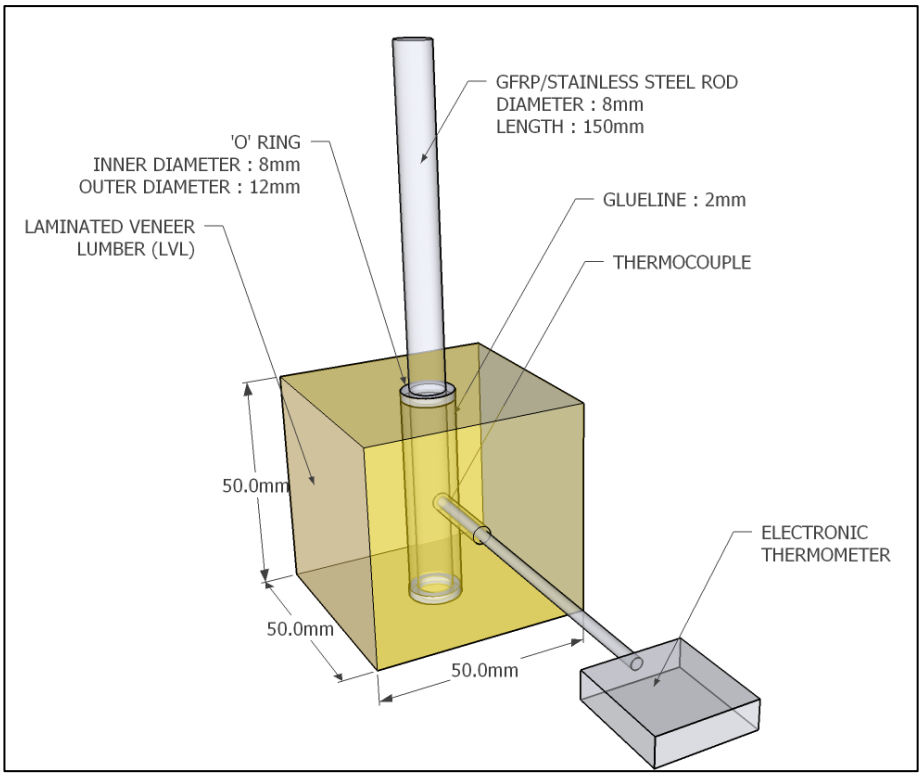

Fig. 11.6 Position of thermocouple at the glue line of bonded-in joint

11.2.4 EVALUATION AND ANALYSIS

As stated by Aicher (2003), global slip between the rod and timber is measured by the slip-displacement of the rod (Figure 11.7). In principle, the shear slip behaviour is similar to a lap joint.

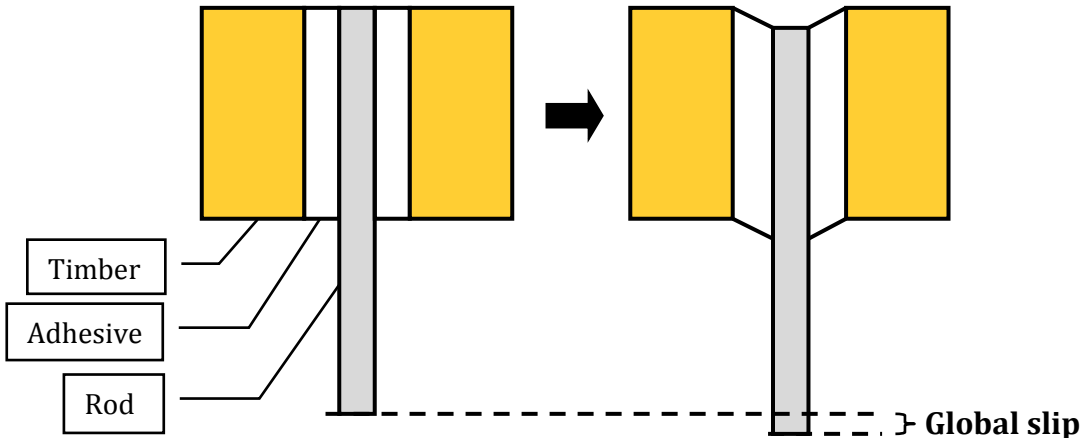

Fig. 11.7 Global slip of a bonded-in rod

Shear stresses at the timber-adhesive and rod-adhesive interfaces were derived as follows:

$$\tau_{\text{ta (timber}-\text{adhesives)}} = \frac{P_{max}}{\pi \emptyset_{hole} L} \quad \text{(Eq. 11.1)}$$

$$\tau_{\text{ra (rod}-\text{adhesives)}} = \frac{P_{max}}{\pi \emptyset_{rod} L} \quad \text{(Eq. 11.2)}$$

Where, the maximum force used to test the sample to failure is denoted as P_{max}, while $\emptyset_{hole}$ and $\emptyset_{rod}$ are the diameter of the hole and rod respectively. L is the anchorage length of the rod. The means of shear strengths for samples tested at room temperature and high temperature were analysed statistically using ANOVA.

11.2.5 SCANNING ELECTRON MICROSCOPY (SEM)

Fractured pull-out samples were imaged using a JEOL model JSM SEM (Figure 11.8) which accommodates large specimens. Prior to examination, the samples were coated with gold in a sputter coater and mounted on a metal disk before insertion into the sample chamber (Figure 11.9).

Fig. 11.8 SEM JEOL JSM.

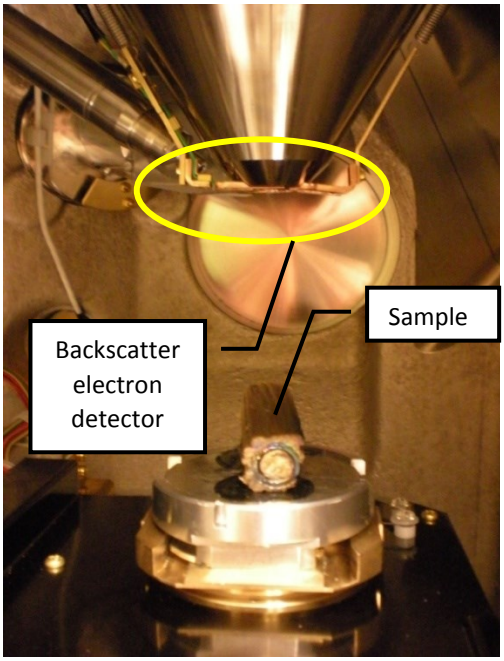

Fig. 11.9 A fractured sample within the SEM viewing chamber.

The effect of adhesive type, wood substrate and rod material on shear strength is reported in the following three sub-sections.

11.3.1 EFFECT OF ADHESIVE TYPE ON SHEAR STRENGTH

Figure 11.10 summarises the pull-out failure loads as a function of adhesive type. The average peak shear stress at the timber-adhesive and rod-adhesive interfaces is presented in Figure 11.11 and Table 11.6 at the timber-adhesive and rod-adhesive interface.

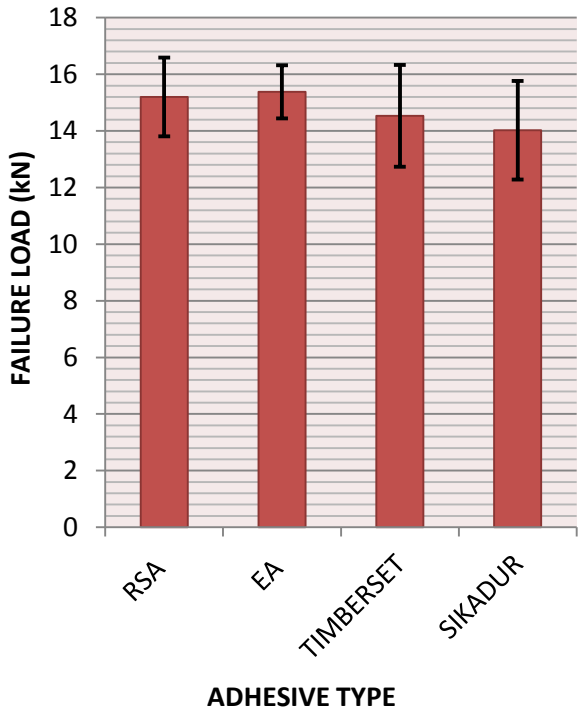

Fig. 11.10 The effect of adhesive type on average failure load including standard deviation

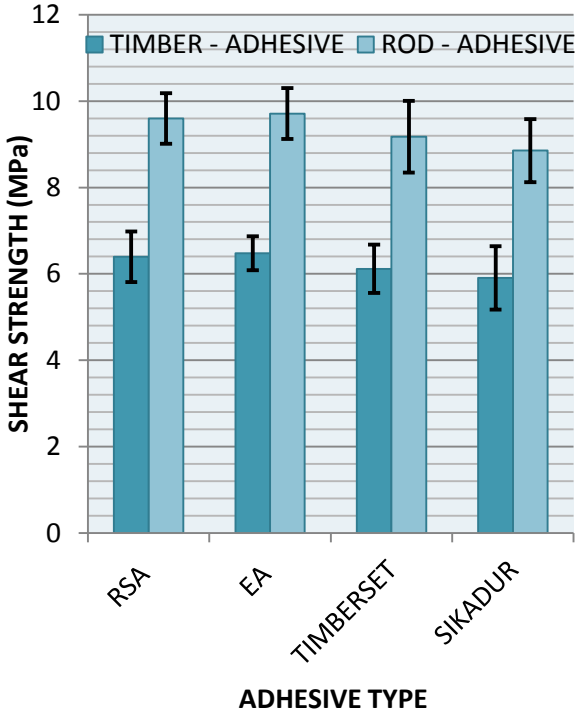

Fig. 11.11 The effect of adhesive type on average peak interfacial shear stress including standard deviation

Table 11.6 Effect of adhesive types on bonded shear strength

Adhesive	No. of Samples	Shear strength (MPa)		COV (%)
		Timber-Adhesive Interface	Rod-Adhesive Interface	
RSA	10	6.40	9.16	9.16
EA	10	6.47	9.71	6.07
TIMBERSET	10	6.11	9.17	11.45
SIKADUR	10	5.90	8.86	10.42

The magnitude of the average shear stress varies from 5.90 to 6.47 MPa at the timber-adhesive interface and 8.86 to 9.71 MPa at the rod-adhesive interface. EA has marginally the highest value of shear strength, followed by RSA, Timberset and Sikadur, suggesting that ductile adhesives possess a marginally higher shear strength compared to brittle adhesive due to the difference in rheology of the adhesives. This observation correlates well with the trend in shear strength of bulk adhesives reported in Chapter 8 and the work of Feligioni *et al.* (2003). The ductility of the adhesive is likely to influence the creep behaviour of the joint and this topic which will be addressed in Chapter 12. However, a statistical analysis of variance at 0.05% probability level was performed for the comparison of means. The value of $p>0.05$ (Table 11.7) indicates that there is no statistical difference between the shear strength of the four adhesives.

Table 11.7. ANOVA of shear strength for pull-out test of main adhesives bonded with LVL

Pull-out test	F value	p-value
Shear Strength at Timber-Adhesive Interface (MPa)	1.195	0.325
Shear Strength at Rod-Adhesive Interface (MPa)	1.195	0.325

As stated in several publications (Davis, 1997; Bainbridge *et al*., 2002; Gardele & Morlier, 2007), failure modes of a single axially loaded glued-in rod can be categorized into 4 types based on the failure mode listed in the Structural Timber Education Programme (STEP):

- MODE 1 Rod failure through yielding
- MODE II Shear failure in the adhesives/adhesive-rod interface failure
- MODE III Localised timber failure around the bond
- MODE IV Failure of the host timber member

Figure 11.12 displays the failure location of the glued-in rods where most of the failure is mode III occurring mainly around the bonded area close to the glue-line. Mode III failure occurs when the strength of the wood is lower than the strength of the adhesive and the rod/adhesive interface. The mean shear strength for all adhesives is above the shear strength value of the LVL which is ~5MPa.

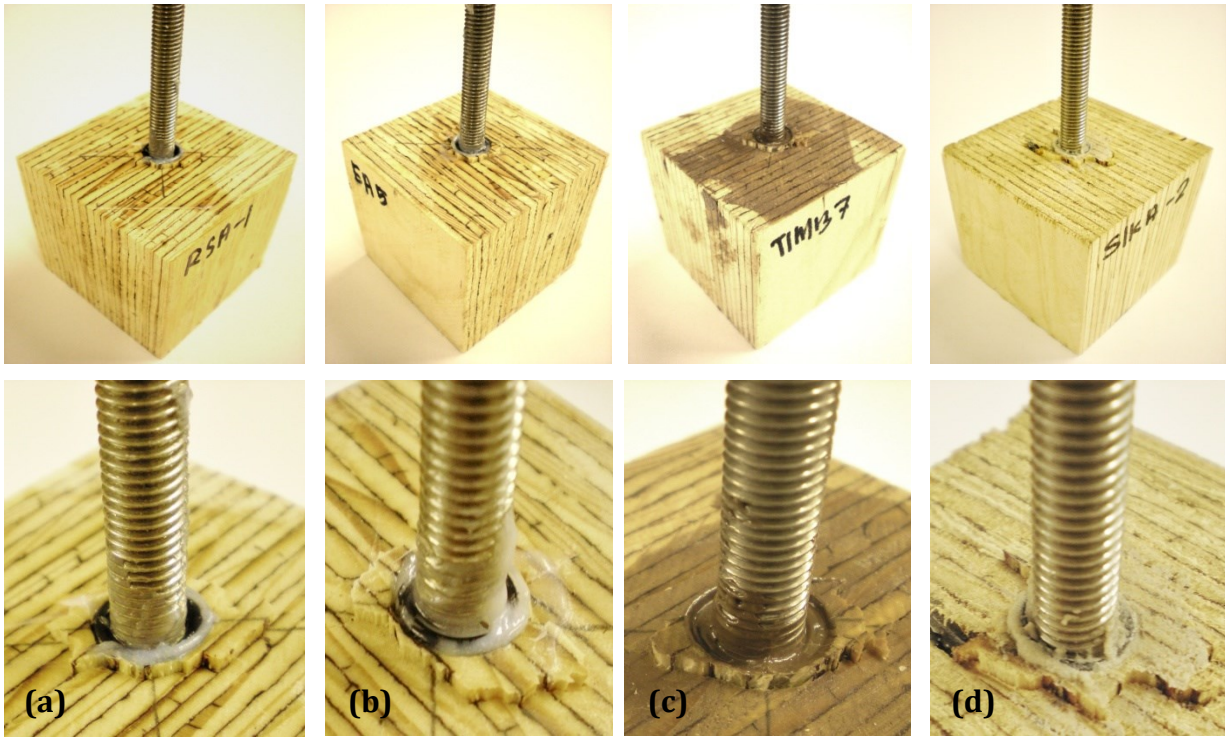

Fig. 11.12 Adhesive-timber failure for (a) RSA (b) EA (c) Timberset and (d) Sikadur.

11.3.2 EFFECT OF WOOD TYPES ON SHEAR STRENGTH

The mean value of the pull-out load and shear strengths are presented as a function of wood type in Figures 11.13 and 11.14 respectively. As indicated in Table 11.8 the LVL samples exhibit the lowest pull-out strength at means of 6.40 MPa (τ_{ta}) and 9.60 MPa (τ_{ra}). Resak samples exhibited the highest mean shear strength at means of 12.52 MPa (τ_{ta}) and 18.78 MPa (τ_{ra}), which are 49% higher than values for LVL samples.

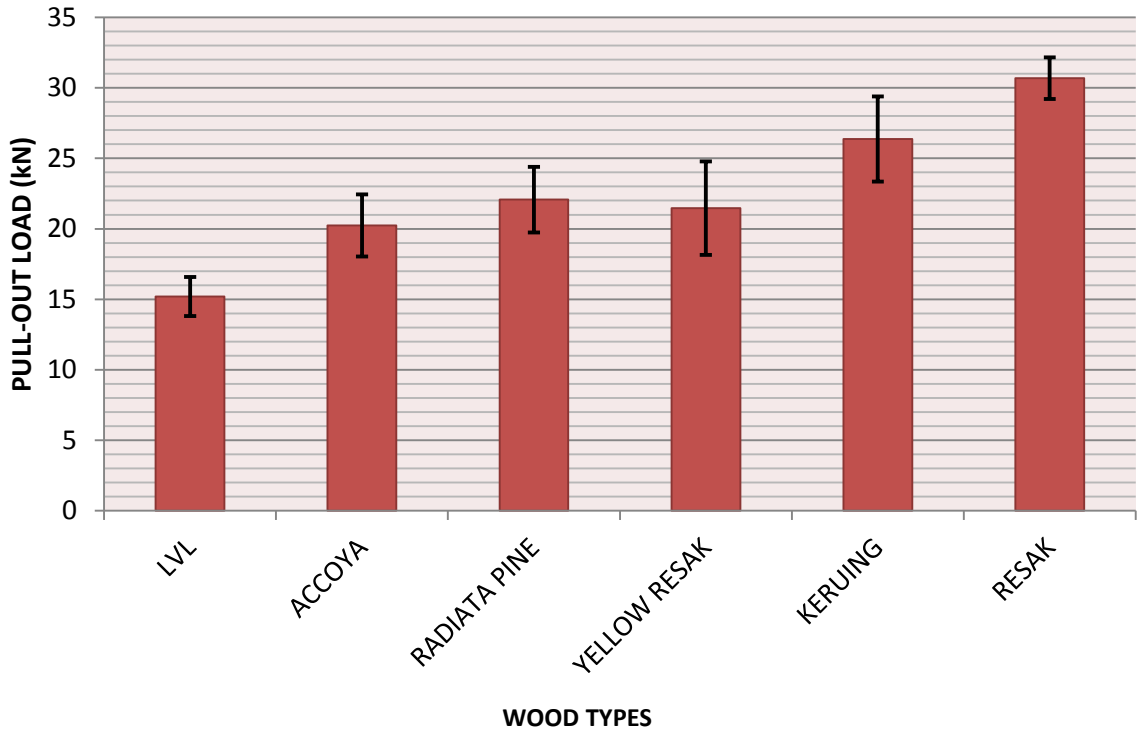

Fig. 11.13 Mean pull-out load and standard deviation of samples bonded using various types of wood.

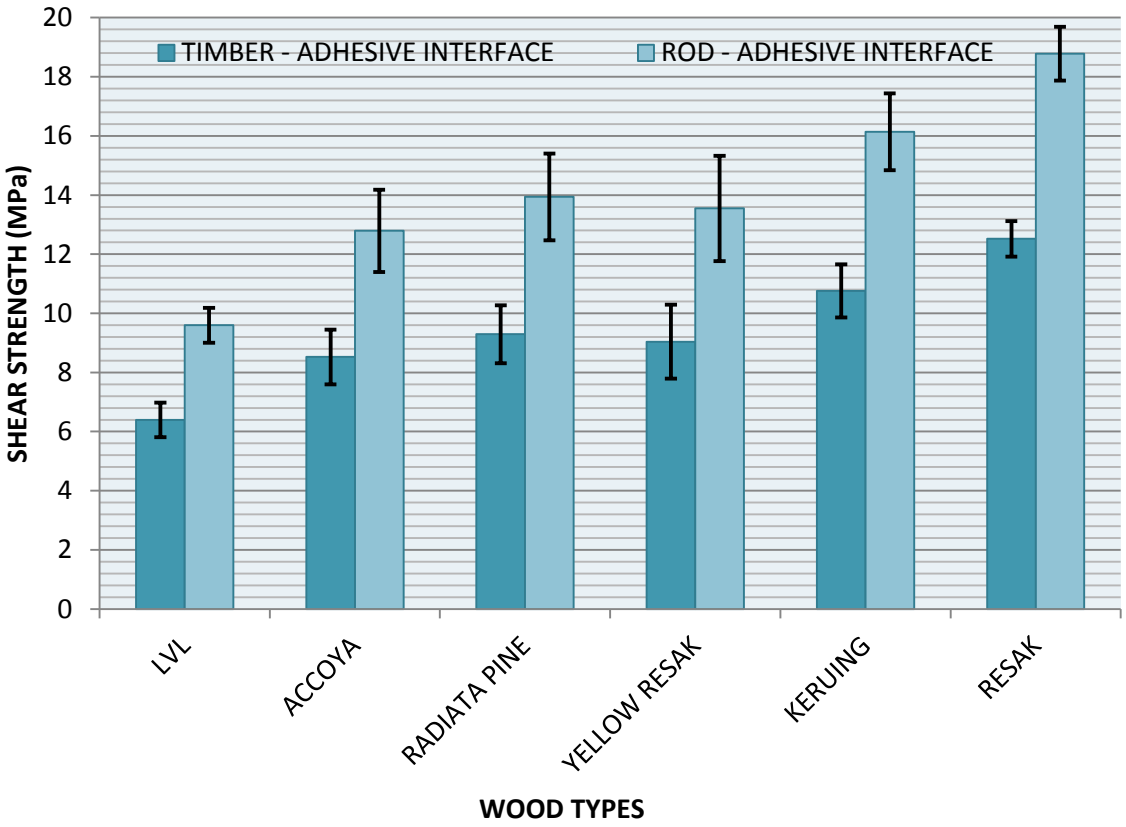

Fig. 11.14 Mean shear strength and standard deviation of samples bonded using various types of wood.

Table 11.8 Data of mean pull-out force and mean shear strength for RSA bonded using various types of wood.

Wood types	Density (kg/m^3)	No. of samples	Pull out force (kN)	Shear Strength (MPa)		COV (%)
				Timber-Adhesive Interface	Rod-Adhesive Interface	
LVL	490	10	15.20	6.40	9.60	9.16
ACCOYA (acetylated Radiata pine)	512	10	20.25	8.53	12.79	10.87
RADIATA PINE	498	10	22.07	9.29	13.94	10.50
YELLOW RESAK	873	10	21.46	9.04	13.55	8.10
KERUING	817	10	26.36	10.76	16.14	7.85
RESAK	905	10	30.68	12.52	18.78	4.82

The density of each wood type and the mean shear strengths from the pull-out tests are recorded in Table 11.2 and 11.8 respectively. In general, the pull-out shear strength of bonded samples increases steadily with the density wood which agrees well with the result reported by Steiger *et al.* (2005), Broughton & Hutchinson (2001) and Serrano (2001) although other studies indicates otherwise (Bengtsson & Johansson, 2000; Bernasconi, 2001).

The investigation of the pull-out strength of untreated Radiata pine and acetylated Radiata pine (Accoya) indicates that treated samples are denser but exhibit a decrease of 8% in mean shear strength compared to untreated samples. Various studies report a lower bonding strength for acetylated wood using epoxy, EPI, polyvinyl acetate (PVAc), resorcinol formaldehyde and phenol resorcinol formaldehyde adhesives (Vick *et al*., 1993; Frihart, 2006). The chemical modification appears to interfere with the bonding process by affecting the wetting of the surface. This is due to the lower affinity of the treated wood to water as a result of a reduction in the number of hydrophilic sites on the wood surface. Bonding strength at the yellow resak surface could be reduced by the presence of excessive extractive according to Marra (1992) and Pizzi *et al*. (2003).

From Duncan multiple comparison analysis, it is clear that there is a highly significant difference in the mean shear strength of LVL, Keruing and Resak. The test also indicates no significant difference between the means of Accoya, Radiata

pine and Yellow resak as depicted in Table 11.9, 11.10 and 11.11 for the timber to adhesive and rod to adhesive interfaces.

Table 11.9 ANOVA of shear strength at timber-adhesive and rod-adhesive interfaces for rods bonded-in with RSA

Pull-out test	F value	p-value
Shear Strength at Timber-Adhesive Interface (MPa)	34.548	<0.05
Shear Strength at Rod-Adhesive Interface (MPa)	34.548	<0.05

Table 11.10 Duncan multiple comparison of shear strength for various woods at the timber-adhesive interface

WOOD TYPES	Subset for alpha = 0.05			
	1	2	3	4
LVL	6.40			
ACCOYA		8.53		
RADIATA PINE		9.29		
YELLOW RESAK		9.04		
KERUING			10.76	
RESAK				12.52

Table 11.11 Duncan multiple comparison of shear strength for RSA bonded with different types of wood at the rod-adhesive interface

WOOD TYPES	Subset for alpha = 0.05			
	1	2	3	4
LVL	9.60			
ACCOYA		12.79		
RADIATA PINE		13.94		
YELLOW RESAK		13.55		
KERUING			16.14	
RESAK				18.78

The finding on the influence of wood density on pull-out shear strength agrees well with the result reported by Broughton & Hutchinson (2001), Steiger *et al.* (2005) and Serrano (2001) although other studies indicates otherwise (Bengtsson & Johansson, 2000; Bernasconi, 2001).

In section 12.3.1 only two types of failures were observed as a function of adhesive type. In contrast the tests using various types of wood exhibited all four types of failure mode. Figure 11.15 depicts types of failures which include Mode I, II, III and IV for the various wood types. The percentages of each failure mode according to the wood type are recorded in Figure 11.16 and Table 11.12 respectively.

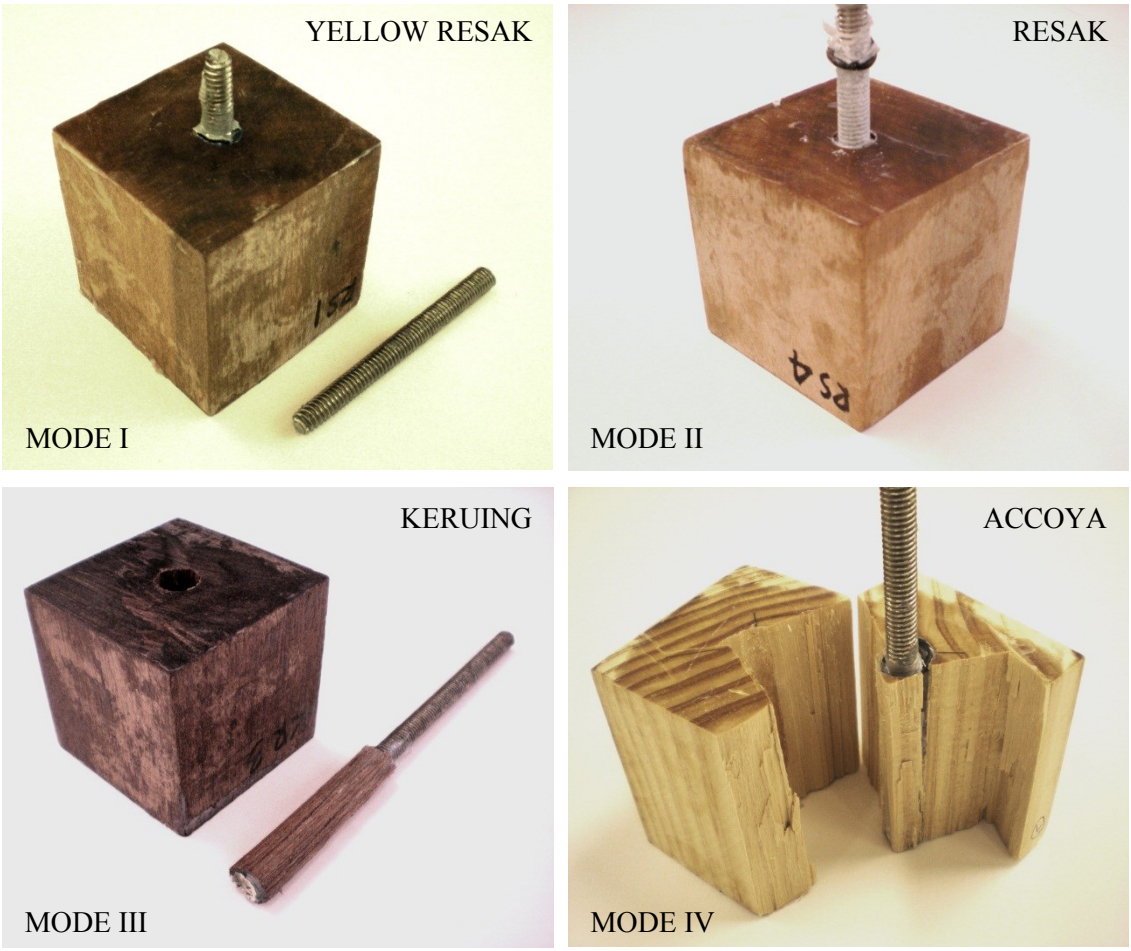

Fig. 11.15: A composition on types of failure modes for various types of wood bonded with RSA.

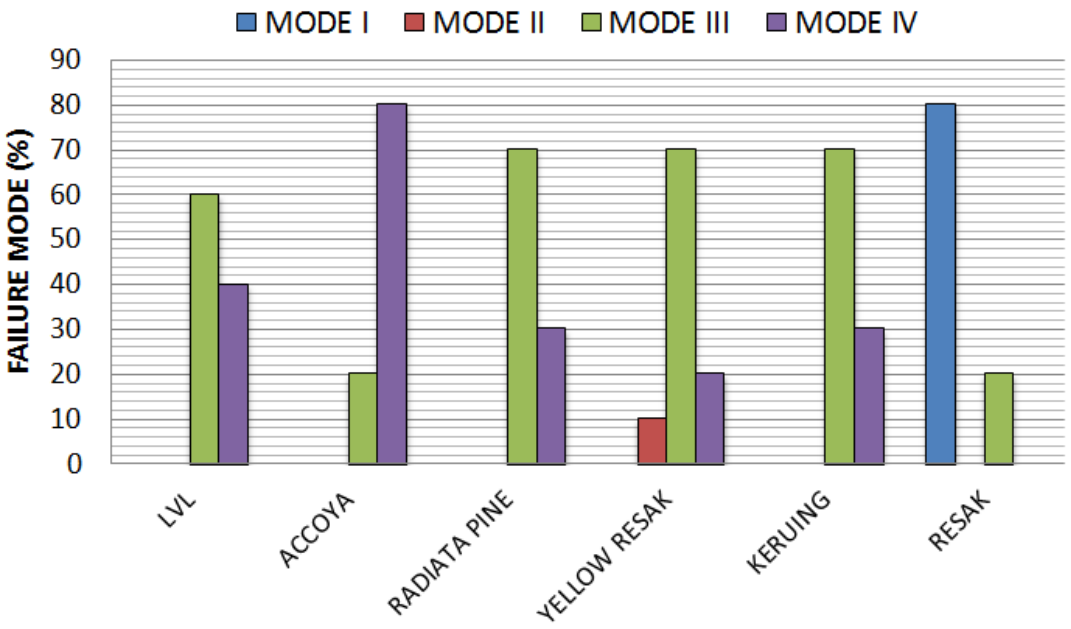

Fig. 11.16 Failure modes according to wood types

Table 11.12 Distribution of failure mode for various wood types

Wood types	Failure mode (%)			
	MODE I	MODE II	MODE III	MODE IV
LVL	0	0	60	40
ACCOYA	0	0	20	80
RADIATA PINE	0	0	70	30
YELLOW RESAK	0	10	70	20
KERUING	0	0	70	30
RESAK	80	0	20	0

Mode I is the most desirable mode of failure where intrinsic failure of the bonded steel rod occurs as a result of yielding. 80% of Resak samples exhibited failures in Mode I, demonstrating good adhesion at the bonded interfaces. 10% of bonded Yellow resak failed in Mode II due to cohesive failure of the bond or failure at the rod to adhesive interface. Either the adhesive was improperly cured or surface contamination (eg. presence of extractives) prevented the development of a good bond. The most significant failure for LVL, Radiata pine, Yellow resak and Keruing was localised timber failure around the bond which can be categorised as Mode III. Part of the wood that was bonded to the rod was pulled out from the bonded interface while a plug of adhesive was still intact around the rod. The failure occurred in the wood in close proximity to the adhesive/timber glueline.

Failure in Mode IV occurred when a wider portion of wood was pulled out from the wood block and in most cases the timber block splits in half. This failure mode was prevalent in Accoya bonded samples. As depicted in Figure 11.17, it is found that the fracture pattern in Radiata pine and Accoya (both are softwood) is influenced by the location of growth rings and the direction of ray parenchyma (depicted by arrow). The crack on the tested sample propagates along the direction of the ray cells and across the region between earlywood and latewood. During crack propagation, it is believed that the weakest points lie within the location where there is an abrupt transition between earlywood and latewood cells. SEM evidence supporting this assumption is discussed in section 12.3.3. It is interesting to note that Radiata pine and Accoya wood exhibited significant differences in failure mode although the mean shear strength of both type of wood indicates no statistical difference. This further highlights the importance material selection in respect to mode of failure during timber joint designing.

The highest shear strength is exhibited by hardwoods which is a function of the high shear strength of the wood itself. Figure 11.18 depicts the fracture pattern of Resak, Keruing and Yellow Resak respectively. The direction of ray cells is indicated by the direction of the white arrow. The figure indicates that the crack propagate perpendicular to the ray cells, rather than along the ray cells as depicted in softwood. Without the presence of growth rings, the cell lumen and cell wall thickness of hardwood behaves uniformly. It can be concluded that the high shear strength exhibited by hardwoods is partly influenced by the absence of growth rings which serves as the weakest point during crack propagation in softwood. In all cases a good bond between the rod and adhesive and the adhesive and wood is essential to cause fracture in the wood.

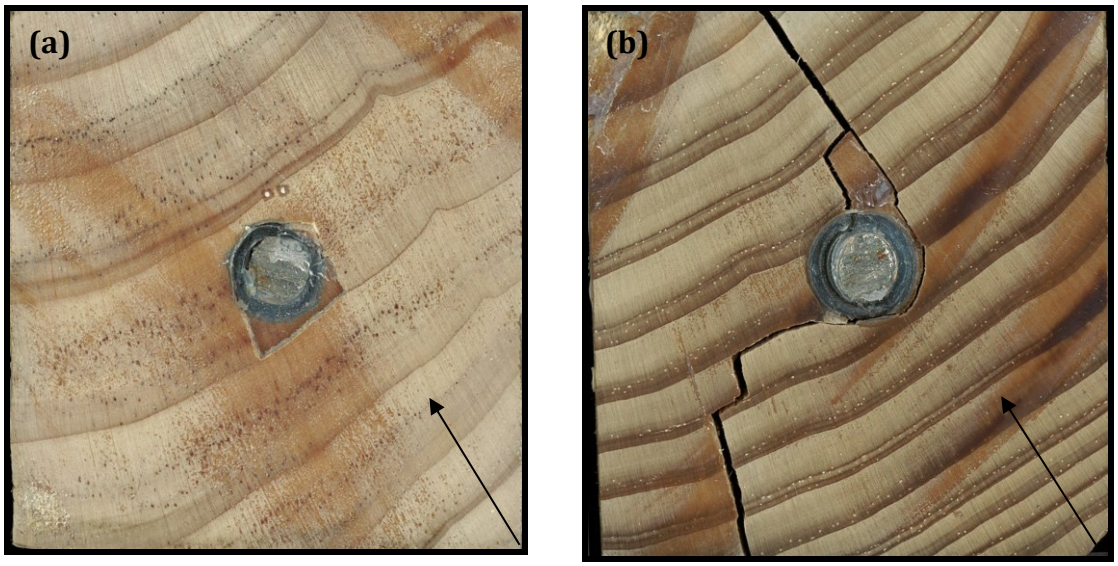

Fig. 11.17 The fracture pattern of (a) Radiata pine and (b) Accoyawood. Black arrows indicate the orientation of ray cells.

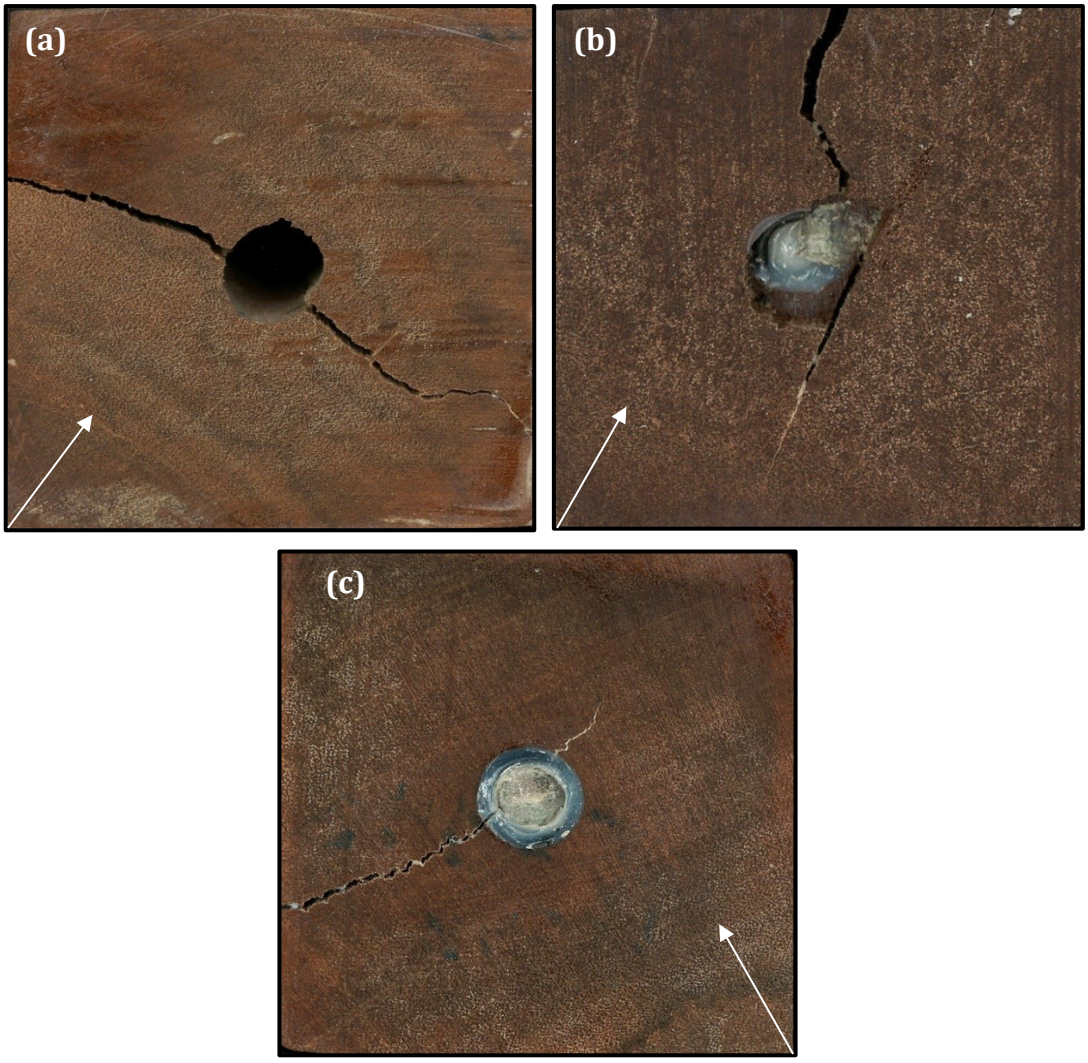

Fig. 11.18 The fracture pattern of (a) Yellow resak (b) Keruing and (c) Resak. White arrows indicate the direction of ray cells.

This study also highlighted the failure behaviour of acetylated wood compared to unacetylated wood. The result from the pull-out test indicates 80% of failure mode occurs in mode IV failure for acetylated wood. This observation suggests that acetylated wood has the tendency to split during testing. As indicated in Figure 11.17, Radiata pine samples exhibit mainly mode III failure where localised failure occurs around the bond line. It is observed that the acetylated wood is more brittle than untreated radiate pine. This comes into the conclusion that acetylation process has significant influence on the mechanical properties by affecting the stiffness of the wood thus influencing the failure behaviour of the bonded joints. It is interesting to note that Radiata pine and Accoya wood exhibited significant differences in failure mode although the mean shear strength of both type of wood

indicates no statistical difference. This further highlights the importance material selection in respect to mode of failure during timber joint designing.

11.3.3 EFFECT OF ROD TYPE AND TEMPERATURE OF TEST ON SHEAR STRENGTH

The shear strength of GFRP bonded-in connections is recorded in Figure 11.19 as a function of treatments A1, B1, C1 and D1 (see Table 11.5) using RSA adhesive. Each treatment denotes the mode of post curing and testing conditions. The control samples (A1) was cured for 20 days at room temperature. Treatment B1 and C1 were each cured at room temperature and post cured for 50 and 70°C for 24hours. Testing for A1, B1 and C1 was conducted at ambient temperature. The curing and post-curing treatment of D1 is similar as C1 apart from testing condition of 50°C. Shear strengths at the timber to adhesive (τ_{ta}) and rod to adhesive (τ_{ra}) interfaces are as presented in Table 11.13.

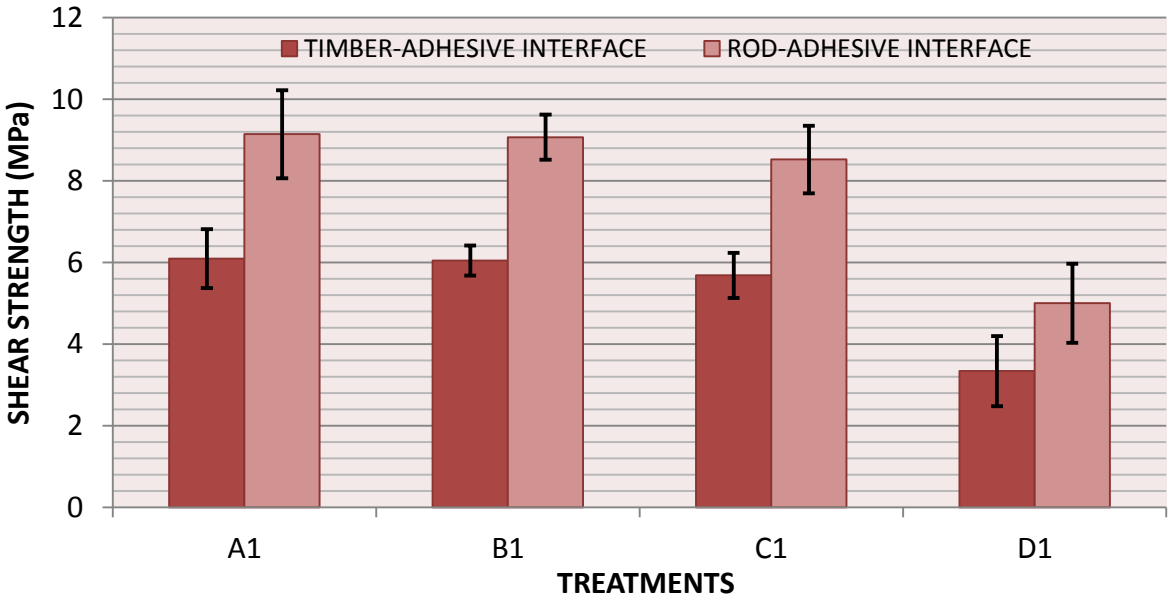

Fig. 11.19 Mean shear strength and standard deviation of GFRP bonded samples according to various treatments

Table 11.13 Details of pull-out force and mean shear strength for GFRP bonded samples

Treatments	No. of samples	Pull out force (kN)	Shear Strength (MPa)		COV(%)
			Timber-Adhesive Interface	Rod-Adhesive Interface	
A1	15	11.49	6.10	9.14	7.81
B1	15	11.40	6.05	9.07	5.10
C1	15	10.71	5.68	8.52	6.73
D1	15	6.29	3.34	5.00	8.53

Analysis by Tamhane multiple comparisons (ANOVA) was made based on the data obtained from the control and post cured samples tested at 20 ± 3ºC (treatment A1, B1 and C1). Difference in the values of mean shear strength at the rod/adhesive interface (τ_{ra}) and shear strength at the timber/adhesive interface (τ_{ta}) were statistically insignificant. This indicates that the shear strength values of the tested specimens were not affected by the post curing treatments although the results indicate a declining value of average shear strength due to the post curing treatments. ANOVA analysis of pull-out tests on 70^{o}C post cured specimens tested at 50^{o}C and control specimens has confirmed a significant decrease in values of τ_{ra} (*p-value* < 0.05) and τ_{ta} (*p-value* < 0.05). This observation relates to the fact that Tg of RSA adhesive is lower than 50^{o}C although further cross linking may result from post curing. Therefore, a significant reduction in shear strength when tested at 50^{o}C as compared to tests conducted at room temperature may be expected.

A similar standard pull-out test was also conducted on 8mm diameter threaded stainless-steel rod. The objective of the study using steel rod was to investigate the contribution of mechanical interlocking to the shear strength of the bond. The shear strength at the rod-adhesive and timber-adhesive interfaces is presented in Figure 11.20 and Table 11.14 respectively.

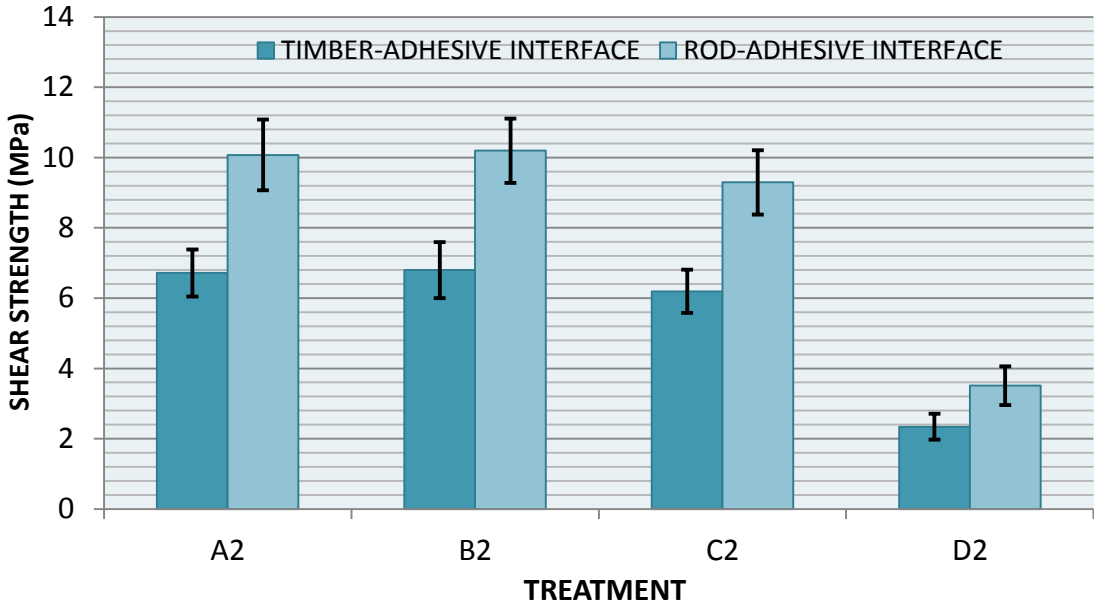

Fig. 11.20 Mean shear strength and standard deviation of stainless steel bonded samples according to various treatments

Table 11.14 Details of pull-out force and mean shear strength for stainless steel bonded samples

Treatments	No. of samples	Pull out force (kN)	Shear Strength (MPa)		COV(%)
			Timber-Adhesive Interface	Rod-Adhesive Interface	
A2	15	12.66	6.72	10.08	5.96
B2	15	12.81	6.80	10.20	8.13
C2	15	11.68	6.20	9.29	7.85
D2	15	4.41	2.34	3.51	6.71

A slight increase of 1% in shear strength at both interfaces was recorded in the sample that was post-cured at 50°C for 24 hours (B2). Post curing at 70°C (C2) however, results in a decrease of 8% in shear strengths as compared to the control sample (A2). Similar to the GFRP rods, differences in the shear strength of the pulled-out steel rods in conditions A2, B2 and C2 were shown to be statistically insignificant. ANOVA test results indicate that the only treatment with significant different in shear strength (*p-value* < 0.05) was the post-cured sample which was tested at 50°C (D2). A significant drop of 65% in shear strength at both timber/adhesive and rod/adhesive interfaces was recorded for sample D2.

The trends in shear strength at the rod/adhesive and timber/adhesive interfaces have proven to be similar for both GFRP and steel rods. A reduction of shear strength has been recorded due to the post-curing treatment of the bonded-in samples although all

results for tests conducted at ambient temperature are insignificantly different. Studies subjecting epoxy adhesives to increasing temperature curing regimes have reported a significant degradation of performance and durability of epoxy adhesives. A study was performed by Richter and Steiger (2005) on the post-curing of wood-wood and wood-FRP bonding with the aim of improving thermal stability. Joints were post-cured at a temperature of 80˚C for 4 hours. The joints were subjected to short term (1-2 minutes) and long term (24 hours) tensile tests at various temperatures (20, 50, 60, 70 and 80˚C). Although the study indicated an increase in glass transition temperature, the post-curing of the adhesive lowered the shear modulus. The result of the study concurred with this current study which indicates that the effect of post-curing at high temperature has not contributed to an improvement in the strength of the joint. This study also concludes that testing at 50˚C, which is much higher than ambient temperature (21˚C), has a detrimental effect on the shear strength.

This study is important in evaluating the performance of glue lines in a structural joint in a variable service temperature environment. Aicher *et al*. (2002) investigated transient temperature evolution in glulam for hidden and exposed glued-in steel rods. Coinciding with the findings of this current study, Aicher *et al*. (2002) measured a strong strength reduction due to testing at elevated temperature thus contradicting the commonly held assumption that bonded-in joints are less susceptible to thermal degradation due to glue lines being hidden. The effect of test temperature on the strength of the bond is much influenced by the behaviour of wood-epoxy interface. Pizzo *et. al* (2002) investigated the thermal expansion coefficients (α) of epoxy-bonded wood joints. The study indicates a significant difference in the α values between the bonded wood and epoxy adhesives. The differences in the magnitude of thermal expansion coefficient between substrate and adhesive result in internal stress within the bonded joint, which affects the durability of the joint.

Another interesting observation from the comparison of using GFRP and steel rod is the differences in shear strength at the test condition A, B, C and D. The value of shear strength for all pull-out tests using steel rod conducted at ambient temperature were higher than the results for GFRP joint samples. The surface of threaded or deformed steel rod provides an extra mechanical interlock in addition to the intrinsic adhesion

provided by the adhesive (Rossignon and Espion, 2008, Broughton and Hutchinson 2001). However, it has been observed that steel rod pull-out samples exhibit a slightly lower value of shear strength than GFRP samples when conducted at 50˚C. High temperature causes internal stress in the bonded-in joint due to differences in the thermal expansion coefficients (α) of the rods and the LVL. The α value of epoxy lies in a range of 58-117 μstrain/˚C which means that it is sensitive to temperature changes. This value is much higher than the α value for both of the rods. Steel has an almost similar expansion coefficient value (16-22 μstrain/˚C) to GFRP (20-30 μstrain/˚C). Therefore, bonded-in steel rods would experience similar internal stress to GFRP bonded-in rods when samples are tested at temperatures as high as 50˚C. As indicated by Cruz *et al.* (2005) and Cruz and Custódio (2006), the types of rod used in bonded-in joints make very little difference to the failure mode due to thermal expansion of the adhesive.

Two-way ANOVA analysis was conducted to investigate the interaction between the two types of rod and post-curing/test temperature treatment as indicated in Table 11.15. Profile plots shown in Figure 11.21 indicate significant interaction which suggests large size effect based on the values of partial eta squared (η^2), see Table 11.16.

Table 11.15 Two-way ANOVA of shear strength for pull-out test of RSA post-cure treatment at timber-adhesive and rod-adhesive interfaces

Shear strength pull-out sample	F value	p-value	Partial eta squared (η^2)
Rod	1.815	0.182	0.022
Treatment	109.081	0.000	0.804
Rod*Treatment	6.148	0.001	0.187

Table 11.16 Reference on assessing values of partial eta squared (Gray & Kinner, 2012)

Size effect	Partial eta squared (η^2)
Small	$0.01 \leq \eta^2 \leq 0.06$
Medium	$0.06 \leq \eta^2 \leq 0.14$
Large	$\eta^2 \geq 0.14$

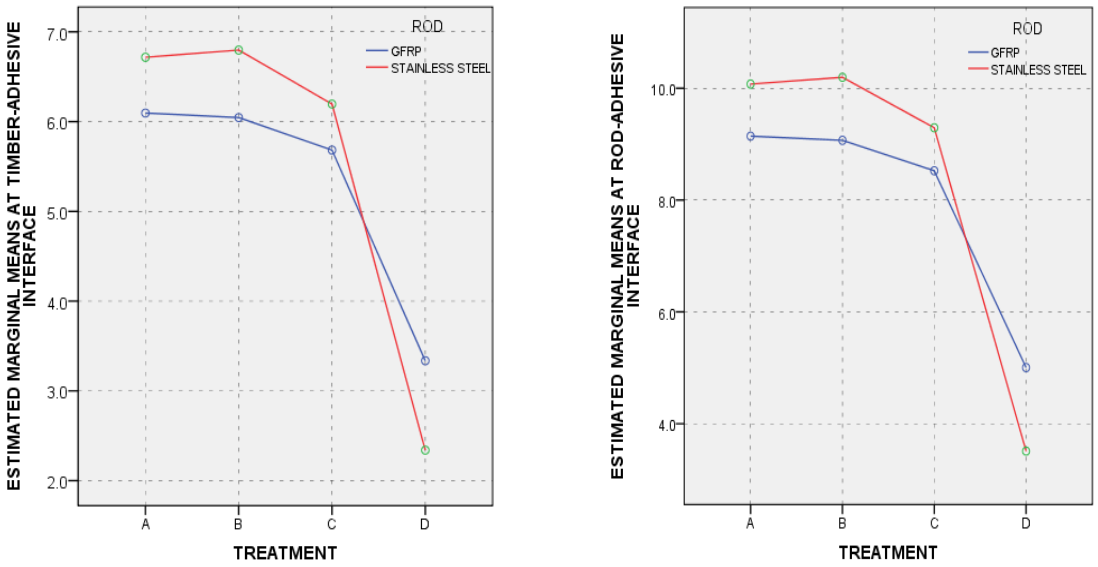

Fig. 11.21 Profile plots of level suggesting interaction between the type of rod and post-cure/temperature effects

Although both of the rods showed similar trends in shear strength properties, differences in failure mode were recorded due to the post-curing treatment. Figure 11.22 depicts samples of single ended bonded-in joints that have been tensile tested until failure. The modes of failure of tensile tested bonded-in connections can be categorised into failure mode II, mode III and mode IV.

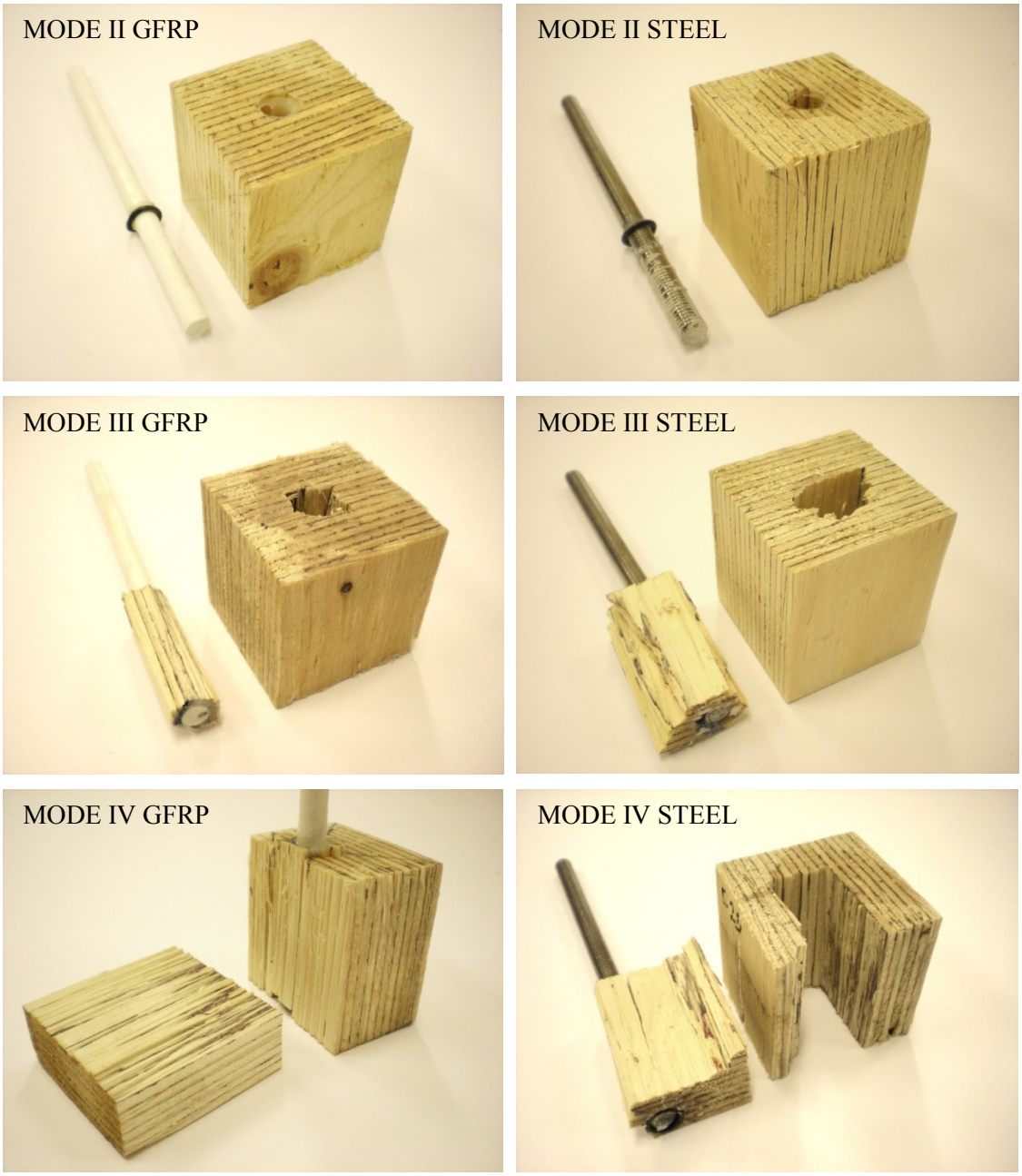

Fig. 11.22 A composition on types of failure modes for GFRP and steel rod bonded sample

Figures 11.23 and 11.24 compare the failure modes which relate to the post-curing treatments and type of rod. The failure mode percentages according to type of rod are as presented in Table 11.17 (GFRP) and 11.18 (steel).

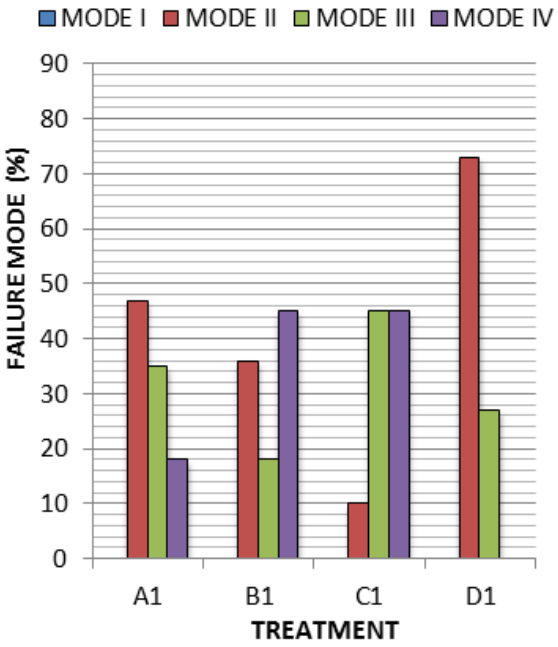

Fig. 11.23 Percentages of failure according to the mode of failure for GFRP bonded samples

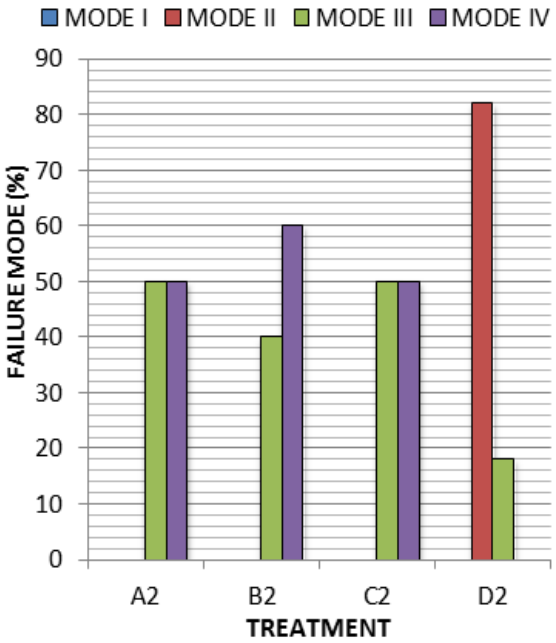

Fig. 11.24 Percentages of failure according to the mode of failure for stainless steel bonded samples

Table 11.17 Details of shear strength and percentages of failure mode for GFRP bonded sample

Adhesive	τ ta (timb/adh) (MPa)	τ ra (rod/adh) (MPa)	Failure mode (%)			
			MODE I	MODE II	MODE III	MODE IV
A1	6.10	9.14	0	47	35	18
B1	6.05	9.07	0	36	18	45
C1	5.68	8.52	0	10	45	45
D1	3.34*	5.00*	0	73	27	0

*Significant difference

Table 11.18 Details of shear strength and percentages of failure mode for stainless steel bonded sample

Adhesive	τ ta (timb/adh) (MPa)	τ ra (rod/adh) (MPa)	Failure mode (%)			
			MODE I	MODE II	MODE III	MODE IV
A2	6.72	10.08	0	0	50	50
B2	6.80	10.20	0	0	40	60
C2	6.20	9.29	0	0	50	50
D2	2.34*	3.51*	0	82	18	0

*Significant difference

The failure mode from the pull-out test indicates that GFRP bonded-in joints are more sensitive to the post-curing treatment than steel bonded-in joints. The tendency for a shift from rod/adhesive failure towards timber failure from ambient to 50˚C to 70˚C

post-cure for GFRP bonded-in samples tested at ambient temperature was observed. The effect of post-curing on failure mode was less obvious with the steel rod. The post-curing treatment may change the intrinsic properties of the epoxy which might affect the bonding properties of the adhesive to the substrate. This issue is very important for wood-GFRP bonding since the results of the test in terms of failure mode entirely depend on the quality of the glue line. As for steel rod, the thread on the surface of the rod would provide an extra element to the bonding mechanism of the joint due to the existence of mechanical interlocking. The increasing percentages of timber failure for GFRP pull-out sample due to post curing at 50˚C and 70˚C might indicate that the epoxy-GFRP bond has exceeded the strength of the wood itself. But since the post-curing has not increased the shear strength, the result suggests that the failure occurs due to brittle timber rupture caused by the 70˚C temperature treatment. Tests conducted at 50˚C for GFRP and steel rod bonded-in samples resulted in a predominance of rod/adhesive failure. The outcome was as expected since it was tested at a temperature that is higher than the adhesive's glass transition temperature.

11.3.4 MACROSCOPIC AND SEM ANALYSIS OF TIMBER FAILURE

The pattern of fracture on tensile tested rods bonded into LVL was analysed macro- and microscopically. The aim of the study was to investigate the effect of micro-movement of wood anatomical structure within the engineered wood due to the shear stresses.

Tensile tested pull-out samples with visible wood failure on the rod were imaged macroscopically to investigate crack patterns formed due to the application of shear stress close to the bonded-in joint. Cracks in the wood occur in two separate orientations both, tangential-longitudinal and radial-longitudinal. The tangential-longitudinal crack as depicted in Figure 11.25 occurred in early wood which has thinner cell walls compared to the late wood. The early wood layer is less rigid and more porous and serves as a weak point for cracks to propagate.

Radial-longitudinal cracks originate from the small fissures in the veneers. As is well known, veneer is produced by rotary peeling process on a tree trunk. During manufacturing, the originally curved layer is then pressed to produce a flat veneer sheet. Due to the tension and compression which occurred within the layer during the process,

small fissures are formed particularly at ray cells. As depicted in Figure 11.26 the crack propagates from horizontal to vertical orientation across several layers of veneers. This crack propagates through small fissures which serve as the weak point within the veneer.

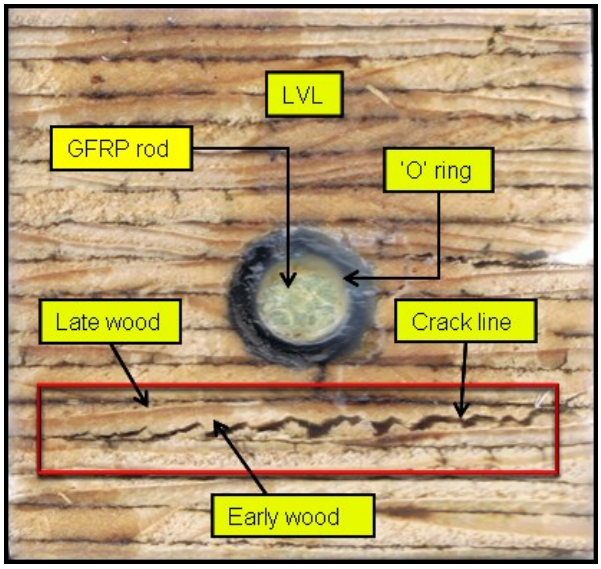

Fig. 11.25 Tangential-longitudinal crack formed following pull-out.

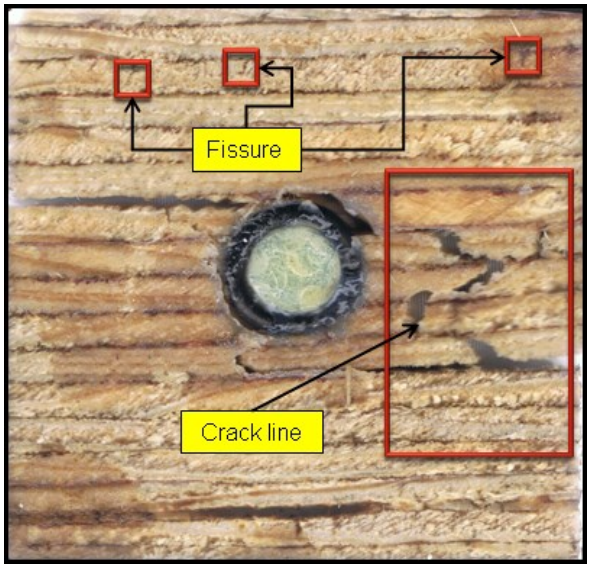

Fig. 11.26 Radial-longitudinal cracks formed following pull-out.

To further investigate the fracture behaviour of tensile tested bonded-in connections, the pulled-out portion of the LVL was examined by scanning electron microscopy (SEM). The examination was conducted on the tangential and radial planes of the LVL. Wood is an anisotropic material which means that the behaviour of wood is determined by the orientation of cells (Desch and Dinwoodie, 1996). Bonded-in rods are oriented parallel to the grain direction so fracture surface are a combination of radial-longitudinal and tangential-longitudinal failure modes.

Figure 11.27 provides an overview of the tangential-longitudinal section of the tensile tested sample. A typical tangential-longitudinal section of softwood is characterised by tracheid and ray cells (uniseriate).

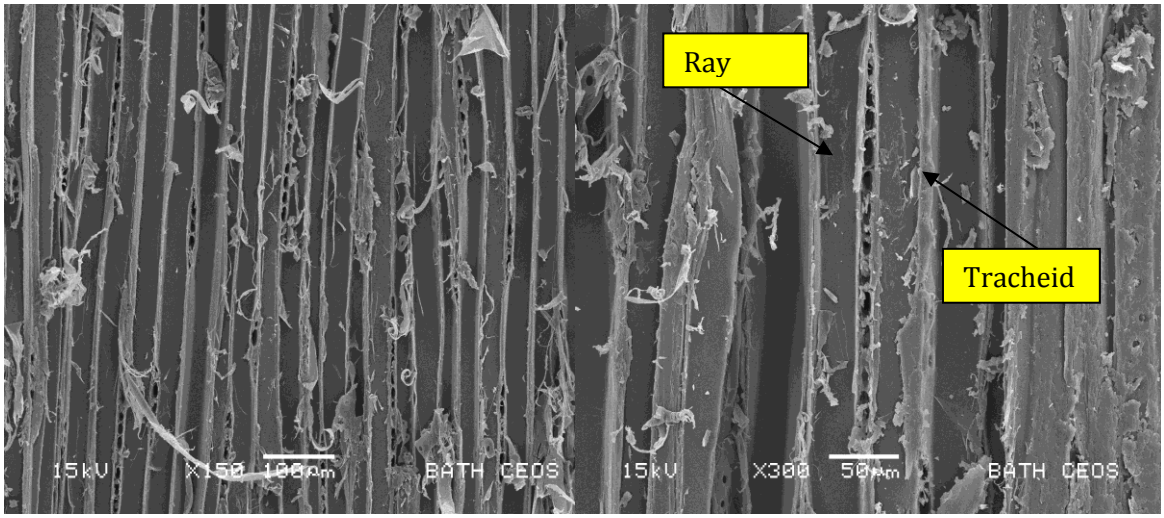

Fig. 11.27 An overview of tangential-longitudinal surface

Observation of the tangential-longitudinal plane of the shear tested sample reveals the occurrence of slipped and fractured wood cells. Figure 11.28 indicates slips and gaps due to fracture of tracheids. This behaviour is consistent with the shear stress causing micro-movement of wood cell in different directions. The fusiform ray in these images are less affected. Gradual separation of cell components such as cell wall and bordered pit are evident in Figure 11.29.

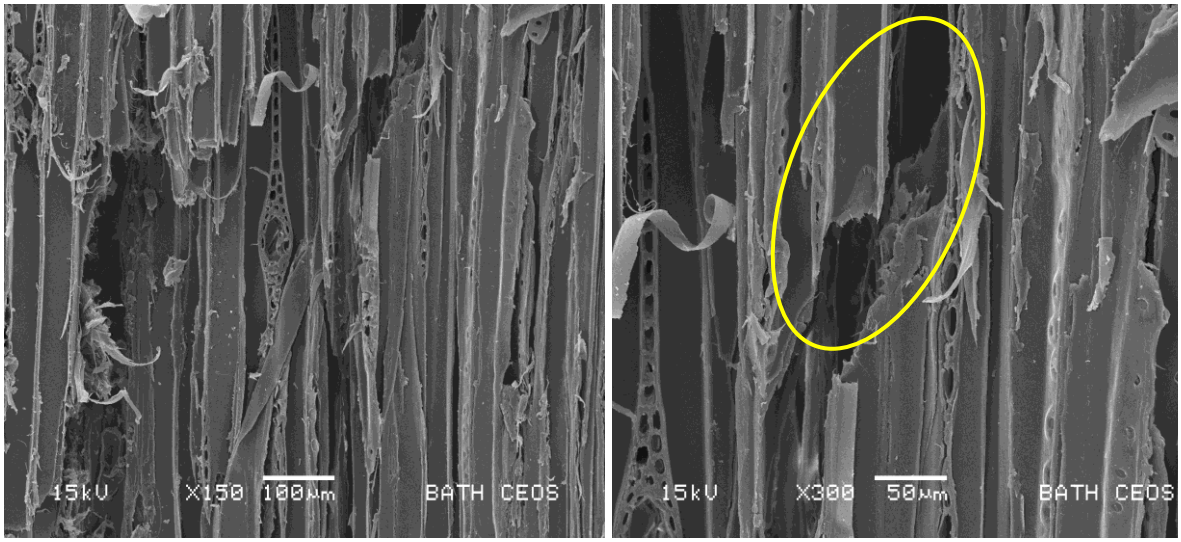

Fig. 11.28 Slip and fracture of wood cells (encircled) (tangential-longitudinal surface)

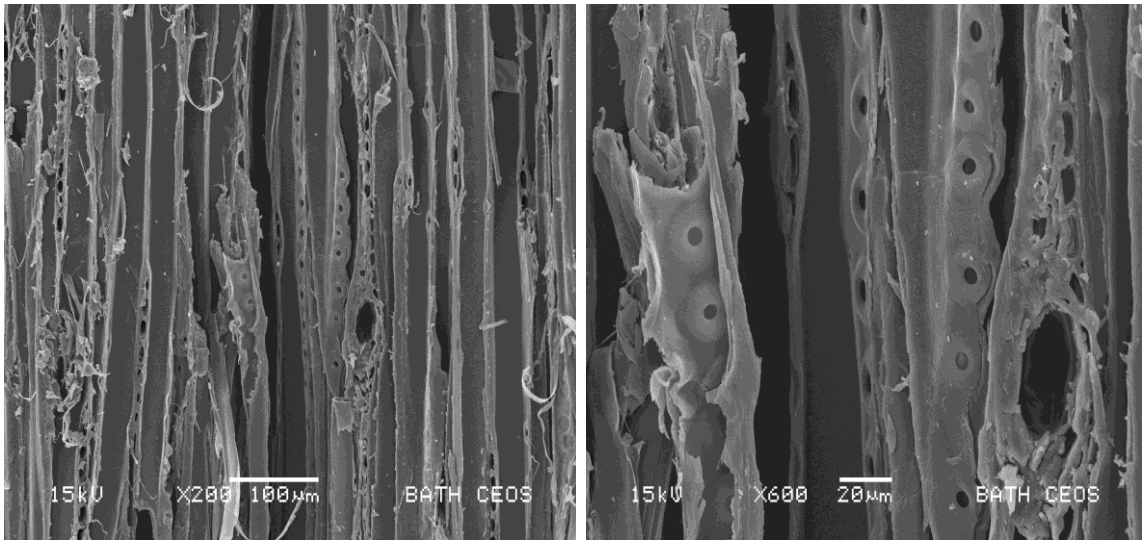

Fig. 11.29 Gradual separation of cell wall and bordered pit

Torn wood cells were observed either individually (Figure 11.30) or in cluster (Figure 11.31). The 'peeling' effect was evidence of shear damage to wood cells as the planes within the wood structure were moved in opposite direction. Gradual separation of cell components was observed with fibrillation of torn cells.

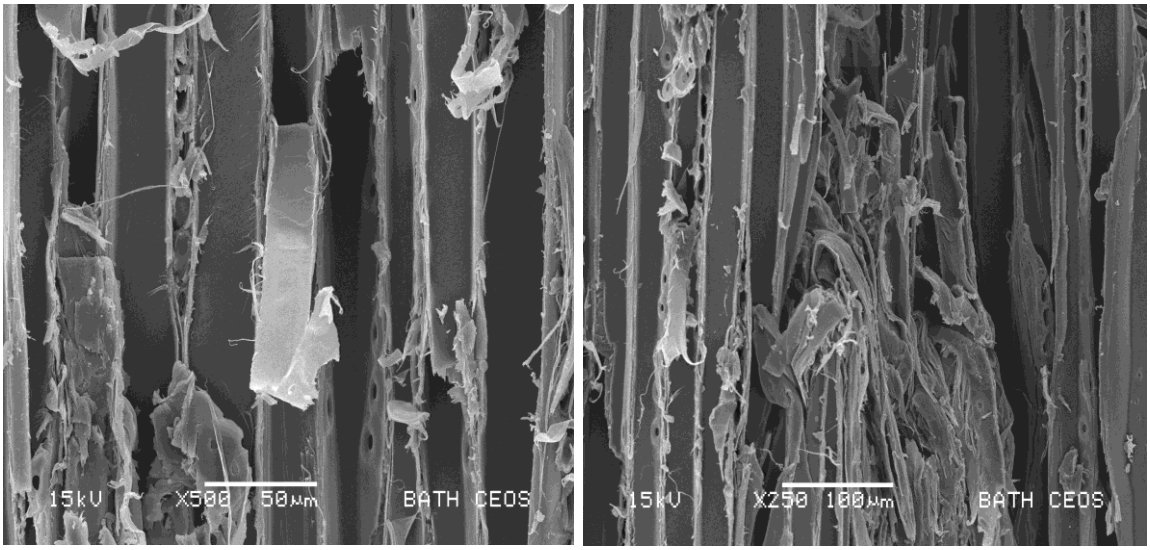

Fig. 11.30 Peeling of individual cell wall. *Fig. 11.31 Peeling of cluster cell walls*

The radial-longitudinal surface of an LVL is characterised by tracheids and ray cells at right angles with bordered pits and cross-field pitting on parenchyma cells (Figure 11.32). A 'peeling' effect due to cell wall separation and fibrillation was observed (Figure 11.33). Macroscopic analysis indicates the tendency of fracture to occur in the

softer and more porous section of earlywood than latewood. This is confirmed by scanning electron microscopy of the crack which runs in between these two regions. Figure 11.34 depicts a portion of earlywood which is adjacent to the latewood. The earlywood is characterised by its larger lumen size and thinner cell wall. Cells of late wood have thicker cell walls and smaller lumens. A crack line was observed to run throughout the length of the earlywood tracheid. The late wood tracheids appear unaffected due to their thicker cell walls. A view of longitudinal radial surface of ray tracheids and ray parenchyma shows portions of torn tracheids (Figure 11.35). Some parts of the tracheid are intact due to the presence of ray tracheid and ray parenchyma cells which run across it. Both cells of ray tracheid and ray parenchyma were less affected by the shear stress. This shows that fracture due to the shear motion occurred easily across the orientation of the ray cells since it provide a weak point for a crack to propagate.

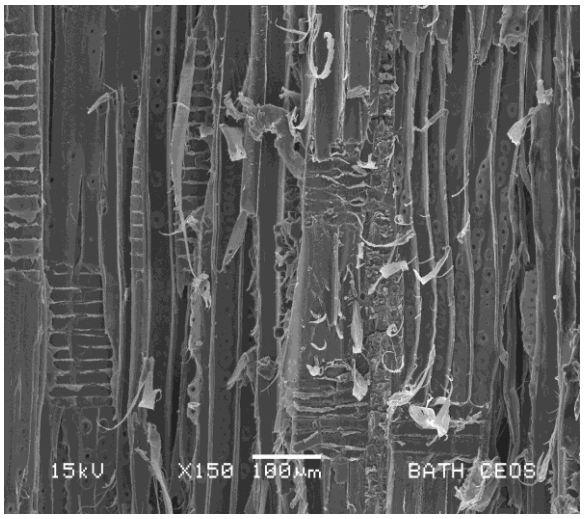

Fig. 11.32 An overview of radial-longitudinal plane

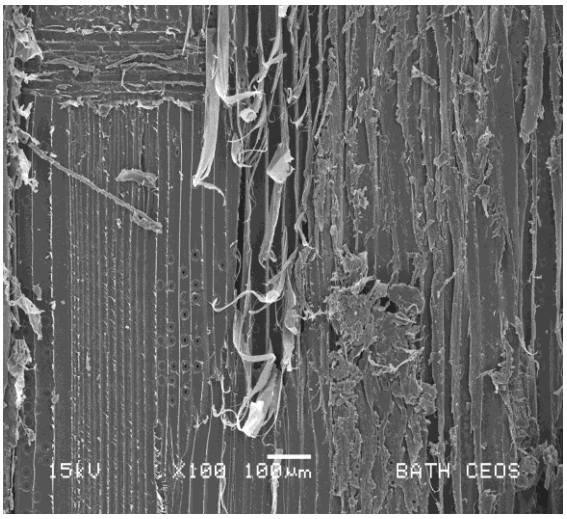

Fig. 11.33 Peeling effect of fibres due to fibrillation

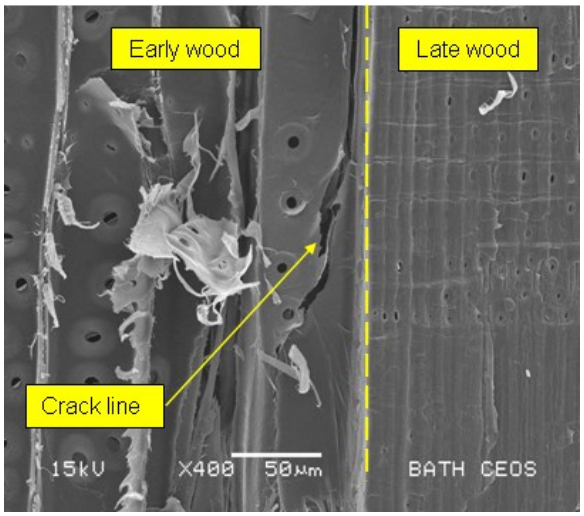

Fig. 11.34 Crack line of early wood

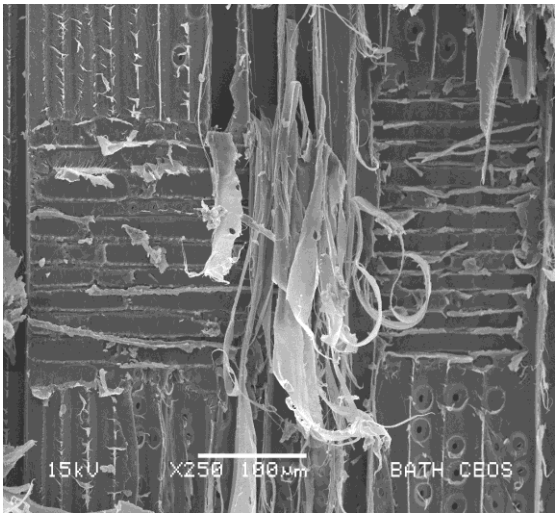

Fig. 11.35 Torn tracheid with ray tracheid and parenchyma.

11.4 CONCLUDING REMARKS

The pull-out strength of single bonded-in rods has been analysed by comparing the effect of using various types of adhesive fillers, woods, rods, post curing treatments and testing temperatures. By comparing the values of mean shear strength and modes of failure, the following conclusion can be drawn:

a) Filler type : The highest mean shear strength was achieved by using a ductile nano-epoxy type filled adhesive which has been modified with liquid rubber. All tested samples failed in Mode III.

b) Wood type : There is a strong correlation between the density of the wood and mean shear strength. The highest mean shear strength was exhibited by Resak where most failure occurs in Mode I. The study indicates a different failure mode according to wood type. Failure mode in softwood and hardwood is mostly related to the anatomical properties of the wood which influences crack propagation. Growth ring interfaces (earlywood to latewood) serve as weak zoness leading to crack propagation. Brittle failure is predominant in Accoya wood where 80% of failure occurs within timber.

c) Rod types : The results demonstrate no significant difference in mean shear strength between tested samples bonded using smooth GFRP and threaded stainless steel rods.

d) Post curing treatments: The study indicates no significant difference between the mean shear strength of the samples exposed to the different post-cure treatments when tested at 20ºC although the post curing treatment was expected to result in a slight increase in the Tg of the epoxy adhesive.

e) Testing temperatures : The study has shown that samples which were tested at a temperature (50ºC) that is higher than the glass transition temperature of the adhesive will exhibit a significant reduction in the mean shear strength.

CHAPTER 12 : CREEP TESTING OF THE ADHESIVE INTERFACE BETWEEN AN LVL SUBSTRATE AND BONDED-IN PULTRUDED ROD

12.1 INTRODUCTION

Creep of adhesives is a time-dependant process which depends on the influence of temperature and humidity. In this chapter, the creep properties of the adhesive interface between LVL and bonded-in pultruded rods are evaluated. All four types of epoxy-based adhesive studied in previous chapters were used in this creep investigation. The effect of different temperatures (20, 30, 40 and 50^{o}C) and relative humidities (65, 75, 85 and 95%) on the creep of the adhesive interface under constant load were investigated. Creep deformation is modelled using Kelvin-Voigt theory and model creep curves are fitted to experimental data.

12.2 DEVELOPMENT OF A CREEP TEST METHODOLOGY

As described in Chapter 12, the adhesive interface in a bonded-in joint which is subjected to tensile or compressive loading will ultimately deform under a shear stress. The bonded-in creep specimen described in this study is a development of a standard pull-out test, which is based on the pull-out of a pultruded rod from a 63mm cube LVL in a mechanical testing machine. For the application of a constant creep load, a scaled-down creep sample was developed. Several test methods for the application of creep were considered including a hydraulic jack system with a feedback loop and a compressed automotive spring. The initial design of the creep sample was based on a single ended sample and a chuck was used to grip the end of the GFRP rod. Due to the physical properties of the glass fibre pultrusion, the chuck slipped during the test invalidating the results. Hence a double-ended sample was designed to counteract the problem of grip-slipping.

12.2.1 MATERIALS : ADHESIVE, ROD AND LVL

RSA, EA, Timberset and Sikadur adhesives were selected for the shear creep tests under constant load. The rod was a glass fibre pultrusion (GFRP) with polyester matrix, available in several diameters. The rod diameter for a standard pull-out test from a 63cm LVL cube is 8mm. Based on the calculated interfacial shear stress in a gravity creep test the rod diameter was reduced to 4mm. The Young's modulus, thermal expansion coefficient (α) and glass transition temperature properties (T_g) of the materials used to fabricate the bonded-in joint are listed in Table 12.1. The behaviour of bonded-in joints subjected to creep under extreme environmental conditions is influenced by these properties.

Table 12.1 Bonded-in sample materials properties

Type	Material	Young's Modulus (E) GPa	Thermal Expansion Coefficient ($10^{-6}C^{-1}$)	Glass Transition Temperature (T_g)
Epoxy	RSA	1.69	71.5	36.8
Epoxy	EA	3.59	55.8	55.6
Epoxy	TIMBERSET	1.39	63.0	35.4
Epoxy	SIKADUR	6.38	37.3	42.5
Rod	GFRP	17.0	10	N/A
Substrate	LVL	13.8	N/A	N/A

12.2.2 STATIC TEST: FABRICATION AND TEST CONFIGURATION

Two types of sample were prepared for static and creep tests. A static test was performed to determine the ultimate shear strength of the adhesive bond whilst double-ended samples were fabricated for the creep test. A schematic diagram of the single ended sample is depicted in Figure 12.1. Blocks of $50mm^3$ Kerto Laminated Veneer Lumber (LVL) were centrally drilled with 7.3mm diameter hole to accommodate the epoxy adhesive and the rod. The blocks were reduced in thicknesses to 30mm (Figure 12.2) to increase the shear stress experienced at the adhesive interface for any given load. Blocks with a thickness of 20 and 10mm were proposed earlier in the study which resulted in failures mainly in the timber. A 4mm diameter glass fibre pultrusion (GFRP) was inserted into the epoxy adhesive which was back-filled into the drilled hole. Rubber

'O' rings were used to centralise the rod at each end of the drilled hole. Prior to bonding, the surface of the GFRP rod was lightly abraded and degreased with acetone to remove surface contaminants such as die release agent. The thickness of the glueline was set at 1.65mm and it was left to cure at 20°C and 65% relative humidity for 20 days prior to testing.

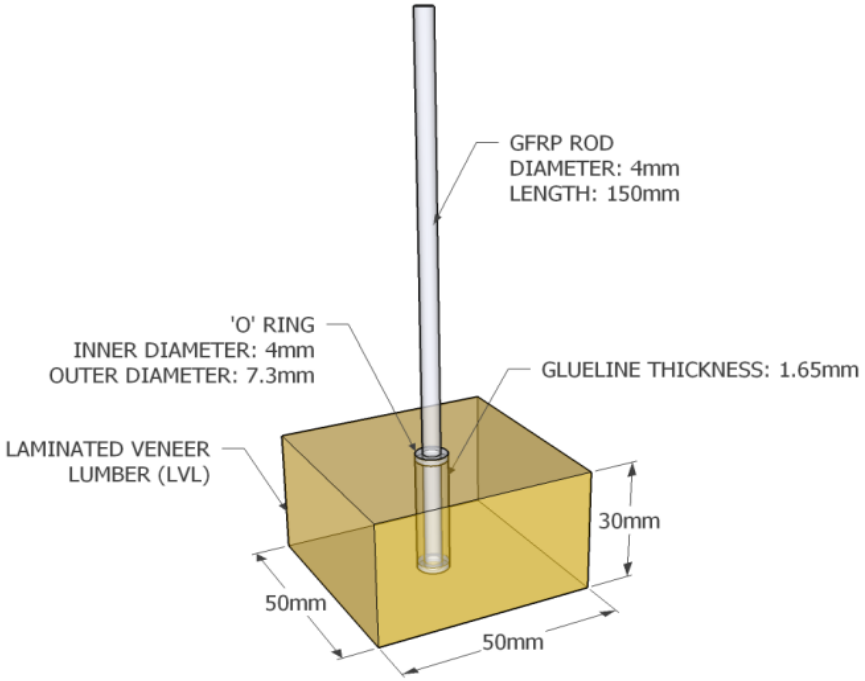

Fig. 12.1 Schematic diagram of a single ended model for static test

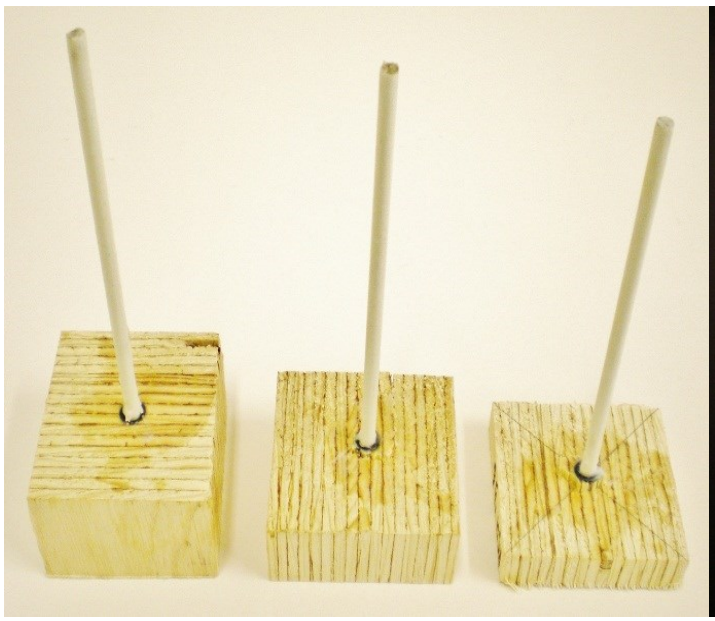

Fig. 12.2 Single-ended model for static test at various thickness; 30mm (left), 20mm (centre) and

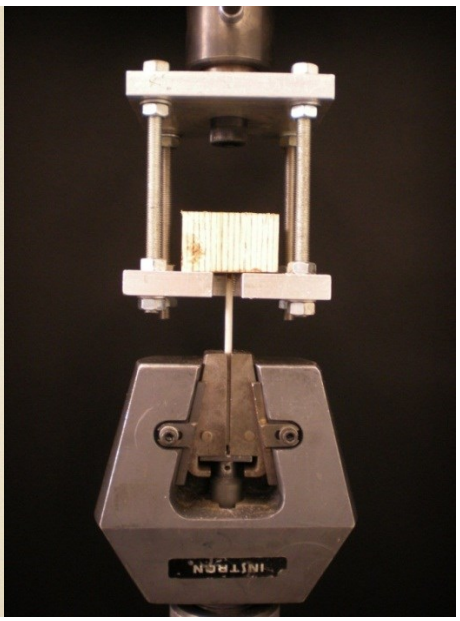

Fig. 12.3 Static test of bonded samples.

10mm (right).

The single ended samples were then tested using an Instron 3369 universal testing machine equipped with load cell of 50kN capacity. The Instron machine was fitted with a customised frame to support the sample (Figure 12.3). The GFRP end of the sample was secured by the grooved lower wedge grips. The tensile test was conducted at a cross-head rate of 2mm/min until sample failure. A total of 10 single-ended samples were tested to failure for each adhesive under investigation. The test data were captured using Bluehill2 software and presented in the form of load (kN) versus displacement (mm) graphs. The peak force (N) can be converted into equivalent vertical load (kg) via Equation 12.1.

$$F = mg \qquad \text{(Eqn. 12.1)}$$

where g is the acceleration due to gravity. The maximum shear stress at the timber-adhesive interface and the adhesive-rod interface was calculated using Equation 12.2.

$$\tau = \frac{F}{2\pi r l} \qquad \text{(Eqn. 12.2)}$$

Where, *F* is the maximum force applied during the static test. The radius of the interface and the embedded length of the rod are represented by *r* and *l* respectively. The diagram of the interface area is represented in Figure 12.4.

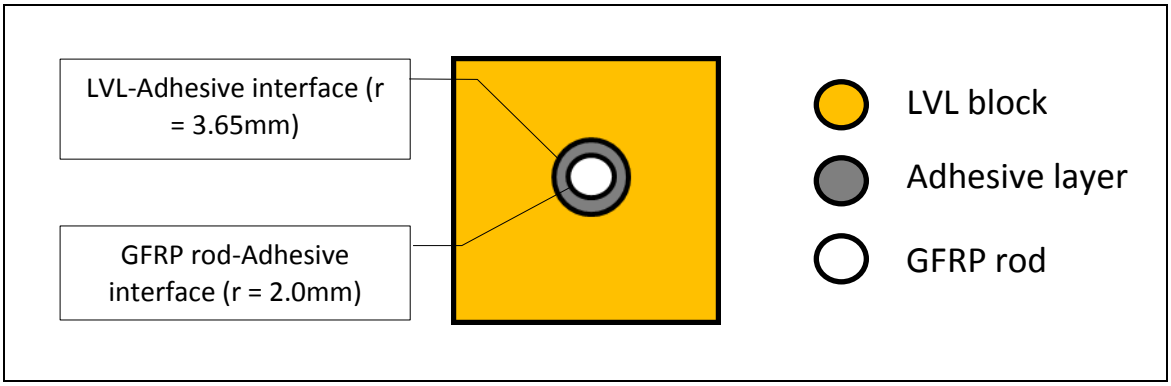

Figure 12.4 Diagram of rod-adhesive and LVL-adhesive interface indicating the radii used in the equation for maximum shear strength.

12.2.3 CREEP TEST : SAMPLE FABRICATION

The samples were fabricated by connecting two LVL blocks with a 4mm diameter GFRP pultruded rod as depicted in Figure 12.5. The blocks were separated by a distance of 70 mm. The LVL blocks were drilled centrally through their entire length and filled with epoxy adhesive. The thickness of glue-line was 1.65mm, the same as for the single ended model. During the insertion of the GFRP rod into the epoxy filled hole, the rod was rotated to minimise the formation of air bubbles and to ensure consistency of the adhesive layer along the embedded length. A rubber 'O' ring was placed at each end of the blocks to centralise the inserted rod. The test-end of the sample where creep strain was monitored had an embedded length of 30mm. The other end with an embedded length of 75mm served to support the creep load which was applied by using steel weights. This method was adopted due to the failure of an earlier test using a metal chuck to grip the end of the GFRP rod which crushed the pultruded rod. The GFRP rod was attached to an aluminium plate which allowed laser sensor displacement measurements to be made. As depicted in Figure 12.6, the distance of the creep block and the aluminium plate was set at 40mm since it is the minimum working distance for the laser sensor. The fabricated samples were then left to cure at 20ºC and 65% RH for 20 days for the adhesive to achieve its optimum state of cure.

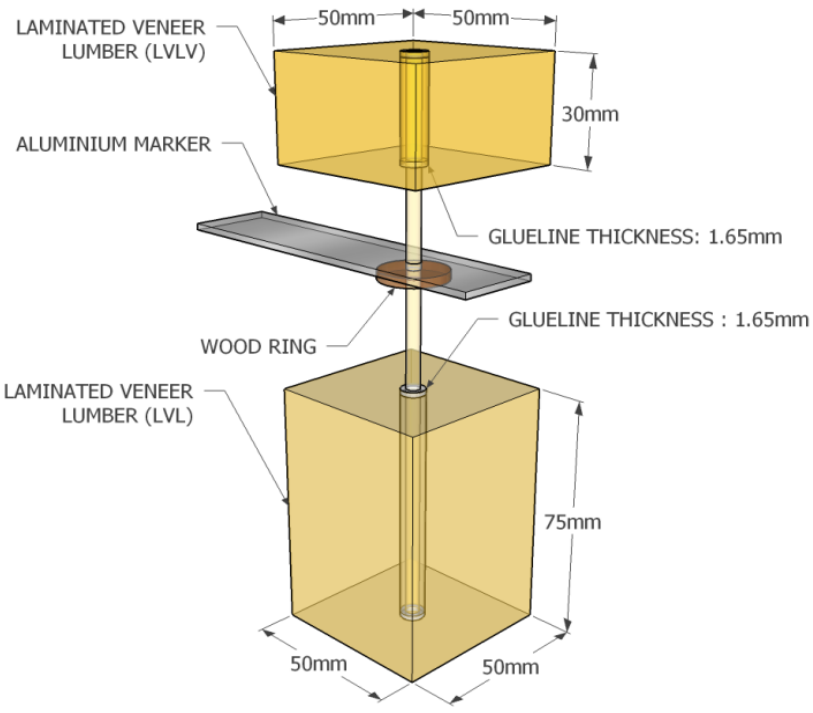

Fig. 12.5 An isometric view of the double-ended creep model

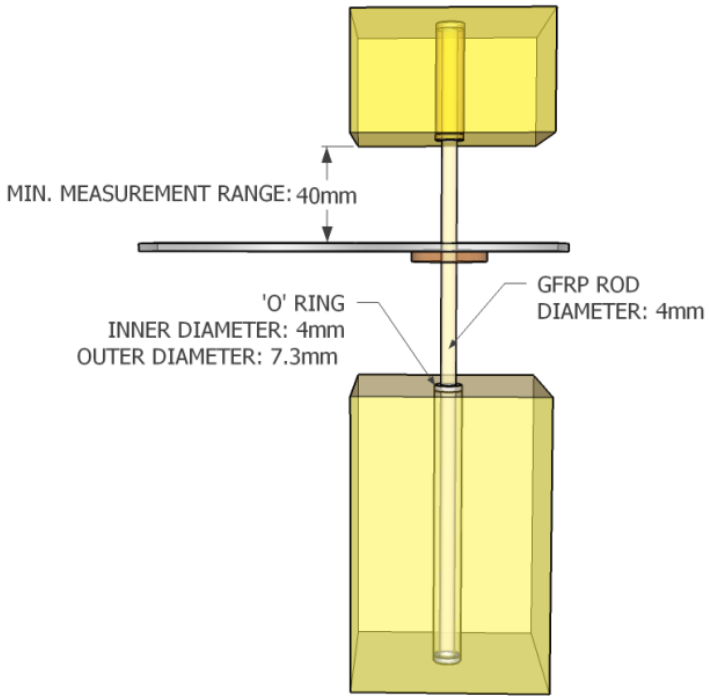

Fig. 12.6 A side view of the double-ended creep model

12.2.4 CREEP TEST RIG SETUP AND THE HUMIDITY CHAMBER

The creep test rig was designed to support the larger end of the creep sample and the attached weight, as depicted in Figure 12.7, and was made of two 10mm thick aluminium plates. The plates were milled to obtain the final dimensions as indicated in Figure 12.8.

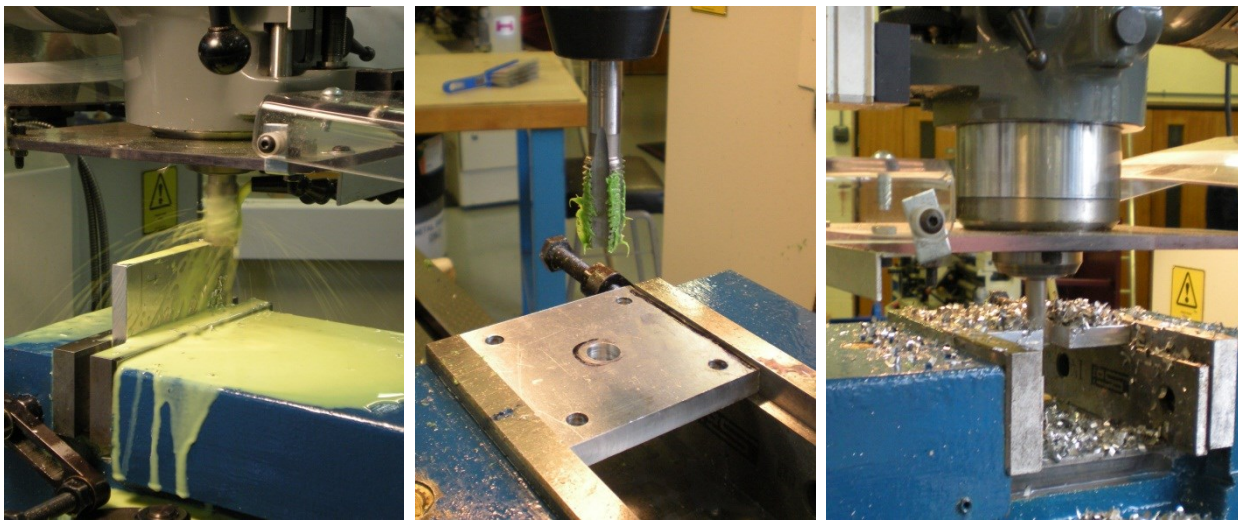

Fig. 12.7 Machining of the creep jig using milling machine

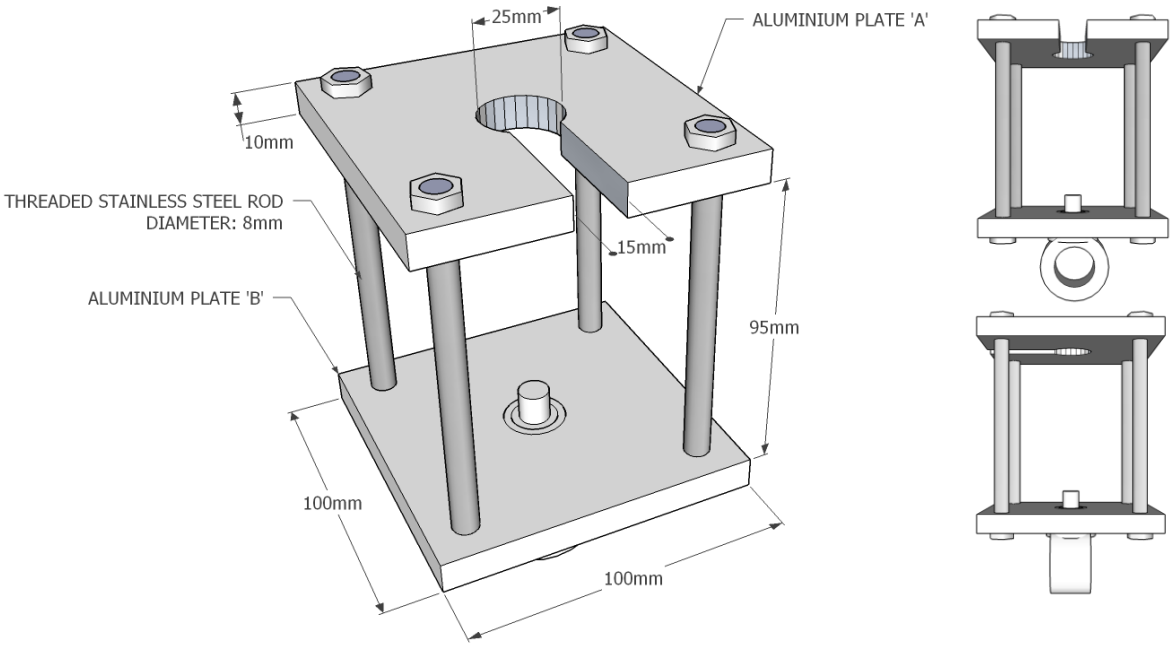

Fig. 12.8 Dimension of the creep jig

As shown in Figure 12.9, the test-end of the double-ended sample was mounted on a pair of steel bars which supported the sample and laser sensor. The larger LVL block functioned as support for the attachment of the dead weights. A constant static tensile creep load was applied equal to 20% of the ultimate shear strength.

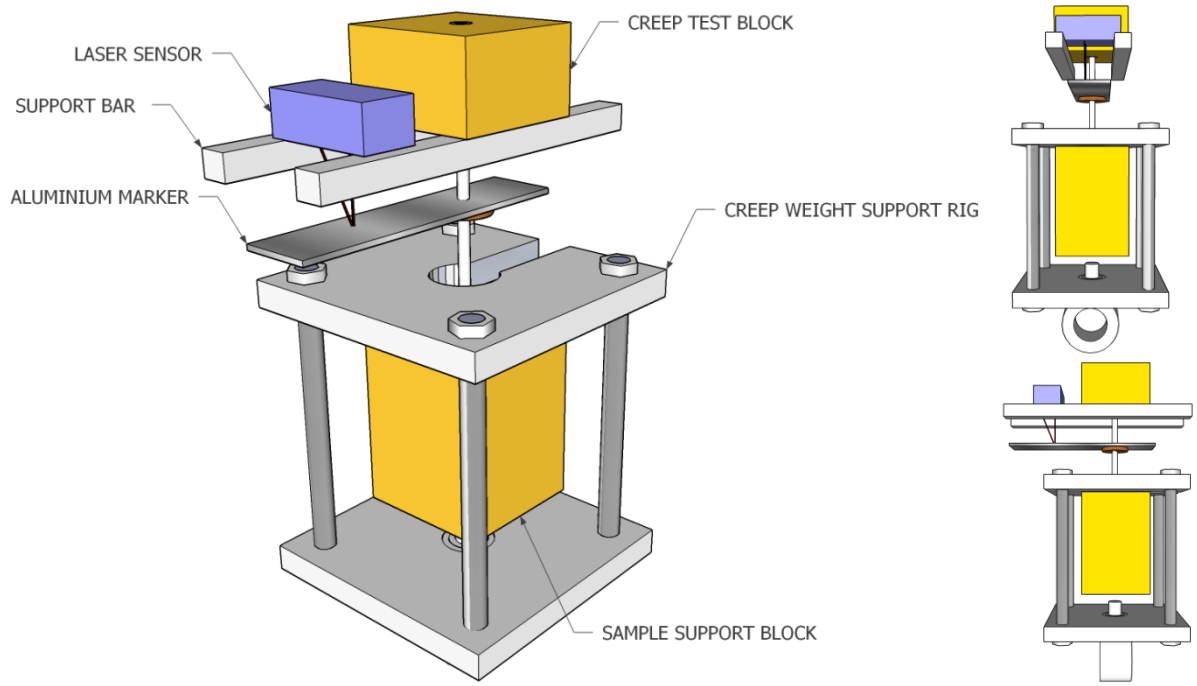

Fig. 12.9 A diagram of the creep jig and bonded-in creep sample

The creep load was comparable to existing working loads. Creep loads were added in 5kg steps. The creep testing of the bonded-in joint samples was conducted in a walk-in environmental chamber. The samples were preconditioned at the temperature/humidity for 30 minutes prior testing. Figure 12.10 shows two creep samples being tested simultaneously with weight hangers attached to the creep jig.

Fig. 12.10 The complete configuration of the creep test in a walk-in humidity chamber

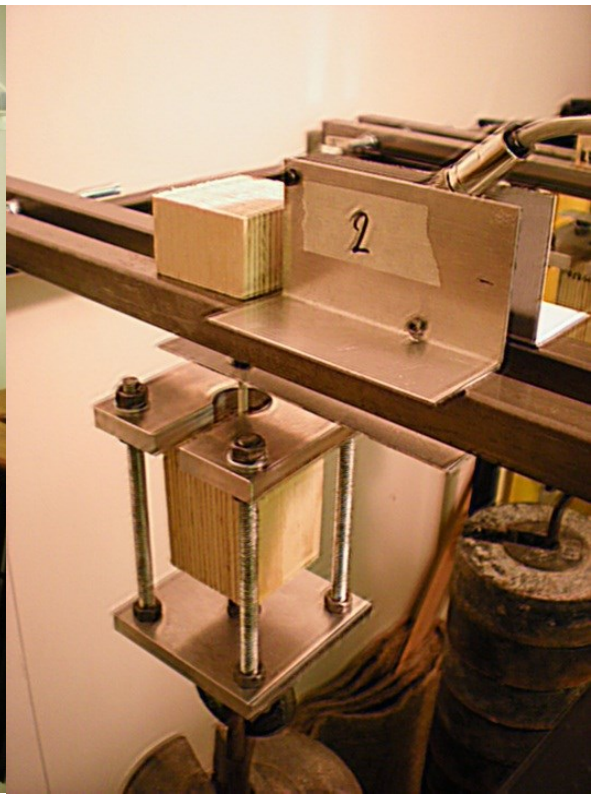

Fig. 12.11 A closer view of the creep test jig and attached laser sensor

A laser sensor was attached on the support bar (Figure 12.11) to measure creep displacement. Prior to the placement of the samples, the test condition (temperature and humidity) was held constant for at least 30 minutes. The combinations of temperature and humidity for the creep studies are listed in Table 2 and tests were performed on three samples for each condition. Laser displacement data were captured at 1 minute intervals using a data logging system via Labview software until the experiment reached a 4000 minute limit.

Table 12.2: Bonded-in creep test matrix

Adhesive	Temperature (°C)	Relative Humidity (%)	Duration (min)
RSA	20	65	4000
	30	75	
	40	85	
	50	95	
EA	20	65	4000
	30	75	
	40	85	
	50	95	
TIMBERSET	20	65	4000
	30	75	
	40	85	
	50	95	
SIKADUR	20	65	4000
	30	75	
	40	85	
	50	95	

12.2.5 DATA ANALYSIS AND MATHEMATICAL MODEL OF CREEP

Data obtained from the creep tests were recorded in the form of shear strain versus time (minutes). As indicated in Figure 12.12, displacement is defined as downward displacement of the GFRP rod due to the shear creep of the glueline

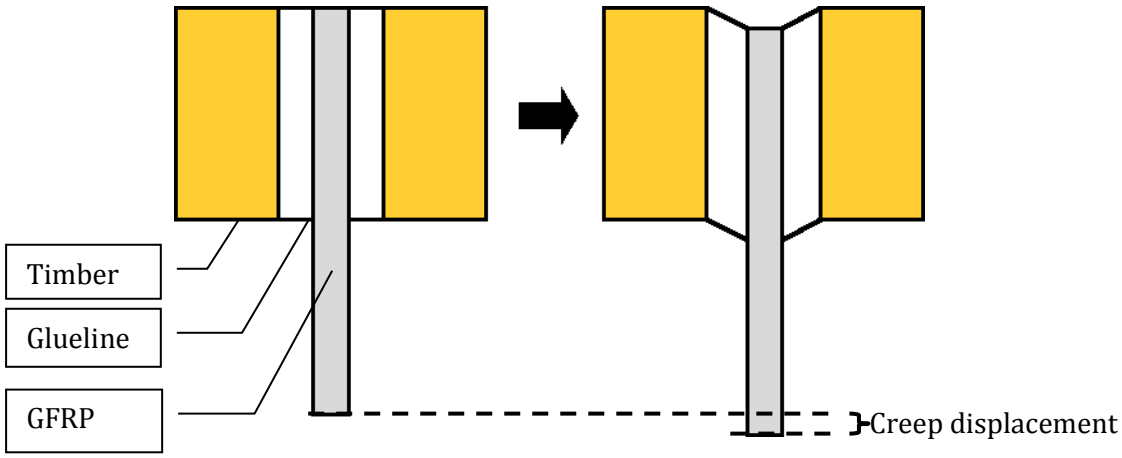

Fig. 12.12 Creep displacement of a tested sample

Shear strain was calculated using Equation 12.3:

$$\text{Shear strain} = \frac{\text{Creep displacement (mm)}}{\text{Glue} - \text{line thickness (mm)}} \quad \text{(Eqn. 12.3)}$$

Viscoelastic creep was modelled using the Kelvin-Voigt equation for creep strain ε(t) which under constant creep stress (σ_0) can be described as:

$$\varepsilon\,(t) = \frac{\sigma_o}{E} \cdot \left[1 - exp\left(-\frac{t}{\tau}\right)\right] \quad \text{(Eqn. 12.4)}$$

E is the elastic modulus of the spring and τ is the characteristic retardation time which is the ratio of dashpot viscosity η to E. This can be visualised as creep element as shown in Figure 12.13.

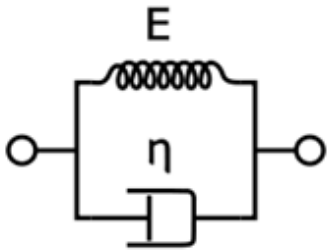

Fig. 12.13 Kelvin-Voigt creep element

A series creep model comprising two Kelvin-Voigt elements was introduced to improve the goodness of fit of the model to experimental data. The equation for Model 2 is given as:

$$\varepsilon(t) = \frac{\sigma_o}{E_1} \cdot \left[1 - \exp\left(-\frac{t}{\tau_1}\right)\right] + \frac{\sigma_o}{E_2} \cdot \left[1 - \exp\left(-\frac{t}{\tau_2}\right)\right] \quad \text{(Eqn. 12.5)}$$

Referring to Figure 12.14, the $\sigma o/E_1$ and retardation time τ_1 correspond to the left side of the elements whilst the remaining $\sigma o/E_2$ and retardation time τ_2 corresponds to the right hand element.

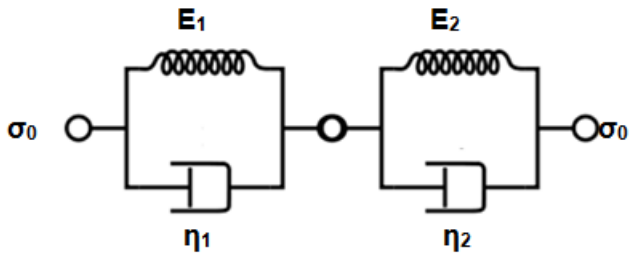

Fig. 12.14 A series of Kelvin-Voigt creep model with two elements

12.2.6 MICROSCOPY

Deformation and failure modes were observed using a Leica M205 C stereo microscope equipped with a Leica DFC425 digital camera (Figure 12.15).

Fig. 12.15 Leica M205 C stereo microscope

Failure of samples occurred in the timber, at the interface between the adhesive and the timber and at the interface between the GFRP rod and the adhesive. Sample preparation prior to observation involved the machining of the samples to expose the centre part of the creep tested block. The samples were cut into two-halves by using a band saw. The deformation of the glueline was a result of the movement of the rod depending on the tensile loading and the temperature and relative humidity. The shearing effect on the glueline due to constant loading can be observed at the top end of the bonded block. This effect is known as ‘dimpling’ (Figure 12.16).

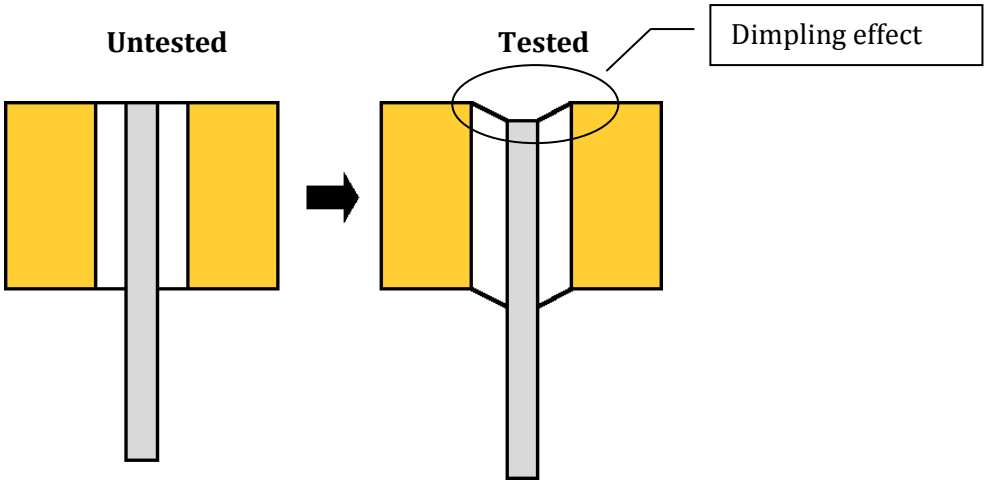

Fig. 12.16 Dimpling effect on tested sample

12.3 RESULTS AND DISCUSSIONS

12.3.1 STATIC TEST OF BONDED IN ROD

In order to determine the tensile strength of epoxy bonded joints, static tensile tests were performed on 10 single-ended samples for each adhesive. The results of the static tests is summarised in Table 12.3 along with the equivalent mass and the calculated shear stress corresponding to the respective interfaces.

Table 12.3: Results of pull-out test on single-ended samples

Adhesive	Maximum load (kN)	Equivalent weighting (kg)	Maximum shear strength (MPa)		20% of UTS (kg)
			Timber-Adhesive Interface	Rod-Adhesive Interface	
RSA	3.16	322	4.59	8.38	64
EA	3.60	367	5.23	9.54	73
TIMBERSET	3.00	305	4.36	7.96	61
SIKADUR	4.19	427	6.08	11.11	85

The average force required to pull-out the GFRP rod ranges between 3.00 to 4.19 kN. The maximum load values were converted to equivalent masses which ranged from 322 to 427kg. The creep load selected was 20% of the tensile strength (UTS) for each adhesives; RSA, EA, Timberset and Sikadur. The percentage load was selected to ensure that a creep response under ambient conditions was observed without causing failure to the tested sample and corresponded to previous work on

the creep behaviour of adhesives by Ahmad *et al.* (2012). At elevated temperatures and relative humidities creep rates were expected to increase.

12.3.2 CREEP TESTING OF BONDED IN ROD

The creep response can be defined in three distinctive phases illustrated in Figure 12.17 which depicts the creep strain curve of EA bonded-in samples tested at 50°C/95%RH.

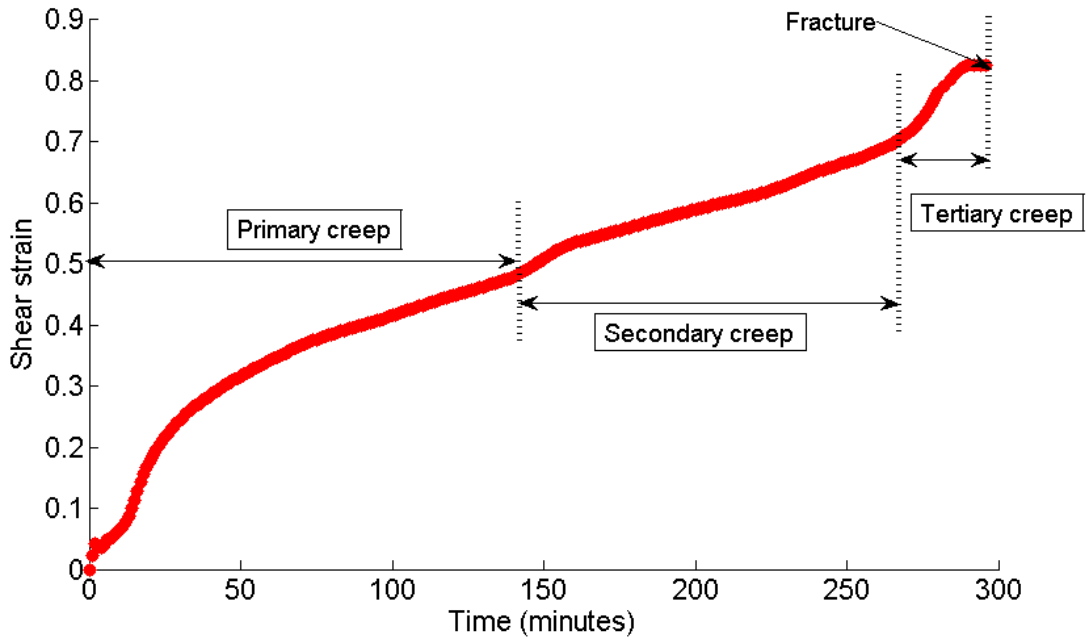

Fig. 12.17: Creep response in shear strain versus time depicts three main phases of creep

The initial primary phase of viscoelastic creep is followed by a second phase of steady state viscoelastic behaviour. The tertiary phase involves an increase in creep rate resulting in failure. The creep response of joints adhesively bonded with RSA, EA, Sikadur and Timberset are presented at four combinations of temperature and relative humidity (RH). The duration of each test was 4000 minutes equivalent to 2.7 days. The full duration of 4000 minutes and the initial 400 minutes of the test were presented for the purpose of clarity. The graphs for RSA (Figure 12.18), EA (Figure 12.19), Timberset (Figure 12.20) and Sikadur (Figure 12.21) are presented below.

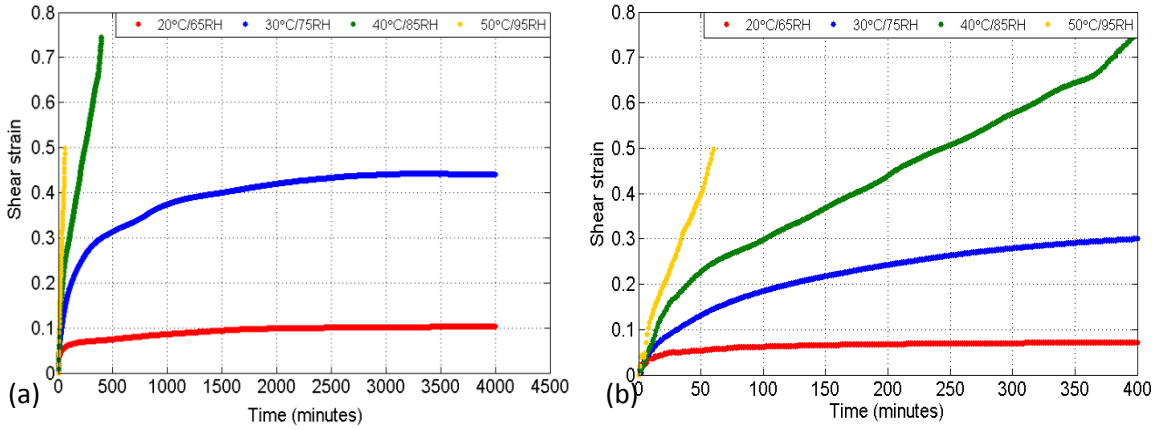

Fig. 12.18. Creep shear strain of RSA at (a) 4000 minutes and (b) 400 minutes

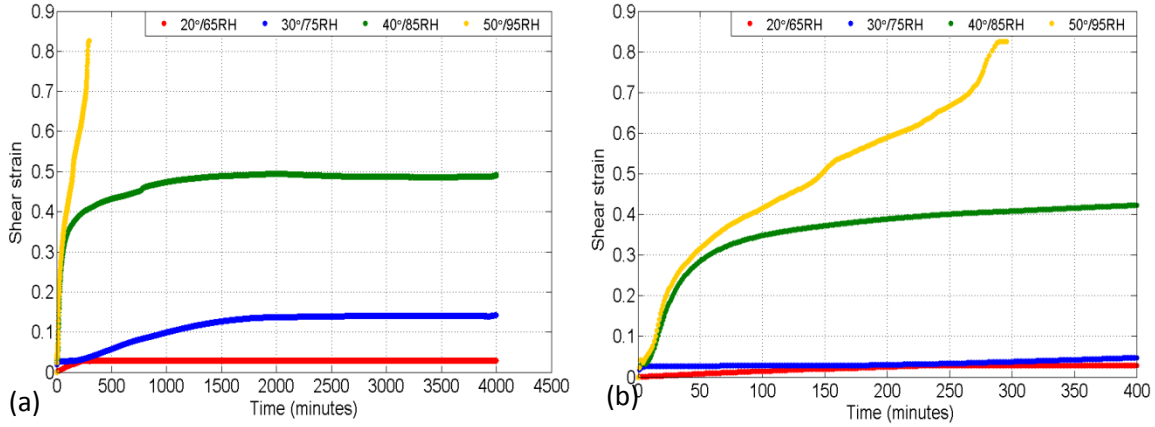

Fig. 12.19. Creep shear strain of EA at (a) 4000 minutes and (b) 400 minutes

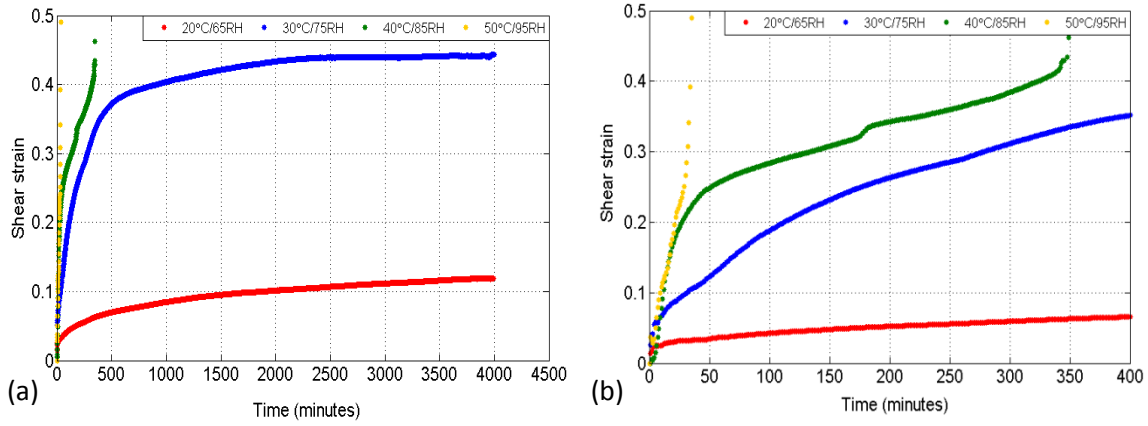

Fig. 12.20. Creep shear strain of Timberset at (a) 4000 minutes and (b) 400 minutes

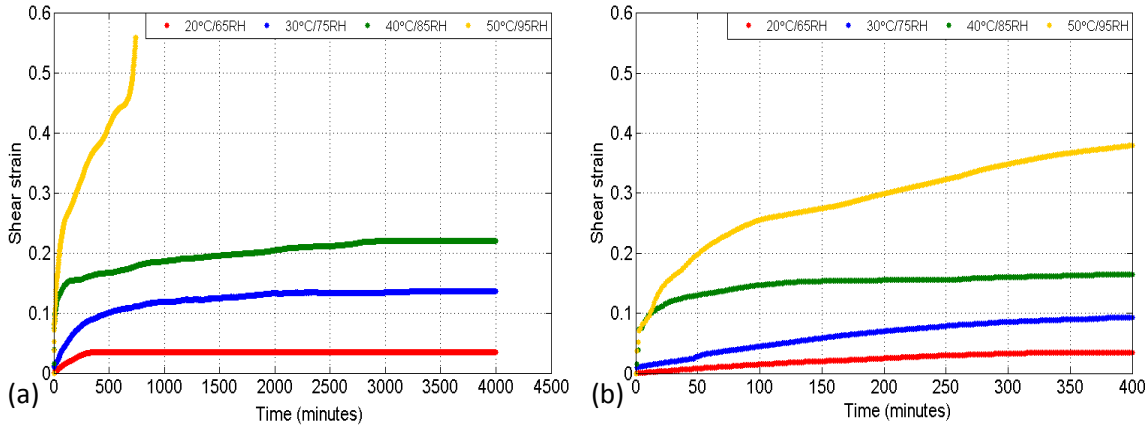

Fig. 12.21. Creep shear strain of Sikadur at (a) 4000 minutes and (b) 400 minutes

At an approximate constant stress of 2N/mm^2, both nano- and micro-filled epoxy adhesive exhibited the almost similar creep characteristic at 20ºC and 65%RH. All adhesives experience a constant increase in shear strain within the first 500 minutes testing before levelling well below 15% of shear strain. None of the sample tested under this climatic condition failed during testing. This observation suggests that all adhesives under study are stable at the temperature which is lower than the adhesive's glass transition temperature. It is worth noting that test condition of 20ºC and 65%RH may reflect the climatic condition of Service 1. This concludes that under climatic condition of Service 1, all epoxy adhesive will experience minor movement and is not likely to fail under suitable loading condition.

At 30ºC and 75%RH, most adhesives exhibited primary and secondary creep. Steep increase in primary creep strain was observed since the samples were preconditioned at the temperature/humidity for 30 minutes prior testing. This observation is typical when the testing temperature is close to the Tg of the adhesives. Larger creep strain was observed for RSA and Timberset since both adhesive has the lowest Tg. Nano-particulate filled EA and micro-particulate Sikadur are more resistant to creep at this temperature and relative humidity. As depicted in Figures 12.19 and 12.21, both epoxy exhibited mostly primary creep strain, similar to the samples which were tested at 20ºC and 65%RH. None of the adhesive tested at 30ºC and 75%RH failed during testing. This observation agrees well with finding in Chapter 9 on creep testing of bulk adhesive using DMTA. The study indicates a significant increase in strain of adhesive creep tested in tension mode at temperature region which is close to the Tg of the adhesive.

At 40ºC and 85%RH, both RSA and Timberset predominantly experienced secondary creep, resulting failure before reaching 500 minutes of testing time. At this test condition, a steep increase in creep strain exhibited by all adhesive following primary and secondary creep phases indicates the onset of tertiary viscous deformation when the testing temperature nearing or exceeds the Tg of adhesives. Tertiary creep eventually results in the failure of the bonded-in joint, in particular for adhesive of Tg below than 40°C. After 400 minutes, nano-composite adhesive RSA exhibited larger creep strain compared to EA. Referring to Figure 12.19a, EA was observed as more stable in creep than RSA because the tested sample lasted for 4000 minutes. The modification of the DGEBA/F based adhesive containing silica nanoparticles with liquid rubber has contributed stability and toughness to EA (Table 8.14). These samples experienced more primary creep than RSA and subsequently settled down to a constant strain at 40°C and 85% RH. Sikadur experienced much lesser creep strain in shear compared to EA due to the stability of the adhesive with regards to high content of microfillers.

Much larger displacements were observed when the samples were tested under the most extreme condition at 50°C and 95% RH. For all samples tested, primary creep proceeded rapidly into secondary followed by tertiary creep stages. At the end of the tertiary creep stage, Timberset and RSA samples failed after approximately 50 minutes of testing. EA failed in tertiary creep after almost 300 minutes. This observation suggests that the rubbery network within the nano-silica EA is more stable compared to un-modified system RSA. Sikadur outperformed other adhesives by lasting more than 600 minutes. As expected, the combination of high temperature and humidity clearly increases the susceptibility of the adhesive to creep failure.

Under conditions which relate to service class 1, 2 and 3, a certain degree of creep should be expected in bonded timber joints. The behaviour of creep strain for RSA, EA, Timberset and Sikadur at 20°C/65%RH represents the creep mechanism of bonded timber joints under the condition of Service Class 1. None of the samples tested under the condition failed during testing.

12.3.3 DEFORMATION AND FAILURE MODE

The appearance of deformation and failure modes for RSA, EA, Timberset and Sikadur are presented in Figure 12.22, 12.23, 12.24 and 12.25 respectively. The composite figures are presented according to the corresponding condition of the samples, prior and post creep testing. The samples conditions are categorized as:

a) Untested sample (prior testing)
b) Minor viscoelastic deformation and yield
c) Major viscoelastic deformation and yield
d) Failure at the rod to adhesive interface

} Post testing

Figure 12.22a shows a longitudinal section through an untested sample for RSA depicting the rod at the centre of the bonded-in joint embedded between the adhesive layers and the LVL. All three components (LVL, adhesive and rod) are horizontally level, indicating that no load has been applied to this sample. A sample that has been loaded at 20ºC and 65% RH exhibited a receding glue line due to the downward movement of the rod (Fig. 12.22b). This type of deformation can be referred to minor viscoelastic yielding. The observation indicates the adhesive as stable and capable of transferring stress under a condition which is similar to ambient temperature and humidity. The *'dimpling effect'* on the annular bondline also occurs on samples loaded at 30ºC and 75%RH (Fig.22c). Since the testing temperature at this point was close to the Tg of the adhesive, it is apparent that the glue-line of RSA has experienced reduction in shear modulus due to the elevation of temperature. Major yielding was observed on RSA samples tested at 30ºC which completed the 4000 minutes testing duration. As indicated in the creep strain Figure 12.18 in section 12.3.2, samples of RSA which were tested at 40ºC/85% RH and 50ºC/95% RH, failed after short time under load. On both occasions, the sample failure occurred at the rod to adhesive interface as shown in Figure 12.22d.

The results for EA, Timberset and Sikadur at associated temperature and humidity combinations indicate almost similar findings. Minor yielding of the glueline was observed at 20ºC/65% RH as indicated in Figure 12.23b, 12.24b and 12.25b. At a temperature/relative humidity of 30ºC/75%RH and 40ºC/85%RH, major yielding and

pronounced *'dimpling effect'* was observed particularly on EA and Timberset samples. It is noticeable that, at 40ºC/85%RH, EA (Fig. 12.23c) is still stable with only minor creep strain compared to RSA which failed after 50 minutes of testing (Fig. 12.22d). The hypothesis put forward is that, the increase in ductility and toughness of EA is contributed by the addition of carboxyl-terminated butadiene acronitrile (CTBN) rubber filler to the standard formulation which includes reactive diluents and silica nanoparticles. Under 40ºC/85%RH condition, Sikadur samples did not exhibit much yielding or receding of glue-line as depicted by other adhesives. This shows that an adhesive system which is highly-filled with rigid micro particulate is less susceptible to creep.

Creep failure occurs within the first 60 minutes of testing at 50ºC/95%RH on RSA and Timberset samples. As for EA and Sikadur, creep life was extended past 300 and 600 minutes respectively. Failure at the adhesive to rod interface was observed in these samples. Figure 12.22d, 12.23d, 12.24d and 12.25d shows tested samples with central void area in which the GFRP rod has been debonded and pulled out. The creep deformation for RSA, EA, Timberset and Sikadur are consistent with the increasing level of temperature and humidity.

A very interesting observation was discovered on the mode of failure of all adhesives under investigation. In static tests of bonded-in joints, failure can occur thereby four mechanisms, namely failure in the adhesive, failure in the wood, failure at the interface between rod and adhesive and failure at the interface between rod and wood. Evidence from Fig 12.22d, 12.23d, 12.24d and 12.25d respectively indicates local debonding which takes place at elevated temperatures and humidity occurs at the interface area between the rod and adhesive layer rather than the rod-wood interface. Comparison was made between the surface morphology of adhesive and the interface area between adhesive and rod as indicated in Figures 12.26 and 12.27. Broken glass fibres on the inside surface of the interface suggested debonding of glass fibre prior to the pull-out of the rod which leads to the failure of the bond. The morphology of a single glass fibre is as depicted in Figure 12.28.

Focusing on the temperature aspect of the study, the measurement factor which needs to be considered is thermal expansion coefficient (TEC) of the material used to fabricate

the model joint. The magnitude of expansion on adhesive, wood and GFRP rod increases correspondingly with the increment of temperature. The behavior within wood-epoxy and GFRP-epoxy interfaces are significantly related to the TEC which influenced the compatibility of bond itself. Differences in TEC value of wood, epoxy and GFRP induces stress at the interfaces thus propagating cracks and delamination. Rise of temperature would affect the integrity of the interface between wood-epoxy and GFRP-epoxy to a different extent. This observation confirms that differential in thermal expansion between the GFRP rod and the adhesive debonds a thin layer of glass fibres from the rod surface which initiates failure at this interface. The theory of the effect of thermal expansion is supported by a related study by Pizzo *et al.* (2002) on TEC of wood and epoxy joints. The study indicates on higher bonding strength of samples which was bonded with epoxy of similar thermal expansion behaviour to wood. Debonding which occurs at GFRP-epoxy interface may also cause by larger stress over the interface area. It is likely that elevated temperature would result post-curing of the adhesive which later contribute to the increase in short-term bonded strength. However, the integrity of the glueline is severely affected at temperature that is close or higher than the glass transition temperature of the adhesive. The finding of this study also confirms to an earlier finding of adhesive testing using DMTA. As reported in Chapter 10, the adhesive is still stable and capable of transferring stress in its rubbery state although tested at temperature which is higher than its *Tg*. This supports the observation that cohesive failure does not occur within the adhesive layer due to the stability of the molecular structure even at elevated temperature.

The result from the creep test also indicates humidity may contribute to the creep behaviour. This may relate to several factors which includes the kinetic of diffusion of water molecules within the bonded system and the epoxy-filler interaction during moisture absorption. Ahmad *et al.* (2010) indicates type of filler as major factor which influences water absorption. The study shows CTBN rubber modified system and epoxy which contains ceramic micro-particles are less susceptible to moisture ingress. Kinloch (1983) suggested that moisture has the capability to displace the bond between epoxy and filler used in the adhesive system. As suggested by Adamson (1980), the kinetic of moisture below Tg can be distinguished into three main stages. In the first phase, the absorbed moisture occupies the free volume within the polymer. The transportation of water into polymer can either be in the form of liquid or vapour. Mikols *et al.* (1982)

and Pethrick *et al.* (1996) supported this theory by suggesting on free water which fills the free volumes and holes within the polymer. At this point, dimensional changes are unlikely. In the second stage water molecule infiltrates the polymer chain through hydrogen bonding. Water molecule which has lost its mobility due to attachment via hydrogen bonding is referred as bound molecules. This increases the space between polymer chains as the water molecules slide between polymer chains and hydrogen bonds. At the same time, the void volume increases as free water molecules continues to diffuse throughout the polymer. The enlargement of voids induces stresses within the filler (eg. silica and alumina) and matrix interface region. As suggested by Kinloch (1983), water molecule caused the filler-matrix bond to become thermodynamically unstable. This creates swelling and plasticisation effect on the polymer. In the final stage of the transport process, water molecule penetrate densely crosslinked region of the polymer.

The test shows on significant decrease in creep strength at elevated moisture, an effect which accelerates with raised temperature. This is supported by Nogueira *et al.* (2001) which indicate that water diffusion in epoxy resin increases with temperature although further crosslinking may have taken place. The temperature supplies the required activation energy to overcome intra-molecular energy barriers. At 40°C and 50°C the diffusion of moisture intensifies due to the increase in molecular mobility. Ahmad *et al.* (2010) observed moisture diffusion rate of nano- and micro-particulate epoxy-based adhesives. The study suggest the diffusion of moisture into the epoxies conforms to the Fickian behavior when aged at 20 days and 30°C/95% RH and deviates from Fickian diffusion behavior when aged at 50°C/95% RH.

A study by Zanni-Deffarges & Shanahan (1995) compares the diffusion of water into bulk epoxy adhesive as compared to adhesive joints. This particular study was made to understand the kinetic of water molecule diffusion within bonded-in joints. The study suggest that the values of *coefficient of diffusion*, D, for adhesive joint is considerably greater than bulk adhesive. It was proposed that the greater value in the diffusion of water within the adhesive joint was due to *capillary diffusion*. It is likely that high surface tension near the interfacial layer of substrate-polymer would draw the water diffusion into the zone. It is also worth to note that surface treatment on the bonded surfaces (e.g substrates and rod) affects the interfacial diffusion of the bond. Surface

treatments such as sandblasting and sanding of stainless steel and GFRP rod to enhance bonding would produce a surface quality which rapidly degrades with moisture. This supports the theory that water ingress via interfaces leads to breakage of bonded joints. The same study also suggests that the increased value of diffusion coefficient in bonded joints was due to the effect of shrinkage stress. Shrinkage of polymer may occur during the curing of the adhesive. An adhesive joint is like to be under shrinkage stress due to the adhesive being constrained by the adherend. This would lead to formation of voids thus creating a porous polymeric material. According to Thomason (1995), the cause on formation of voids can be distinguished into two types. Voids can be formed due to entrapment of air bubbles during resin formulation and also due to volatile components which vaporized during the curing process. This finding is in good agreement with the evidence from Chapter 8 which indicates the presence of voids within cured resin. It is likely that the presence of voids would lead to water ingress and higher diffusion coefficient.

Blackman *et al.* (2008) suggested the presence of pre-bond moisture which affected the fracture behavior of adhesively bonded joints. The pre-bond moisture which originates from the atmosphere enters the joint via the substrate (e.g wood) or via the adhesive prior to fabrication of the joint. The diffusion of moisture from the substrate into the adhesive resulted on formation of voids, plasticization of the adhesive and degradation to the interfacial adhesion.

The structure and/or orientation of the substrate/polymer also contribute to the diffusion of moisture near the interfacial region (Deffarges & Shanahan, 1995). Relating to this study, movement of moisture likely occurs within the cell of the wood. It is known that moisture moves faster parallel to the grain than perpendicular to the grain. The surface area of the bonded model and fastener holes serves as end grain surfaces. Movement of moisture between the environment and timber is more distinct through end grain thus resulting local weak point within the immediate area of the bond. The size of the sample also influences the susceptibility of the joint to moisture. A joint within a larger member would be less affected by temperature variance compared to a smaller wood block. Moisture ingress may cause reduction of mechanical strength of the bond by causing physico-chemical changes within the substrate-adhesive interface and/or degradation of the adhesive polymer itself.

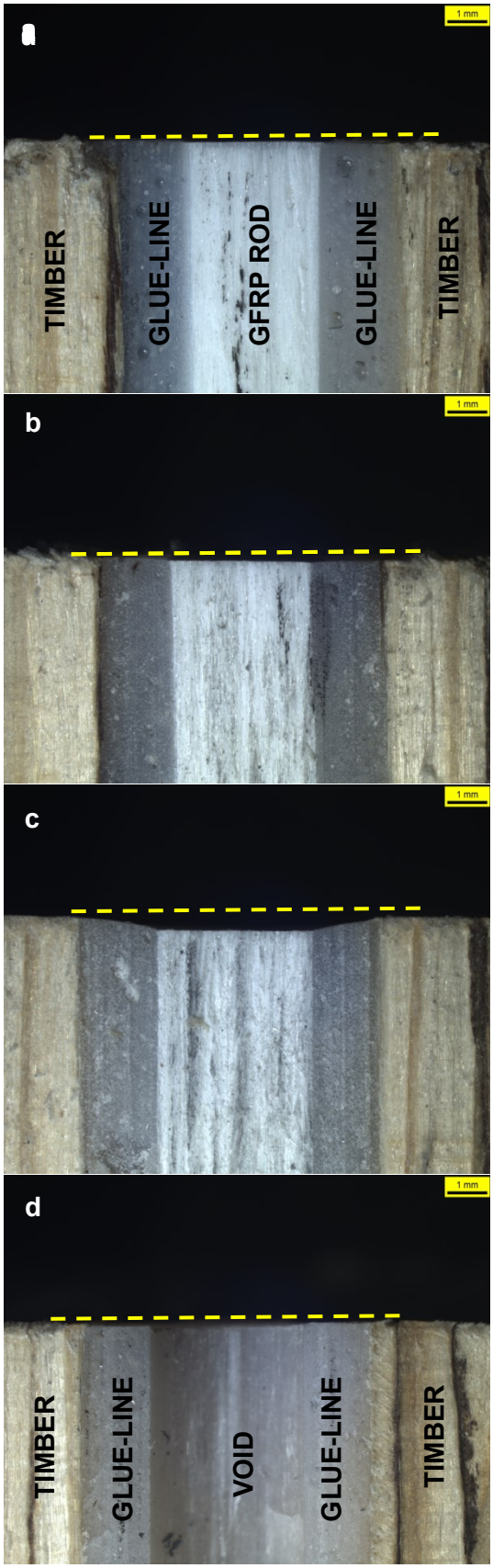

Fig. 12.22. RSA: (a) untested sample (b) minor deformation and yield (c) major deformation and yield (d) failure at rod adhesive interface.

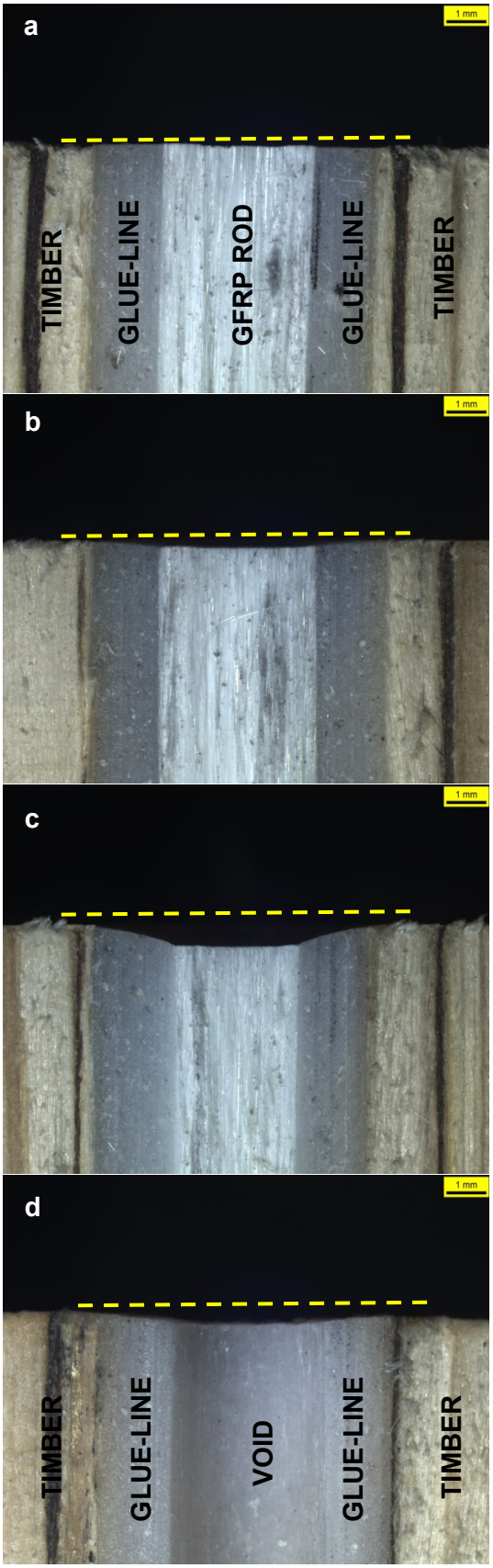

Fig. 12.23. EA: (a) untested sample (b) minor deformation and yield (c) major deformation and yield (d) failure at rod adhesive interface.

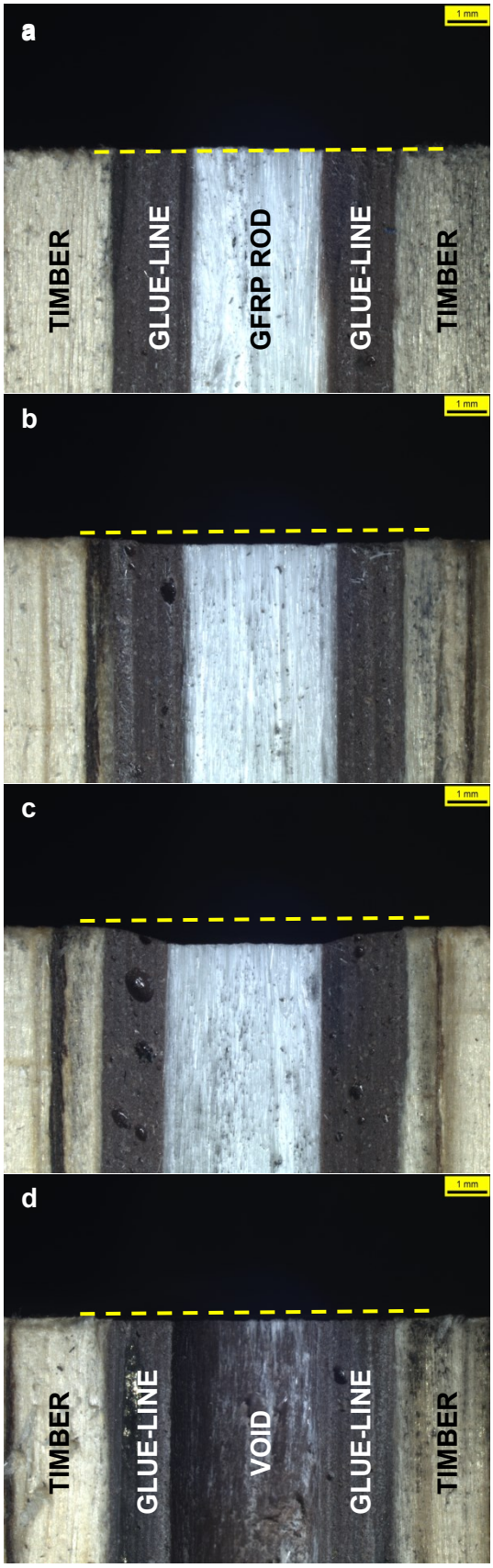

Fig. 12.24. Timberset: (a) untested sample (b) minor deformation and yield (c) major deformation and yield (d) failure at rod adhesive interface.

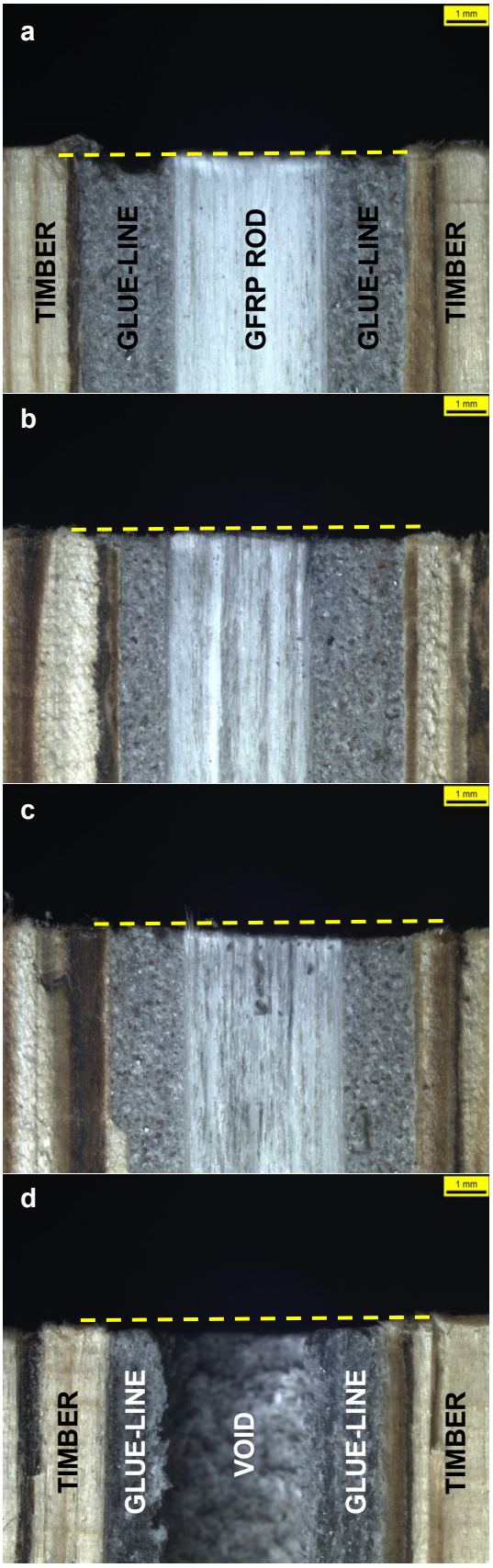

Fig. 12.25. Sikadur: (a) untested sample (b) minor deformation and yield (c) major deformation and yield (d) failure at rod adhesive interface.

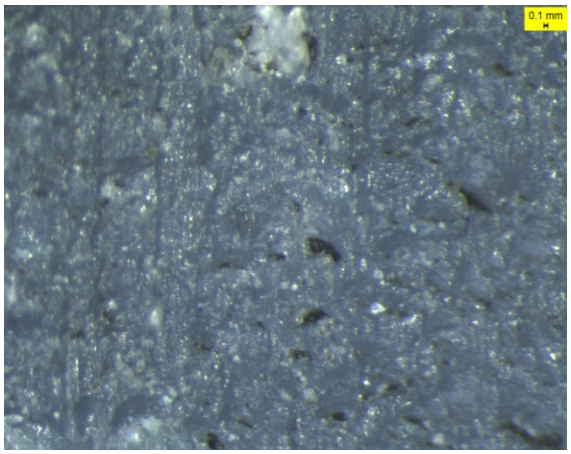

Fig. 12.26. Surface morphology of adhesive area

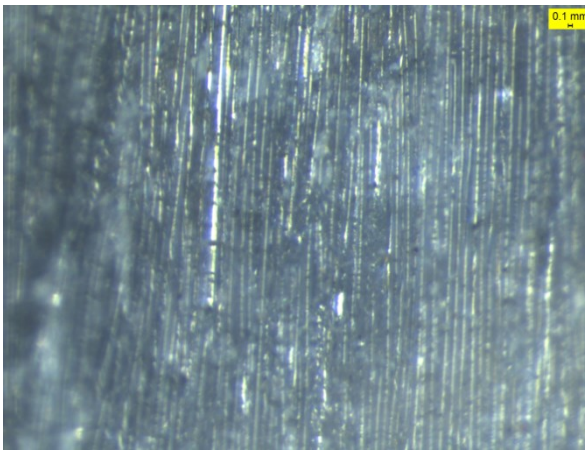

Fig. 12.27. Surface morphology of adhesive-rod interface area. Debonded glass fibre attached to the inner wall of void area.

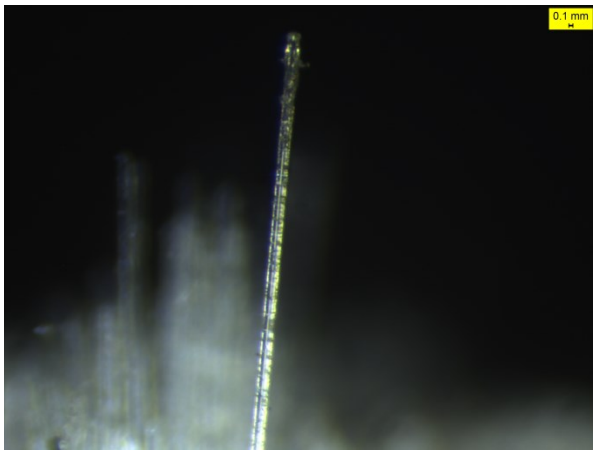

Fig. 12.28. Single glass fibre

12.3.4 MATHEMATICAL MODELLING

To apply the theoretical model proposed above to the experimental results, consideration on the assumption of the model were made. The objective of mathematical modelling was mainly to determine the goodness of fit of the experimental data to the viscoelastic creep equations based on Kelvin-Voigt's theory. The Kelvin-Voigt theory of viscoelasticity is only valid for primary and secondary creep. Based on this assumption, data of tertiary creep at 40ºC and 50ºC for RSA and 50ºC for EA, Timberset and Sikadur was excluded from the modelling. Two model equation (Model 1 and Model 2) based on the number of exponential model were

presented in this study. A summary on creep coefficients for RSA, EA, Timberset and Sikadur are presented in Table 12.4, 12.5, 12.6 and 12.7 respectively.

The modelling indicates that the creep strain obtained from the study conforms to the creep equation of Eqn. (12.4). As depicted in Table 12.4 to 12.7, the results on the coefficient of determination (R^2) for all adhesive under investigation suggest satisfactory goodness of fit. The retardation time, τ (in minutes) for Model 1 suggests a steady declined as the temperature increases from 20°C to 40°C. An example from Table 12.6 on Timberset indicates on gradual reduction of τ from 1225 minutes at 20°C/65%RH to 92.35 minutes at 40°C/85%RH. The increase of temperature expands the free volume within the polymer thus resulting movements to the localised bond (bending and strecting) and side chains. As the heating continues, large-scale chain slippage occurs and the material begins to flow which contributes to shorter retardation time on high-temperature tested samples.

An extra exponential model was added to the equation to provide better fit to the model. Model 2 as depicted in the respective tables indicates the two-element Kelvin-Voigt model as represented by retardation time τ_1 and τ_2. In all cases, the value of τ_1 is more than τ_2. This observation signifies different time constant which takes place simultaneously during creep progression. Based on the improvisation, the value of coefficient of determination is close to unity. Figure 12.29, 12.30, 12.31 and 12.32 shows the curve corresponding to Eqn. 12.4 and 12.5, including the experimental results. As can be seen, Model 2 simulation provides a better fit to the experimental results.

The modelled creep coefficient also exhibits steady decline of elastic modulus E following the increase of temperature and humidity. It was observed that for EA (Table 12.5), elastic modulus (E) at 20°C/65%RH (0.074 GPa) drops progressively to 0.007GPa at 40°C/85%RH. Similar trend was also observed on RSA, Timberset and Sikadur. This supports earlier investigation which indicates that absorption of heat would change the viscoelasticity behaviour of the epoxy, thus contributing to the loss in stiffness and increase in flow.

Table 12.4. Modelled creep coefficient for RSA

		MODEL 1				MODEL 2						
T (°C)	RH(%)	σ_o/E	τ (min)	E(GPa)	R^2	σ_o/E	τ_1 (min)	E_1 (GPa)	σ_o/E	τ_2 (min)	E_2(GPa)	R^2
20	65	0.0498	897.5	0.0402	0.9426	0.069	557.800	0.029	0.756	5.495	0.003	0.975
30	75	0.2991	619	0.007	0.9518	0.314	505.000	0.006	0.698	10.940	0.003	0.968
40	85	Response not viscoelastic										
50	95	Response not viscoelastic										

Table 12.5. Modelled creep coefficient for EA

		MODEL 1				MODEL 2						
T (°C)	RH(%)	σ_o/E	τ(min)	E(GPa)	R^2	σ_o/E	τ_1(min)	E_1(GPa)	σ_o/E	τ_2(min)	E_2(GPa)	R^2
20	65	0.0281	109.7	0.071	0.963	0.027	123.7	0.075	0.005	1.247	0.083	0.965
30	75	0.143	866.9	0.014	0.954	0.143	867.1	0.014	0.003	0.0006	0.667	0.980
40	85	0.286	232.9	0.007	0.889	0.159	465.6	0.013	0.331	32.79	0.006	0.992
50	95	Response not viscoelastic										

Table 12.6: Modelled creep coefficient for Timberset

		MODEL 1				MODEL 2						
T (°C)	RH(%)	σ/E	τ(min)	E(GPa)	R^2	σ/E	τ_1(min)	E_1(Gpa)	σ/E	τ_2(min)	E_2(GPa)	R^2
20	65	0.0796	1225	0.0251	0.986	0.0714	2276	0.028011	0.03341	227.7	0.0598	0.9985
30	75	0.3488	308.2	0.0057	0.9791	0.1023	987.7	0.01955	0.2969	174.5	0.0067	0.9983
40	85	0.3009	92.35	0.0066	0.9094	6.336	1224.0	0.000316	0.2347	19.01	0.0085	0.9908
50	95	Response not viscoelastic										

Table 12.7. Modelled creep coefficient for Sikadur

		MODEL 1				**MODEL 2**						
T (°C)	RH(%)	σ/E	τ(min)	E(GPa)	R^2	σ/E	τ_1(min)	E_1(GPa)	σ/E	τ_2(min)	E_2(GPa)	R^2
20	65	0.09731	218.1	0.0206	0.9871	0.0968	219.9	0.0207	0.0268	132.1	0.0746	0.9873
30	75	0.1086	443.3	0.0184	0.9802	0.0618	794.9	0.0323	0.0686	149.8	0.0292	0.9978
40	85	0.08957	1235	0.0223	0.9505	0.0851	1560	0.0235	0.0959	23.22	0.0208	0.9918
50	95	Response not viscoelastic										

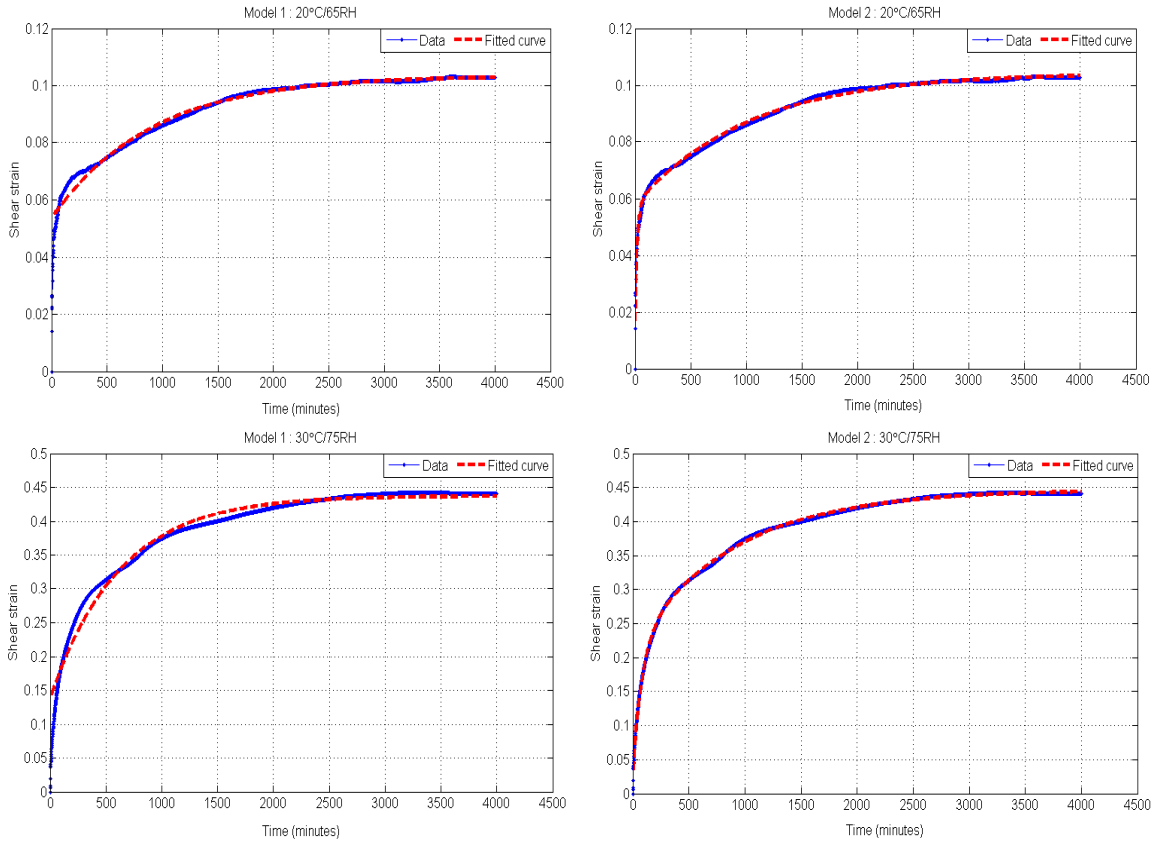

Fig. 12.29. Graphical representation of fitted data based on Kelvin-Voigt model of RSA bonded creep samples. The figure indicates Model 1 (left column) and Model 2 (right column) at various temperature and humidity.

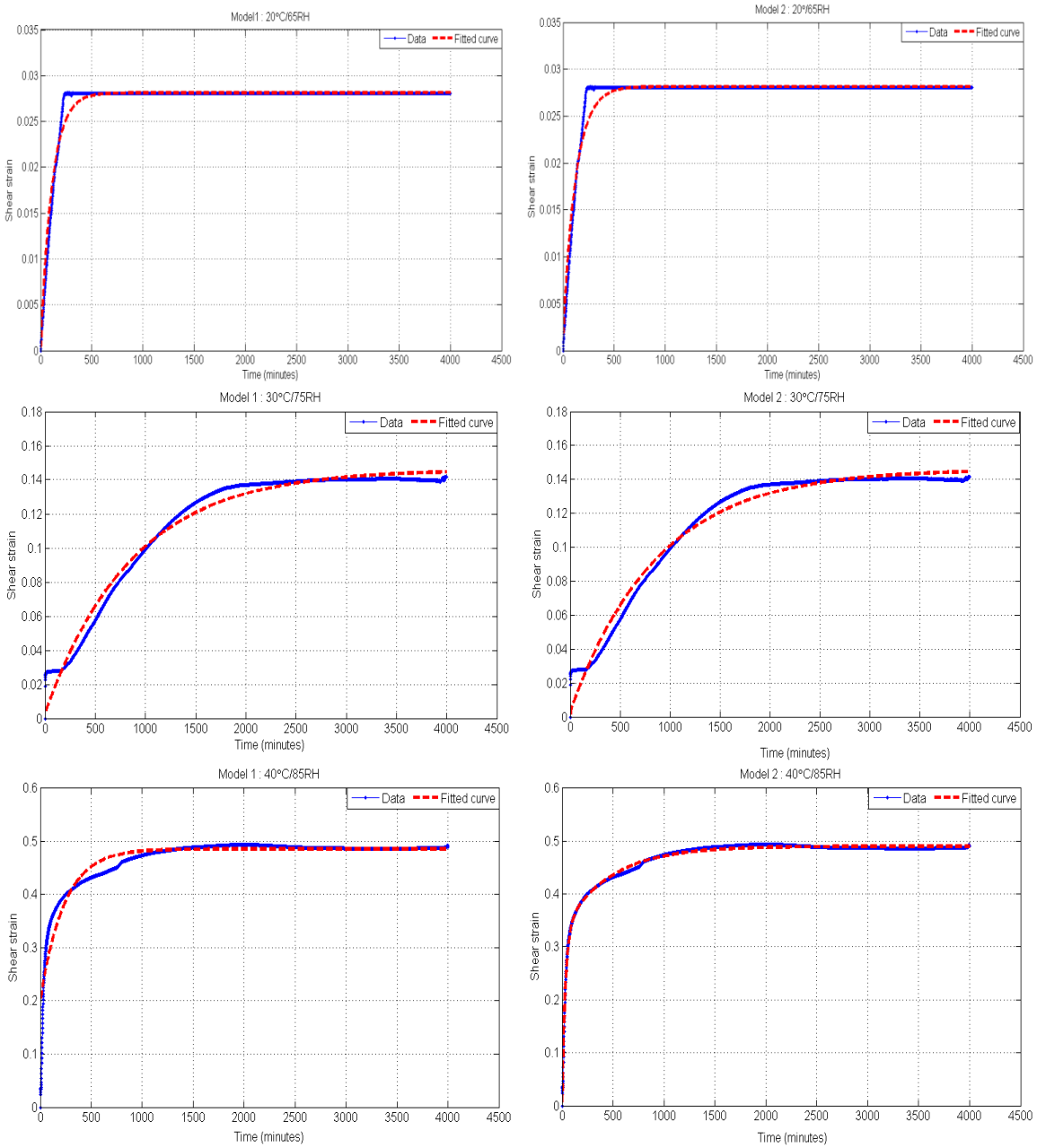

Fig. 12.30. Graphical representation of fitted data based on Kelvin-Voigt model of EA bonded creep samples. The figure indicates Model 1 (left column) and Model 2 (right column) at various temperature and humidity.

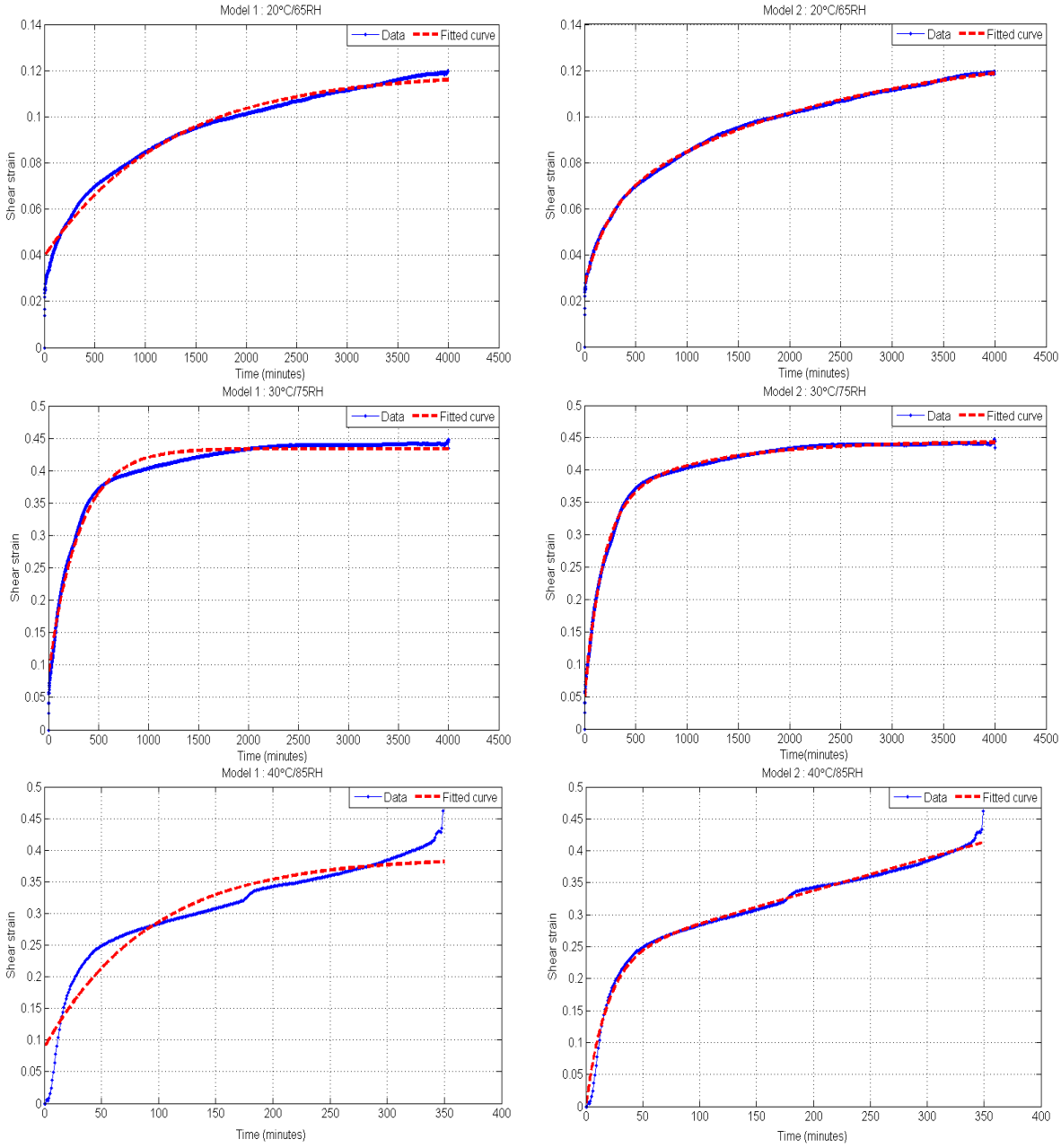

Fig. 12.31. Graphical representation of fitted data based on Kelvin-Voigt model of EA bonded creep samples. The figure indicates Model 1 (left column) and Model 2 (right column) at various temperature and humidity.

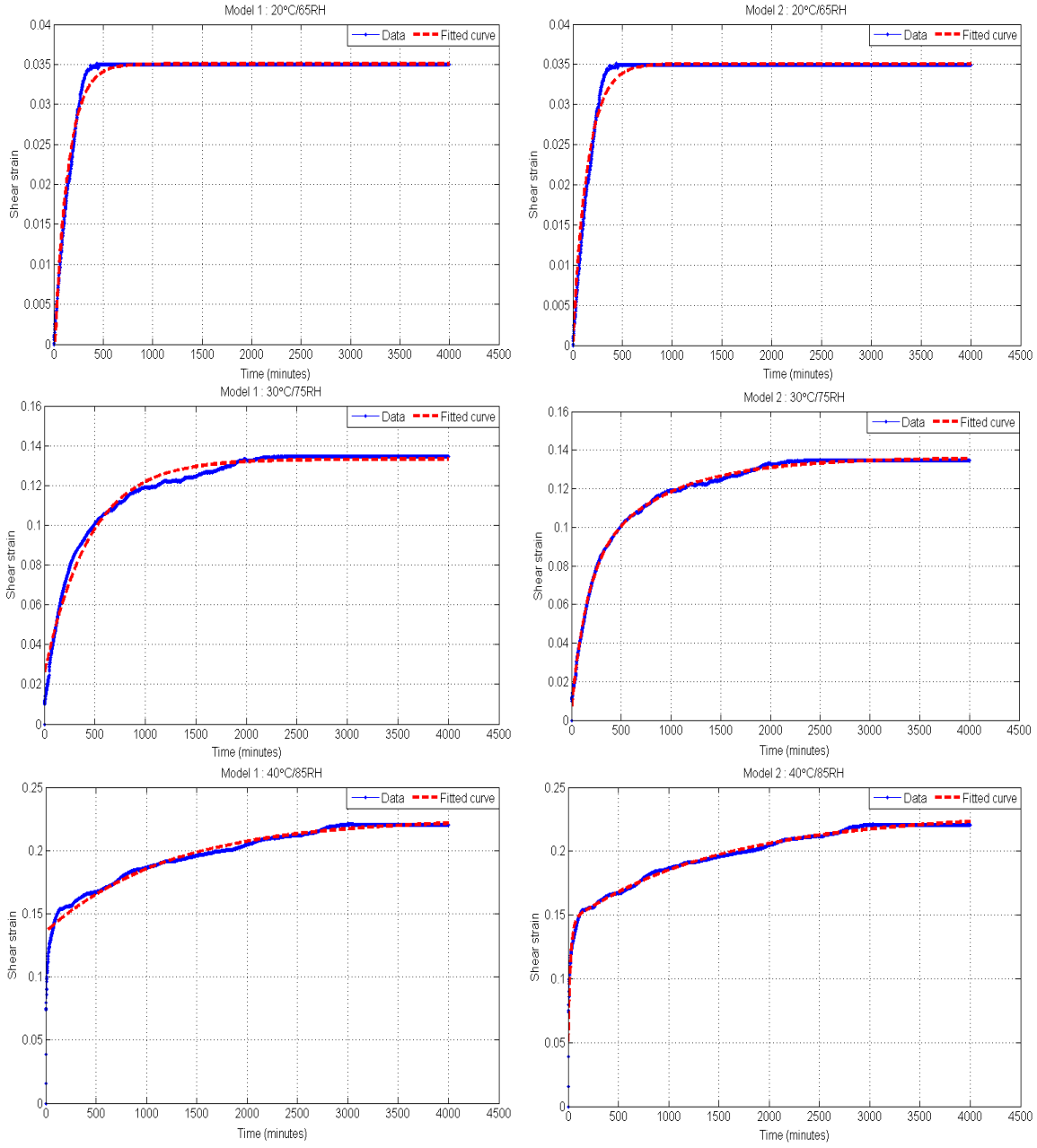

Fig. 12.32. Graphical representation of fitted data based on Kelvin-Voigt model of Sikadur bonded creep samples. The figure indicates Model 1 (left column) and Model 2 (right column) at various temperature and humidity.

12.4 CONCLUDING REMARKS

This chapter reviews the characteristic of bonded-in joint models in relation to creep loading. The effect of surrounding temperature and relative humidity on the bonded-in joints tested under constant load were also investigated in this study. Kelvin-Voigt creep models were applied and the following conclusions were obtained.

- The creep performance of nano- and micro particulate timber adhesive has been examined as a function of temperature and relative humidity. Comparison between the two thixotropic nano-silicate adhesive has indicated that CTBN rubber-filled system (EA epoxy) has more resistance to creep under extreme conditions as compared to standard RSA. Under the most extreme condition, micro particulate filled Sikadur has outperformed other adhesive by lasting more than 600 minutes. The general trends in creep resistance are summarised as follows: Sikadur > EA > Timberset > RSA.
- The above study shows that creep resistance is strongly dependant on the combination of testing temperature and humidity. All adhesives experienced creep failure when tested under the condition of 50°C/95%RH. A significant increase in strain was recorded for samples tested under the temperature close to the glass transition temperature of the adhesive.
- The empirical data on creep behaviour conforms to the Kelvin-Voigt creep equation. The creep curve is consistent to the equation as with higher temperature and humidity test condition.

CHAPTER 13 : FINAL DISCUSSIONS AND CONCLUSIONS

13.1 INTRODUCTION

The research framework of this study was built based on three basic elements of bonded-in joints; adhesive, substrate and rod. The purpose of this thesis is to study the interaction between these elements and how does it contribute to a strong bond. Therefore, the characterisation on the properties and response of the elements was defined into three phases:

a) *Adhesive*
b) *Adhesive + wood*
c) *Adhesive + wood + rod*

The investigation on the microscopic, mechanical and thermal properties of bulk adhesive is as presented in Chapter 7, 8 and 9 respectively. The interaction between adhesive and wood are investigated based on shear creep using DMTA and static shear using TAST as reviewed in Chapter 9 and 10. Chapter 11 and 12 presented the analysis on static shear strength and creep of bonded-in joint, which concludes the phase on the assessment of adhesive + wood + rod interaction.

13.2 PARAMETER EFFECT STUDY

13.1.1 EFFECT OF FILLER TYPES ON MECHANICAL PROPERTIES OF BULK ADHESIVE

The effect on filler types and modification of epoxy adhesives was examined through flexural, inter-laminar shear, tensile and fracture toughness test. Based on micro analysis study as presented in section 7.3.1 and 7.3.2, the adhesives under investigation contains micro- and nano size particulate to improve strength and toughness of the epoxies. The study on flexural strength finds that inclusion of rubber to the standard nano-silica adhesive has resulted in an improvement of flexural strength (section 8.2.2.1). Similar finding was reported by Bussi & Ishida, 1994 and

Nigam *et al*. 1999. Micro-particle filled adhesive had the lowest flexural strength due to the brittle nature of the material.

The investigation on the inter-laminar shear strength (section 8.3.2.1) indicates that adhesives containing micro-size particulates performed poorly in ILS compared to adhesives modified with nano-size particles which impart efficient stress transfer due to the large contact area. Wetzel *et al.* (2003) proposed the importance of filler-matrix interaction in which large uneven distributed micro-particulate will act as stress concentration sites and initiate crack propagation and failure within adhesives. The addition of liquid rubber to nano-silica filled epoxy contributes to enhanced shear strength due to the presence of the dispersed rubber phase. The toughening effect is due to flexibility of the matrix which promotes shear yielding at low stresses. Other observations which supported this finding are reported Ratna & Banthia (2000) and Kar & Banthia (2004).

The highest tensile modulus (TMOE) is exhibited by the micro-particle filled epoxy (section 8.4.2.1). The stiffness of the adhesive is contributed by the inclusion of rigid microfillers as confirmed in studies by Wetzel *et al*. (2003), Wang *et al*. (2002), Imanaka *et al.* (2001) and Smith *et al.* (1991). This study also indicates improvement in tensile properties of the liquid rubber nano-silica composite, which enhancement suggest good bonding between filler and matrix, thus enabling efficient stress transfer via the interface. Failure in a heavily filled micro particle adhesive may occur at the filler-matrix interface but failure in a nanoparticle-filled adhesive may occur by both particle debonding and cohesive failure of the epoxy (Haupert and Wetzel, 2005).

This study indicates that increased fracture toughness can be achieved with the inclusion of rubber and rigid particulates (section 8.5.2.1). Both rubber and rigid-particulates act as initiation sites for shear yielding and deformation in an epoxy resin matrix. These particulates are responsible for crack pinning and localised plastic deformation. During crack propagation, the crack becomes pinned and deviates to produce secondary cracks. The formation of new surfaces requires energy thus contributing to the high value of *GIc.*

It can be concluded that mechanical performance of modified epoxies depends on the filler, the type of matrix and also chemical and physical interaction at the interface.

13.1.2 EFFECT OF FILLER TYPE ON BONDED STRENGTH

The effect of adhesive filler type on the strength of bonded surfaces is demonstrated by the thick adherend shear test (section 10.3.2) and static pull-out test of bonded-in joint (section 11.3.1). Lap joints made from liquid-rubber modified adhesive had better shear strength than the standard nano-silica adhesive. Statistical analysis indicates that the types of adhesive used in the study and the resultant shear strength were significant.

The magnitude of the average shear stress for bonded-in joint varies from 5.90 to 6.47 MPa at the timber-adhesive interface and 8.86 to 9.71 MPa at the rod-adhesive interface (section 11.3.1). Liquid rubber modified epoxy had the highest value of shear strength. This observation conforms to the shear strength of bulk adhesives reported in Chapter 8. Most of the failure is mode III which occur mainly around the bonded area close to the glue-line. This indicates strength of the wood is lower than the strength of the adhesive and the rod/adhesive interface.

13.1.3 EFFECT OF FILLER TYPE ON GLASS TRANSITION TEMPERATURE (TG)

Analysis on the thermal properties of epoxy adhesive was investigated using DMTA (section 9.3.1). It is found that the storage modulus is strongly influenced by the size of particulate and the presence of liquid rubber within the epoxy matrix. The heavily-filled micro particulate adhesive exhibited the highest modulus which is a reflection of high molecular weight. The incorporation of liquid-rubber improves the storage modulus of nano-silica composite. Broadening of loss factor peak is an indication of highly cross link material which is most evident on micro filled epoxies. The Tg values as indicated by onset E' values are in the subsequent order: EA> Sikadur > RSA > Timberset

13.1.4 EFFECT OF TEMPERATURE AND GLASS TRANSITION TEMPERATURE (TG) ON CREEP PROPERTIES

The influence of temperature on the durability of bulk epoxy adhesive was examined using Dynamic Mechanical Thermal Analyser approach (section 9.3.2.3). Creep test of bulk epoxy was conducted in tension mode. The DMTA has demonstrated that tensile creep strains are a function of temperature and stress, as expected, but above Tg + 15ºC the adhesives behave like rubbers with low elastic moduli. Within temperature range of 25°C to 30°C, the strain as resulted by constant load was very minimal. The strain of the material starts to show significant acceleration as it reaches glass transition temperature, Tg + 15°C of the adhesive. Following the phase of viscoelastic zone, creep strains increases and equilibrate at the end of each temperature steps. At low stresses the adhesives are stable up to 80ºC but as the stress increased the rupture stress falls to temperatures as low as 50ºC. Creep strain continues to increase in second and tertiary creep phase before failure. Creep in shear mode (section 9.3.3) gives an insight on the response of brittle (high modulus) epoxy to shear creep in comparison to ductile epoxy. In shear, creep strain is greater than tensile strain closer to the Tg of the adhesives. Above T_g, the increment of creep strain corresponding to temperature increase is very minimal.

Creep properties of the adhesive interface between LVL and bonded-in pultruded rods are evaluated in Chapter 12. The result as presented in section 12.3.2 shows that creep resistance is strongly dependant on the testing temperature and humidity. All adhesive experienced creep failure when tested under the condition of 50°C/95%RH. A significant increase in strain was observed on samples tested under the temperature nearing to the T_g of the adhesive.

13.1.5 EFFECT OF POST CURING TREATMENT ON PROPERTIES OF POLYMER

The study on post curing effect of nano-silica filled epoxy was investigated on bulk polymer and bonded-in joints. In Chapter 8, bulk epoxy samples post cured at 50 and 70°C were tested for flexural (section 8.2.2.2), shear (section 8.3.2.2), tensile strength (section 8.4.2.2) and fracture toughness (section 8.5.2.2). In general, it was found that the influence of the post curing was not significant on mechanically tested

bulk epoxy. Prolonged post curing at temperature higher than the Tg value of the adhesive resulted in the degradation of the polymer. The exposure to high temperature may have increased the Tg but lowers the mechanical strength of the material as supported by research studies (Ahmad, 2008 and Richter & Steiger, 2005).

The effect of post curing on bonded-in joints in Laminated Veneer Lumber (LVL) is presented in section 11.3.3 (Chapter 11). For this particular section, the effect on the types of rod used for bonding is taken into consideration. Types of bonded rod selected for the study was stainless steel and GFRP. The study indicates a declining value of average shear strength due to the post curing treatments although statistically insignificant. The trend is similar for both GFRP and steel bonded-joints in which reduction of shear strength has been recorded due to the post-curing treatment of the bonded-in samples. Differences in failure mode of were recorded due to the post-curing treatment. The investigation indicates that GFRP bonded-in joints are more sensitive to the post-curing treatment than steel bonded-in joints. The tendency for a shift from rod/adhesive failure towards timber failure from ambient to 50˚C to 70˚C post-cure for GFRP bonded-in samples tested at ambient temperature was observed.

13.1.6 EFFECT OF TESTING TEMPERATURE ACCORDING TO TYPES OF ROD

The study also shows that the value of shear strength is higher for steel rod (in section 11.3.3) when tested at ambient temperature. The surface of threaded or deformed steel rod provides an extra mechanical interlock in addition to the intrinsic adhesion provided by the adhesive. The steel rod pull-out samples exhibit a slightly lower value of shear strength than GFRP samples when tested at 50˚C. This may be due to internal stress in the bonded-in joint due to differences in the thermal expansion coefficients (α) of the rods and the LVL. ANOVA analysis indicates valid interaction between types of rod and test temperature treatment.

13.1.7 EFFECT OF WOOD TYPES AND SPECIES ON SHEAR STRENGTH

The effect on the type of substrate to bonded-in shear strength is presented in Chapter 11 (section 11.31). The pull-out shear strength of bonded samples increases steadily

with the density wood which agrees well with the result reported by Steiger *et al.* (2005) and Serrano (2001) although other studies indicates otherwise (Bengtsson & Johansson, 2000; Bernasconi, 2001). The highest shear strength is exhibited by hardwoods in which it represents the high shear strength of the wood itself.

The investigation of the pull-out strength of untreated Radiata pine and acetylated Radiata pine (Accoya) indicates that treated samples are denser but exhibit a decrease of 8% in mean shear strength compared to untreated samples. Various studies report a lower bonding strength for acetylated wood using epoxy, EPI, polyvinyl acetate (PVAc), resorcinol formaldehyde and phenol resorcinol formaldehyde adhesives (Vick *et al*., 1993; Frihart, 2006).

13.3 FUTURE WORK

The continuity to the Dynamic Mechanical Thermal Analysis (DMTA) study should be carried out. Creep analysis of polymer via DMTA has many potential in an insight into the viscoelastic response of a polymer. The DMA apparatus which is equipped with a humidity controller unit could be use to study the effect of temperature and humidity on the creep of epoxies. This would give a more realistic condition on to emulate durability of bonded joints due to environmental factors.

Testing of creep in shear for wood-wood bonded model (such as lap joint) could be carried out in an environmental chamber. Strain gauge or laser displacement instrument could be used to measure the accurate measurement. This would give more understanding on the shear creep properties within bonded model. Finite element analysis on inelastic behaviour of bonded models could also be introduced in future work.

The bonded creep model which was introduced by this study is a novel approach. The future work on model for bonded joint should be into introduction of different type of substrates and rods. By varying the temperature, humidity and stress level, a meaningful database could be established for reference.

Temperature, humidity and displacement monitoring on joints of an existing bonded-in structure could be an interesting future work. This is to justify on the durability of room temperature curing epoxy under the influence of high temperature and humidity. A similar preliminary study was conducted by Smedley *et al*. (2012) on the newly erected MTIB exhibition hall.

13.4 CONCLUSIONS

The experimental testing and results from this research provided a deeper understanding on factors which contributed to the durability of a bonded joint. Creep response is a factor of time, temperature and humidity as proven by the presented results. This research has resulted in the following conclusions:

- On mechanical properties of bulk adhesive
  - Modification of RSA to produce EA: The reinforcement of RSA adhesive by incorporating nano-particles and nano-rubber significantly increased the flexural (112%), shear (21%), tensile (87%) and fracture toughness properties, K_{1C} and G_{1C} (55% and 12%) of the EA adhesive.

- On pull-out shear strength of bonded-in joint
  - The highest static mean shear strength was achieved by using the ductile nano-epoxy type adhesive which had been modified with liquid rubber.
  - There is a strong correlation between the density of the wood and mean shear strength. Higher density wood produces higher mean pull-out shear strength.
  - There is no significant difference in mean shear strength between tested samples bonded using smooth GFRP and threaded stainless steel rods
  - The study indicates no significant difference between the mean shear strength of the samples exposed to the different post-cure treatments
  - The study has shown that steel rod and GFRP bonded samples tested at a temperature higher than the glass transition temperature of the adhesive (50°C) exhibited a significant reduction of 109% and 81% in the mean shear strength.

❖ On creep testing of bulk adhesive using DMTA

- Tensile creep strains are a function of temperature and stress, but above Tg + 15ºC the adhesives behave like rubbers with low elastic moduli.
- Shear creep occurs more rapidly than tensile creep but settles down to a constant creep strain once the viscoelastic range of temperature has been exceeded
- Micro-particulate filled epoxy adhesive exhibit less creep but failed in shorter time compared to nano-silica filled epoxy
- The two element Kelvin-Voigt model is sufficient to model creep of thixotropic adhesives

❖ On creep testing of bonded-in joints

- Creep resistance is strongly dependant on the testing temperature and humidity. All adhesive experienced creep failure when tested under the condition of 50°C/95%RH.
- Rubber-filled nanosilica system has more resistance to creep under extreme conditions as compared to standard nano-silica adhesive.
- Under the most extreme condition (50°C/95%RH), micro-particulate adhesive outperformed other adhesive.

REFERENCES

Adachi, T., Osaki, M., Araki, W., Kwon, S. (2008). Fracture toughness of nano- and micro-spherical silica-particle-filled epoxy composites. Acta Materialia, vol.56, pp.2101-2109.

Adamson, M.J. (1980). Thermal expansion and swelling of cured epoxy resin used in graphite/epoxy composite materials. Journal of Material Science 15 : 1736-1745.

Ahmad, Z. PhD thesis dissertation (2008).

Ahmad, Z., Ansell, M.P., and Smedley, D. (2010). Effect of nano- and micro-particle additions on moisture absorption in thixotropic room temperature cure epoxy-based adhesive for bonded-in timber connections. Internation Journal of Adhesion & Adhesive, 30 : 448-455.

Ahmad, Z., Ansell, M.P., Smedley, D., and Paridah, M.T. (2012). Creep behavior of epoxy-based adhesive reinforced with nanoparticles for bonded-in timber connection. Journal of Materials in Civil Engineering, 24 : 825-831.

Aicher, S. (2003). Structural adhesives joints including glued-in bolts. In S. Thelandersson & H.J. Larsen (Eds.), *Timber engineering*. (pp.333-363) John Wiley, England, UK.

Aicher, S., Kalka, D. and Scherer, R. (2002). Transient temperature evolution in glulam with hidden and non-hidden glued-in steel rods. Otto Graf Journal, vol.13, pp. 199-213.

Aicher, S., Wolf M. & Dill-Langer, G. (1998). Heat flow in a glulam joint with a GISR subjected to variable ambient temperature. Otto Graf Journal, vol.9, pp. 185-204.

Altenbach, H., “Creep Analysis of Thin-Walled Structures.” Z. Agnew. Math. Mech., Vol 82, No.8, pp. 507-533, 2002.

Ansell, M.P. and Smedley, D. (2007). Bonded-in technology for structural timber. Proceedings of the Institution of Civil Engineers. Construction Materials 160, Issue CM3, pp.95-98.

Apicella, A., Nicolais, L., Astarita, G., and Drioli, E. (1979). Effect of Thermal History on Water Sorption, Elastic Properties and the Glass Transition of Epoxy Resins. Polymer, Vol.20., pp. 1143 – 1148.

Arias, M.L, Frontini, P.M. and Williams, R.J.J. (2003). Analysis of the damage zone around the crack tip for two rubber-modified epoxy matrices exhibiting different toughenability. Polymer vol.44, pp. 1537 – 1546.

Ashby, M., Shercliff, H. and Cebon, D. (2010). Materials: engineering, science, processing and design (2nd ed.). Butterworth-Heinemann, UK, pp. 12 – 59.

Ashcroft, I.A., Abdel Wahab, M.M., Crocombe, A.D., Hughes, D.J., and Shaw, S.J. (2001). The Effect of Environment on the Fatigue of Bonded Composite Joints. Part 1: Testing and Fractography. Composites, vol.32, pp. 45-58.

Backman, A.C. & Lindberg, K.A.H. (2002). Interaction between wood and polyurethane-alkyd lacquer resulting in a decrease in the glass transition temperature. Journal of Applied Polymer Science, vol. 85, pp- 595-605.

Bainbridge, R., Mettem, C., Harvey, K., and Ansell, M. (2002). Bonded-in Rod Connection for Timber Structures-Development of Design Methods and Test Observations. International Journal of Adhesion and Adhesive, vol.22, pp. 47-59.

Bainbridge, R.J. and Mettem, C.J. (1998). A review of moment-resistant structural timber connections. In Proceeding Institution of Civil Engineers Structures & Buildings, pp. 323-331.

Batchelar, M.L. and McIntosh, K.A. (1998). Structural joints in glulam. NZ Timber Design Journal, Issue 4, vol. 7, pp. 13-20.

Bengtsson, C., Johansson, C.J. (2000). Test methods for glued-in rods for timber structures. Proceedings of the CIB-W18 Meeting Thirty-Three, The Netherlands, Paper 33-7-8.

Berglund, L. and Rowell, R. M. (2005). Wood composites. In R. M. Rowell (Ed.) *Handbook of wood chemistry and wood composites*. Taylor and Francis, New York, pp. 281-301.

Bernasconi, A. (2001). Behaviour of axially loaded glued-in rods – requirements and resistance, especially for spruce timber perpendicular to the grain direction. Proceedings of the CIB-W18 Meeting Thirty-Four, Venice, Italy, Paper 34-7-6.

Bishop, J. (2005a). Epoxide adhesive. In Handbook of Adhesion. Edited by Packham, D.E. John Wiley and Sons, pp 147-150.

Bishop, J. (2005b). Epoxide adhesive : curatives. In Handbook of Adhesion. Edited by Packham, D.E. John Wiley and Sons, pp 150-155.

Blackman, B.R.K., Johnsen, B.B., Kinloch, A.J. and Teo, W.S. (2008). The effects of pre-bond moisture on the fracture behavior of adhesively-bonded composite joints. The journal of adhesion, 84 (3): 256-276.

Blass, H.J. (2003). Joints with dowel-type fasteners. In S. Thelandersson & H.J. Larsen (Eds.), *Timber engineering*. (pp.315-331) John Wiley, England, UK.

Bodig, J and Jayne, B.A. (1982). Mechanics of wood and wood composites. Van Nostrand Reinhold Company Inc. pp. 55-58.

Bonfield, P.W., Mundy, J., Robson, D.J and Dinwoodie, J.M. (1996). The modelling of time-dependant deformation in wood using chemical kinetics. Wood Science and Technology, vol. 30, pp. 105-115.

Broughton, J.G., and Hutchinson, A.R. (2001a). Adhesive system for structural connections in timber. International Journal of Adhesive Adhesion, 21:177-186.

Broughton, J.G, and Hutchinson, A.R. (2001b). Effect of timber moisture content on bonded-in rods. Construction and Building Materials, vol. 15, pp.17 – 25.

Broughton, J.G, and Hutchinson, A.R. "LICONS: Low Intrusion Conservation System for Timber Structures." 2003.

Brown, S.K. The British Polymer Journal, Vol. 14, 1982

Buchanan, A.H. (2007). *New Zealand Timber Design Guide (3rd ed.)*. Timber Industry Federation, NZ.

Bussi, P. and Ishida, H. (1994). Partially miscible blends of epoxy resin and epoxidized rubber: Structural characterization of the epoxidized rubber and mechanical properties of the blends. Journal Applied Polymer Science, vol. 53, pp. 441-454.

Campbell, D., Pethrick, R.A., and White, J.R. (2000). Polymer characterization : physical techniques. Stanley Thornes Ltd. UK. 386-399.

Chen, T.K. and Jan, Y.H. (1992). Fracture mechanism of toughened epoxy resin with bimodal rubber-particle size distribution. Journal of Materials Science 27, pp. 111-121.

Chikhi, N., Fellahi, S. and Bakar, M. (2002). Modification of epoxy resin using reactive liquid (ATBN) rubber. European Polymer Journal, vol.38, pp. 251-264.

Chu, Y.P. (1987). Structural timber joints. Sinar Suria, Kuala Lumpur, Malaysia

Comyn J. Polymer Marine Environment: 153, 1989.

Cruz, H. & Custódio J.E.P. (2006). Thermal performance of epoxy adhesives in timber structural repair. In 9th World conference on timber engineering – WCTE, Portland, Oregon, USA.

Cruz, H., Custódio J.E.P. & Machado, J.S. (2004). Temperature effects on the performance of epoxy adhesives used in structural reinforcements. In: 2nd Construction national congress on re-think construction – Construćão, Porto, Portugal.

Cruz, H., Custódio J.E.P. & Machado, J.S. (2005). High service temperature and the timber embedment effects on the performance of epoxy structural adhesives. Int. J Construlink, vol. 3, pp. 1-8.

Dagher, H. J. and Bragdon, M. (2001). Advanced FRP-wood composite in bridge applications. Proceedings of the SEI/ASCE Structure Congress, Washington, DC.

Davis, G. (1997). The Performance of Adhesives Systems for Structural Timbers. Int. Journal of Adhesion and Adhesives, Vol.17, pp. 247-255.

Desch, H.E. and Dinwoodie, J.M. (1996). Timber structure, properties, conversion and use, Macmillan Press Ltd. Basingstoke, U.K.

Dinwoodie, J. M. (2000). Timber: its nature and behaviour (2nd ed.). Taylor and Francis, New York, pp. 234-255.

Ellis, B. (1993). Chemistry and technology of epoxy resins, B. Ellis, ed., Blackie Academic Professional, New York, 72-116.

Faherty, K.F. (1998). Mechanical fasteners and connectors. In K.F Faherty & T.G Williamson (Eds.), *Wood engineering and construction handbook (3rd ed.)* (pp.5-1 – 5-152) McGraw-Hill.

Feligioni, L., Lavisci, P., Duchanois, G., De Ciechi, M., and Spinelli, P. (2003). Influence of glue rheology and joint thickness on the strength of bonded-in rods. Holz als Roh- und Werkstoff 61: 281-287.

Feng, C.W., Keong, C.W., Hsueh, Y.P., Wang, Y.Y. and Sue, H.J. (2005). Modelling of long-term creep behaviour of structural epoxy adhesives. International Journal of Adhesion and Adhesive, vol. 25, pp. 427-436.

Findley, W.N. (1960). Mechanism and mechanics of creep in plastics. SPEJ, vol. 16, pp. 57-65.

Frigione, M., Lettieri, M., and Mecchi, A. (2006). Environmental effect of epoxy adhesives employed for restoration of historical buildings. Journals of materials in civil engineering, 18: 715-722.

Frihart, C.R & Hunt, C.G. (2010). Adhesives with wood materials: Bond formation and performance. In *Wood handbook: wood as an engineering material (2010 edition.)*, (pp. 10-1 – 10-24) Forest Product Society, US.

Frihart, C.R. (2006). Wood structure and adhesive. In D.D Stokke & L.H. Groom (Eds), Characterization of the cellulosic cell wall, (pp. 242-251) Blackwell publishing.

Frihart, C.R. (2005). Are epoxy-wood bonds durable enough?. Wood Adhesive 2005: Discussion Forum, California, USA, 2005.

Frihart, C.R. 2005. Are Epoxy-Wood Bonds Durable Enough? Wood Adhesive 2005: Discussion Forum, California, USA.

Gardelle, V. and Morlier, P. (2007). Geometric parameters which affect the short term resistance of an axially loaded glued-in rod. Materials and structures 40: 127-138.

Gere, J.M (2006). Mechanics of Materials. Thomson ltd. Pp. 15-17

Glos, P. & Horstmann, H. (1989). Strength of glued lap timber joints. Proceedings CIB-W18A meeting 22, East Berlin, Germany, paper 22 – 7-8, pp.1-17.

Goland, M. and Reissner. (1944) E. J. Appl. Mech. 2, A-17.

Goodhew, P.J and Humphreys, F.J (1988) Electron Microscopy and Analysis, 2nd Ed. London : Taylor and Francis.

Goulding, T.M (1994). Epoxy resin adhesive. In Handbook of Adhesive Technology Edited by Pizzi, A and Mittal K.L, Marcel Dekker Inc. pp. 531-547.

Hanhijärvi.A. (2000a). Advances in the knowledge of the influence of moisture changes on the long-term mechanical performance of timber structures. Materials and Structures., vol 33., pp 43-49.

Hanhijärvi.A., (2000b). Computational method for predicting the long-term performance of timber beams in variable climates. Materials and Structures., vol.33, pp.127 – 134.

Hanhijärvi, A. and Hunt, D. (1998). Experimental indication of interaction between viscoelastic and mechanosorptive creep. Wood and Science Technology, vol. 32, pp. 57 – 70.

Harvey, K., and Ansell, M.P. (2000). Improved Timber Connections Using Bonded-in GFRP Rods. In Proceeding of World Conference on Timber Engineering, Whistler, Canada.

Haupert, F. & Wetzel. B. (2005). Reinforcement of thermosetting polymers by the incorporation of micro- and nanoparticles. In K., Friedrich, S., Fakirov & Z., Zhang, *Polymer Composites : from nano- to macro-scale*. (page 45-62) Springer, NY.

Huiwen, H. and Sun, C.T. (2000). The characterisation of physical aging in polymeric composites. Composite Science and Technology, vol. 60, pp. 2693-2698.

Imanaka, M., Takeuchi, Y., Nakamura, Y., Nishimura, A. and Iida, T. (2001). Fracture toughness of spherical silica-filled epoxy adhesives. Internation Journal of Adhesion & Adhesives, vol.21, pp. 389-396.

Johnsen, B.B., Kinloch, A.J., Mohammed, R.D., Taylor, A.C., and Sprenger, S. (2007). Toughening mechanism of nanoparticle-modified epoxy polymers. Polymer 48, pp. 530-541.

Kar, S. and Banthia, A.K. (2004). Use of acrylate-based liquid rubbers as toughening agents and adhesive property modifiers of epoxy resin. Journal of Applied Polymer Science, vol. 92, pp. 3814-3821.

Kim, D.S., Cho, J., Kim, K. and Park, C.E. Polymer Engineering and Science, Vol.36, Pp 755, 1996.

Kinloch, A.J. (1983). Fracture behavior of polymers. Elsevier Applied Science, London and New York, 188-189.

Kinloch, A.J and Young, R.J. (1983). Toughened multiphase plastics. In: Fracture behaviour of polymers. New York: Applied Science Publishers, pp.422.

Kinloch, A.J., Maxwell, D.L., and Young, R.J. (1985a). The fracture of hybrid-particulate composites. Journal of Materials Science, vol.20, pp. 4169-4184.

Kinloch, A.J., Maxwell, D.L., and Young, R.J. (1985b). Micromechanisms of crack propagation in hybrid-particulate composites. Journal of Materials Science Letters 4, pp. 1276-1279.

Kinloch, A.J., Mohammed, R.D., Taylor, A.C., Eger, C., Sprenger, S., and Egan, D. (2005). The effect of silica nano particles and rubber particles on the toughness of multiphase thermosetting epoxy polymers. Journal of Materials Science, vol.40 (18), pp.5083-5086.

Kwon, S., Adachi, T., Araki, W., and Yamaji, Akihiko. (2008a). Effect of composing particles of two sizes on mechanical properties of spherical silica-particulate-reinforced epoxy composites. Composites: part B 39, pp. 740-746.

Kwon, S.C., Adachi, T., and Araki, W. (2008b). Temperature dependence of fracture toughness of silica/epoxy composites: related to microstructure of nano- and micro-particles packing. Composites: Part B 39, pp. 773-781.

Larsen, H.J. (2003). Introduction: fasteners, joints and composite structures. In S. Thelandersson & H.J. Larsen (Eds.), *Timber engineering*. (pp.303-313) John Wiley, England, UK

Lee, J. K., Hwang, J.Y., and Gillham, J.K. (2001). Erasure below glass-transition temperature of effect of isothermal physical aging in fully cured epoxy/amine thermosetting system. Journal Applied Polymer Science, 81(2), pp.396-404.

Lorenzis, L.D., Scialpi, V. and Tegola, A.L. (2005). Analytical and experimental study on bonded-in CFRP bars in glulam timber. Composites: Part B 36: 279-289.

Lou, Y.C and Schapery, R.A., "Viscoelasticity Characterisation of a Nonlinear Fibre-Reinforced Plastic." Journal of Composite Materials, Vol.5, pp. 208 – 234, 1971.

Maazouz, A., Sautereau, H. and Gerard, J.F. Hybrid-particulate composites based on an epoxy matrix, a reactive rubber, and glass beads: morphology, viscoelastic and mechanical properties. Journal of Applied Polymer Science, vol.50, issue 4 (1993) 615-626.

Manzione, L.T., Gillham, J.K. and McPherson, C.A. Rubber-modified epoxies. I. Transition and morphology. Journal of Applied Polymer Science, vol. 26 (1980) 889-905.

Marra A.A. (1992). Technology of wood bonding – principles in practice. Van Nostrand Reinhold.

Mårtensson, A. (1994). Creep behaviour of structural timber under varying humidity conditions. Journal of Structural Engineering, vol. 9, pp. 2565-2580.

Matějka, L., Dukh, O. and Kolařík, J. (2000). Reinforcement of crosslinked rubbery epoxies by in-situ formed silica. Polymer 41, pp. 1449-1459.

McMurray, M.K and Amagi, S. The Effect of Time and Temperature on Flexural Creep and Fatigue Strength of a Silica Particle Filled Epoxy Resin. Journal of Materials Science, Vol.34, Pp. 5927 – 5936, 1999.

Meek, G.A (1976) Practical Electron Microscopy for Biologists 2nd Ed. London-New York-Sydney-Toronto : John Wiley and Sons.

Menard, K.P. (2008). Dynamic mechanical analysis: a practical introduction (2nd ed.). (pp. 15 – 75) Taylor & Francis Group, US.

Meyer, F., Sanz, G., Eceiza, A., Mondragon, I., and Mijovic, J. (1995). The effect of stoichiometry and thermal history during cure on structure and properties of epoxy networks. Polymer, 36(7), pp.1407-1414

Mikols, W.J., Seferis, J.C., Apicella, A., Nicolais, A. (1982). Evaluation of structural changes in epoxy systems by moisture sorption-desorption and dynamic mechanical studies. Polymer Composites 3(3) : 118-124.

Millington, S. (2005). Standards for adhesives and adhesion. In Handbook of Adhesion. Edited by Packham, D.E. John Wiley and Sons, pp 483-485.

Miyano, Y., Nakada, M., Kasamori, M. and Muki, R. (2000). Effect of physical aging on the creep deformation of an epoxy resin. Mechanics of Time-Dependant Materials, vol. 4, pp. 9-20.

Naturally:Wood. (2012). Richmond Olympic Oval. Retrieved May 25, 2013, from http://www.naturallywood.com.

Nielsen, J. (2003). Trusses and joints with punched metal plate fasteners. In S. Thelandersson & H.J. Larsen (Eds.), *Timber engineering*. (pp.365-382) John Wiley, England, UK.

Nigam, V., Setua, D.K. and Mathur, G.N. (1998). Wide-angle x-ray scattering, Fourier Transform Infrared Spectroscopy, and Scanning Electron Microscopy studies on the influence of the addition of liquid functional rubber in epoxy thermoset. Journal of Applied Polymer Science 70, pp.537 – 543.

Nigam, V., Setua, D.K, Mathur, G.N. (1999). Characterization of liquid carboxy terminated copolymer of butadiene acrylonitrile modified epoxy resin. Polymer Engineering Science, vol. 39, pp. 1425-1432.

Ning Su, R.I., Mackie and Harvey, W.J. (1991). The Effects of Ageing and Environment on the Fatigue Life of Adhesive Joints." International Journal of Adhesion and Adhesive, Vol.12. Pp. 85-93.

Nishimura, A., Yaguchi, A. and Kawai, S. Zairyou, (1989).Vol. 38, Pp. 434.

Nogueira, P., Ramírez, Torres, A., Abad, M.J., Cano, J., López-bueno, I., and Barral, L. (2001). Effect of water sorption on the structure and mechanical properties of an epoxy resin system. Journal of Applied Polymer Science, 80 : 71-80.

Ozturk, A., Kaynak, C. and Tincer, T. (2001). Effect of liquid rubber modification on the behaviour of epoxy resin. European Polymer Journal, no. 37, pp. 2353-2363.

Pearson, R.A and Yee, A.F. (1986). Toughening mechanism in elastomer-modified epoxies. Part 1: Mechanical studies. Journal of Materials Science, 21, pp. 2462 – 2474.

PerkinElmer (2013). Dynamic mechanical analysis (DMA) : A beginner's guide.

Pervin, F., Zhou, Y., Rangari, V.K., and Jeelani, S. (2005). Testing and evaluation on the thermal and mechanical properties of carbon nano fiber reinforce SC-15 epoxy. Materials Science and Engineering: A, vol. 405 (1), pp. 246-253.

Pethrick, R.A., Hollins, E.A., Mc Ewan, I., Pollock, E.A., Hayward, D. (1996). Effect of cure temperature on the structure and water absorption of epoxy/amine thermosets. Polymer International 39(4), pp. 275-288.

Pierce, C. B. and Dinwoodie, J.M.. (1977). Creep in chipboard. Part 1: fitting 3- and 4-element response curves to creep data. Journal Materials Science, vol. 12, pp. 1955 – 1960.

Pierce, C.B and Dinwoodie, J.M. (1985). Creep in chipboard. Part 5: an improved model for prediction of creep deflection. Wood Science Technology, vol.19, pp. 83-91.

Pizzi, A. and Mittal, K.L. (2003). Handbook of adhesives technology. 2nd ed. CRC Press LLC.

Pizzo, B., Rizzo, G., Lavisci, P., Megna, B. and Berti, S. (2002). Comparison of thermal expansion of wood ad epoxy adhesives. Holz als Roh- und Werkstoff 60: 285-290.

Qiao, L., and Easteal, A.J. (2001). Aspects of the performance of PVAc adhesives in wood joints. Pigment & Resin Technology, vol. 30(2), pp. 79-87.

Rammer, D.R. (2010). Fastenings. In, *Wood handbook: wood as an engineering material (2010 edition.)*, (pp. 8-1 – 8-27) Forest Product Society, US.

Ranta-Maunus,A. (1990). Impact of Mechano-sorptive Creep to the Long-term Strength of Timber." Holz als Roh-und Werkstoff., vol. 48, pp. 67 – 71.

Ratna, D. and Banthia, A.K. (2000). Toughened epoxy adhesive modified with acrylate based liquid rubber. Polymer International, vol.49, pp. 281-287.

Reimer, L. and Kohl, H. (2008). Transmission Electron Microscopy : Physics of Image Formation. Springer.

Richter, K., and Steiger, R. (2005). Thermal stability of wood-wood and wood-FRP bonding with polyurethane and epoxy adhesives. Advance Engineering Material, 7(5):419-426.

Rong, M.Z., Zhang, M.Q., Liu, H., Zheng, H.M., Wetzel, B., Friedrich, K. (2001). Microstructure and tribological behaviour of polymeric nano-composites. IndLubrTribol; 53(2):72-77.

Rossignon, A., and Espion, B. (2008). Experimental assessment of the pull-out strength of single rods bonded in glulam parallel to the grain. Holz Roh Werkst, 66:419-432.

Russel, B. and Chartoff, R. (2005). The influence of cure conditions on the morphology and phase distribution in a rubber-modified epoxy resin using scanning electron microscopy and atomic force microscopy. Polymer 46, pp. 785 – 798.

Serrano, E (2001a). Glued-in rods for timber structures – an experimental study of softening behaviour. Materials and structures 34 : 228-234.

Serrano, E. (2001b). Glued-in rods for timber structures – a 3D model and finite element parameter studies. International Journal of Adhesion & Adhesives, vol. 21. pp.115-127.

Shmulsky, R. and Jones, P. D. (2011). Forest products and wood science : an introduction (6th ed.), Wiley-Blackwell, UK, pp. 316-350.

Smedley, D., Tiew, J., Roseley, A., Ahmad, Z., Ansell, M.P. (2012). Innovative timber exhibition hall in Johor Malaysia, constructed from indigenous hardwood using bonded-in moment resisting connections. World Conference in Timber Engineering, Auckland, NZ.

Smith, J.W., Cantwell, W.J., Demarmels, A. and Kausch, H.H. (1991). Creep failure mechanism in a particulate-filled epoxy resin. Journal of Material Science, vol. 26, pp. 5534-5542.

Steiger, R., Gehri, E. and Widmann, R. (2005). Pull-out strength of axially loaded steel rods bonded in glulam parallel to the grain. Materials and structures 40:69-78.

Sue, H. (1992). Craze-like damage in a core-shell rubber-modified epoxy system. Journal of materials science 27, pp.3098-3107.

Thomason, J.L. (1995). The interface region in glass fibre-reinforced epoxy resin composites: 2. Water absorption, voids and the interface. Composites 26(7): 477-485.

TRADA Wood Information. (2003) Subject: Joint and jointing, pp. 51.

TRADA Wood Information. (2007) Up-to-date information for builders: Mechanical fixings for wood.

Van de Kuilen, J.W.G. (1999). Duration of load effects in timber joints. PhD dissertation, Delft University of Technology, The Netherlands.

Vick, C.B., Larsson, P.Ch., Mahlberg, R.L., Simonson, R. and Rowell,R.M. (1993). Structural bonding of acetylated Scandinavian softwoods for exterior lumber laminates. International journal of adhesion and adhesives 13: 139-149.

Vincent, J. (2012). Basic elasticity and viscoelasticity. In, *Structural Biomaterials (3rd ed.)*, (pp. 1 – 28) Princeton University Press.

Volkersen, O. (1938) Luftfahrtforsch, 15, 14.

Wang, H., Bai, Y., Liu, S., Wu, J. and Wong, C.P. (2002). Combined effects of silica filler and its interface in epoxy resin. Acta Materialia, vol.50, pp. 4369-4377.

Ward, I.M & Sweeney, J. (2004). An introduction to the mechanical properties of solid polymers (2nd ed.). (pp. 53 – 71) John Wiley & Sons, England.

Watt, M.I (1997) The Principles and Practice of Electron Microscopy 2nd Ed. Cambridge University Press.

Wetzel, B., Haupert, F. and Zhang, M.Q. (2003). Epoxy nanocomposites with high mechanical and tribological performance. Composite Science and Technology, no.63, pp. 2055-2067.

Wolfrum, J., Ehrenstein, G.W. and Avondet, M.A. (2000). Dynamical mechanical thermo analysis of high performance composites-influences and problems. Journal of Composite Materials, vol. 34, pp. 1788-1807.

Yamamoto, I., Higashihara, T., Kobayashi, T. (2003). Effect of silica-particle characteristics on impact/usual fatigue properties and evaluation of mechanical characteristics of silica-particle epoxy resins. JSME International Journal, 46(2): pp. 145-153.

Yamanaka, K. and Inoue, T. (1990). Phase separation mechanism of rubber-modified epoxy. Journal of Material Science, 25, pp. 241-245.

Yee, A.F. and Pearson, R.A. (1989). Toughening mechanism in elastomer-modified epoxies. Part 3: The effect of cross-link density. Journal of Materials Science, 24 pp. 2571 – 2580.

Young, R.J. (1986). Rigid-particulate thermosetting polymers. In Structural Adhesives : Development in Resin and Primers, (A.J Kinloch Ed.), Elsevier, London & New York, pp. 163-198.

Young, R.J., Maxwell, D.L. and Kinloch, A.J. (1986). The deformation of hybrid-particulate composites. Journal of materials science 21, pp. 380-388.

Zanni-Deffarges, M.P., and Shanahan, M.E.R. (1995). Diffusion of water into an epoxy adhesive: comparison between bulk behavior and adhesive joints. Int. Journal of Adhesion and Adhesives 15: 137-142.

Zhang, H. and Berglund, L.A. (2004). Deformation and fracture of glass bead/CTBN-rubber/epoxy composites. Polymer Engineering and Science, vol. 33, issue 2 100-107.

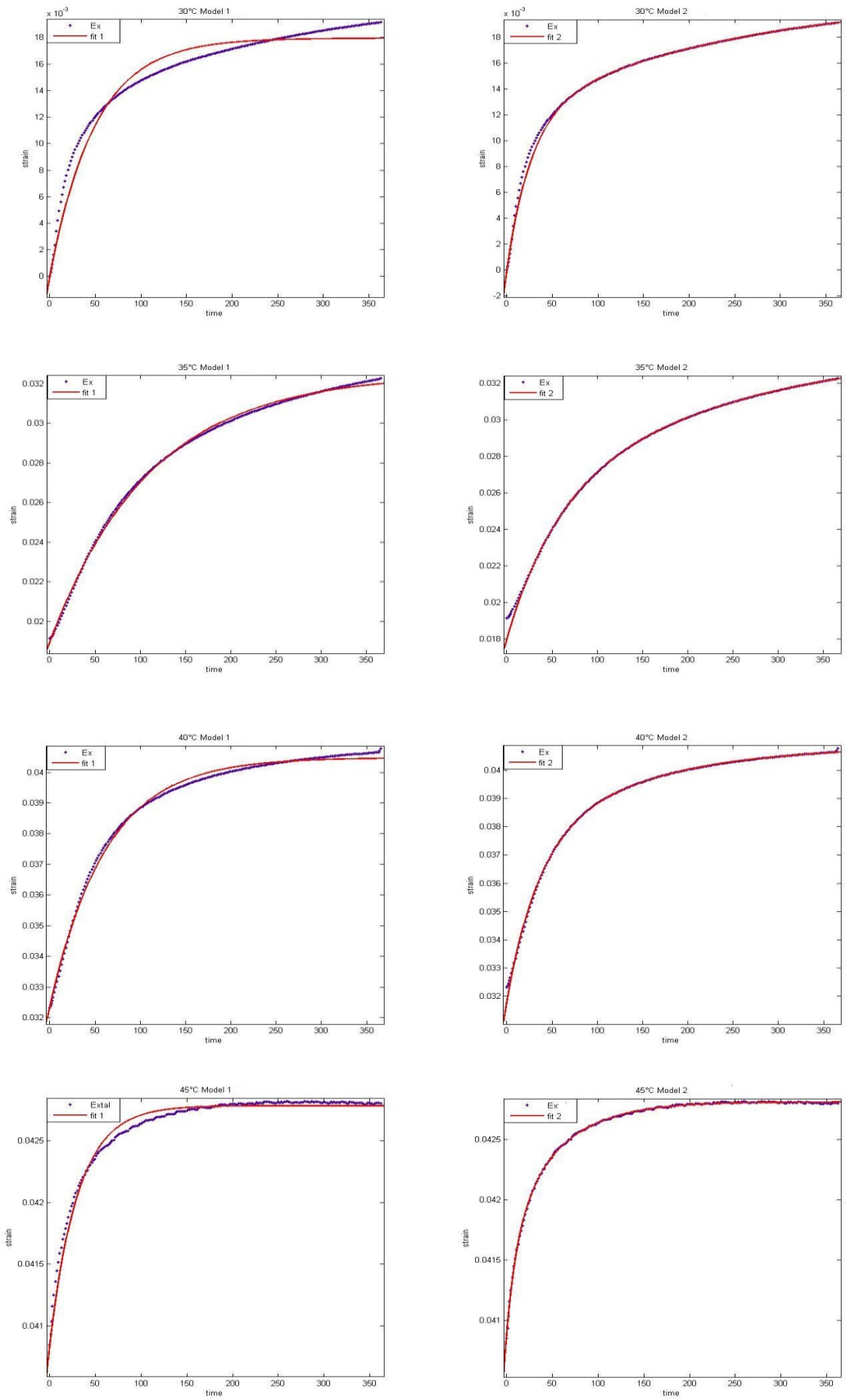

Fig. A1.1. Graphical representation of fitted data based on Kelvin-Voigt model of RSA samples. The figure indicates Model 1 (left column) and Model 2 (right column) at 30 to 45°C.

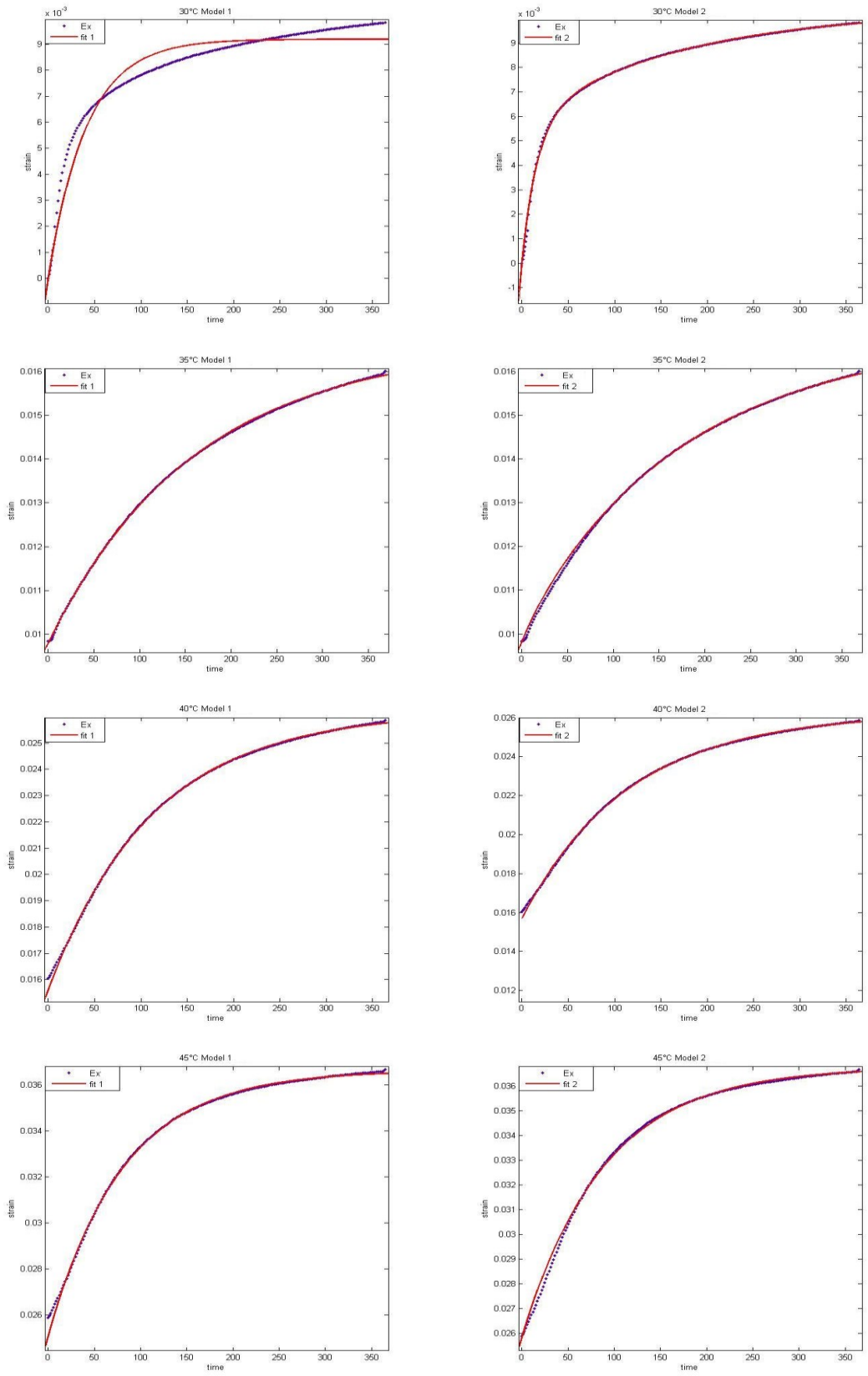

Fig. A2.1. Graphical representation of fitted data based on Kelvin-Voigt model of EA samples. The figure indicates Model 1 (left column) and Model 2 (right column) at 30 to 45°C.

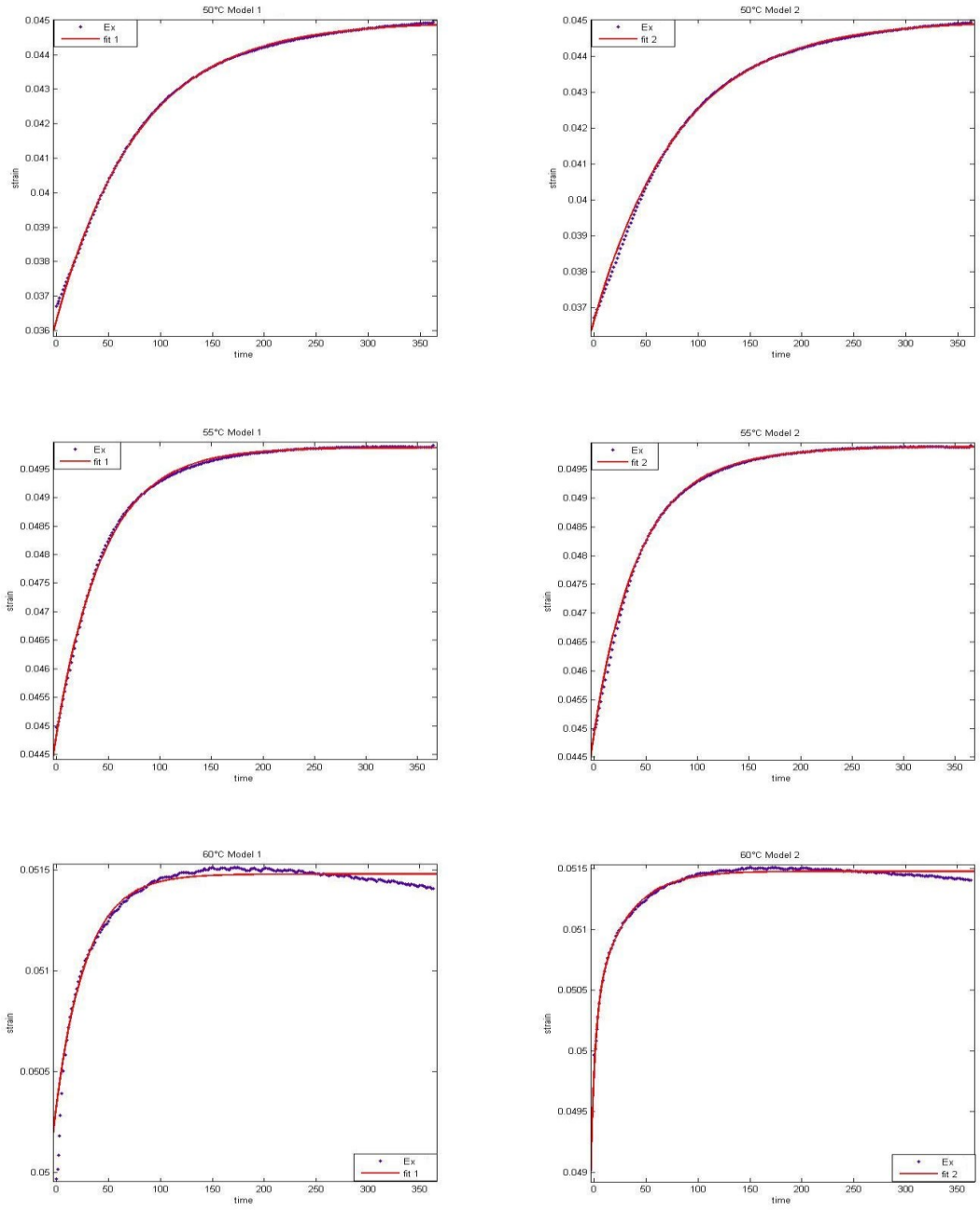

Fig. A2.2. Graphical representation of fitted data based on Kelvin-Voigt model of EA samples. The figure indicates Model 1 (left column) and Model 2 (right column) at 50 to 60°C.

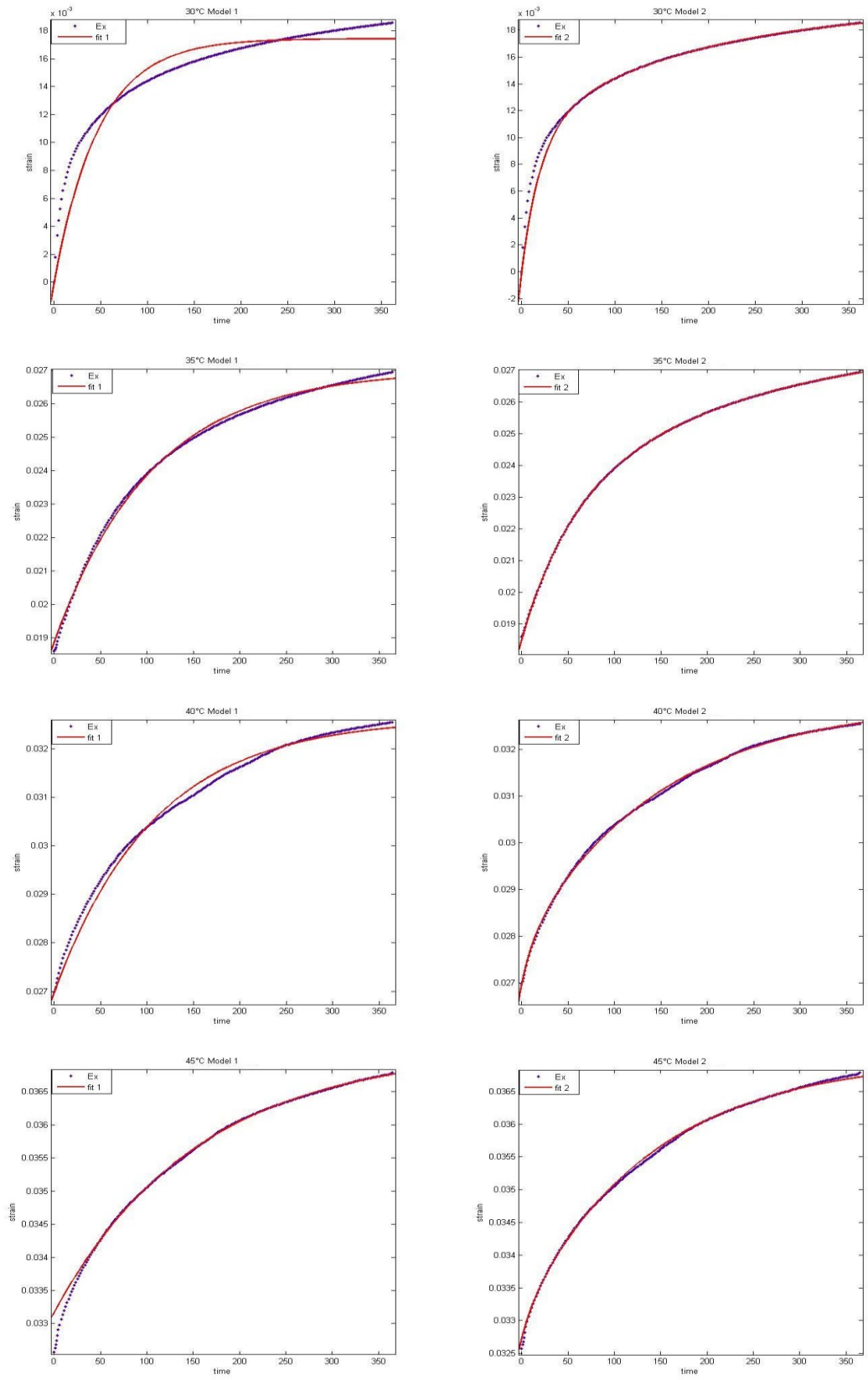

Fig. A3.1. Graphical representation of fitted data based on Kelvin-Voigt model of Timberset samples. The figure indicates Model 1 (left column) and Model 2 (right column) at 30 to 45°C.

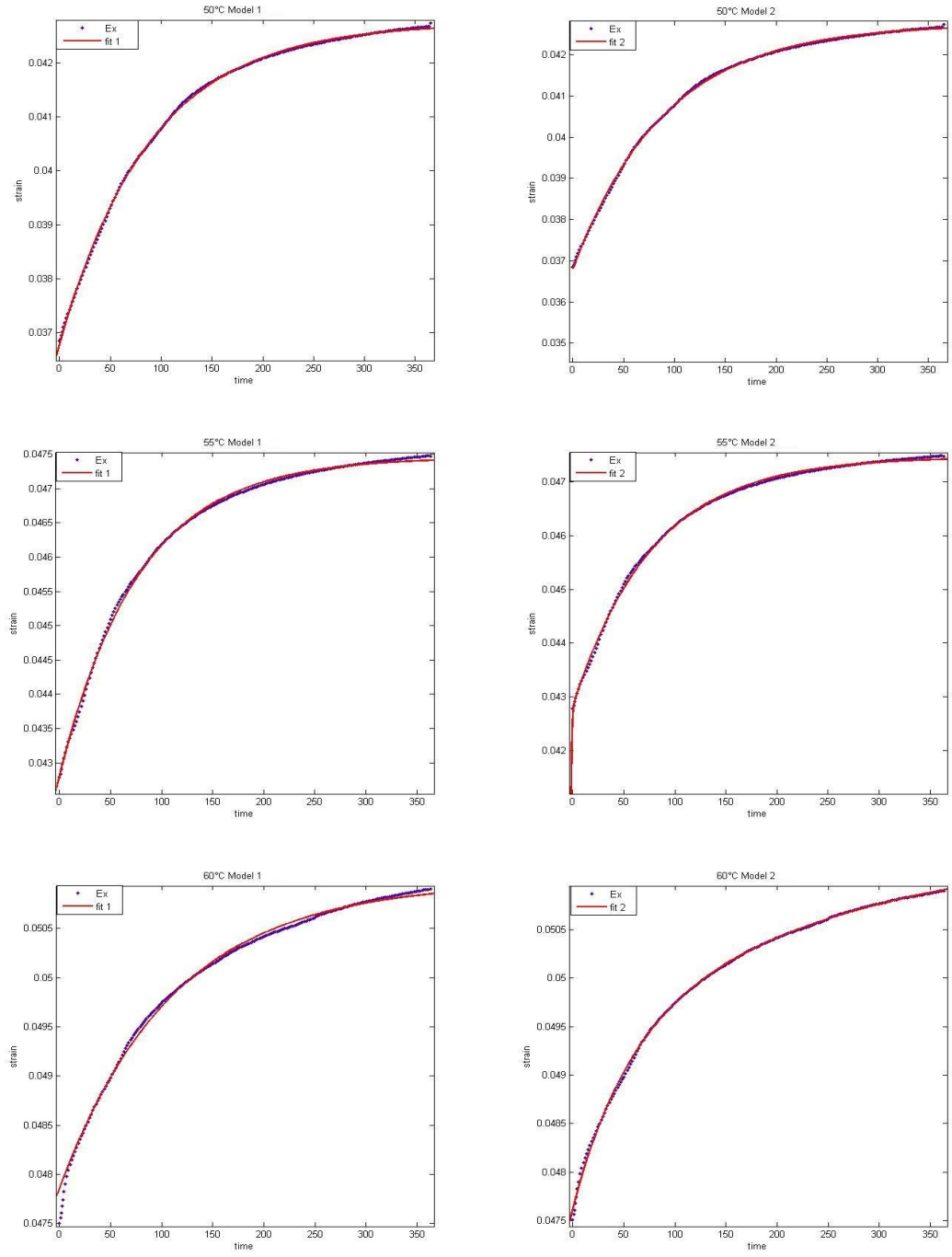

Fig. A3.2. Graphical representation of fitted data based on Kelvin-Voigt model of Timberset samples. The figure indicates Model 1 (left column) and Model 2 (right column) at 50 to 60°C.

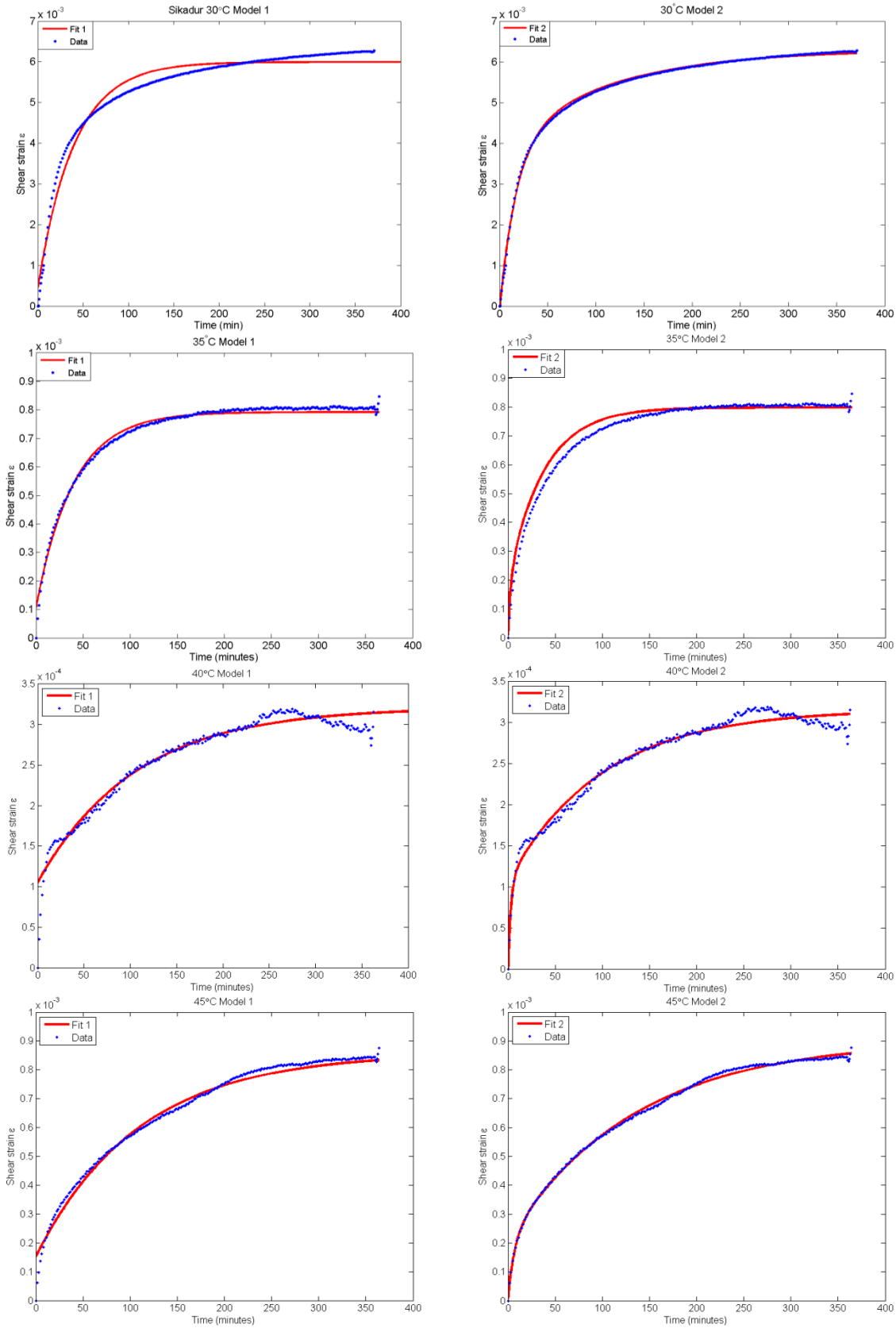

Fig. A4.1. Graphical representation of fitted data based on Kelvin-Voigt model of Sikadur samples. The figure indicates Model 1 (left column) and Model 2 (right column) at 30 to 45°C.

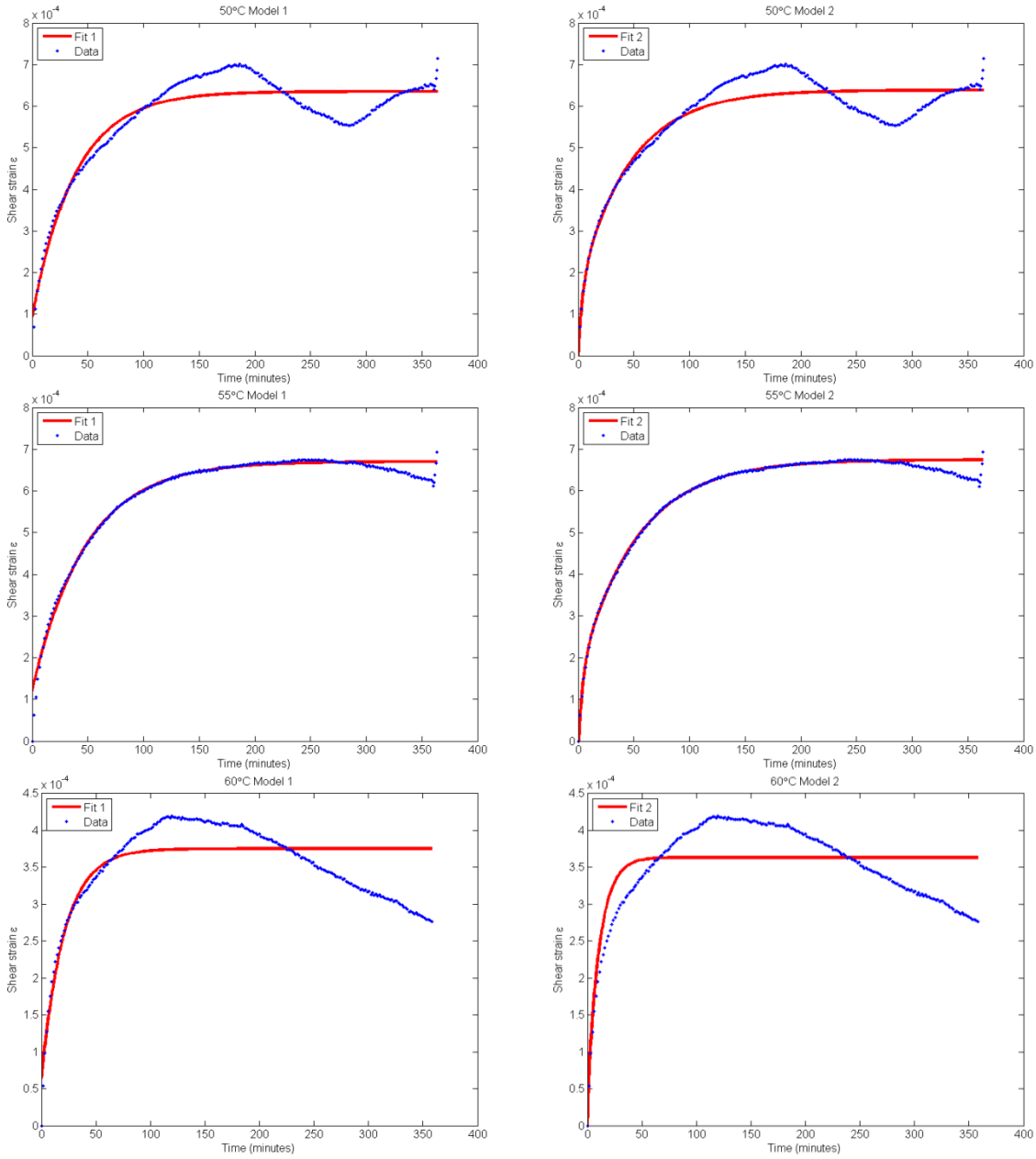

Fig. A4.2. Graphical representation of fitted data based on Kelvin-Voigt model of Sikadur samples. The figure indicates Model 1 (left column) and Model 2 (right column) at 50 to 60°C.